International Atomic Energy Agency

INDC(NDS)-146
Distribution: L

INDC

INTERNATIONAL NUCLEAR DATA COMMITTEE

IAEA Consultants' Meeting on
THE U-235 FAST-NEUTRON FISSION CROSS-SECTION, and
THE Cf-252 FISSION NEUTRON SPECTRUM

Smolenice, Czechoslovakia
28 March - 1 April 1983

Proceedings edited by

H.D. Lemmel, D.E. Cullen

July 1983

IAEA NUCLEAR DATA SECTION, WAGRAMERSTRASSE 5, A-1400 VIENNA

Printed by the International Atomic Energy Agency
Austria
July 1983
83-6258

INDC(NDS)-146
Distribution: L

IAEA Consultants' Meeting on THE U-235 FAST-NEUTRON FISSION CROSS-SECTION, and THE Cf-252 FISSION NEUTRON SPECTRUM

Smolenice, Czechoslovakia
28 March - 1 April 1983

Proceedings edited by

H.D. Lemmel, D.E. Cullen

July 1983

Abstract

The two IAEA Consultants' Meetings on the U-235 fast-neutron fission cross-section and the Cf-252 fission neutron spectrum were held simultaneously in the castle of Smolenice near Bratislava, hosted by the Slovak and Czechoslovak Akademies of Sciences, in the period 28 March to 1 April 1983.

The topics of the meetings concern two nuclear reactions that are recognized as important standard reference data. Experts reviewed recent progress in experiment and theory which will lead to significantly improved accuracy of the data.

This report contains the papers presented and the conclusions and recommendations of the meeting.

Contents

IAEA Consultants' Meeting on
The U-235 Fast-Neutron Fission Cross-Section

Smolenice, Czechoslovakia
28 March - 1 April 1983

List of papers presented

IAEA Consultants' Meeting on
The Cf-252 Fission Neutron Spectrum

Smolenice, Czechoslovakia
28 March - 1 April 1983

List of papers presented

Session 1. Direct spectrum measurements

Compare also paper 5 of the U-235 meeting.

Session 2. Theory

(Nr. 6 is not included in this document)

Supplementary papers relevant to this meeting see also K.H. Böckhoff (ed.): Proceedings of the International Conference on Nuclear Data for Science and Technology, Antwerp, 6-10 Sept. 1982, Reidel Publishing Company 1983, in particular the following papers:

A.D. Carlson, J.W. Behrens: Measurement of the U-235(n,f) cross-section from 0.3 to 3.0 MeV using the NBS Electron Linac. (p.456)

W.P. Poenitz, T. Tamura: Investigation of the prompt-neutron spectrum for spontaneously-fissioning Cf-252. (p. 465)

D.G. Madland, J.R. Nix: Calculation of the prompt-neutron spectrum and average prompt-neutron multiplicity for the spontaneous fission of Cf-252. (p. 473)

M.V. Blinov, G.S. Boykov, V.A. Vitenko: New experimental data on the energy spectrum of Cf-252 spontaneous fission prompt neutrons. (p. 479)

R. Böttger, H. Klein, A. Chalupka, B. Strohmaier: The neutron energy spectrum from the spontaneous fission of Cf-252 in the energy range from 2 MeV to 14 MeV. (p. 484)

H. Märten, D. Seeliger, B. Stobinski: The high-energetic part of the neutron spectrum from spontaneous fission of Cf-252. (p.488)

Meeting Schedule

Part 1: The U-235 Fast-Neutron Fission-Cross Section

Chairmen: A.D. Carlson (NBS Washington)
B.H. Patrick (Harwell)

Scientific Secretary: D.E. Cullen (IAEA)

Monday, 28 March:

Presentation of papers

Tuesday, 29 March and Thursday, 31 March

Working group sessions

Friday, 1 April

Conclusions and Recommendations

Part 2: The Cf-252 Fission Neutron Spectrum

Chairmen: M.V. Blinov (R.I. Leningrad)
H. Klein (PTB Braunschweig)

Scientific Secretary: H.D. Lemmel (IAEA)

Tuesday, 29 March

Working group sessions

Wednesday, 30 March

Presentation of papers

Thursday, 31 March

Working group sessions

Friday, 1 April

Conclusions and Recommendations

List of Participants

R. Arlt (27 + 28 March)	International Atomic Energy Agency Wagramerstr. 5 P.O. Box 100 A-1400, Vienna, Austria
M.R. Bhat	National Nuclear Data Center Bldg. 197D Brookhaven National Laboratory Upton, New York 11973, U.S.A.
M.V. Blinov (Chairman, U-235 meeting)	Radievyj Institut V.G. Khlopina Ul. Rentgena 1 Leningrad P-22, U.S.S.R.
C. Budtz-Jörgensen	Bureau Central de Mesures Nucléaires Steenweg naar Retie B-2440 Geel, Belgium
A.D. Carlson (Chairman, U-235 Meeting)	Radiation Physics Building Room B119 National Bureau of Standards Washington, D.C. 20233, U.S.A.
A. Chalupka	Institut für Radiumforschung und Kernphysik Boltzmanngasse 3 A-1090 Vienna, Austria
D.E. Cullen (Scientific Secretary, U-235 Meeting)	International Atomic Energy Agency Wagramerstr. 5 P.O. Box 100 A-1400 Vienna, Austria
J. Davidova (Local Secretary)	Czechoslovak Academy of Sciences 2, Slesca Ul. CS-180 40 Prague 8, Czechoslovakia
Z. Dezsö	Institute of Experimental Physics Kossuth Lajos University P.O. Box 105 H-4001 Debrecen, Hungary
Z. Dlouhy	Institute of Nuclear Physics of the Czechoslovak Academy of Sciences CS-250 68 Rez u Prahy, Czechoslovakia
D.B. Gayther	Nuclear Physics Division Bldg. 418 U.K. Atomic Energy Authority AERE Harwell, Didcot OXON OX11 ORA, United Kingdom

P.I. Johansson	Neutron Physics Laboratory Studsvik Energiteknik AB Fack S-8-611 82 Nykoeping, Sweden
H. Klein (Chairman, Cf-252 Meeting)	Physikalisch Technische Bundesanstalt Abteilung 7 Bundesallee 100 D-3300 Braunschweig, Fed. Rep. Germany
A. Lajtai	Central Research Institute for Physics The Hungarian Academy of Sciences P.O. Box 49 H-1525 Budapest, Hungary
H.D. Lemmel (Scientific Secretary, Cf-252 Meeting)	International Atomic Energy Agency Wagramerstr. 5 P.O. Box 100 A-1400 Vienna, Austria
H. Märten	Sektion Physik Technische Universität Dresden Mommsenstrasse 13 DDR-8027 Dresden, German Dem. Rep.
W. Mannhart	Physikalisch Technische Bundesanstalt Abteilung 7 Bundesallee 100 D-3300 Braunschweig, Fed. Rep. Germany
C. Nordborg	NEA Data Bank B.P. N° 9 (Bât. 45) F-91190 Gif sur Yvette, France
P. Oblozinsky (Local Secretary)	Department of Nuclear Physics Fyzikalny Ustav SAV CS-842 28 Bratislava, Czechoslovakia
H.G. Ortlepp	Sektion Physik Technische Universität Dresden Mommsenstrasse 13 DDR-8027 Dresden, German Dem. Rep.
B.H. Patrick (Chairman, U-235 Meeting)	Nuclear Physics Division Bldg. 418 U.K. Atomic Energy Authority AERE Harwell, Didcot OXON OX11 ORA, United Kingdom
W.P. Poenitz	Applied Physics Division Bldg. 314 Argonne National Laboratory 9700 South Cass Avenue Argonne, Illinois 60439, U.S.A.

V.G. Pronyaev (28 March)	International Atomic Energy Agency Wagramerstr. 5 P.O. Box 100 A-1400 Vienna, Austria
V. Shpakov	Radievyj Institut V.G. Khlopina Ul. Rentgena 1 Leningrad P-22, U.S.S.R.
C. Wagemans	Centre d'Etude de l'Energie Nucléaire C.E.N./S.C.K. Boeretang 200 B-2400 Mol, Belgium
I. Wilhelm	Charles University Prague

Part-time observers from the Institute of Physics,
Slovak Academy of Sciences, Bratislava:

M. Blazek
E. Betak
S. Hlavac
J. Kristiak
A. Luchavova
J. Pivarc

IAEA Consultants' Meeting on The U-235 Fast-Neutron Fission Cross-Section

Smolenice, near Bratislava, Czechoslovakia
28 March - 1 April 1983

Chairmen: A.D. Carlson (NBS Washington)
B.H. Patrick (Harwell)

CONCLUSIONS AND RECOMMENDATIONS

1. INTRODUCTION

The meeting re-affirmed the importance of the U-235 fission cross-section as a primary standard in the energy range 100 keV to 20 MeV. The accuracy required was briefly discussed and the current uncertainty was established as a function of neutron energy. There was considerable discussion on the main contributions to the uncertainties in the measurements of the cross-section and on what steps might be taken to reduce those uncertainties. Lastly, the work which must be carried out to allow the cross-section to be determined to within the required accuracy was identified.

2. ACCURACY REQUIREMENTS

It was agreed that the use of the U-235 fast fission cross-section as a primary standard is the main reason for requiring high accuracy and it was felt that the objective should be an uncertainty of ±1% (1 standard deviation) over the energy range 100 keV to 20 MeV. Such a value will ensure that the contribution from this standard to the overall error in any measurement should be very small. In addition, the U-235 fission cross-section is used as a 'test-bed' against which new techniques are tried and tested. If measurements are unable to produce accurate values for the favourable case of the U-235 fission cross-section, what hope is there of obtaining high quality data for unfavourable nuclides with, for example, high alpha-activity or low cross-sections?

Besides its importance as a standard, the U-235 fast fission cross-section has application in the fast reactor field. For that purpose, requests in WRENDA are typically seeking an accuracy of between 1 and 2% up to $\sim$5 MeV, and above that energy an uncertainty of $\gtrsim$2% is probably acceptable. If an accuracy of 1% for a standard can be achieved over the energy range 100 keV to 20 MeV, all of the requests for U-235 fast fission cross-sections in WRENDA would be satisfied.

The nuclear data needs for fusion are not yet sufficiently detailed to require the U-235 high energy fission cross-section to a high accuracy, although the situation may change in the course of time.

3. CURRENT UNCERTAINTIES IN THE U-235 FAST FISSION CROSS-SECTION

An accurate estimate of the uncertainties in any cross-section can only be obtained by detailed evaluation of the appropriate measurements and therefore it is quite clear that the present meeting could do no more than make an intelligent estimate of the accuracy to which the U-235 fast fission cross-section is currently known. Rather than quoting accuracies in energy intervals, which leads to apparent discontinuities in the uncertainties, it was decided to specify values at specific energies from which the magnitudes at other energies can be inferred by a smooth interpolation. The meeting felt that the following uncertainties apply at the present time.

E_n (MeV)	$\frac{\Delta\sigma_{nf}}{\sigma_{nf}}$ (%)
0.1	2-3
1.0	2-3
3.0	2-3
5.0	3-4
8.0	3-4
13	4
14	1.0
15	2
20	6

However, one participant felt that the cross-section is known to 1-2% over much of the energy range below 13 MeV.

The region giving most cause for concern at the present time is that from ∿3 to 6 MeV. Here, the data tend to divide into two groups, one having a convex shape and high cross-section values, and the other with a concave shape and low values. (See, for example, Fig. 3 of the contribution by Bhat). The two groups differ by up to ∿10% although the contributing measurements claim accuracies in some cases of ∿2%. During the meeting, some reasons were put forward for doubting the accuracy of certain measurements (see the paper by Gayther and Patrick) and those reasons might lead to a downweighting of the data from those measurements.

There was some slight concern about the uncertainty in the region of 600 keV, where it was felt that the spread in the data might warrant a larger uncertainty than quoted in the above table.

It is encouraging to note that there appears to be very good agreement among the 'modern' (i.e. post 1975) 14 MeV measurements. However, this apparent strength must be viewed with caution as all of the measurements have employed the same technique, namely the time correlated associated particle (TCAP) method, and there may be unknown systematic errors present.

It was noted that the U-235 cross-section averaged over the Cf-252 fission neutron spectrum is very insensitive to the shape of that spectrum and therefore such measurements provide a useful normalisation value for shape measurements and evaluations. At the present time, the most accurate measurements are in agreement within the experimental uncertainties of 1.5-2%.

4. MAIN CONTRIBUTIONS TO UNCERTAINTIES IN MEASUREMENTS

It was clear from the discussions that, as experimental techniques are examined more critically, and, as a result, refined, more and more of the problems of making accurate measurements are being understood. As a consequence, a comparison of older to newer measurements might appear to indicate that little progress has been made, but this may only be because the older measurements may have been too optimistic in their error estimates. There are clear signs that the main problem areas are now recognised and being tackled with vigour. These areas must be divided into two main components, covering problems arising from fission counting and those from neutron flux determination.

On the fission counting side of any measurement, the following are the problem areas.

(a) Extrapolation of the fission fragment pulse height spectrum to zero energy

In a well-designed experiment, the extrapolation to zero pulse height introduces a correction of $\sim$1-1.5%, and in most cases, it is assumed that this extrapolation is linear and has a constant magnitude equal to the measured pulse height spectrum in the region just above the bias. But is this assumption justified or could the neglect of the ionisation defect cause undetected systematic errors? More work needs to be done to understand these effects and also more attention paid to the electronic methods used in processing the signals from fission chambers.

(b) Loss of fission fragments

Corrections for loss of fragments require a knowledge of the angular distribution as a function of the neutron energy and of the range of fragments in the fissionable material used. In the case of U-235, the uncertainty in the range may have a significant effect and may be more of a problem than any inaccuracies in the angular distributions. More work needs to be done to understand the effect of surface conditions (of both the backing and the deposit) on the loss of fission fragments. Direct measurements of fission chamber efficiency might be the best way of solving problems (a) and (b).

(c) Sample assay

Considerable attention is currently being focussed on the problems of sample assay and the international intercomparison of the mass determinations of fission foils should produce very valuable results. Of the main methods employed, comparisons of fission counting in a thermal field relative to very accurately assayed foils, seem to lead to more accurate results than alpha-particle assay. Further details of the results of the international intercomparison are to be found in the Appendix.

For the TCAP method, however, the areal density, rather than the total mass, is the important quantity. In this case, the alpha-counting technique using at least two apertures seems to be favourable.

Turning to the neutron counting aspect of a typical experiment, it appears that the most accurate method currently in use is the TCAP method. Problem areas which could lead to systematic errors are:

(i) inscattering through large angles of the associated particle. Estimations for the worst case of the 2.6 MeV TCAP measurements on a neutron generator suggest that this effect could lead to an error ∿0.5%.

(ii) the shape of the neutron cone corresponding to the associated particle acceptance. Scattering effects need to be carefully calculated and verified by direct measurement.

(iii) pile-up and count loss corrections. As high counting rates are employed, very careful attention needs to be paid to these effects if undetermined systematic errors are to be avoided.

(iv) high sample uniformity. Sample non-uniformity has to be carefully measured and taken into account.

The meeting also discussed the errors arising out of attempting to produce accurate cross-sections up to high energy by successive normalisations of essentially independent measurements, beginning at thermal energy. It was concluded that this is very unlikely to lead to accurate values due to the fact that the statistical uncertainty at each normalisation region becomes a systematic error in the succeeding values and these errors add up to produce large uncertainties at high energy.

It must also be remembered that problems may arise in the application of a standard. For example, the measurement of the response of a detector using the TCAP method is largely unaffected by scattered neutrons. However, if this detector is then used in a different experimental set-up, corrections for scattering may be required.

5. WHAT CAN BE DONE TO REDUCE THE UNCERTAINTIES IN MEASUREMENTS?

There is no doubt that the problems identified in the previous section must be solved if we are to reach the 1% goal which seems desirable. Currently, new measurements are in progress or planned in a number of laboratories, in particular at the National Bureau of Standards, Argonne National Laboratory, Khlopin Radium Institute and at the Technical University of Dresden. The following suggestions for methods, either currently in use or to be used, were put forward.

The inefficiency of fission chambers may be investigated by one or more of several possible techniques. For example, neutron fragment coincidence/anticoincidence measurements may be useful in determining missing events and hence shed light on the problem of extrapolating the fission fragment pulse height spectrum to zero pulse height, as well as on the absorption problem. Another method, the angular distribution approach described in a contribution from Budtz-Jørgensen, may prove to be a very powerful tool for these purposes. Yet another approach may be the use of U-235/Cf-252 mixed source counting techniques.

The loss of fission fragments may also be determined by the application of thermal beams to low geometry fission counting with varying foil thicknesses, coupled with alpha-particle assay. Another method is to compare 2π fission counting with low geometry counting, again using thermal fields.

There is a general need to investigate these problems and all possible sources of systematic error. It was suggested that this should be done through more international intercomparisons. Already such an intercomparison of fissile foil mass assay is in progress and a second round of intercomparisons of flux determinations has been started. This can only lead to improved methods and one suggestion for a possible new intercomparison would involve an exchange of fission chambers.

In the case of shape measurements done with white neutron spectra, the main points which require further investigation are the determination of the neutron energy scale at high energies and the backgrounds associated with the fission counting and flux measurements. The energy scale of experiments in which the flux is measured by detecting recoil protons in a silicon detector can be affected by a considerable time walk in the discriminator from which the timing is derived. The time walk may not be the same as that measured using an alpha-particle source (or a pulser) and simulating protons by altering the pulse height using an amplifier.

Background determination at high neutron energies (i.e. energies above the region where notch filters can be used) in time-of-flight measurements on white neutron sources has long been a problem. The methods used are sometimes rather indirect and of a "hand-waving" variety and more attention needs to be paid to this aspect.

Experiments on linear accelerators have to cope with the intense gamma-flash which precedes the arrival of the neutron burst and as a result they have to recover from the effect of the gamma-ray burst in sufficient time to record neutron reactions with full efficiency. In a typical case of a 50m flight path, this means recovering in less than 1μs. It is essential for measurers to show that their equipment has properly recovered during the full duration of their counting period.

During the course of the meeting, it became apparent that there were significant differences in the fission fragment ranges adopted by different groups in making calculations of corrections. There appears to be no single compilation of this type of data and such a publication should be encouraged. Following that, an evaluation should be performed so that consistent values can be used by all groups and to identify where any further work is required. However, it has to be realised that ranges obtained elsewhere may not solve the problems for a particular measurer, as the chemical composition of the foil may not be well known and surface effects as well as impurities may cause errors.

6. RECOMMENDATIONS

The need for full documentation of measurements was stressed; this is vital if evaluators are to be able to make proper assessments of data. If sufficient detail cannot be given in a journal, because of space restrictions, then it is recommended that more detailed laboratory reports should be issued.

It was agreed that there is essentially no value in producing more measurements of the fast fission cross-section of U-235 with accuracies in the range 2-3% or worse using established techniques. As we already have a number of such measurements, additional ones will contribute little towards the reduction of the uncertainties. However, this should not be interpreted as an attempt to stifle new and innovative techniques. On the contrary, new methods, which may provide independent determinations, are to be encouraged even if they produce accuracies in the 2-3% range.

It is clear that if higher accuracies are to be achieved, one must pay particular attention to understanding the properties of the fission and flux detectors and to the corrections which are applied (e.g. loss of fragments in fission detectors).

The only foreseeable way of improving the accuracy of the cross-section is to perform

(a) accurate mono-energetic measurements (using the TCAP method at as many energies as possible) with the focus on discrepant regions, but also paying attention to lower neutron energies where the applied needs are greatest.

(b) accurate shape measurements which can be used to determine the cross-section between the spot point data.

These recommendations are certainly not novel but that can hardly be surprising. However, that does not make them any less valid. There can be no substitute for very careful, detailed and thorough investigations of all possible sources of systematic errors, using a variety of techniques. Science is founded on questioning and this approach must be applied vigorously and nothing must be taken for granted. Given a concerted effort, the problems can be solved and the U-235 fission cross-section can be determined to an accuracy of ±1% using existing experimental techniques.

APPENDIX

Results of Sample Comparison (W.P. Poenitz, Argonne National Laboratory, USA)

Absolute alpha-decay rates and relative fission ratios were determined for 15 samples from ANL, LANL, NBS, KRI, BRC, Harwell, and CBNM in measurements at ANL. Comparisons for the alpha-decay rates can be made for those samples for which such values have been stated or can be inferred from stated masses based on alpha counting:

Sample	Quoted, αps	ANL, αps	Δ, %
NBS	50.89±0.25	50.97±0.13	~0.1
KRI VI	62.6 ±2.0	62.94±0.2	~0.5
KRI XV	74.4 ±2.2	73.97±0.2	~0.6
HAR A	911.2±4.6*	914.1±3.2	~0.3
HAR B	915.6±4.6*	914.9±3.2	~0.1
CBNM 33	476.3±4.1	476.7±1.2	~0.1
CBNM 36	976.9±8.3	977.3±2.5	~0.1

* subject to revision

The comparison of sample masses, which includes questions of fission fragment absorption, is shown here only for some selected samples. The quoted values are shown as well as those derived from the ratio determinations and quoted masses:

Sample	Quoted, μg	Av. Ratios x Quoted, μg	Δ, %
ANL 5-2	834.6±2.7	833.5±3.3	~0.13
LANL S1	298.7±0.3	298.4±1.2	~0.10
NBS	228.5±1.2	228.4±0.9	~0.04
KRI	758±25 757.9±7.6	760.6±3.0	~0.34 ~0.36
CBNM 36	250.0±0.4	250.9±1.0	~0.36
HAR A	343.4±2.7*	346.5±1.4	~0.90

* subject to clarification of the specific activity

IAEA Consultants' Meeting on The Californium-252 Fission-Neutron Spectrum

Smolenice, near Bratislava, Czechoslovakia
28 March - 1 April 1983

Chairmen: H. Klein, PTB Braunschweig
M.V. Blinov, RI Leningrad

CONCLUSIONS AND RECOMMENDATIONS

Summary

Since the last review of Blinov [1] improvement in the knowledge of the neutron energy spectrum from the spontaneous fission of ^{252}Cf is remarkable in several aspects:

- the energy range, where the neutron spectrum has recently been measured, was extended to the limits 1keV and 28MeV. Various detectors in overlapping energy ranges were used, and the analysis and correction of the data was refined;

- spectrum averaged cross sections, measured in the Cf-field, and interpreted with improved cross section evaluations confirmed the spectral shape in the energy range from 1MeV to 18MeV;

- the theoretical understanding was improved by two different approximations of the evaporation model and by Hauser-Feshbach calculations.

Consequently the data from the independent sources, i.e. differential data, integral data and theoretical approaches, appear now to be in rather good agreement, while partially disagreeing with earlier data. For this reason a new evaluation is strongly recommended.

In addition to this improved description of the spectral shape guidelines are required for the different applications of Cf-sources as a reference in order to avoid systemtic errors.

1. Status of the TOF-experiments

The progress of various time-of-flight experiments, covering the neutron energy range from 1keV to 28MeV, was reported. The final analysis of all experiments is expected for the end of 1983. The experimentalists are recommended, to present their energy spectra as tabulated point data together with the quantitative listing of all corrections (i.e. background subtraction and renormalization of tof-spectra, ff-detection efficiency, in-/out-scattering by constructive materials) and uncertainties (i.e. statistics, n-detection efficiency, corrections). Graphical presentations should be given relative to a Maxwellian distribution with an energy parameter T=1.42 MeV. The NBS segment fit or theoretical approximations may be included in the graph for comparison. Final data will be available for an evaluation either directly from the authors and/or via the NDS of the IAEA.

1.1. Experimental details

Blinov [paper 1, compare ref. 3] presented recent measurements performed with an ^{235}U fission chamber in the energy range from 10keV to 10MeV. Final data are available, but corrections and uncertainties have to be documented and the covariance matrix to be prepared.

Additional data in the energy range 25keV up to 1.2MeV, performed with Li-glass scintillators, are available from Lajtai [paper 3]. This data set agrees well with Blinov's spectrum in this energy region.

The measurements with a black neutron detector in the energy range from 250keV upto 10MeV [paper 2], first presented by Poenitz at the Antwerp conference [4], were revised, but with a noticeable change at highest energies only. The final analysis will be finished before the end of 1983.

The data set in the energy range of 2-14MeV [5] will be supplemented as discussed by Chalupka and Klein [papers 4 and 5]. Final data will be available before the end of 1983.

The high energy data (11-28MeV) [6] are still valid. Märten [paper 6] will make available additional informations on the corrections and uncertainties.

1.2. Summary of the results

The experimental data presented can be described in the energy region from 1keV to 6MeV by a Maxwellian distribution with T=1.42MeV. The deviations between the experimental data and the Maxwellian do not exceed limits of 10% (1-10keV) and 5% (10keV-6MeV). In the upper energy region (6MeV-20MeV) the NBS segment fit [7] is in better agreement with the measurements.

2. Status of integral measurements

Spectrum averaged cross section measurements with threshold reactions sensitive in the range 1MeV to 18MeV were performed by Mannhart [paper 8, ref. 8] with uncertainties of 2-3%, and by Dezsö [paper 9]. After replacing the ENDF/B-V cross sections for some of the threshold reactions investigated by recently evaluated data sets the calculated and measured averaged cross sections are in good agreement if the NBS description is used for the neutron energy spectrum. The covariance matrix for the Cf spectrum deduced from these integral measurements will be available by spring 1984.

Note: The following ENDF/B-V data sets were replaced: Al-27(n,α) by Vonach's evaluation; Ti-47(n,p) by preliminary data of a ANL/PTB cooperation; Ni-58(n,2n) and Cu-63(n,) by Winkler's evaluations.

Additional integral data are expected from Dezsö until July 83 and should be included in this analysis.

3. Theoretical approaches

Besides the latest approach of Madland-Nix, presented at the Antwerp Conference [9], new calculations on the basis of the cascade evaporation model were discussed by Märten [paper 7]. The energy spectrum $n(E_n)$ as well as double differential data $n(P_f; E_n)$ for various fission-fragment parameter sets P_f can be predicted.

Similar calculations on the basis of the Hauser-Feshbach formalism were performed by Rubchenya and compared with double differential data of Blinov [paper 1]. The calculation of the neutron energy spectrum will be completed by the end of 1983.

Presently the theoretical approaches cannot describe the energy spectrum in the entire energy range. To improve these models, additional double differential experiments are recommended in order to determine various parameters of these approaches and to investigate the mechanism of the fission neutron emission (i.e. the fraction of cission neutrons, emission during fragment-acceleration, etc).

4. Evaluation

As soon as the recent experimental data are finally analysed <u>a new evaluation of the Cf neutron energy spectrum is strongly recommended</u>.

The experimental data show that <u>the energy distribution cannot be described by a simple parametrization</u>. For this reason an accurate description may be possible by a pointwise tabulation only.

It has to be investigated, if earlier measurements are sufficiently documented to be included in this evaluation.

Additional <u>experiments presently being performed should be timed for spring 84</u>.

5. Interim solution

Until the time, the evaluation becomes available, the following descriptions should be used:

(a) the NBS segment fit is a satisfactory representation in the energy range from 1MeV to 20MeV. For lower energies, significant deviations are to be expected;

(b) a Maxwellian distribution with T=1.42MeV is suitable for 1KeV upto 6MeV. It is to be expected that the evaluated distribution may deviate within limits of not more than 5% [10% for 1keV to 10keV] from this representation.

6. Applications

The discussion of various experimental difficulties demonstrated that the application of the Cf spectrum as a reference, i.e. calibration of tof-spectrometers or induced fission cross section measurements, should be supported by guidelines to consider the influence of the actual experimental parameters, in particular the properties of the fragment-detectors (efficiency, time interval statistics, etc).

References

[1] M.V. BLINOV: Neutron Energy Spectra of Spontaneous Fission Sources (Review). IAEA Consultants' Meeting on Neutron Source Properties, Debrecen Hungary, 17-21 March 1980. Proceedings edited by K. Okamoto, INDC(NDS)-114 (June 1980). Page 79

[2] International Conference on Nuclear Data for Science and Technology, Antwerp 6-10 Sept. 1982. Proceedings edited by K.H. Böckhoff, Reidel Publishing Company 1983

[3] M.V. BLINOV, G.S. BOYKOV, V.A. VITENKO: New experimental data on the energy spectrum of Cf-252 spontaneous fission prompt neutrons. Antwerp Conference [2] page 479

[4] W.P. POENITZ, T. TAMURA: Investigation of the prompt neutron spectrum for spontaneously-fissioning Cf-252. Antwerp Conference [2] page 465

[5] R. BÖTTGER, H. KLEIN, A. CHALUPKA, B. STROHMAIER: The neutron energy spectrum from the spontaneous fission of Cf-252 in the energy range 2 MeV - 14 MeV. Antwerp Conference [2] page 484

[6] H. MÄRTEN, D. SEELIGER, B. STOBINSKI: The high-energetic part of the neutron spectrum from spontaneous fission of Cf-252. Antwerp Conference [2] page 488

[7] NBS Cf-252 spectrum, available on magnetic tape, e.g. from the IAEA Nuclear Data Section.

[8] W. MANNHART: Measurement and evaluation of integral data in the Cf-252 neutron field. Antwerp Conference [2] page 429.

[9] D.G. MADLAND, J.R. NIX: Calculation of the prompt neutron spectrum and average prompt neutron multiplicity for the spontaneous fission of Cf-252. Antwerp Conference [2] page 473

U-235-Sample-Mass Determinations and Intercomparisons*

by

W. P. Poenitz and J. W. Meadows

Argonne National Laboratory

Argonne,Ill., U.S.A.

* This work has been supported by the US Department of Energy

I. *Introduction*

The neutron-induced fission cross section of U-235 is not only one of the most frequently used references but is also of direct importance in reactor applications. As a consequence, knowledge of this cross section is required with ~1% uncertainty as reflected in corresponding entries in request lists (1,2), which have persisted since the last 10-15 years Measurements to that level of accuracy require the investigation of the contributing components, one of which is the fission mass. The latter is most often determined by others than the experimenter who measures the differential cross sections or integral reaction-rate ratios in a reactor test facility. The isotopic composition and the sample mass are usually obtained from associated chemistry departments or standard laboratories, however, the experimentor has still the responsibility to assure that the values he uses are adequately described by the quoted uncertainties. This can be achieved by comparing samples from different origins. It was in this spirit that an intercomparison of fission samples obtained from different US laboratories, which were involved in cross section measurements, was carried out in 1979 (3). The notable outcome of this effort was that a bias of~0 7% was found between the standard laboratory and other contributing laboratories (which was, however, within the stated uncertainty). The National Bureau of Standards (NBS) has since then worked on a redefinition of the mass asignments of its reference samples, has revised its mass scale by 0.8%, and has reduced its uncertainty by a factor of two (to about ± 0.5%). However, this new mass scale includes values relative to others. In the present work these have been removed in order to compare mass scales as independent from one another as possible. Independence already appears hard to come by. For example, the Los Alamos National Laboratory (LANL) sample mass specifications are mainly determined by the highest-weight entries which are for the isotopic composition from NBS, and for the specific activity (determined by isotopic dilution) from the Central Bureau for Nuclear Measurements (CBNM). The same material, INS-1, is apparently used by LANL and NBS, and samples obtained from the Centre D'Etudes de Bruyeres le Chatel (BRC) and CBNM for the present work were made with the same material originating from NBS.

One of the interesting developements in recent times in the area of precision measurements has been the 14-MeV-neutron fission cross sections of U-235. The praise has surely to go to Cance and Grenier (4) who first observed and reported values which were substantially lower than the data accepted at that time. These new values were subsequently confirmed by Arlt et al. (5) and later by others (6-10).

The 14-MeV values are not of great interest in applied areas at the present time, however, they have substantial importance because of their impact on the normalization of the evaluated U-235 cross section, as will be discussed in Section V. The very precise 14-MeV values affect the evaluated cross sections at much lower neutron energies and as some inconsistencies appear to emerge it was considered interesting to assure that these inconsistencies are not due to discrepant mass scales used in the various experiments. Consequently, the present authors inquired at the 1979 Knoxville conference whether one or two of the samples which were used at the Khlopin Radium Institute in Leningrad (KRI) and at the Technical University of Dresden (TUD) for 14-MeV measurements could be made available for an intercomparison. This sample transfer was subsequently arranged by the International Atomic Energy Agency (IAEA) and the present report describes the comparison which was made at Argonne National Laboratory (ANL).

In order to improve on the validity of possible conclusions, the authors had also asked BRC, the AERE Harwell, and CBNM for contributions to this intercomparison. Samples were obtained from these laboratories and included in the present measurements. All samples are described in Section II.

The measurements consisted of two parts. The first part was the determination of the alpha-decay rates of the samples and the derivation of the absolute sample masses from these data. This is described in Section III. The second part was a set of relative fission-rate measurements and is described in Section IV. Updated data from the 1979 measurements are included in Sections III and IV.

The intercomparison of all the mass scales could only be made after all the reference values became available. This exchange of data took place at the present meeting. The results of the intercomparison are discussed in Section V.

II. Sample Descriptions

Six different fissile materials were involved in the 1979 and 1982/83 intercomparisons discussed here. The isotopic compositions and data on the specific activities which were made available or derived in the present work are given in Table I. Values given for the specific activities based upon the isotopic compositions (IC) and half-lives were derived with the reported IC's and the half-lives given in Table 2. The laboratories which contributed the samples may have used different half-lives. The half-lives given in Table II were mainly from the recent evaluation by Holden (11), however, for the so important U-234, his downweigthing of the latest measurement by Geidel'man et al.(12) was not accepted, and the value obtained by Meadows (13) was not used. This, however, changed the result only from 2.455 to 2.456 · 10^5 ys. The reason for leaving out the value reported by Meadows is that it was concluded that the material M-TH (which figured prominently in the T determination by Meadows) was too uncertain to be used further as a reference. It was excluded in the present work and all data measured with the corresponding sample SST5 were made relative to the first ANL mass scale U5-S-U4.

The isotopic compositions given in Table 1 are as reported, or averages were several values were available. The IC values for the KRI material are as given by KRI. A value for the U-234 content derived from present alpha spectroscopy is in good agreement with the coresponding value from KRI. A material which appears rather similar has been defined in Ref. 10. The coresponding values for the isotopic composition are given in Table 1 in brackets. These values lead to a specific activity which differs by 0.2% from our determination.

The physical descriptions of the samples are sumarized in Table 3. Knowledge of the chemical compound and approximate thickness of the fissile deposit is required for the calculation of corrections for the total fission-fragment absorption. Knowledge of the diameter of the fissile deposit and the material, diameter and thickness of the backing is required for the calculation of the corrections for transmission and scattering effects. The values for the thickness of the deposits given in Table 3 (in $\mu g/cm^2$) are approximate values used for the calculation of the fission-fragment absorption. Most sample backings were plain discs, exceptions were the BRC and the KRI samples. The BRC sample backing was a 0.05-cm thick Ta disc with the thickness under the fissile deposit reduced to 0.03cm. The information on the KRI samples given in Table 3 is from Ref. 5, and as obtained during the present meeting. The Cr-Ni ratio and the density of the backing material is unknown. A 50-50% ratio and a density of 7.9g/cm was assumed. The KRI samples were (apparently by soldering) mounted in carrier rings as indicated in Fig. 1. The additional amount of solder was unknown and has been neglected. The material of the moumting ring is brass. The mounting procedure had apparently positioned the samples slightly and unevenly above and below the top surface of the mounting ring, which was important for determining the alpha-counting-geometry factors.

III. Alpha Counting

The alpha-decay rates of all samples were determined with a low-geometry surface-barrier detector. Samples obtained for the present intercomparison were counted before and after the fission ratio experiments. The ANL samples have been counted repeatedly during the last 10 years. Samples with low decay rates (NBS, KRI, ANL-R5,N3, LANL-S1) and the samples from CBNM were counted with a geometry factor of ~1/220. Other samples were also counted with a geometry factor of ~1/1000 (ANL-5-1, 5-2, SST5, LANL-S3, and BRC). Some of the samples were counted in addition in a second low-geometry counter of similar design with a somewhat different aperture and geometry factor (LANL-S3, ANL-R5,5-2,SST5, AERE-B, KRI-VI). Geometry factors were determined with Monte-Carlo simulations and with a series-expansion approximation. Backgrounds of typically less than 0.3% was subtracted. Decay rates from 1979 were slightly revised for a redetermination of the counter geometry.

The accuracy of the present LG alpha counting has been tested: a) the comparison with the second LG counter shows agreement within 0.1%, b) this second LG counter has been compared with another LG counter at ANL-Idaho (agreement within 0.1%), and c) various uranium, plutonium and neptunium sample counts on different shelves have been compared (1st. shelf/2nd. +0.04%, 2nd./3rd. -0.05%, 1st./3rd. -.16%, and 1st./5th. -0.07%).

Representative alpha spectra obtained with the low-geometry counter are shown in Figs. 2 and 3. The spectra obtained for the KRI samples were used to obtain the contribution from the U-234 decay. A fraction of 3.1±0.1% of the total count rate was found. The AERE samples show an 0.8% count-rate contribution from impurities with energies above the U-234-decay alpha energy for one sample and 1.1% for the other. Decay assignments of these impurities indicate the Th-228 decay chain. It is unknown whether additional contributions from impurities are in the U-235 - U-236 - U-234 alpha-energy range.

The ANL samples were also counted with a 2π counter for which the calibration factors were known for different thicknesses of uranium on SS backings as determined with the second LG counter. Samples of the same material and on identical backings were also counted with this 2π counter in order to determine the ratios with negligible statistical uncertainties.

The results from the present alpha counting and their total uncertainties are given in Table 4. Statistical uncertainties were 0.2% or less. The systematic uncertainties are determined by the "known" uncertainties of the geometry factor (aperture and sample-deposit diameters, sample to aperture distance) and unknown components: 1) nonuniform area densities, which are probably negligible for all but the electroplated samples, 2) sample-backing warping which affects the sample-to-aperture distance, and 3) alpha impurities within the U-235 - U-236 - U-234 alpha-energy range. Some corrections were applied for sample warping based on measurements with a microscope (BRC, NBS, KRI) and estimates have been made on these uncertainties and included in the given systematic uncertainties.

The present values for the ANL samples are identical with the quoted values as they include previous counts. The only other direct alpha-decay rates reported so far are those by AERE and KRI. The average difference of between the present values and the AERE decay rates is o.2%. The values given in Table 4 for the NBS samples were derived from the value quoted by NBS for the alpha-decay rate of its standard-reference sample and relative measurements by NBS between its reference and the sample NBS 25-S-5-2 used in the present experiments. These ratios were obtained by alpha counting (1X) and by fission counting (2X). Our value agrees with NBS within 0.1%. The values quoted for CBNM were derived from the given masses based on alpha counting and the slightly different $T_{1/2}$ used. Agreement between the present counts and those from CBNM is within 0.06%.

The values for the absolute uranium masses given in Table 4 are based on the present alpha-decay rates and the specific activities given in Table 1. Also listed in Table 4 are the values quoted by the owners of the samples. The agreement between the values from ANL and LANL is within 0.13% implying agreement between the alpha counting at both laboratories within that uncertainty. The LANL values were recently revised by a minor amount (<0.1%). Agreement with NBS is very good after the aforementioned revision of the NBS mass scale by 0.8%. The value given in the Table for NBS is as quoted, thus includes measurements relative to LANL samples. The bias of 0.3% between the present values and those quoted by CBNM is due to the high weight of the values based on isotopic dilution. Agreement with the values based on alpha counting is within 0.14%, the difference being mainly due to the different U-234 half-life values used. The value quoted by BRC is based on the U-234 half life of 2.446 10^5 ys., thus 0.4% of the difference with the present value can be understood with the different half-life values.

VI. Fission Ratio Measurements

It should be clear from the outset that in comparing sample masses of different materials and with different backings by fission-rate ratio measurements, one compares a variety of other features of fission counting besides sample masses. The measured fission rates are proportional to the sample masses, but also to the counting efficiency, e. g. the total fission-fragment absorption is involved.

The present fission-ratio measurements were carried out in a back-to-back ionization chamber (14). Measurements were made at 600 ± 100-keV-neutron energy utilizing the Li(p,n)-source reaction and a pulsed and bunched proton beam. The samples were located at a distance of 5 cm from the neutron source. A random-pulser signal which was time correlated with the accelerator pulse was split on an odd-even basis and added to the two preamplifiers. These events were found to be processed by the on-line computer and associated electronics with a better than 0.1% parity. Identifying tags (pulser, detectors 1 and 2) were used to store 8 time-of-flight spectra (TOF) in the computer. Inspection of these TOF spectra showed some random-coincidence events ($\sim$0.2%), which did, however, not affect the ratio results. Different choices of background ranges in the TOF spectra did not affect the result either. Various test measurements (interchange of detector electronics, measurements at different distances from the target, interchange of detectors, proof of reproducibility) were described in the previous report (3).

Measurements were carried out for each of the ratios in two steps: once with one sample facing the target, then with the other sample facing the target. These two sets were obtained with approximately the same statistical uncertainties of typically 0.3%.

Corrections were applied for:

1. Sample distance from the target.

The two samples were separated by the sum of their backing thicknesses, and, in some cases, by an additional 0.0127-cm-thick center mounting plate. The required corrections were typically 2-3%, but substantially larger where the KRI samples were involved (8-10%) However, by averaging the results from the measurements for the two directions of the fission chamber, the uncertainty for this correction becomes negligible.

2. Transmission losses and scattering gains.

Corrections were applied for the transmission losses which occur for the sample facing away from the target by area-weighting the losses through the contributing structural components. Scattering gains for both samples were computed for the various scattering components with the Monte-Carlo technique, taking into account the angular distributions of the elastically scattered neutrons and inelastic processes. The combined effect of transmission losses and scattering gains on the measured ratios was typically less than 1%. Averaging the measurements for the two directions of the fission chamber results in an effective correction factor of 1.0 for a completely symmetrical arrangement of identical samples. The "residual" correction for transmission and scattering effects for the more common case of asymmetrical samples was typically 0.0-0.3% and largest for measurements between the ANL 5-2, SST-5 and the KRI samples (0.5%), because the large diameter ANL sample deposits overlap the brass mounting rings of the KRI samples. The uncertainty of the corrections for transmission and scattering was assumed to be 50% of the residual corrections.

3. Detection losses below the electronic threshold.

The threshold for the detection of fission events was set close to the alpha (pile-up) pulses in the pulse-height spectrum. The fission-pulse losses below this threshold were determined based upon a linear extrapolation from the pulses above the threshold to zero-pulse height. Though this is probably a good approximation, it is not quite correct as Monte-Carlo calculations for thicker samples show a non-linear shape (15). However, the possible error should be substantially reduced in a ratio measurement and should be negligible if both samples have similar thicknesses.

4. Fission events from isotopes other than U-235.

The present measurements were interpreted to yield total uranium-mass ratios. The primary neutron energy was choosen to result in only small contributions from fission in isotopes other than U-235. Thus, the correction depends mainly on the U-235-wt fractions of the materials involved and results in a negligible contribution to the uncertainty of the result

5. *Angular distribution of the source neutrons.*

A correction was applied for the measurements of ratios between samples of different diameters. The evaluation by Liskin et al. (16) was used for the anisotropy of the $^{7}Li(p,n)$ reaction. This correction was most frequently 1.5% but 3.7% for ratios between samples with the smallest and largest deposit diameters.

6. Total fission-fragment absorption.

This correction is surely the most important as it is the most uncertain. The present procedure of measuring the ratio with the two directions of the fission chamber averages over the effect of the neutron momentum. The effect of the angular distribution of the fission fragments is small. The major remaining effect is determined by the range of the fission fragments, *R*, in a specific deposit material. Experimental values of R were known for some of the sample materials (ANL 5-2, 5-1, SST5, NBS). Values can also be calculated if the chemical composition is known (e. g. r = 6.6 mg U/cm for UO_2, 4.7 for UF_4, 5.9 for U_3O_8). However, the material of the KRI samples was unknown by the present authors until the present meeting took place Thus the following consideration was made: the average energy loss of the 4.397-MeV alpha which occurs with 57% probability in the decay of U-235 should indicate to some extent the energy loss of charged particles in an unknown material. The energy loss of these alphas, determined from the energe spread (detector resolution subtracted), in the low-geometry alpha spectra is proportional to the sample thickness, δ, (for thin samples), thus:

$$\Delta E_{\alpha} \sim \delta$$

The fission-fragment range would be expected to be in some form inversely related to the alpha energy loss, therefore

$$\Delta E_{\alpha} \cdot R \sim \delta$$

was considered, searching for an empirical relationship with the help of the many other samples for which the range was known. Fig. 13 shows that the relationship appears to be linear and clearly indicates that the assumption of a range of 7.5 mg U/cm for the KRI samples was wrong. The fission fragment absorption losses of the KRI samples were finally determined based on the FF ranges which follow from the straight line in Fig. 3. This may not have been the best choice, the dashed line in Fig. 3 represents the majority of the data better and the consequent failure to explain the heaviest sample S3 could be accepted based on the energy dependence of dE_{α}/ds.

The fission fragment-range alone is not what determines the total absorption. The structure or smoothness of the backing affects in addition the total absorption to be accounted for. Consideration of the geometry of the ionizatiion chamber leads to the understanding of the observed pulse-height spectrum: the sharp drop from the maximum in the pulse-height spectrum toward lower pulse heights comes from a "geometrical" cut-off of the FF due to the collector plate. Smaller pulses are from FF's emitted with angles close to 90°, thus losing most of their energy. Because total FF losses are caused by those emitted extremely close to 90°, one would expect that the number of pulses below the geometric cut-off are in first order proportional to the total FF losses -- for a perfect backing. However, an imperfect backing would cause additional pulses in the low energy part of the spectrum and additional FF losses not explained by the FF range of the material. This would be specifically expected for thinner samples. The ratio between the fraction of pulses below the geometrical cut-off and the fraction of total FF losses calculated with the ranges for the various materials is shown in Fig. 4. Some features are as expected, for example, the KRI samples appear to have the best polished backing (based on qualitative inspection under a microscope) and the ratio in Fig. 4 is consequently low. The backings of the ANL samples SST5 and 5-2 had not been polished but appear to be smooth, though a few larger scratches can be observed. The backing of the sample R5 has been polished, but polishing marks are visible, thus it is not surprising to find a high ratio as it is a very thin sample. In most other cases, however, the rato does not clearly correspond to the merely qualitative nature of the microscope observation and the figure seems to be inconclusive as to required additional corrections. No further action was taken, but measurements are planned for the ANL samples in which the 2π-ionization-chamber count rates will be compared with LG-FF counting.

V. Results and Discussion

Fifteen samples were involved in the present intercomparison, thus measurements of 14 ratios would be sufficient to obtain the ratio between any two sample masses. A sensible 105 ratios could be measured between the 15 samples, however, one of the ratio measurements took about an average of 6 hours and a total of 28 ratios was measured. This overdetermines the number of unknowns by a factor of 2 A consistent set of 14 unknowns can be derived with least-squares adjustments

$$\delta = (A^T C^{-1} A)^{-1} A^T C^{-1} M$$

where A is the coefficient matrix, and C is the variance-covariance matrix of the measurement vector M. This has been simlified with C - I, the identity matrix, thus neglecting the correlations:

$$\delta = (A^T A)^{-1} A^T M.$$

The corresponding results are given in Table 6. Measured values are identified by the % difference between the measured and the consistent value. Besides the 28 fission ratio measurements (round brackets) additional 10 ratios derived from the alpha counting were included in the consistency fit (winged brackets). The latter were confined to ratios between samples of the same material with the exception of two ratios where materials were involved for which the isotopic composition was exceptionally well known.

The uncertainties of the input data were typically 0.3-0.5%. The uncertainties of the results from the present measurements given in Table 6 are typically 0.2-0.3%. The results from the present ratio measurements can be used to determine absolute sample masses either based upon the values derived from the present alpha counting or with masses quoted by the owners of the samples. Both types of data are given for each sample in the Appendix.

Comparison of all four values which can be obtained for the mass of each sample from.

1) The mass quoted by the owners of the sample,
2) The mass determined from the present alpha counting,
3) The mass determined from the present ratio measurements relative to all other sample masses and the masses determined by the present alpha counting
4) The mass determined as under 3), but using the masses quoted by the owners of the samples,

are typically within a range of ±0.3% or better, thus indicate a better knowledge of the sample masses than the quoted uncertainties. Knowledge of the U-235 sample mass in a cross section measurement or reaction-rate-ratio measurement in a reactor within 0.3% is considered sufficient.

One of the conclusions of the 1979 intercomparison was that the U-234 half life may be the source of some of the inconsistencies noted at that time. Very accurate values were available for the isotopic compositions of two of the fissile materials involved in the present intercomparison (AERE, CBNM). The ANL, LANL, NBS, and CBNM mass scales are mainly determined by independent isotopic dilution measurements (though the isotopic dilution measurement for the LANL samples was done at CBNM, this was quite some time ago). Thus, the half life of U-234 can be determined from the present alpha decay rates for the AERE and CBNM samples and their masses based on the ratio measurements and the quoted masses for the ANL, LANL, and NBS samples. The value is

$$T_{1/2}(\text{U-234}) = (2\ 460+0.005)\cdot 10^5 \text{ yrs.}$$

which is in very good agreement with the latest measurement by Geidel'man et al. (12):

$$T_{1/2}(\text{U-234}) = (2.459+\ 0.007)\cdot 10^5 \text{ yrs.}$$

It is concluded from the present investigations, that U-235 sample masses are well enough known for future measurements and have not been a source of errors in recent high accuracy measurements. However, corrections for total ff absorption may have been too low. The U-234 half life is now known with sufficient accuracy to determine sample masses of spiked U-235 material to within 0.3%.

After recieving final values for the AERE samples, a final report will be distributed to the contributing laboratories. This report will contain uncertainty specifications.

References

1. "Compilation of Requests for Nuclear Data", compiled and edited by the National Nuclear Data Center for the Department of Energy Nuclear Data Committee, DOE/NDC-22U (1981).

2. "World Request List for Nuclear Data", N. DayDay, Editor, WRENDA 81/82, International Atomic Energy Agency, INDC (SEC)-78/URSF (1981).

3. W. P. Poenitz, J. W. Meadows, and R. J. Armani, "U-235 Fission Mass and Counting Comparison and Standardization", Argonne National Laboratory Report ANL/NDM-48 (1979).

4. M. Cance and G. Grenier, Nucl. Sci. Eng. 68, 197 (1978).

5. R. Arlt et al., Kernenergie 24, 48 (1979).

6. I. D. Alkhazov et al., Atom. Energ. 47, 416 (1979).

7. O. A. Wasson, A. D. Carlson and K. C. Duvall, Nucl. Sci. Eng. 80, 282 (1982).

8. M. Mahdavi, G. F. Knoll, and J. C. Robertson, "Measurements of the 14 MeV Fission Cross Sections for U-235 and Pu-239", Proc. Conf. on Nuclear Data for Technology, Antwerp (1982), to be published.

9. LiLingwen et al., Proc. Conf. on Nuclear Data for Technology, Antwerp (1982), to be published.

10. M. Varnagy, S. Juhasz, and J. Csikai, Proc. Conf. on Neutron Physics, Vol. 3, 13, Kiev (1980).

11. N. E. Holden, "The Uranium Half-lives: A Critical Review", Brookhaven National Laboratory Report BNL-NC5-51320 (1981).

12. A M. Geidel'man et al., Izv. Aead. Nauk. SSSR, Ser. Fiz. 44, 927 (1980).

13. J. W. Meadows, "The alpha half-life of U-234", Argonne National Laboratory Report ANL-7610, 44 (1970).

14. J. W. Meadows, Nucl. Sci. Eng. 68, 360 (1978).

15. K. Kari, Nuclear Research Center Karlsruhe Report, KFK 2673 (1977).

16. H. Liskien and A. Paulsen, "An Evaluation for Cross Sections of the Reaction ^{7}Li(p,n)", EANDC(E) - 159 "L" (1973).

Table 1. Isotopic Compositions and Specific Activities

Material	Isotopic Compositions/wt%				Specific Activities/αpmpμg				
	U-234	U-235	U-236	U-238	Isotopic Dilution	Isot. Comp. Half-L. (b)	Colorim.	Others	Average (c)
LANL (a) INS-1	0.0607	99.7457	0.0655	0.1277	13.338 ± .024	13.26 ± .13	-----	13.30 ± .08	13.33 ± .02
NBS INS-1					13.412 ± .067	13.26 ± .13	-----	13.38 ± .16	13.38 ± .07
ANL U5-S-U4	1.027	98.397	0.450	0.125	146.24 ± .25	147.2 ± .7	146.1 ± .9		146.3 ± .3
ANL M-Th	0.852	93.244	0.334	5.570		122.6 (e) ± .7	124.1 (e) ± .7		
KRI U5-P	0.00111 0.00111 (d) (0.0010	99.9972 99.9955	0.0017 0.0035)(f)			4.954 ±.015 (4.941)			
AERE U5-92	1.1104	92.409	0.315	6.165		158.3 ± .5			
CBNM/ BRC U5-97	1.6582	97.663	0.1497	0.5296		233.9 ± .7			

(a) Isotopic composition is an average of CBNM, NBS and LANL determinations.
(b) Present values.
(c) Uncertainty limited to lowest uncertainty of individual values.
(d) From present alpha spectroscopy.
(e) Values not used. Mass defined relative to ANL U5-S-U4.
(f) From Ref. 10. Wt% assumed. It is not sure that this is the same material.

Table 2. Constants used for the Present Specific-activity Determinations.

Isotope	Half-life, Y	Atomic weight, g/mol
U-234	$2.456 \cdot 10^{5}$	234.0409
U-235	$7.037 \cdot 10^{8}$	235.0439
U-236	$2.342 \cdot 10^{7}$	236.0456
U-238	$4.468 \cdot 10^{9}$	238.0507

1 mol = $0.60225 \cdot 10^{24}$
1 year = 365.25 days

Table 3. Sample Specifications.

	Fissile Sample Deposit					Backing		
Sample	Material	Compound	Dep. Techn.	Diam. cm	Approx. Thickness $\mu g/cm^2$	Material	Thickness cm	Diameter cm
ANL-R5	U5-S-U4	U_3O_8	EP	2.22	20.6	SS	0.0127	4.445
ANL-N3	U5-S-U4	U_3O_8	EP	1.27	41.1	SS	0.0254	1.905
ANL-5-1	U5-S-U4	$UO_2 \cdot H_2O$	EP	2.49	210.4	SS	0.0254	6.985
ANL-5-2	U5-S-U4	$UO_2 \cdot H_2O$	EP	2.50	164.2	SS	0.0254	6.985
ANL-SST5	U5-Th	UF_4	EV	2.54	81.2	SS	0.0254	6.985
LANL-S1	INS-1	U_3O_8	EV	2.00	95.1	Pt	0.0127	4.763
LANL-S3	INS-1	U_3O_8	EV	2.00	537.9	Pt	0.0127	4.763
NBS25-S-52	INS-1	UO_2	EV	1.27	182.0	Pt	0.0127	1.905
KRI VI	U5-P	U_3O_8	HFS	2.1	220.7	Cr-Ni	0.010+	2.100+
KRI XV	U5-P	U_3O_8	HFS	2.1	260.2	Cr-Ni	0.010+	2.100+
BRC	U5-NBS	U_3O_8	?	1.2945	85.8	Ta	0.03 (0.05)	2.771
AERE-A	U5-UK	U_3O_8	EV	2.0	110.4	SS	0.0394	2.699
AERE-B	U5-UK	U_3O_8	EV	2.0	110.6	SS	0.0394	2.699
CBMN-33	U5-NBS	UF_4	EV	1.27	96.0	SS	0.015	1.905
CBMN-36	U5-NBS	UF_4	EV	1.27	197.0	SS	0.015	1.905

EV = Evaporation, EP = Electroplating, HFS = High Frequency Sputtering,
SS = Stainless Steel
\+ = Additional Material due to the Brass Mounting Ring

Table 4. Results from the Present Alpha Counting.

	Alpha Decay Rate, αps		Sample Masses,	μg Uranium
Sample	Quoted	Present	Quoted	Present
ANL R5		194.1 ± 0.6		79.60 ± 0.29
ANL N3		127.2 ± 0.4		52.17 ± 0.19
ANL 5-1		2602 ± 6		1067 ± 4
ANL 5-2		2035 ± 5		834.6 ± 2.7
ANL SST5		847.8 ± 1.7		418.1 ± 1.6
LANL S1		66.52 ± 0.2	298.7 ± 0.3	299.4 ± 1.2
LANL S3		375.1 ± 1.1	1688.3 ± 3.0	1688.6 ± 5.7
NBS	50.66 ± .25 (a1) 51.00 ± .25 (a2)	50.97 ± .13	228.5 ± 1.2	228.6 ± 1.3
KRI VI	62.6 ± 2.0	62.94 ± 0.2 (b)	758 ± 25 757.9 ± 7.6 (e)	762.7 ± 3.3
KRI XV	74.4 ± 2.2	73.97 ± 0.2 (b)	901 ± 30 901.0 ± 9.0 (e)	896.2 ± 3.9
BRC		454.9 ± 1.4	115.6	116.7 ± 0.5
AERE A	911.2 ± 4.6	914.1 ± 3.2 (c)	343.4 ± 2.7 (d)	346.5 ± 1.6
AERE B	915.6 ± 4.6	914.9 ± 3.2 (c)	345.1 ± 2.8 (d)	346.8 ± 1.6
CBNM 33	476.3 ± 4.1	476.7 ± 1.2	122.1 ± 1.0 (f) 121.9 ± 0.4 (g)	122.3 ± 0.5
CBNM 36	976.9 ± 8.3	977.3 ± 2.5	250.4 ± 2.1 (f) 249.9 ± 0.9 (g)	250.7 ± 1.0

(a) Obtained from NBS ratio measurement relative to NBS standard by (1) alpha counting, (2) fission counting.
(b) Including the 3.1% contribution from U-234.
(c) Excluding contributions from impurities with alpha-energies above 4.77 MeV.
(d) Preliminary.
(e) Based on given areal density and total area.
(f) Based on alpha counting and specific activity.
(g) Based on isotopic dilution.

Table 5. Results from the Present Ratio Measurements.

Nominator

Denominator	R5	N3	5-1	5-2	SST5	S1	S3	NBS	KRI VI	KRI XV	BRC	HAR A	HAR B	CBNM33	CBNM36
ANL R5	-	0.6562	13.461	10.515	5.2576	3.765 (+.3)	21.231	2.8828	9.5904	11.249	1.4700	4.3725	4.3791	1.5421	3.1656
ANL N3	1.5240	-	20.53	16.033	8.0128	5.738	32.357	4.3934	14.616	17.143	2.2404	6.6627	6.6739	2.3502	4.8245
ANL 5-1	0.0743	0.0487 {+.4}	-	0.7816	0.3906	0.2797	1.5773	0.2142	0.7125	0.8357	0.1092	0.3248	0.3253	0.1146	0.2352
ANL 5-2	0.0951 {+.3}	0.0624	1.2795 (+.1)	-	0.4998	0.3579 (+.2)	2.0182	0.2740 (-.5)	0.9117	1.0693	0.1397	0.4156	0.4163	0.1466	0.3009
ANL SST5	0.1902 (0)	0.1248 (-.5)	2.5602	2.0009 (-.1)	-	0.7161 (+.1)	4.0382 (0)	0.5483 (-.1)	1.8241	2.1395 (+.2)	0.2796 (-.1)	0.8315	0.8329 (+.3)	0.2933	0.6021
LANL S1	0.2652	0.1743	3.5752	2.7941	1.3965	-	5.6402	0.7657	2.5473	2.9877	0.3904	1.1612	1.1631	0.4096	0.8408
LANL S3	0.0471	0.0309	0.6340	0.4955	0.2476	0.1773 {0}	-	0.1358	0.4517	0.5298	0.0692	0.2059	0.2063	0.0726	0.1491
NBS	0.3469	0.2276	4.6693	3.6496	1.8238	1.3060 (-.6) {+.1}	7.3649	-	3.3256	3.9021	0.5099	1.5165	1.5191	0.5349	1.0981
KRI VI	0.1043	0.0684	1.4035	1.0969 (+.1)	0.5482	0.3926	2.2138	0.3007 (-.6)	-	1.1729 (-.2) {+.3}	0.1533	0.4558	0.4566	0.1608	0.3306 (+.8)
KRI XV	0.0889	0.0583	1.1966	0.9352	0.4674	0.3347	1.8875	0.2563	0.8526	-	0.1307	0.3886	0.3893	0.1371	0.2814
BRC	0.6803	0.4464	9.1567	7.1563	3.5765	2.5612	14.443	1.9612 (0)	6.5247 (+.2)	7.6520	-	2.9742 (0)	2.9789	1.0490	2.1538
HAR A	0.2287 (-.1)	0.1501	3.0790	2.4063 {0}	1.2026	0.8612	4.8565	0.6594 (-.7)	2.1938 (-.1)	2.5731	0.3362	-	1.0017 (-.3) {+.1}	0.3527	0.7242
HAR B	0.2284	0.1498	3.0738	2.4023	1.2006	0.8598	4.8484	0.6583	2.1901	2.5687	0.3357	0.9983	-	0.3521	0.7229
CBNM 33	0.6485	0.4255	8.7289	6.8212 (+.3)	3.4095	2.4415	13.768	1.8694	6.2192	7.2946	0.9533	2.8350	2.8398	-	2.0527 {-.1}
CBNM 36	0.3159 {+.2}	0.2073	4.2521	3.3230 (+.3)	1.6609	1.1893	6.7069	0.9106	3.0248	3.5534	0.4643 {+.2}	1.3809 (-.4)	1.3833	0.4872	-

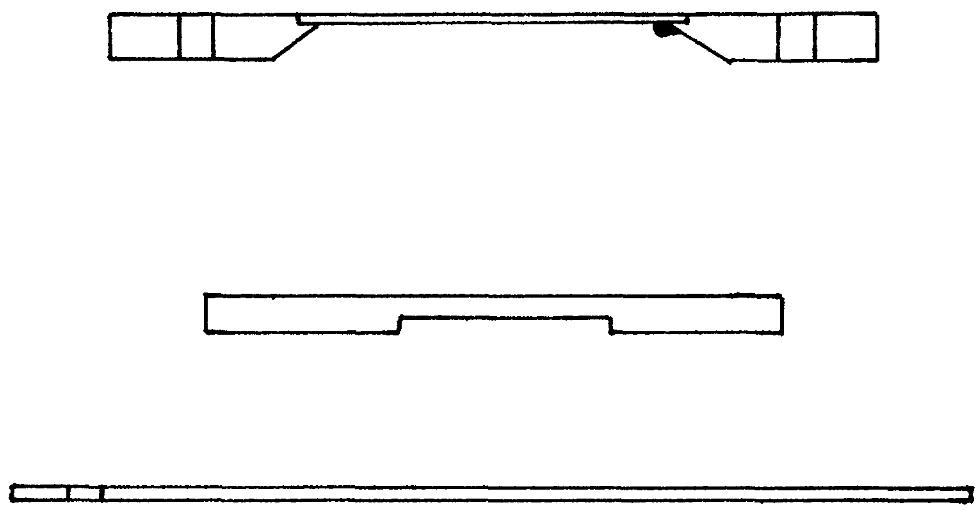

Fig. 1. Schematic of the KRI, BRC, ANL SST5+5-2 Samples.

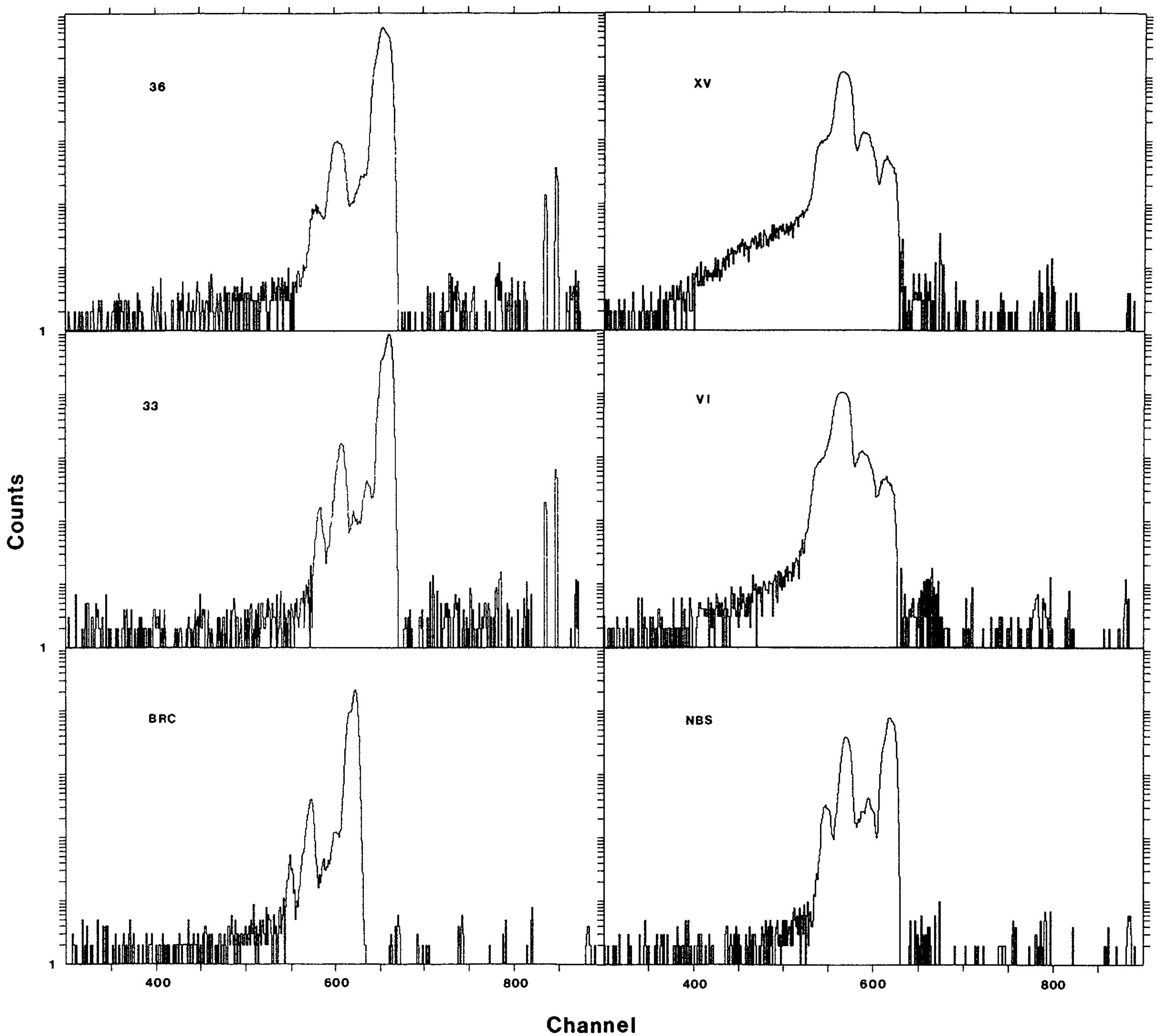

Fig. 2. Representative LG Alpha Spectra.

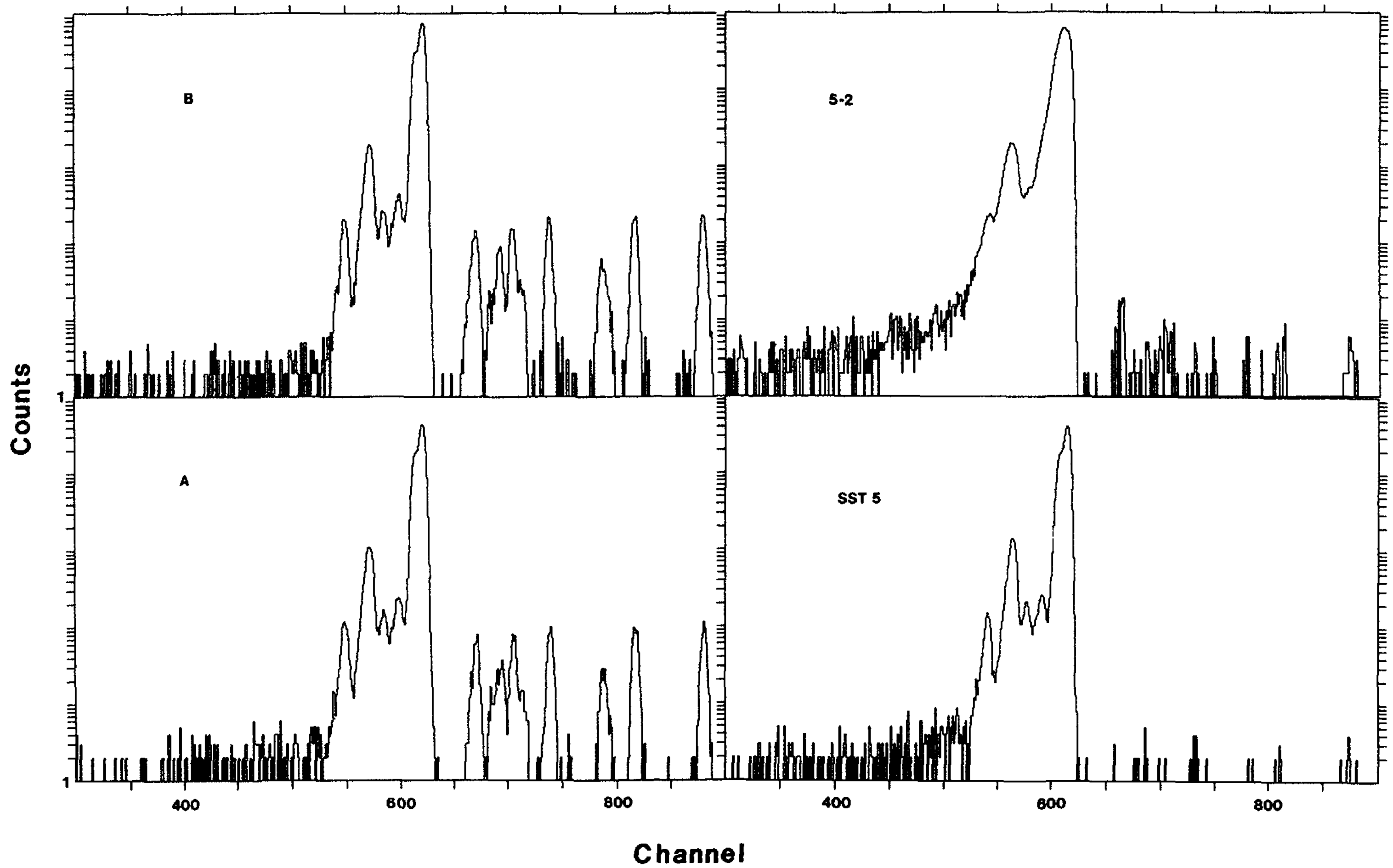

Fig. 3. Representative LG Alpha Spectra.

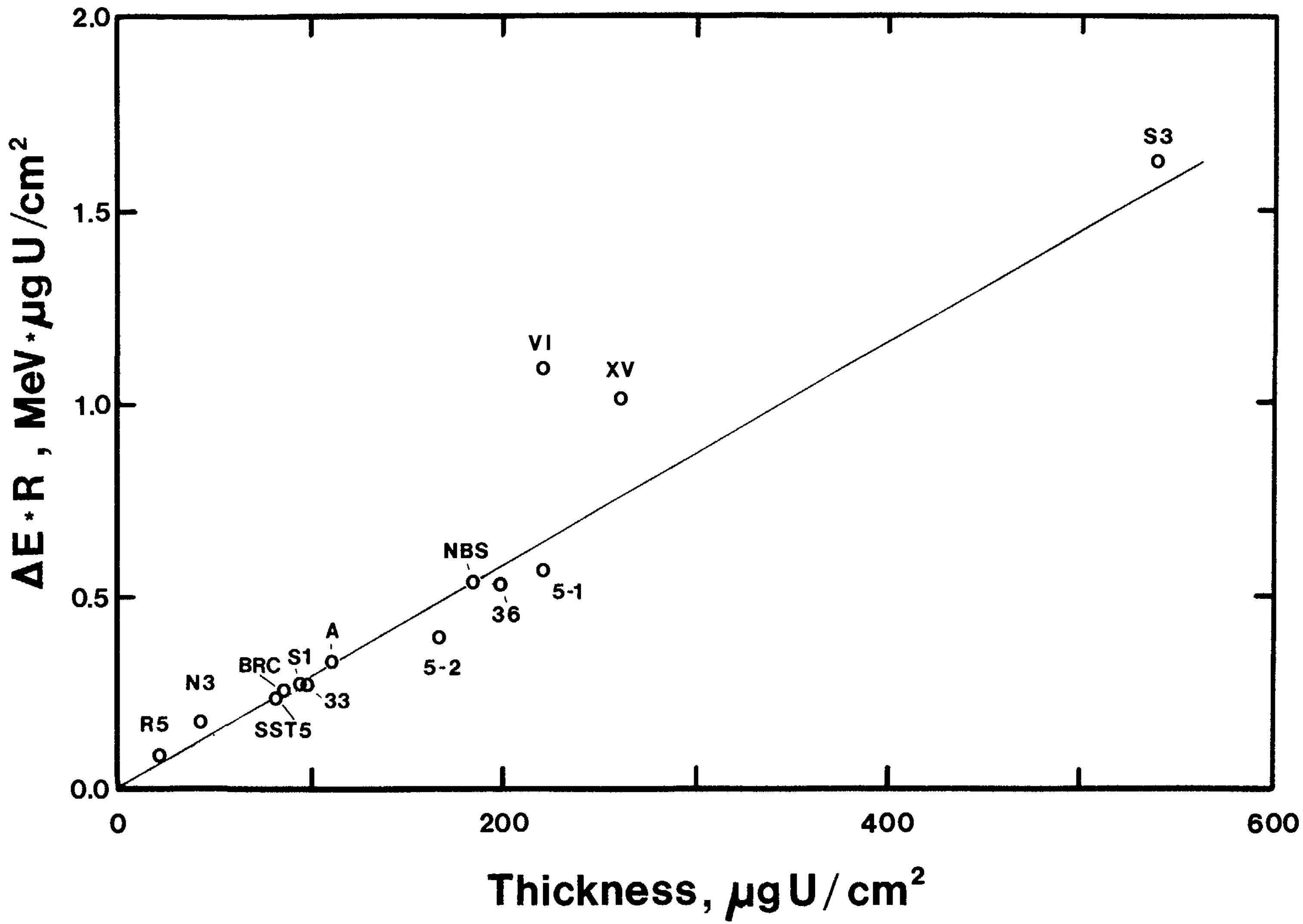

Fig. 4. Alpha Energy Loss Multiplied with the FF Range as a Function of the Sample Thickness. The Values for the KRI Samples is shown for an Assumed UO_2.

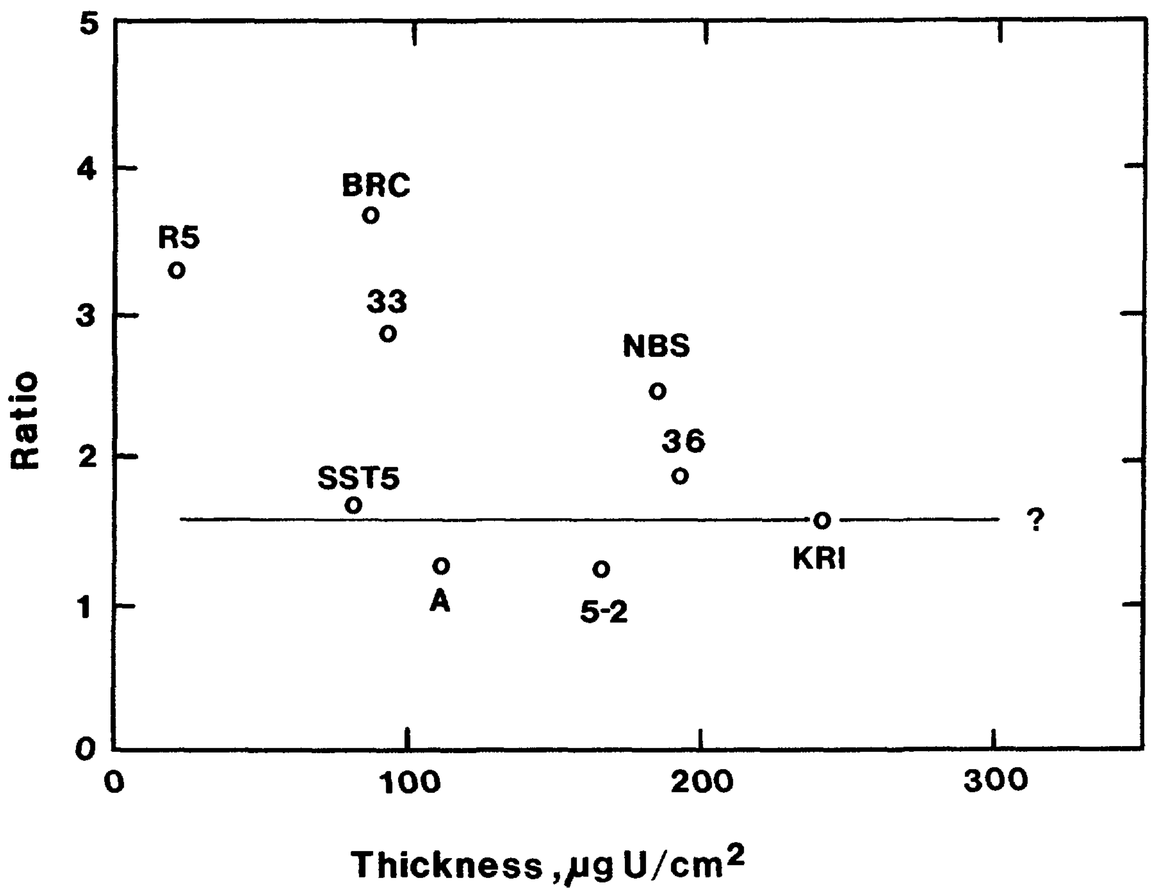

Fig. 5. The Ratios of the Fraction of Pulses Below the Geometrical Cut-off vs. the Fraction of Calculated FF Absorption Losses.

ANL R5

QUOTED MASS 79.6

MASS FROM FISSION RATIO MEASUREMENT

REL. TO	MASS BASED ON ANL ALPHA COUNT		QUOTED MASSES	
ANL R5	.0		.0	
ANL N3	79.5		79.5	
ANL S-1	79.3		79.3	
ANL S-2	79.4		79.4	
ANL SST5	79.5		79.5	
AV. ANL		79.4		79.4
LANL S1	79.5		79.3	
LANL S3	79.5		79.5	
AV. LANL		79.5		79.4
NBS	79.3		79.3	
AV. NBS		79.3		79.3
KRI VI	79.5		79.0	
KRI XV	79.7		80.1	
AV. KRI		79.6		79.6
BRC	79.4		78.6	
AV. BRC		79.4		78.6
AERE A	79.2		78.5	
AERE B	79.2		78.8	
AV. AERE		79.2		78.7
CBNM 33	79.3		79.0	
CBNM 36	79.2		79.0	
AV. CBNM		79.3		79.0
AVERAGE		79.4		79.1

ANL ALPHA COUNT 79.6

ANL N3

QUOTED MASS 52.2

MASS FROM FISSION RATIO MEASUREMENT

REL. TO	MASS BASED ON ANL ALPHA COUNT		QUOTED MASSES	
ANL R5	52.2		52.2	
ANL N3	.0		.0	
ANL S-1	52.0		52.0	
ANL S-2	52.1		52.1	
ANL SST5	52.2		52.2	
AV. ANL		52.1		52.1
LANL S1	52.2		52.1	
LANL S3	52.2		52.2	
AV. LANL		52.2		52.1
NBS	52.0		52.0	
AV. NBS		52.0		52.0
KRI VI	52.2		51.9	
KRI XV	52.3		52.6	
AV. KRI		52.2		52.2
BRC	52.1		51.6	
AV. BRC		52.1		51.6
AERE A	52.0		51.5	
AERE B	52.0		51.7	
AV. AERE		52.0		51.6
CBNM 33	52.0		51.9	
CBNM 36	52.0		51.8	
AV. CBNM		52.0		51.8
AVERAGE		52.1		51.9

ANL ALPHA COUNT 52.2

ANL 5-1

QUOTED MASS 1067.0

MASS FROM FISSION RATIO MEASUREMENT

REL. TO	MASS BASED ON ANL ALPHA COUNT		QUOTED MASSES	
ANL R5	1071.3		1071.3	
ANL N3	1071.3		1071.3	
ANL 5-1	.0		.0	
ANL 5-2	1067.8		1067.8	
ANL SST5	1070.4		1070.4	
AV. ANL		1070.2		1070.2
LANL S1	1070.4		1067.9	
LANL S3	1070.6		1070.4	
AV. LANL		1070.5		1069.2
NBS	1067.2		1066.8	
AV. NBS		1067.2		1066.8
KRI VI	1070.5		1063.7	
KRI XV	1072.4		1078.1	
AV. KRI		1071.4		1070.9
BRC	1068.7		1058.6	
AV. BRC		1068.7		1058.6
AERE A	1066.8		1057.3	
AERE B	1066.1		1060.9	
AV. AERE		1066.5		1059.1
CBNM 33	1067.2		1063.7	
CBNM 36	1065.9		1062.9	
AV. CBNM		1066.5		1063.3
AVERAGE		1069.0		1065.4

ANL ALPHA COUNT 1067.0

ANL 5-2

QUOTED MASS 834.6

MASS FROM FISSION RATIO MEASUREMENT

REL. TO	MASS BASED ON ANL ALPHA COUNT		QUOTED MASSES	
ANL R5	837.0		837.0	
ANL N3	836.1		836.1	
ANL 5-1	833.9		833.9	
ANL 5-2	.0		.0	
ANL SST5	836.5		836.5	
AV. ANL		835.9		835.9
LANL S1	836.5		834.6	
LANL S3	836.7		836.5	
AV. LANL		836.6		835.6
NBS	834.3		833.9	
AV. NBS		834.3		833.9
KRI VI	836.6		831.3	
KRI XV	838.1		842.6	
AV. KRI		837.3		837.0
BRC	835.4		827.5	
AV. BRC		835.4		827.5
AERE A	833.7		826.3	
AERE B	833.1		829.0	
AV. AERE		833.4		827.6
CBNM 33	834.2		831.5	
CBNM 36	833.2		830.8	
AV. CBNM		833.7		831.2
AVERAGE		835.4		832.7

ANL ALPHA COUNT 834.6

ANL SST5

QUOTED MASS 418.1

MASS FROM FISSION RATIO MEASUREMENT

REL. TO	MASS BASED ON ANL ALPHA COUNT		QUOTED MASSES	
ANL R5	418.5		418.5	
ANL N3	418.0		418.0	
ANL 5-1	416.8		416.8	
ANL 5-2	417.1		417.1	
ANL SST5	.0		.0	
AV. ANL		417.6		417.6
LANL S1	418.1		417.1	
LANL S3	418.2		418.1	
AV. LANL		418.1		417.6
NBS	416.9		416.7	
AV. NBS		416.9		416.7
KRI VI	418.1		415.5	
KRI XV	418.9		421.1	
AV. KRI		418.5		418.3
BRC	417.4		413.4	
AV. BRC		417.4		413.4
AERE A	416.7		413.0	
AERE B	416.4		414.3	
AV. AERE		416.5		413.7
CBNM 33	417.0		415.6	
CBNM 36	416.4		415.2	
AV. CBNM		416.7		415.4
AVERAGE		417.5		416.1

ANL ALPHA COUNT 418.1

LANL S1

QUOTED MASS 298.7

MASS FROM FISSION RATIO MEASUREMENT

REL. TO	MASS BASED ON ANL ALPHA COUNT		QUOTED MASSES	
ANL R5	300.2		300.2	
ANL N3	299.3		299.3	
ANL 5-1	298.4		298.4	
ANL 5-2	298.7		298.7	
ANL SST5	299.4		299.4	
AV. ANL		299.2		299.2
LANL S1	.0		.0	
LANL S3	299.4		299.3	
AV. LANL		299.4		299.3
NBS	298.6		298.4	
AV. NBS		298.6		298.4
KRI VI	299.4		297.5	
KRI XV	300.0		301.6	
AV. KRI		299.7		299.6
BRC	298.9		296.1	
AV. BRC		298.9		296.1
AERE A	298.4		295.7	
AERE B	298.2		296.7	
AV. AERE		298.3		296.2
CBNM 33	298.6		297.6	
CBNM 36	298.2		297.3	
AV. CBNM		298.4		297.5
AVERAGE		299.0		298.0

ANL ALPHA COUNT 299.4

LANL S3

QUOTED MASS 1698.3

MASS FROM FISSION RATIO MEASUREMENT

REL. TO	MASS BASED ON ANL ALPHA COUNT		QUOTED MASSES	
ANL R5	1690.0		1690.0	
ANL N3	1688.3		1688.3	
ANL 5-1	1683.0		1683.0	
ANL 5-2	1684.4		1684.4	
ANL SST5	1688.6		1688.6	
AV. ANL		1686.9		1686.9
LANL S1	1688.7		1684.7	
LANL S3	.0		.0	
AV. LANL		1688.7		1684.7
NBS	1683.4		1682.6	
AV. NBS		1683.4		1682.6
KRI VI	1688.5		1677.9	
KRI XV	1691.6		1700.6	
AV. KRI		1690.0		1689.3
BRC	1686.4		1670.5	
AV. BRC		1686.4		1670.5
AERE A	1682.9		1667.8	
AERE B	1681.0		1672.8	
AV. AERE		1682.0		1670.3
CBNM 33	1684.6		1679.1	
CBNM 36	1681.4		1676.7	
AV. CBNM		1683.0		1677.9
AVERAGE		1685.9		1680.3

ANL ALPHA COUNT 1688.6

NBS

QUOTED MASS 228.5

MASS FROM FISSION RATIO MEASUREMENT

REL. TO	MASS BASED ON ANL ALPHA COUNT		QUOTED MASSES	
ANL R5	229.5		229.5	
ANL N3	229.2		229.2	
ANL 5-1	228.5		228.5	
ANL 5-2	228.7		228.7	
ANL SST5	229.2		229.2	
AV. ANL		229.0		229.0
LANL S1	229.2		228.7	
LANL S3	229.3		229.2	
AV. LANL		229.3		229.0
NBS	.0		.0	
AV. NBS		.0		.0
KRI VI	229.3		227.9	
KRI XV	229.7		230.9	
AV. KRI		229.5		229.4
BRC	228.9		226.7	
AV. BRC		228.9		226.7
AERE A	228.5		226.4	
AERE B	228.3		227.2	
AV. AERE		228.4		226.8
CBNM 33	228.6		227.9	
CBNM 36	228.3		227.7	
AV. CBNM		228.5		227.8
AVERAGE		228.9		228.1

ANL ALPHA COUNT 228.6

KRI VI

QUOTED MASS 797.9

MASS FROM FISSION RATIO MEASUREMENT

REL. TO	MASS BASED ON ANL ALPHA COUNT		QUOTED MASSES	
ANL R5	763.2		763.2	
ANL N3	762.7		762.7	
ANL 5-1	760.2		760.2	
ANL 5-2	760.9		760.9	
ANL SST5	762.7		762.7	
AV. ANL		761.9		761.9
LANL S1	762.6		760.8	
LANL S3	762.8		762.6	
AV. LANL		762.7		761.7
NBS	760.2		759.9	
AV. NBS		760.2		759.9
KRI VI	.0		.0	
KRI XV	764.1		768.2	
AV. KRI		764.1		768.2
BRC	761.3		754.1	
AV. BRC		761.3		754.1
AERE A	760.2		753.4	
AERE B	759.5		755.8	
AV. AERE		759.9		754.6
CBNM 33	760.6		758.1	
CBNM 36	758.3		756.2	
AV. CBNM		759.4		757.1
AVERAGE		761.4		759.7
ANL ALPHA COUNT	762.7			

KRI XV

QUOTED MASS 901.0

MASS FROM FISSION RATIO MEASUREMENT

REL. TO	MASS BASED ON ANL ALPHA COUNT		QUOTED MASSES	
ANL R5	895.4		895.4	
ANL N3	894.9		894.9	
ANL 5-1	891.7		891.7	
ANL 5-2	892.4		892.4	
ANL SST5	894.5		894.5	
AV. ANL		893.8		893.8
LANL S1	894.5		892.4	
LANL S3	894.6		894.5	
AV. LANL		894.6		893.5
NBS	891.9		891.5	
AV. NBS		891.9		891.5
KRI VI	894.6		888.9	
KRI XV	.0		.0	
AV. KRI		894.6		888.9
BRC	892.9		884.5	
AV. BRC		892.9		884.5
AERE A	891.7		883.7	
AERE B	890.8		886.5	
AV. AERE		891.2		885.1
CBNM 33	892.0		889.1	
CBNM 36	890.9		888.4	
AV. CBNM		891.5		888.8
AVERAGE		893.1		889.4
ANL ALPHA COUNT	896.2			

BRC

QUOTED MASS 115.6

MASS FROM FISSION RATIO MEASUREMENT

REL. TO	MASS BASED ON ANL ALPHA COUNT		QUOTED MASSES	
ANL R5	117.0		117.0	
ANL N3	116.9		116.9	
ANL 5-1	116.5		116.5	
ANL 5-2	116.6		116.6	
ANL SST5	116.9		116.9	
AV. ANL		116.8		116.8
LANL S1	116.9		116.6	
LANL S3	116.9		116.9	
AV. LANL		116.9		116.8
NBS	116.6		116.5	
AV. NBS		116.6		116.5
KRI VI	116.9		116.2	
KRI XV	117.1		117.7	
AV. KRI		117.0		117.0
BRC	.0		.0	
AV. BRC		.0		.0
AERE A	116.5		115.5	
AERE B	116.4		115.8	
AV. AERE		116.5		115.7
CBNM 33	116.6		116.2	
CBNM 36	116.4		116.1	
AV. CBNM		116.5		116.1
AVERAGE		116.7		116.5
ANL ALPHA COUNT	116.7			

AERE A

QUOTED MASS 343.4

MASS FROM FISSION RATIO MEASUREMENT

REL. TO	MASS BASED ON ANL ALPHA COUNT		QUOTED MASSES	
ANL R5	348.1		348.1	
ANL N3	347.6		347.6	
ANL 5-1	346.5		346.5	
ANL 5-2	346.8		346.8	
ANL SST5	347.7		347.7	
AV. ANL		347.3		347.3
LANL S1	347.7		346.8	
LANL S3	347.7		347.6	
AV. LANL		347.7		347.2
NBS	346.7		346.5	
AV. NBS		346.7		346.5
KRI VI	347.7		345.5	
KRI XV	348.3		350.2	
AV. KRI		348.0		347.8
BRC	347.1		343.8	
AV. BRC		347.1		343.8
AERE A	.0		.0	
AERE B	346.2		344.5	
AV. AERE		346.2		344.5
CBNM 33	346.8		345.6	
CBNM 36	346.2		345.2	
AV. CBNM		346.5		345.4
AVERAGE		347.2		346.1
ANL ALPHA COUNT	346.5			

AERE B

QUOTED MASS 345.1

MASS FROM FISSION RATIO MEASUREMENT

REL. TO	MASS BASED ON ANL ALPHA COUNT		QUOTED MASSES	
ANL R5	348.5		348.5	
ANL N3	348.3		348.3	
ANL 5-1	347.1		347.1	
ANL 5-2	347.4		347.4	
ANL SST5	348.2		348.2	
AV. ANL		347.9		347.9
LANL S1	348.2		347.4	
LANL S3	348.3		348.2	
AV. LANL		348.3		347.8
NBS	347.3		347.1	
AV. NBS		347.3		347.1
KRI VI	348.2		346.1	
KRI XV	348.9		350.8	
AV. KRI		348.6		348.4
BRC	347.6		344.4	
AV. BRC		347.6		344.4
AERE A	347.1		344.0	
AERE B	.0		.0	
AV. AERE		347.1		344.0
CBNM 33	347.3		346.2	
CBNM 36	346.8		345.8	
AV. CBNM		347.1		346.0
AVERAGE		347.8		346.5

ANL ALPHA COUNT 346.8

CBNM 33

QUOTED MASS 121.9

MASS FROM FISSION RATIO MEASUREMENT

REL. TO	MASS BASED ON ANL ALPHA COUNT		QUOTED MASSES	
ANL R5	122.7		122.7	
ANL N3	122.6		122.6	
ANL 5-1	122.2		122.2	
ANL 5-2	122.4		122.4	
ANL SST5	122.6		122.6	
AV. ANL		122.5		122.5
LANL S1	122.6		122.3	
LANL S3	122.6		122.6	
AV. LANL		122.6		122.5
NBS	122.3		122.2	
AV. NBS		122.3		122.2
KRI VI	122.6		121.9	
KRI XV	122.9		123.5	
AV. KRI		122.7		122.7
BRC	122.4		121.3	
AV. BRC		122.4		121.3
AERE A	122.2		121.1	
AERE B	122.1		121.5	
AV. AERE		122.2		121.3
CBNM 33	.0		.0	
CBNM 36	122.1		121.8	
AV. CBNM		122.1		121.8
AVERAGE		122.5		122.0

ANL ALPHA COUNT 122.3

CBNM 36

QUOTED MASS 250.0

MASS FROM FISSION RATIO MEASUREMENT

REL. TO	MASS BASED ON ANL ALPHA COUNT		QUOTED MASSES	
ANL R5	252.0		252.0	
ANL N3	251.7		251.7	
ANL 5-1	250.9		250.9	
ANL 5-2	251.2		251.2	
ANL SST5	251.7		251.7	
AV. ANL		251.5		251.5
LANL S1	251.7		251.2	
LANL S3	251.8		251.7	
AV. LANL		251.8		251.4
NBS	251.0		250.9	
AV. NBS		251.0		250.9
KRI VI	252.1		250.6	
KRI XV	252.2		253.6	
AV. KRI		252.2		252.1
BRC	251.3		249.0	
AV. BRC		251.3		249.0
AERE A	250.9		248.7	
AERE B	250.7		249.5	
AV. AERE		250.8		249.1
CBNM 33	251.0		250.2	
CBNM 36	.0		.0	
AV. CBNM		251.0		250.2
AVERAGE		251.5		250.6

ANL ALPHA COUNT 250.7

STATISTICAL ANALYSIS OF FISSION CROSS SECTION MEASUREMENTS ON $^{233,235,238}U$, ^{237}Np, $^{239,242}Pu$ AT NEUTRON ENERGIES OF 2.6, 8.5 AND 14.7 MEV

Dushin V.N., Fomichev A.V., Kovalenko S.S., Petrzhak K.A., Shpakov V.I.
(Khlopin Radium Institute, USSR)
Arlt R., Josch M., Musiol G., Ortlepp H.G., Wagner W.
(Technical Univercity of Dresden, GDR)

Within the scope of the joint measurement programme of the V.G. Khlopin Radium Institute, Leningrad, USSR, and the Technical Univercity of Dresden, GDR, absolute fission cross-section measurements have been carried out on heavy nuclei at the spot point neutron energies of 2.6, 8.5, and 14.7 MeV. The measurements were performed at the neutron generators of the Radium Institute and the Technical Univercity and at the tandem generator of the Central Institute of Nuclear Research, Rossendorf (GDR). The experimental technique has been continuously improved during the period of several years needed for the design and construction of the measuring equipment and for the completion of the time consuming measurements. The fission cross-section determinations on all isotopes were manifold repeated, employing different set ups, in order to gain a higher accuracy. For the main isotopes several independent measurements were carried out. In this way a large amount of experimental results has been obtained and published (e.g. [1 - 4]).

The aim of this work is a comprehensive analysis of the results and of the uncertainties of the measurements by means of a correlation analysis. As the result the final fission cross-section values including all the measurements carried out in Leningrad and Dresden are evaluated.

The time correlated associated particle method (TCAPM) was used in all the fission cross-section measurements. This method was described in details elsewhere (e.g. [2]). It is worthwhile therefore to mention shortly its principal features. The neutron sources were $^3H(d,n)^4He$ or $^2H(d,n)^3He$ reactions. The ^3He or ^4He particles associated with the neutrons were registered in some solid angle, which was defined by the detector entrance diaphragm. The neutron cone corresponding to these associated particles irradiated a fission target. Both the associated particles and the coincidences fission-associated particle were recorded. Under condition, that the neutron cone is completely situated inside the fission target, the fission cross section is defined by the formula:

$$\sigma_f = \frac{N_c}{N_{ap}\, n}\,, \qquad [1]$$

where N_c is the number of coincident fission events, N_{ap} is the number of associated particles registered, and n is the number of target nuclei per cm^2.

The following corrections were applied to the rough data of the measurements:

i) background of random coincidences
ii) background of the assiciated particle counter
iii) neutron attenuation and scattering
iv) inefficiency of the parallel plate fission chamber
v) fission of other than the main isotopes of a deposit.

Details of the procedures of the correction determination are given in the corresponding publications.

The fission foils were manufactured at the Radium Institute. Low geometry alpha counting was applied to determine both the areal density and nonuniformity of the foils. In the case of $^{235,238}U$ additional X ray microprobe analysis and ellipsometry were used in order to determine the nonuniformity of the layer.

In order to calculate the areal density of tne fission foils, several corrections are to be applied to the measured alpha counting rate:

i) subtraction of the alpha counts of other than the main isotopes
ii) background of the alpha detector
iii) extrapolation to zero alpha energy
iv) efficiency of the alpha counting system

All these corrections cause uncertainties. Besides these additional uncertainties should be taken into account in the evaluation of the final results:

i) statistical uncertainty of the number of coincident fission counts
ii) statistical uncertainty of the number of alpha particles counted in the low geometry alpha assay of the fission foils
iii) statistical uncertainty of the number of associated particles
iv) uncertainty of the value of the half lives used for the calculations of the areal density of the fission foils
v) uncertainty arising from nonuniformity of the fission foils
vi) uncertainty connected with the topography of the neutron cone
vii) uncertainty of the energy of the bombarding neutrons.

The analysis of the experimental data and the calculations of mean values have been performed taking into account the correlation of the uncertainties of the single measurements. Covariance matrices Cov $(\sigma_f^{\,i}, \sigma_f^{\,j})$ of the results have been calculated from the covariance of the partial uncertainties of the cross sections using the expression:

$$\mathrm{Cov}\,(\sigma_f^{\,i}, \sigma_f^{\,j}) = S_i^{T}\, \mathrm{Cov}\,(X_l^{\,i}, X_k^{\,j})\, S_j, \quad \text{where}$$

$\sigma_f^{\,i}, \sigma_f^{\,j}$ - results of different fission cross-section measurement
Cov $(X_l^{\,i}, X_k^{\,j})$ - covariance matrix of the partial uncertainties of the measurements
S_i, S_j - coefficients of sensitivity
$X_l^{\,i}, X_k^{\,j}$ - values which are used to get the fission cross section and its corrections

In order to calculate the covariance the following expressions were put into the formula (1):

$$N_c = (X_1 - X_2)\,(1 + X_3)\,(1 - X_4)\,(1 + X_5)$$

$$N_{ap} = (X_6 - X_7)\,(1 - X_8)$$

$$n = (X_9 - X_{10})\,(1 - X_{11})\,(1 + X_{12})\,X_{13}^{-1}\,X_{14}\,(\ln 2)^{-1}, \quad \text{where}$$

X_1 - statistics of the number of coincident fission counts
X_2 - statistics of the number of random coincidences
X_3 - part of fission fragments, absorbed in the fission foil
X_4 - contribution of the fission events of other than the main isotopes of the fission foil
X_5 - correction for the extrapolation of the fission fragments spectrum to zero energy
X_6 - statistics of the number of associated particles
X_7 - background of the associated particle counter
X_8 - neutron beam attenuation
X_9 - statistics of the number of alpha counts in the low geometry alpha assay

X_{10} - statistics of the background of the low geometry alpha assay

X_{11} - contributions of alpha counts from other than the main isotopes in the low geometry alpha assay

X_{12} - correction for the extrapolation of the alpha spectrum to zero energy

X_{13} - solid angle of the low geometry alpha counter

X_{14} - half life.

All these values X as well as their uncertainties X were introdused as variables in the statistical analysis. In addition the following uncertainties have been concidered:

ΔX_{15} - uncertainty due to the nonuniformity of the fission target

ΔX_{16} - uncertainty of the topographyof the neutron cone

ΔX_{17} - uncertainty of the energy of the bombarding neutrons

The total nonuniformity of the fission foils have been used as a partial uncertainty ΔX_{15} though that leads to an overestimation of the uncertainty. Careful investigation have been accomplished in order to determine the topography of the neutron cone. The maximal value of a possible "tail" of the neutron cone taking into account the accurasy of the measurements of its topography was used as a measure of the partial uncertainty ΔX_{16}. The partial uncertainty ΔX_{17} has been obtained from the theoretical and experimental determination of the dispersion of the neutron energy, the gradient of the energy dependence of the fission cross section being allowed for.

The main question of the generation of the covariance matrices is the estimation of the degree of correlation between the partial uncertainties. After a subdivision of the uncertainties into sufficient elementary components corresponding to the structure of the experiment it seems to be correct based on an experts estimation to relate one of the following three degrees of correlation between the partial uncertainties: zero correlation (k = 0), total correlation (k = 1), and intermediate correlation (k = 0.5 - 0.7).

In this work the results of publications [1 - 3] have been analized. The data obtained in [1] for ^{239}Pu and ^{237}Np have been excluded because this analysis made clear that these values contain systematical error. These results had been obtained at an early stage of measurement programme. In this case very thick backings of the fission deposits were used (up to 3 mm) and the deposits contained rather large amount of admixtures. In the publication [3] a preliminary result for ^{235}U at the neutron energy of 8.5 MeV was given, which now has been finalized [4]. The value for the fission cross section of ^{238}U given in [1] has been revised. Additional measurements carried out indepehdently in Leningrad and in Dresden in 1981/1982 at neutron energies of 2.56 MeV (^{235}U), 8.5 MeV (^{237}Np), and 14.7 MeV (^{233}U, ^{237}Np, $^{239,242}Pu$) [4] have been included in the analysis too.

In cases when the data published were based on several subsequent runs of measurements the results of these runs were considered separately instead of final results. All the data which were included in the analysis together with the covariance matrices are given in tables 1 and 2. The abbreviations TUD and RIL indicate the laboratory in which the measurement was performed - Technical Univercity of Dresden and Khlopin Radium Institute, Leningrad.

The analysis of the data has been carried out employing the χ^2 approach. In order to identify "outrunners" the uncertainty of the ratio σ_f^i/σ_f^j has been considered in addition. By accounting the covariances the uncertainty of the ratio decreased by a factor of 3.5. In this way two runs (one for ^{235}U and the other for ^{239}Pu) have been excluded, for which the deviation of the ratio from 1 was some 4 times larger than the uncertainty.

The evaluation of the final values of the fission cross sections has been performed employing the generalized least square method (e.g. [5]). The results of the separate analysis of the different nuclei are given in table 3 together with the results of different evaluations and other measurements employing the time correlated associated particle method. The analysis indicates a statistical discrepancy in the results for ^{239}Pu. The large value of χ^2 (~ 6) points to an unaccounted systematical uncertainty.

Besides the set of all measurements has been considered too, taking into account the mutual correlations. The covariance matrix of the complete set of the measurements on all isotopes and at all energies has elements of the same order of magnitude, as the matrix of the ^{235}U measurements (table 1) and therefore is omitted here because of its large size. The mean values obtained on the basis of this covariance matrix together with their mutual covariances are presented in table 4. When comparing table 4 with table 3 a slight shift of the mean values and some decrease (up to 30 per cent) of the uncertainties of the separate cross sections are evident, the statistical agreement being satisfying (χ^2 = 12.9).

To compare our results with the data obtained using TCAPM by other authors the attenuation of the neutron flux has been calculated for the experimental arrangement used in [7]. The correction obtained shows a difference of 7 % as compared with corresponding value given in [7]. This would lead to decrease of the fission cross section obtained in [7] by 0.2 - 0.4 %. Such a shift (within the limits of uncertainties) demonstrates the stability of the method used but on the other hand the need of a mutual intercomparison of the programmes used for the corrections calculations is evident.

The comparison of the results of this work for ^{235}U with the results of the latest measurements employing a black neutron detector [9] and relative to the (n,p)-scattering cross section [10] shows a good agreement.

From the results of this work it may be concluded that excluding ^{239}Pu all our measurements are in good agreement. Futhermore an excelent agreement with the results obtained at different laboratories employing the same measurement principle [6,7] can be stated. In this way the time correlated associated particle method can be regarded as the most reliable one for the performance of the normalization of shape measurements in the range of fast neutron energies.

References

1. Adamov V.M. et al. In Proc. of the Internat. Conf. on Nuclear Cross, Sect. for Technology, Knoxwille, 1979, NBS Spec. Publicat. 594, Washington, 1980, p. 984
2. Arlt R. et al. Ibid, p. 990
3. Arlt R. et al. Neutrn Physics, Proc. of the 5-th AllUnion Conf. on Neutron Physics, Kiev, 1980. Moscov, 1980, v. 4, p.192.
4. Alkhazov I.D. In Theses of the 3-d AllUnion Conf. on Metrology of Neutr. Irradiation, Moscov, 1982, p. 155.
5. Mannhart W. A Small Guide to Generatihg Covariances of Experim. Data. PTB-FMRB-84, ISSN 0341-6666, Braunschweig, 1981.
6. Cance M., Grenier G., Nucl. Sci. and Eng., 68, 197 (1978).
7. Wasson O.A., Meier M.M., Duvall K.C. Nucl. Sci. and Eng. 80, 882 (1982).
8. Lemmel H.D. editor. INDL/A Nuclear Data Library for Evaluated Neutron Reaction Data of Actinides. May, 1982.
9. Poenitz W.P. Nucl. Sci. and Eng. 64, 894 (1977)
10. Carlson A.D., Patrick B.H. Proc. of Internat. Conf. on Neutron Phycics and Nucl. Data, Harwell, 1978, p. 880.

Table 1

Covariance matrix of the fission cross-section measurements on ^{235}U

σ_f (barns)			Covariance matrix (in $\%^2$)										
RIL	2.0714	(14.7 MeV)	2.08	0.92	0.73	0.82	0.82	0.82	0.41	0.41	0.41	0.41	0.41
RIL	2.1348	(14.7 MeV)		2.08	0.73	0.82	0.82	0.82	0.41	0.41	0.41	0.41	0.41
RIL	2.0755	(14.7 MeV)			3.03	0.67	0.67	0.67	0.45	0.39	0.39	0.39	0.39
RIL	2.0960	(14.7 MeV)				1.90	0.74	0.74	0.31	0.31	0.31	0.31	0.31
RIL	2.1010	(14.5 MeV)					3.02	0.74	0.31	0.31	0.31	0.31	0.31
RIL	2.0840	(14.0 MeV)						3.02	0.31	0.31	0.31	0.31	0.31
TUD	2.083	(14.7 MeV)							1.76	1.05	1.06	1.05	1.06
TUD	2.087	(14.7 MeV)								1.45	1.06	1.05	1.06
TUD	2.075	(14.7 MeV)									2.76	1.05	1.07
TUD	2.073	(14.7 MeV)										1.51	1.06
TUD	2.075	(14.7 MeV)											1.81

Table 2

Covariance matrices of the fission cross-section measurements

	Nuclide	E_n (MeV)	σ_f (barn)	Covariance matrix ($\%^2$)			
TUD	^{235}U	2.6	1.214	3.41	2.44		
TUD			1.215		5.17		
TUD	^{235}U	8.5	1.801	6.12			
TUD	^{239}Pu	14.7	2.377	0.92	0.62	0.24	0.24
TUD			2.394		1.02	0.24	0.24
RIL			2.309			1.60	0.65
RIL			2.349				3.64
TUD	^{237}Np	14.7	2.226	1.08	0.41	0.53	
RIL		14.7	2.214		3.26	0.82	
TUD		8.5	2.163			4.40	
RIL	^{233}U	14.7	2.254	4.00	2.02		
TUD			2.244		3.48		
RIL	^{242}Pu	14.7	2.125	2.90	1.49		
TUD			2.143		2.94		
RIL	^{238}U	14.7	1.171	3.98	0.38		
TUD			1.166		2.96		

Table 3

Mean values of the fission cross sections obtained by the separate analysis on different nuclides in comparison with the results of evaluations and the measurements employing TCAPM

Nuclide	σ_f (barn)	$\pm\Delta$	$\pm\Delta\sqrt{\chi^2/_{N-1}}$	Data of evaluations		Experimental results of other authors using TCAPM
^{233}U (14.7 MeV)	2.248	1.7 %	1.7 %	2.28 ± 4 % ENDL-76		
^{235}U (14.7 MeV)	2.086	0.9 %	0.9 %	2.101 ± 4 % ENDF-B/V		2.061 ± 0.039 [6]
						2.074 ± 0.030 [7]
^{235}U (8.5 MeV)	1.810	2.5 %	2.5 %	1.782 ± 3.5 % ENDF-B/V		
^{235}U (2.6 MeV)	1.214	1.8 %	1.8 %	1.259 ± 3% ENDF-B/V		
^{238}U (14.7 MeV)	1.168	1.4 %	1.4 %	1.180 ± 4.3 % ENDF-B/V		1.149 ± 0.025 [6]
^{237}Np (14.7 MeV)	2.224	1.0 %	1.0 %	2.179 ± 5 % INDC(FR)-42L	8	
^{237}Np (8.5 MeV)	2.163	2.0 %	2.0 %	2.165 ± 5% INDC(FR)-42L	8	
^{239}Pu (14.7 MeV)	2.361	0.8 %	1.2 %	2.343 ± 5 % INDC(CCP)-166	8	2.310 ± 0.021 [6]
^{242}Pu (14.7 MeV)	2.134	1.5 %	1.5 %	2.15 ± 5.5 % INDC(CCP)-150	8	

Table 4

Mean values of the fission cross sections obtained by the analysis on the complete set of measurements together with their covariance matrix

Nuclide	σ_f (barns)	Covariance matrix										
^{235}U (14.7 MeV)	2.087	274*	161	159	92	77	83	89	127	67	71	78
^{235}U (14.5 MeV)	2.097		1040	160	61	53	53	64	75	50	52	75
^{235}U (14.0 MeV)	2.078			1020	60	53	52	64	74	50	52	74
^{235}U (8.5 MeV)	1.804				1210	260	40	34	74	170	43	32
^{235}U (2.6 MeV)	1.221					307	36	30	53	38	32	30
^{239}Pu (14.7 MeV)	2.360						304	90	140	87	76	72
^{237}Np (14.7 MeV)	2.221							417	110	197	75	74
^{233}U (14.7 MeV)	2.243								1190	115	87	120
^{237}Np (8.5 MeV)	2.165									1570	76	47
^{242}Pu (14.7 MeV)	2.134										910	46
^{238}U (14.7 MeV)	1.167											212

* read as $274 \cdot 10^{-6}$ (barn)^2

NBS MEASUREMENTS OF THE ^{235}U FISSION CROSS SECTION

A. D. Carlson

National Bureau of Standards

Washington, DC 20234 USA

The neutron standards program at the National Bureau of Standards has focused much of its attention on measurements of the ^{235}U fission cross section. In this paper the results of the various experiments performed at the NBS linac, Van de Graaff and ^{252}Cf facilities will be reviewed.

The first differential measurements of the $^{235}U(n,f)$ cross section were made at the linac neutron time-of-flight facility (Wasson 1976). These data were measured relative to the hydrogen scattering cross section using a hydrogen gas proportional counter (Wasson 1978). For these data, as well as all subsequent differential measurements, computer based two-parameter (pulse height and time-of-flight) data acquisition systems were employed. The measurements cover the energy region from 5 to 800 keV neutron energy. These shape data which were obtained with a 200 m flight path were normalized to a second experiment performed with a 23 m flight path. This experiment, which used a ^{6}Li glass flux detector, relies on the 7.8 to 11.0 eV energy interval for the cross section normalization. A change in the evaluated value of the cross section in this interval combined with small corrections to the original analysis of these experiments are discussed in the Appendix of (Wasson 1982b). The final cross section determinations from this investigation are shown in Fig. 1. The total uncertainties (statistical and systematic) are about 3% Also shown is the ENDF/B-V evaluation (Bhat 1979, Poenitz 1979) The evaluation is systematically ~ 2.5% higher than these data.

Measurements which cover the energy region from 0.2 to 1.2 MeV and, therefore, overlap much of the NBS linac data were also made at the NBS Van de Graaff facility (Wasson 1982b). For these determinations the fission rate measurements were made with the same fission chamber used in the linac experiment. However, for this work the mass of the ^{235}U deposits in the chamber was determined so that the cross section measurements could be made absolute. The ^{235}U mass was established relative to a well characterized NBS reference deposit by using fission counting in a thermalized neutron beam (Wasson 1981). By measuring the mass in this manner, problems due to surface conditions of the foils and uncertainty in the range of the fission fragments are simplified. Corrections are made for fission fragment absorption, but due to the normalization to the standard deposit mass, only the change in the absorption between the energy of interest and thermal is important. For these measurements this change is very small.

The neutron flux was measured with a black neutron detector. Monte Carlo calculations of the efficiency of this detector were verified experimentally (Meier 1977) for neutron energies below 900 keV using a $T(p,n)^3He$ associated particle spectrometer. Cross section measurements were made with two different sizes of collimators preceding this detector. The results for the two collimators agree well within their statistical uncertainties. The final data for this experiment are shown in Fig 2. Total uncertainties for all the measurements are ≈ 2 3%. The ENDF/B-V evaluation which is also shown is systematically ~ 2 3% higher than these measurements. Figure 3 shows a comparison of the NBS linac and Van de Graaff measurements They are in excellent agreement in the region of overlap Recent absolute measurements of the ^{235}U fission cross section from other laboratories compared with the ENDF/B-V evaluation are shown in Fig. 4. The NBS linac and Van de Graaff results are near the data of (Poenitz 1974, 1977) and (Szabo 1976).

Measurements of the shape of the cross section (Carlson 1978) have been made in the MeV energy region relative to the hydrogen scattering cross section with an annular proton telescope. The data have uncertainties of 2-3%. Several thicknesses of polyethylene film were used in the telescope in order to cover the total energy range from ~ 1 to 20 MeV with acceptable pulse height resolution and count rate. These data were obtained at the 60 m station of the linac facility. A fission chamber was used as the reaction rate detector.

Since only the shape of the ^{235}U fission cross section was measured, special care was taken to investigate effects which could affect this shape. The complete results of this investigation are given in (Carlson 1978). One of the special tests which was part of this work was to determine if linac associated gain shifts or baseline shifts for either of the detectors were affecting the electronic systems. The time dependence of such shifts was investigated using measurements made with and without a radioactive source near the detector which was in the linac produced neutron beam. The difference between the counting rates from these two runs is the constant rate of the radioactive source modified by the gain or baseline shifts. The radioactive sources used were a ^{252}Cf neutron source for the fission chamber and an ^{241}Am α source for the solid state detector used in the proton telescope. For both detectors there was no indication of shifts within the statistical accuracy of the measurements. One remaining concern is about the time walk of the proton telescope system. The measurements of this walk may not be exactly appropriate since an alpha particle source or pulser is used instead of proton recoils. Investigations are underway to test the quality of the walk corrections by a check of the consistency of the energy scale. The walk correction has limited the range of data reported to 1-6 MeV. These data are compared with the measurements of (Poenitz 1977) and (Szabo 1976) and the ENDF/B-V evaluation in Fig. 5. The present measurements have been normalized to ENDF/B-V at 1.2 MeV. An interesting feature is the lower approximately consistent cross section from ~ 3 to 4 MeV for these three sets of measurements. In Fig. 6 recent measurements from other laboratories are compared with the present values from 1-5 MeV neutron energy. The region from ~ 3 to 4 MeV is seen to be a problem area where a very large spread in the measurements exists.

The NBS 14 MeV measurement was initiated at a time when 5% differences (Alkhazov 1976, Adamov 1977, Cancé 1978) existed in determinations of this cross section The measurement (Wasson 1982a) was made using the time correlated associated particle technique. To obtain the low energy deuteron beam of 250 keV, a shorting bar was used on the NBS Van de Graaff accelerator. The fission chamber used in the experiment employed two fission foils in back to back geometry whose areal densities had been measured relative to a reference deposit using thermal neutron fission counting The reference deposit, Los Alamos National Laboratory spare #1, has been very accurately characterized. As noted previously, uncertainties in the fission fragment absorption correction are reduced with this procedure since only the uncertainty in the change in the absorption correction from thermal to 14 MeV need be considered. The results of the NBS fission cross section measurement are shown in Fig. 7 compared with other time correlated associated particle measurements and ENDF/B-V. The 5% differences referred to earlier have been removed as a result of revisions of the (Alkhazov 1976) and (Adamov 1977) data The agreement among the measurements is excellent and they confirm the ENDF/B-V evaluation. It appears that the ^{235}U fission cross section is now known to < 1% near 14 MeV.

A determination of the ^{235}U fission cross section averaged over the ^{252}Cf spectrum has been made at the NBS ^{252}Cf facility. The results of this experiment have been reported by (Heaton 1976). A reanalysis of this measurement has recently been completed (Grundl 1983). The result of this work has been a small change in the value of the cross section, an increase of 0.9%. The new value of the cross section is 1216 mb (± 1.61%). The error reduction resulting from this analysis has been substantial, an rms reduction of about a factor of 2. This improvement results from

- An investigation of the absolute source strength of NBS-I which led to a reduction in the ^{252}Cf source strength uncertainty from 1.2% to 0.9%.
- A program to improve the mass scale which included various interlaboratory intercomparisons. This led to a reduction in fissionable deposit mass uncertainty from 1.3% to 0.7%.
- Monte Carlo calculations of neutron scattering in the fission chamber and deposit backing. The largest improvement was for the deposit backing where the reduction in uncertainty was from 0.8% to 0.2%.

In addition, a new experiment has been designed with the objective of reducing the uncertainty even further. Data taking has begun for this measurement (Schröder 1983).

Absolute measurements (Carlson 1983) have been made at the NBS linac facility using the same detectors employed in the work of Wasson (1982b). The data cover a larger energy region (0.3-3 MeV) with higher resolution than was possible with the earlier measurements. The fission chamber was located at the 69.5 m station and the black detector was at the 200 m station of the same flight path tube. Backgrounds for both detectors were reduced to negligible levels To eliminate background from neutrons that scatter from the black detector it was necessary to accumulate data in a one count per burst mode with a time window which included the highest energy neutrons from the linac target. With this condition neutrons which would have caused background, produce a pulse in the black detector and stop the accumulation of data for the remainder of that linac pulse, thus the background event is not recorded. This limitation requires a small diameter collimator before the black detector to reduce the counting rate and therefore the dead-time corrections. Also all black detector events were delayed so they occur later in time than the fission chamber events. This procedure eliminated the dead-time shadowing losses to the low rate fission events by the black detector events so that less time was required to obtain the required statistical accuracy of ~ 1%. The experimental data has been taken and analysis is nearly complete. At the present state of the analysis the results indicate values slightly lower than ENDF/B-V thus in agreement with the earlier NBS results (Wasson 1976, Wasson 1982b). In Fig 8 a portion of the present preliminary data are normalized to ENDF/B-V to facilitate a shape comparison with that evaluation. The agreement is good, however, more structure is observed near 1 MeV in the present measurements.

A new plastic scintillator detector (Dias 1983) has been designed and fabricated at NBS for fast neutron flux measurements. With this detector escape of proton recoils is eliminated experimentally and multiple scattering is kept low. The detector consists of two thin plastic scintillators optically separated from each other and independently coupled to photomultiplier tubes. The protons which escape from the first scintillator are detected by the second scintillator which is placed behind the first one. If there is a coincidence between the two scintillators, the linear outputs are added, otherwise only the output of the first scintillator is used. The response of this detector, called the dual thin scintillator (DTS), has been determined by Monte Carlo methods and compared with measurements using the associated particle technique.

As an application of this detector, an absolute measurement has been made of the ^{235}U fission cross section at the linac facility. The experimental conditions for this measurement were the same as those of (Carlson 1983) except the black detector has been replaced with the DTS detector. Data have been obtained from ~ 1-6 MeV and the analysis of these measurements is now in progress. A comparison of a portion of these preliminary data with the black detector measurements of (Carlson 1983) and ENDF/B-V is shown in Fig. 9. Each of the data sets has been multiplied by the same factor to normalize it to the ENDF/B-V evaluation. Thus the comparison of the two sets of measurements is absolute. The two data sets are in good agreement within their statistical uncertainties. Also, the agreement with the shape of ENDF/B-V is excellent.

The feasibility of a measurement of the ^{235}U fission cross section at 2.6 MeV using the associated particle technique is now being investigated. The NBS Van de Graaff with a shorting bar will produce 200 keV deuterons to be used with the $D(d,n)^3He$ reaction for this measurement. Experimental studies have indicated low count rates and concerns about the ultimate accuracy possible in this measurement. Further work is in progress to improve the conditions for this experiment.

The measurements summarized in this paper represent the effort at the National Bureau of Standards towards improving the state of knowledge of the ^{235}U neutron fission cross section. The use of various neutron sources, neutron flux detectors, fission detectors, and different techniques provides the redundancy of work required to understand the systematic errors in fission cross section measurements.

References

Adamov V. M., Alexandrov B. M., Alkhazov I. D., Drapchinsky L. V., Kovalenko S. S., Kostochkin O. I., Kudriavzev G. Y., Malkin L. Z., Petrzhak K. A., Pleskachevsky L. A., Fomichev A. V. and Shpakov V. I. (1977) "Absolute ^{235}U, ^{238}U and ^{237}Np Fast Neutron Fission Cross Section Measurements," in Proc. of the International Specialists Symposium on Neutron Standards and Applications, National Bureau of Standards (Eds. Bowman C. D., Carlson A. D., Liskien H. O. and Stewart L.), NBS Spec. Publ. 493, p. 313.

Adamov V. M., Alkhazov I. D., Gusev S. E., Drapchinsky L. V., Dushin V. N., Formichev A. V., Kovalenko S. S., Kostochkin I., Malkin L. Z., Petrzhak K. A., Pleskachevsky L. A., Shpakov V. I., Arlt R and Musiol G. (1980) "Absolute Measurements of Induced Fission Cross Sections of Heavy Nuclides for Both ^{252}Cf Fission Spectrum Neutrons and 14.7-MeV Neutrons" in Proc. of the Int. Conf. on Nuclear Cross Sections for Technology, Knoxville, TN, (Eds. Fowler J. L., Johnson C. H. and Bowman C. D.) NBS Spec. Publ. 594, p. 995.

Alkhazov I D., Kasatkin V. P., Kostochkin O I., Malkin L Z., Petrzhak K. A., Fomichev A. V., and Shpakov V. I. (1976) "Absolute Measurements of the ^{235}U Fission Cross Section by 14.8 MeV Neutrons," in Proc. of the 1975 Kiev Conf. Vol. 6, p. 9.

Arlt R., Meilung W., Musiol G., Ortlepp H -G., Teichner R , Wagner W., Alkhazov I. D., Kostochkin O. I., Kovalenko S. S., Petrzhak K. A. and Shpakov V. I. (1981a) Kernenergie 24, 48.

Arlt R., Heidrich H. V., Josch M., Musiol G., Ortlepp H. -G., Teichner R. and Wagner W. (1981b) "The Application of the Time Correlated Associated Particle Method (TCAPM) For Fission Cross Section Measurements at 2.6 MeV Neutron Energy" Technical University of Dresden (G.D.R.) Report, 05-22-81, also Kernenergie 25, 199.

Barton D. M., Diven B. C., Hansen G. E., Jarvis G. A., Koontz P. G. and Smith R. K. (1976), Nucl. Sci. Engng. 60, 369.

Bhat M. R. (1979) "ENDF/B-V Summary Documentation for ^{235}U," in ENDF-201 (BNL-17541) "ENDF/B Summary Documentation," Compiled by R. Kinsey.

Cancé M. and Grenier G. (1978) Nucl. Sci. Engng. 68, 197.

Cancé M. (1983) Private communication; Cance M., Gimat D., Grenier G. and Parisot D. (1980) "Measurement of Fission Cross Sections," CEA-N-2134 (INDC(FR) 38/L) p. 54.

Carlson A. D. and Patrick B. H. (1978) "Measurements of the ^{235}U Fission Cross Section in the MeV Energy Region" in Proc. of an Int. Conf. on Neutron Physics and Nuclear Data for Reactors and Other Applied Purposes, Harwell, p. 880.

Carlson A. D. and Behrens J. W. (1983) "Measurement of the $^{235}U(n, f)$ Cross Section From 0.3 to 3.0 MeV Using the NBS Electron Linac," in Proc. of the 1982 Antwerp Conf. on Nuclear Data for Science and Technology, ed. Böckhoff K. H., 456.

Davis M. C , Knoll G F., Robertson J C , and Gilliam D. M. (1978) Ann Nucl. Energy 5, 569

Dias M D , Johnson R. G., and Wasson O A (1983), "An Absolute Neutron Flux Detector for the 1-20 MeV Energy Region," in Proc of the 1982 Antwerp Conf on Nuclear Data for Science and Technology, (Ed Böckhoff K H), Reidel Publishing Co., p. 875

Grundl J. A. and Gilliam D. M. (1983) Trans. Am Nucl Soc 44, 533.

Heaton H. T., Gilliam D. M., Spiegel V , Eisenhauer C and Grundl J. A (1976) "Fission Cross Sections of ^{235}U, ^{238}U and ^{239}Pu Averaged Over the ^{252}Cf Neutron Spectrum" in Proc. of the NEANDC/NEACRP Specialists Meeting on Fast Fission Cross Sections of U-233, U-235, U-238 and Pu-239, Argonne National Laboratory, (Eds. Poenitz W. P. and Smith A. B.) ANL-76-90, p. 333.

Kaeppeler F. (1974) "Measurement of the Neutron Fission Cross Section of ^{235}U Between 0.5 and 1.2 MeV" in Proc. of a panel on Neutron Standard Reference Data, Vienna, IAEA-PL-246-2/27, p. 213.

Kari K. (1978) "Messung der Spaltquerschnitte von ^{239}Pu und ^{240}Pu relativ zum Spaltquerschnitt von ^{235}U und Streuquerschnitt H(n,p) in dem Neutronenenergiebereich zwischen 0.5-20 MeV, Karlsruhe (Germany) report KFK-2673.

Leugers B., Cierjacks S , Brotz P , Erbe D., Groeschel D , Schmalz G and Voss F (1976) "The U-235 and U-238 Neutron Induced Fission Cross Sections Relative to the H(n,n) Cross Section" in Proc of the NEANDC/NEACRP Specialists Meeting on Fast Neutron Fission Cross Sections of U-233, U-235, U-238 and Pu-239, Argonne National Laboratory, (Eds. Poenitz W P. and Smith A B) ANL-76-90, p. 246.

Li Jingwen, Li Anli, Rong Chaofan, Ye Zhongyuan, Wu Jingxia and Hao Xiuhong (1983) "Absolute Measurements of ^{235}U and ^{239}Pu Fission Cross Section Induced by 14.7 MeV Neutrons" in Proc. of the 1982 Antwerp Conf. on Nuclear Data for Science and Technology, ed. Böckhoff K. H., 55.

Meier, M. M. (1977) "Associated Particle Methods" in Proc. of the International Specialists Symposium on Neutron Standards and Applications, National Bureau of Standards (Eds. Bowman C. D., Carlson A. D., Liskien H. O. and Stewart L.), NBS Spec. Publ. 493, p. 221.

Poenitz W. P (1974) Nucl. Sci. Engng. 53, 370.

Poenitz W. P. (1977) Nucl. Sci. Engng. 64, 894.

Poenitz W. P. (1979) "Evaluation of ^{235}U(n,f) Between 100 keV and 20 MeV," USDOE document ANL/NDM-45.

Schröder I. G. (1983) private communication.

Smith R. K., Henkel R. L. and Nobles R. A. (1957) Bull. Am. Phys. Soc. 2, 196, revised by Hanson G. E. (1975), Private communication from Stewart L. (1978).

Szabo I. and Marquette J. P. (1976) "Measurement of the Neutron Induced Fission Cross Sections of Uranium-235 and Plutonium-239 in the MeV Energy Range" in Proc. of the NEANDC/NEACRP Specialists Meeting on Fast Neutron Cross Sections of U-233, U-235, U-238 and Pu-239, Argonne National Laboratory (Eds. Poenitz W. P. and Smith A. B.) ANL-76-90, p. 208.

Wasson O. A. (1976) "The ^{235}U Neutron Fission Cross Section Measurement at the NBS Linac" in Proc. of the NEANDC/NEACRP Specialists Meeting on Fast Neutron Fission Cross Sections of U-233, U-235, U-238 and Pu-239, Argonne National Laboratory (Eds. Poenitz W. P. and Smith A. B.) ANL-76-90, p. 183, see also Wasson (1982b).

Wasson O. A., Schrack R. A. and Lamaze G. P. (1978) Nucl. Sci. Engng. 68, 170.

Wasson O. A. and Meier M. (1981) Nucl. Instr. Meth. 190, 571.

Wasson O. A., Carlson A. D. and Duvall K. C. (1982a) Nucl. Sci. Engng. 80, 282.

Wasson O. A., Meier M. M. and K. C. Duvall (1982b) Nucl. Sci. Engng. 81 196.

White P. H. (1965) J. Nucl. Energy 19, 325.

Figures

Fig. 1. Comparison of the Wasson (1976) ^{235}U fission cross section measurements with the ENDF/B-V evaluation. The statistical and total uncertainties are indicated for each data point by the small and large error bars, respectively.

Fig. 2. Comparison of the Wasson (1982b) ^{235}U fission cross section measurements with the ENDF/B-V evaluation. The statistical and total uncertainties are indicated for each data point by the small and large error bars, respectively.

Fig. 3. Comparison of the Wasson (1976) and Wasson (1982b) ^{235}U fission cross section measurements. The statistical and total uncertainties are indicated for each data point by the small and large error bars, respectively. The ENDF/B-V evaluation is also shown.

Fig. 4. Comparison of recent absolute measurements of the ^{235}U fission cross section from other laboratories. The ENDF/B-V evaluation is also shown.

Fig. 5. Comparison of the Szabo (1976), Poenitz (1977) and Carlson (1978) ^{235}U fission cross section measurements. The ENDF/B-V evaluation is also shown.

Fig. 6. Comparison of recent measurements of the ^{235}U fission cross section for neutron energies from 1 to 5 MeV. The ENDF/B-V evaluation is also shown.

Fig. 7. Measurements of the ^{235}U fission cross section near 14 MeV using the time correlated associated particle technique. The ENDF/B-V evaluation is also shown.

Fig. 8. Preliminary measurements of the ^{235}U fission cross section by Carlson (1983). The data have been normalized to the ENDF/B-V evaluation. The error bars are statistical standard deviations.

Fig. 9. Comparison of the Carlson (1983) and Dias (1983) ^{235}U fission cross section measurements. The error bars are statistical standard deviations. The data sets have been normalized to the ENDF/B-V evaluation.

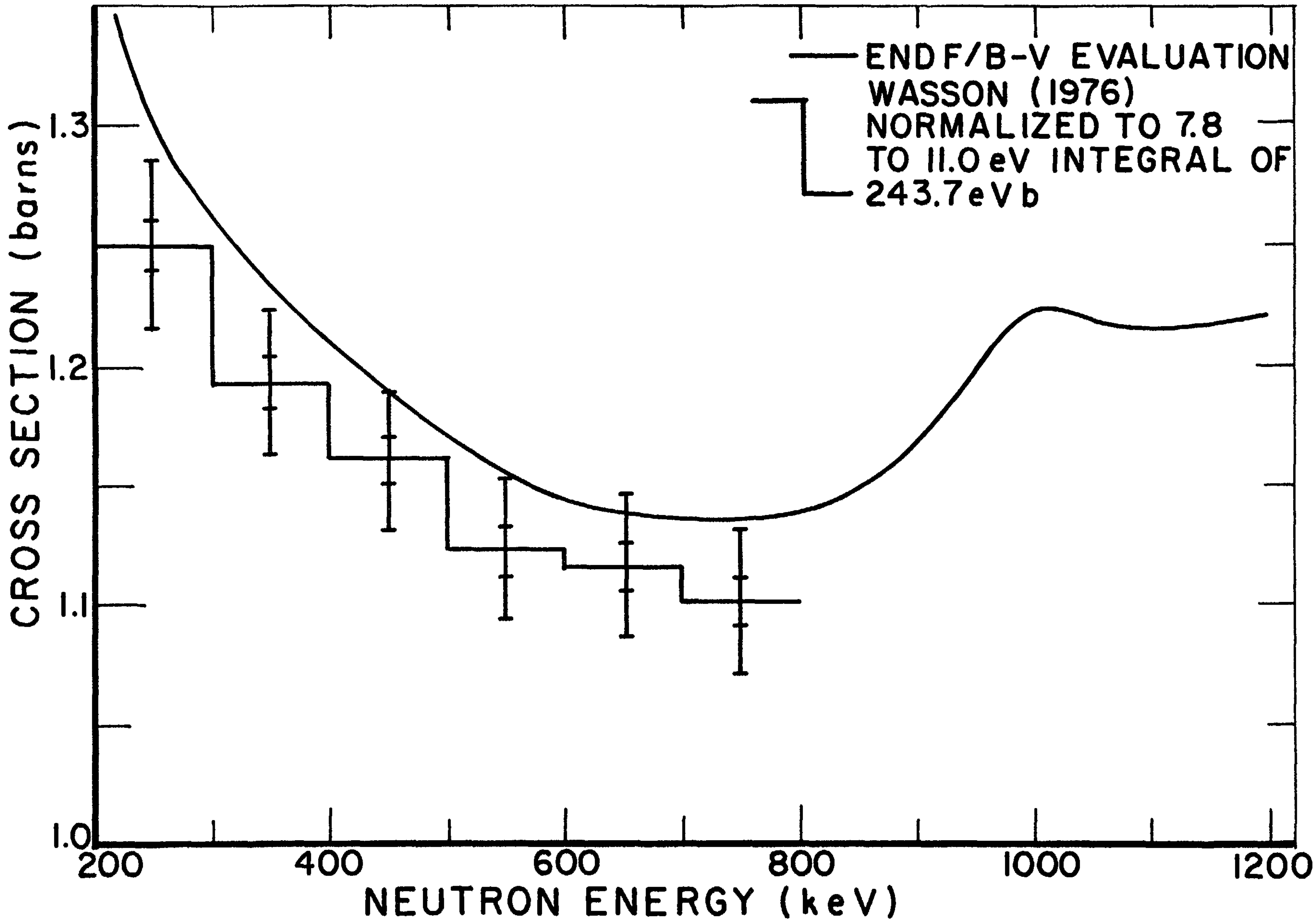

ENDF/B-V EVALUATION
WASSON (1976)
NORMALIZED TO 7.8
TO 11.0 eV INTEGRAL OF
243.7 eV b
CROSS SECTION (barns)
1.3
1.2
1.1
1.0
200
400
600
800
1000
1200
NEUTRON ENERGY (keV)

FIG. 1

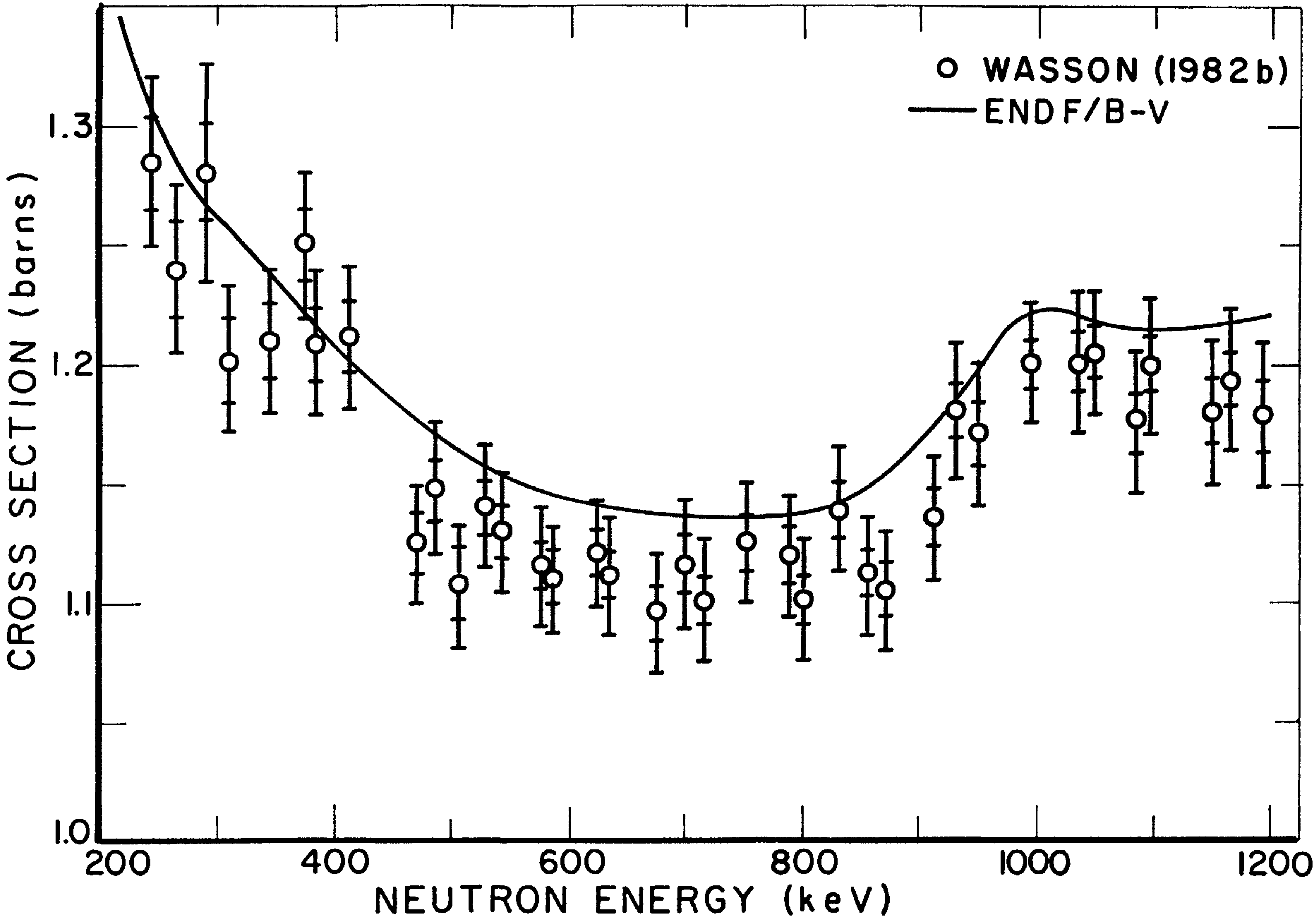

WASSON (1982b)
ENDF/B-V
1.3
1.2
1.1
1.0
CROSS SECTION (barns)
200
400
600
800
1000
1200
NEUTRON ENERGY (keV)

FIG. 2

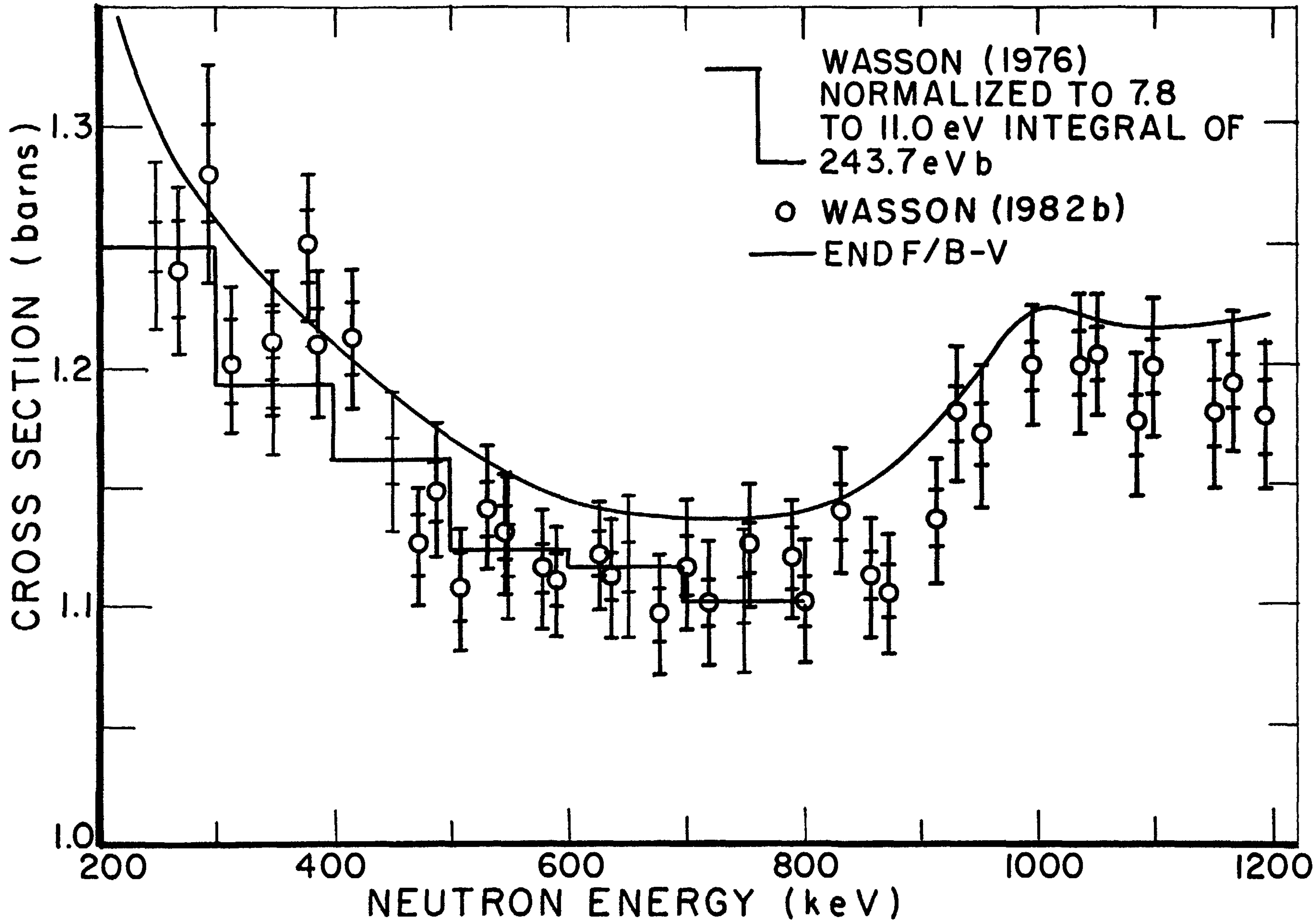
WASSON (1976)
NORMALIZED TO 7.8
TO 11.0 eV INTEGRAL OF
243.7 eV b
o WASSON (1982b)
ENDF/B-V
CROSS SECTION (barns)
1.3
1.2
1.1
1.0
200
400
600
800
1000
1200
NEUTRON ENERGY (keV)

FIG. 3

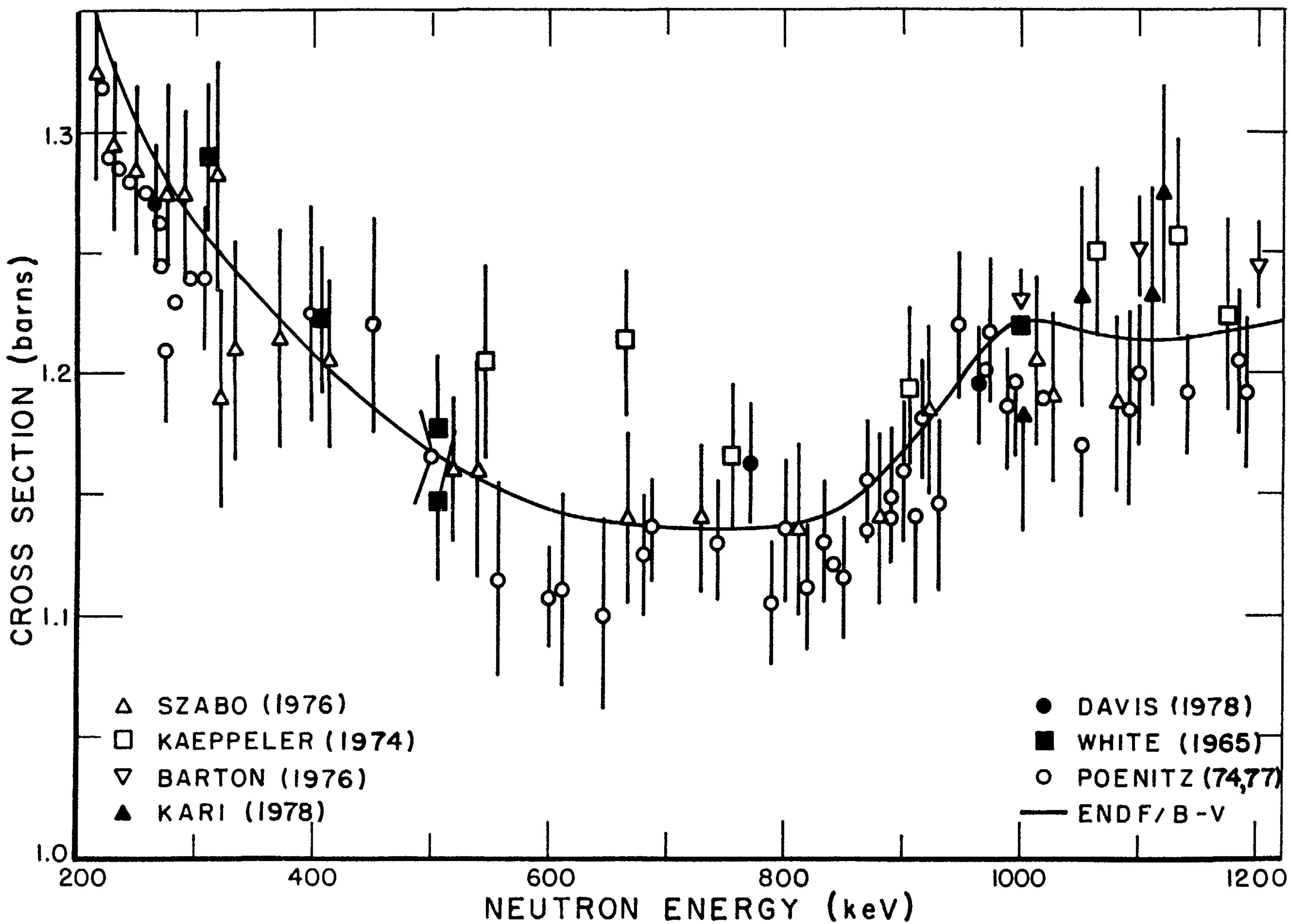
CROSS SECTION (barns)
1.0
1.1
1.2
1.3
200
400
600
800
1000
1200
NEUTRON ENERGY (keV)
SZABO (1976)
KAEPPELER (1974)
BARTON (1976)
KARI (1978)
DAVIS (1978)
WHITE (1965)
POENITZ (74,77)
ENDF/B-V

FIG. 4

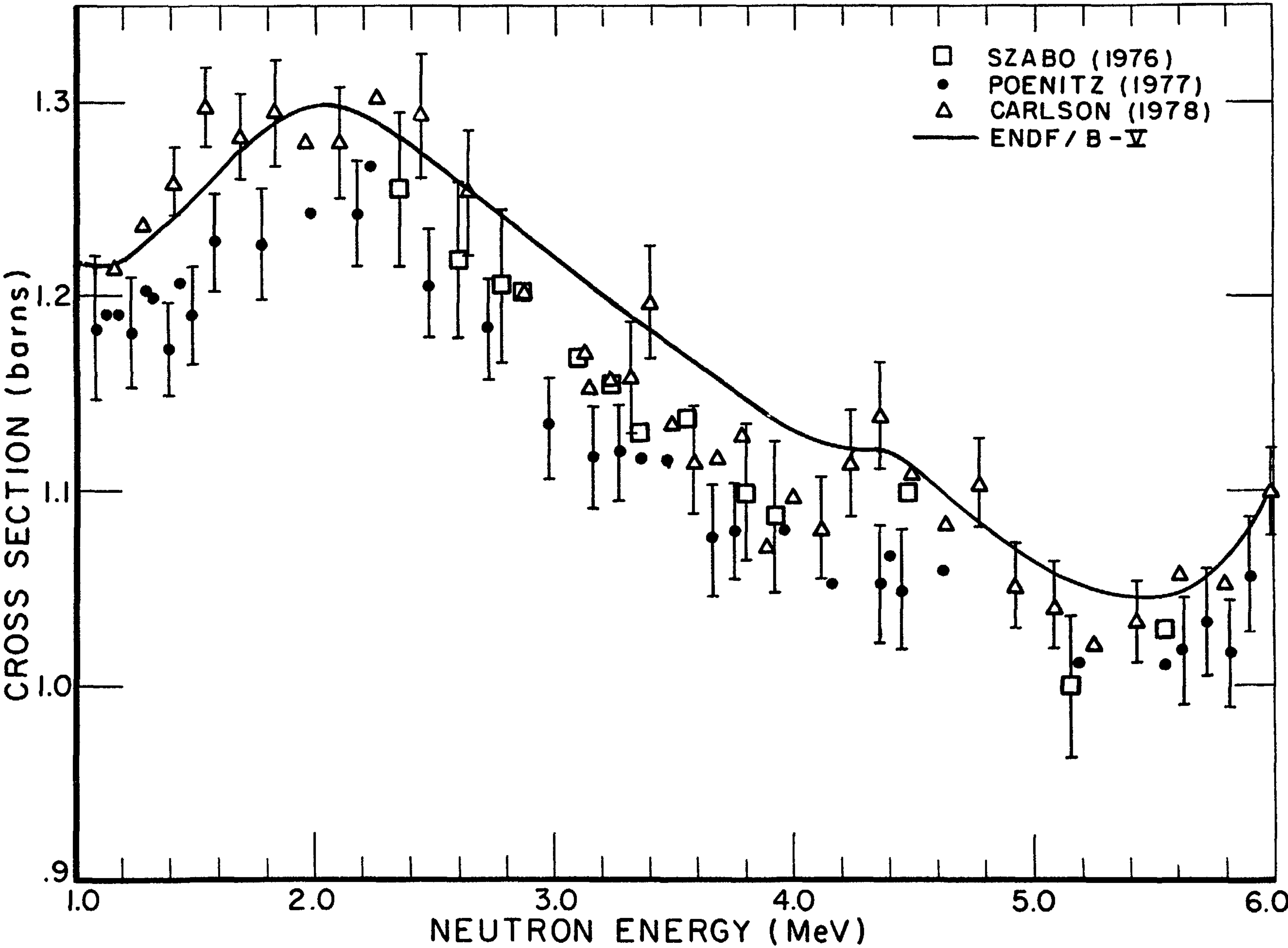
SZABO (1976)
POENITZ (1977)
CARLSON (1978)
ENDF/B-V
CROSS SECTION (barns)
1.3
1.2
1.1
1.0
.9
1.0
2.0
3.0
4.0
5.0
6.0
NEUTRON ENERGY (MeV)

FIG. 5

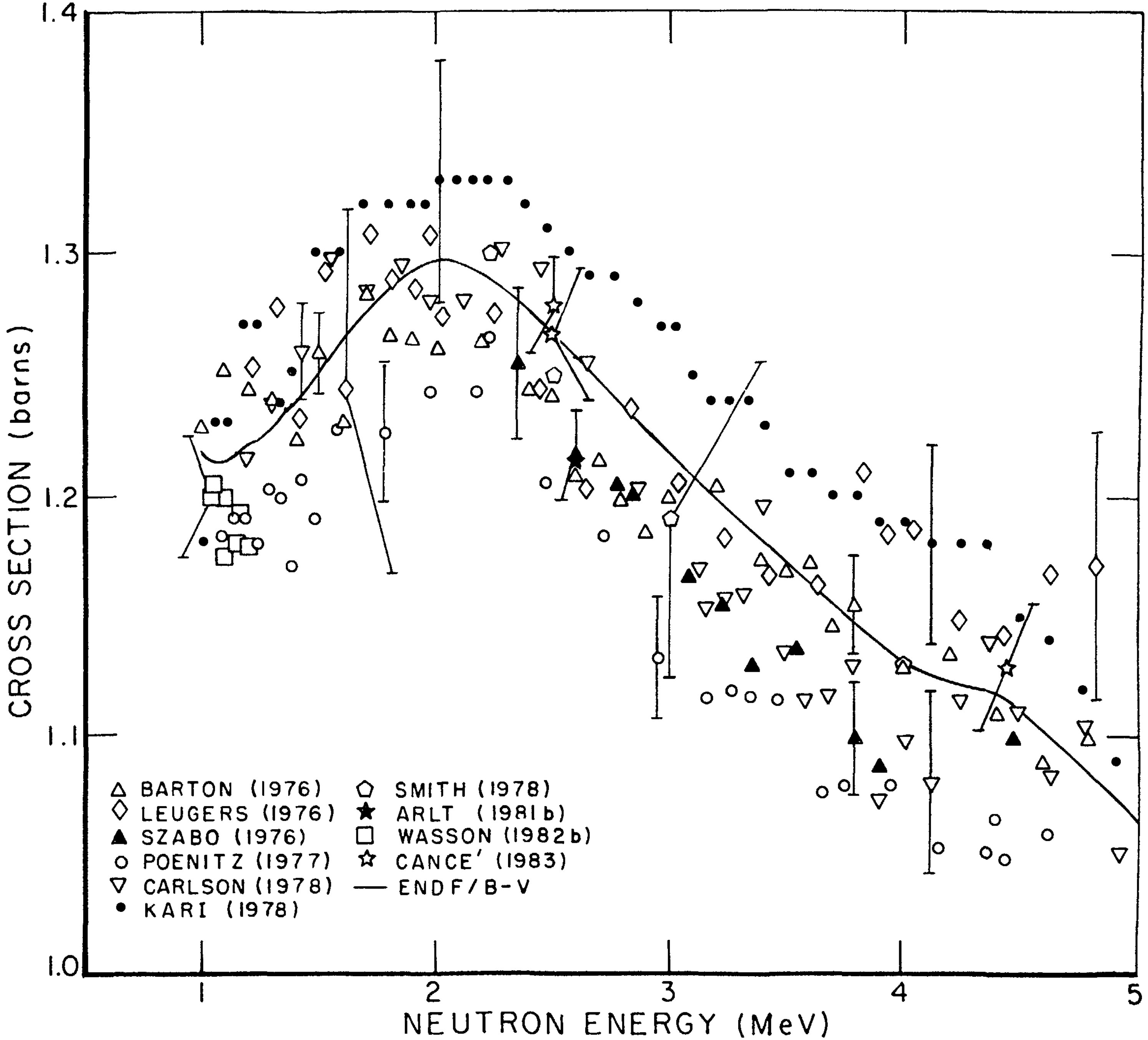
CROSS SECTION (barns)
NEUTRON ENERGY (MeV)
1.4
1.3
1.2
1.1
1.0
1
2
3
4
5
BARTON (1976)
LEUGERS (1976)
SZABO (1976)
POENITZ (1977)
CARLSON (1978)
KARI (1978)
SMITH (1978)
ARLT (1981b)
WASSON (1982b)
CANCE' (1983)
ENDF/B-V

FIG. 6

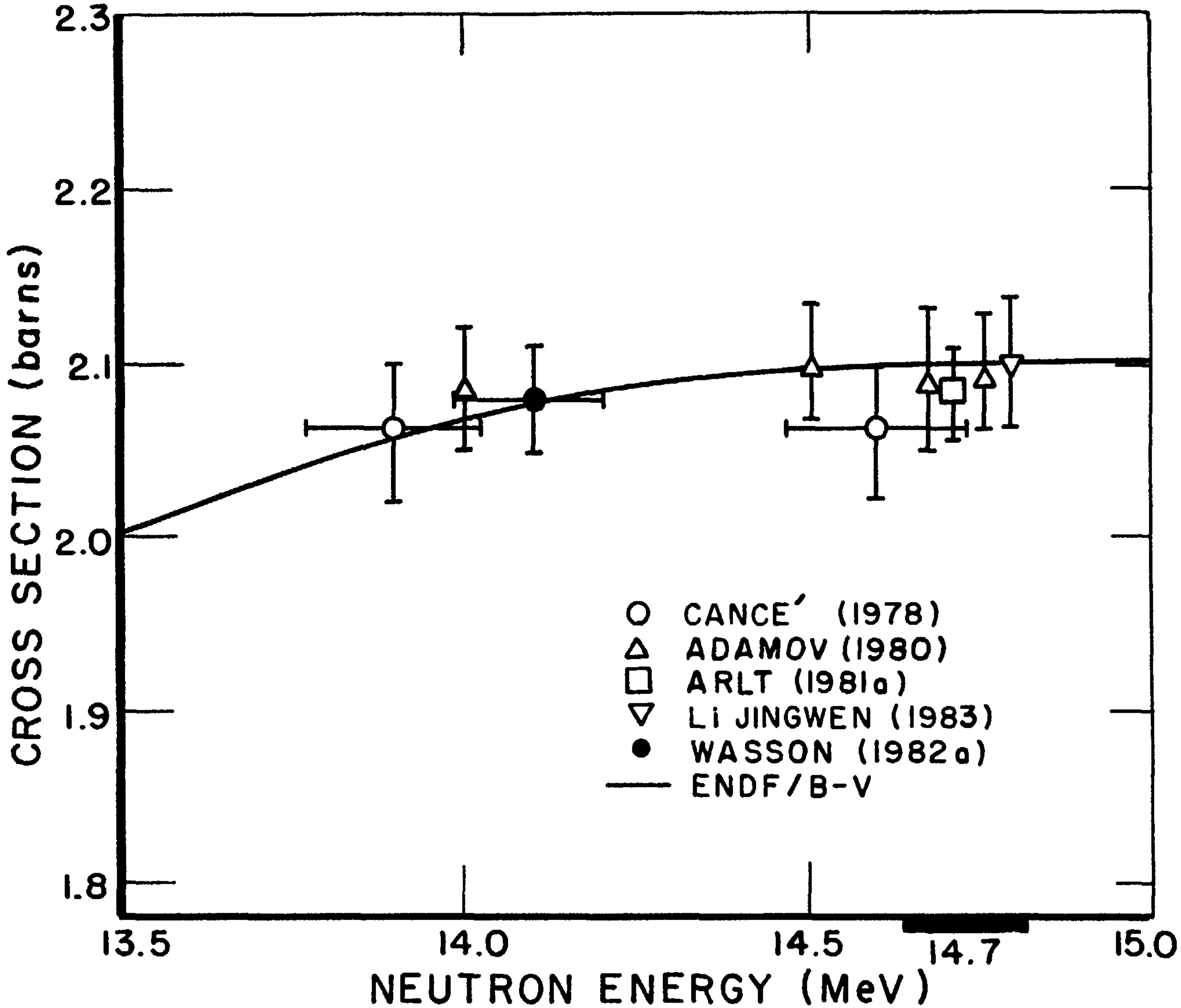

2.3
2.2
2.1
2.0
1.9
1.8
CROSS SECTION (barns)
13.5
14.0
14.5
14.7
15.0
NEUTRON ENERGY (MeV)
CANCE´ (1978)
ADAMOV (1980)
ARLT (1981a)
Li JINGWEN (1983)
WASSON (1982a)
ENDF/B-V

FIG. 7

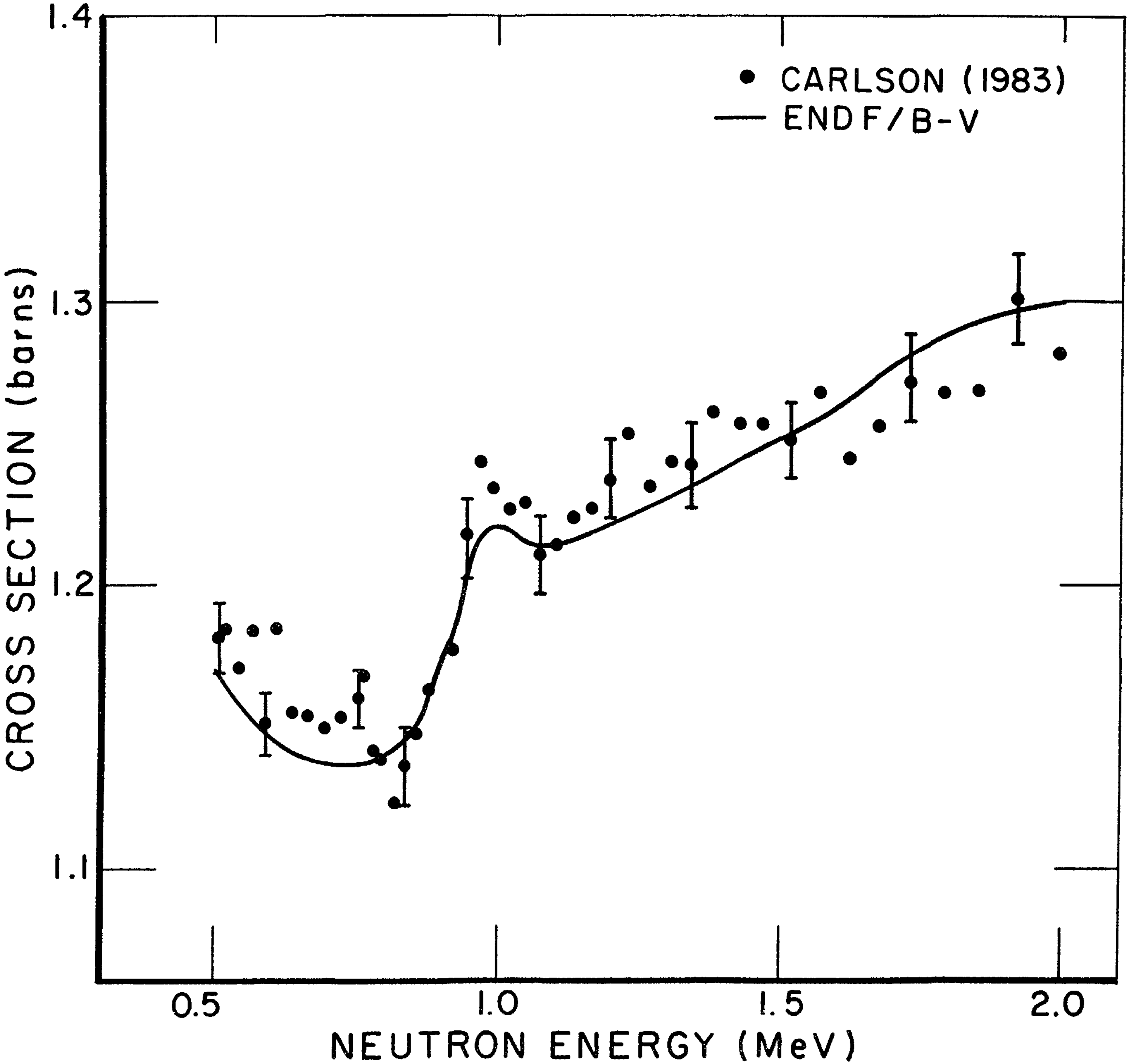
CARLSON (1983)
ENDF/B-V
1.4
1.3
1.2
1.1
CROSS SECTION (barns)
0.5
1.0
1.5
2.0
NEUTRON ENERGY (MeV)

FIG. 8

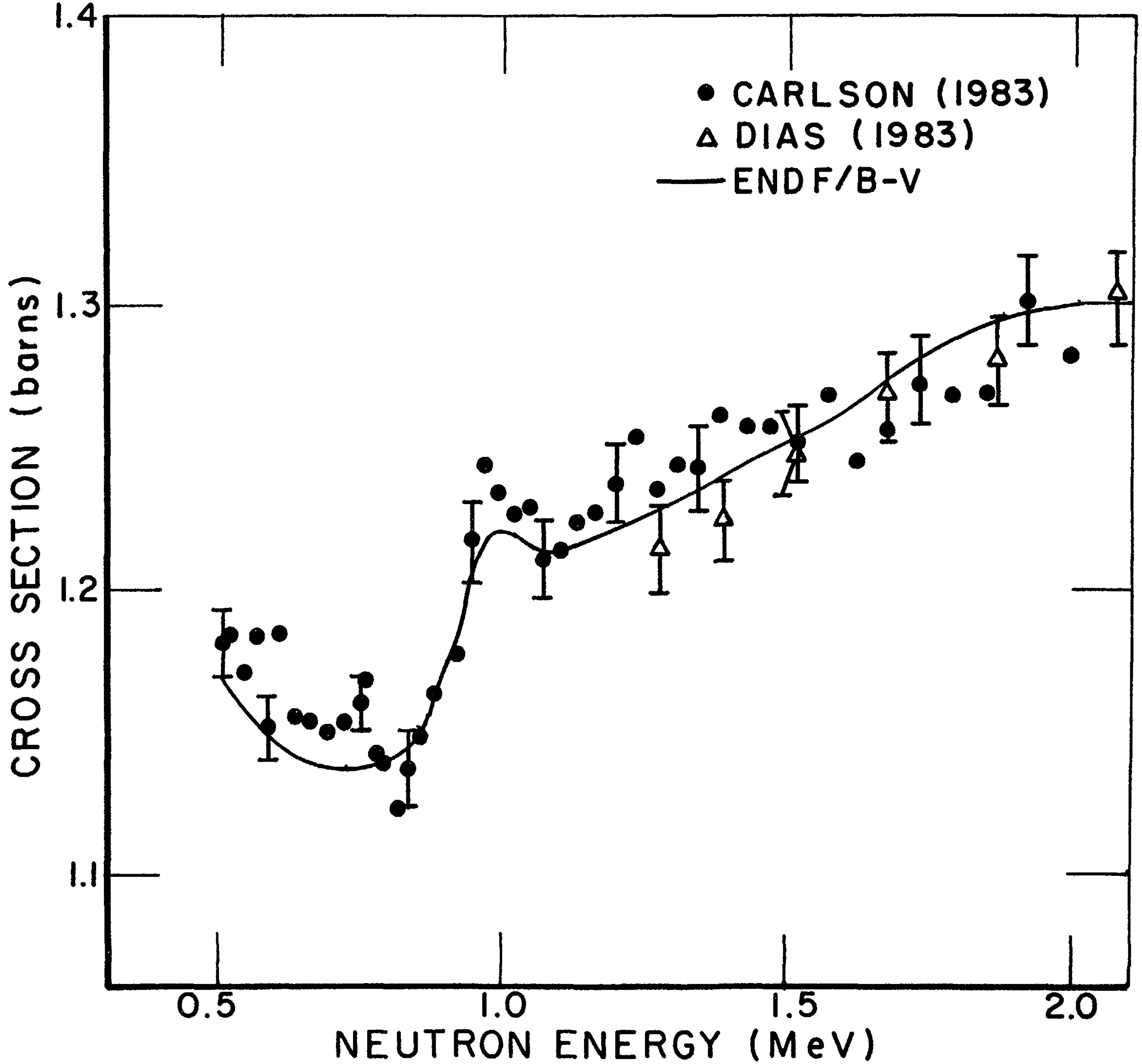
1.4
1.3
1.2
1.1
CROSS SECTION (barns)
0.5
1.0
1.5
2.0
NEUTRON ENERGY (MeV)
CARLSON (1983)
DIAS (1983)
ENDF/B-V

FIG. 9

Invited paper presented at the IAEA Consultants Meeting on "The Uranium-235 Fast-Neutron Fission Cross Section", Smolenice, Czechoslovakia, 28 March - 1 April 1983

FISSION CROSS-SECTION NORMALIZATION PROBLEMS

C. Wagemans*
SCK-CEN, B-2400 MOL and
Nuclear Physics Lab., B-9000 GENT
Belgium

and

A.J. Deruytter
C.E.C. Joint Research Centre
CBNM, B-2440 GEEL
Belgium

* NFWO

INTRODUCTION

Before discussing the fission cross-section normalization problems it is useful to first recall their origin(s). What the measuring society wants to achieve is to determine the $^{235}U(n,f)$ cross-section with 1% accuracy from almost 0 to 20 MeV neutron energy. Two major problems make this hard to realise: First no single neutron source covers the whole energy region of interest, and secondly no single neutron flux detector does so. Hence one has to work with partial measurements which have to be joined together, causing normalization and cross-normalization problems. This is especially true for the shape measurements, in which the shape of the $^{235}U(n,f)$ cross-section is measured relative to that of a reference cross-section ($^{10}B(n,\alpha)$, $^{6}Li(n,\alpha)$, H(n,n'), ...). Such measurements have to be normalized to absolute fission cross-section values, which, however, are only available for a limited number of neutron energies (mainly in the thermal region and between 0.1 and 14 MeV). Ideally all fission cross-section measurements should be normalized in the thermal region, since here one combines at the same time large cross-section values and an isotropic emission of the fission fragments with the availability of very high neutron fluxes. So thin samples can be used, which reduces several experimental uncertainties such as self-absorption, scattering, energy loss etc. As a consequence of these excellent experimental conditions, the (absolute) thermal fission cross-section of ^{235}U can be determined with an accuracy of $\leq 1\%$ (e.g. ref. 1). At higher neutron energies (≥ 100 keV), the accuracy of the absolute fission cross-section measurements is typically 2-3%, with the exception of the 14 MeV region where the favourable kinematics of the $^{3}H(d,\alpha)n$ neutron source enables a 1.5% accuracy (ref. 2). Another reason for the high accuracy achieved in (ref. 2) was the thorough check of samples and detectors with a thermal neutron beam. We strongly recommend such a procedure for all absolute measurements in the high energy region. A thermal neutron beam is indeed a powerful tool for checking targets and detectors and for resolving discrepancies between different targets (detectors). A typical example for the latter application can be found in (ref. 3).

THE USE OF NORMALIZATION INTEGRALS

For various reasons it is often not possible to normalize a fission cross-section shape measurement in the thermal region. This is illustrated in Table 1. Out of 11 measurements performed before 1970, only one (ref. 2) is directly, and three others (refs. 4, 7, 8) are indirectly normalized in the thermal region. Moreover, some of the normalization methods reported

Table 1 COMPARISON OF THE NORMALIZATION METHODS APPLIED IN THE OLDER σ_f MEASUREMENTS OF ^{235}U (before 1970).

SHORE and SAILOR (4)	σ_f normalized to the data of LEONARD (unpublished) in the region 0.1-0.4 eV which are normalized at 0.0253 eV to (582±10) barn (two-step normalization).
MICHAUDON (5)	σ_f normalized to $\int_{8\ eV}^{10\ eV} \sigma_f(E)dE = 208.47$ barn.eV obtained by SHORE and SAILOR.
MICHAUDON et al. (6)	σ_f normalized to $\int_{0.4\ eV}^{1.3\ eV} \sigma_f(E)dE$ obtained by SHORE and SAILOR.
IGNATIEV et al. (7)	σ_f deduced from measurements of σ_t and η, assuming $\sigma_s = \frac{22}{(E+2.3)^2} + 11$ (σ_s in barn, E in eV) and normalized to η=2.07 at 0.0253 eV. Indirect method.
RYABOV et al. (8)	σ_f normalized to $\sigma_f{}^{\circ}$= (582±6 barn). The lowest data point given by the author is 0.15 eV. The error introduced by the normalization is 5 per cent.
BOWMAN et al. (9)	σ_f normalized at 0.0253 eV to the least squares value of (577.1±0.9)barn reported in BNL 325, suppl.2.
BROOKS et al. (10)	σ_f calculated via $\eta = \frac{\bar{\nu}\sigma_f}{\sigma_t - \sigma_s}$ and normalized at 0.06 eV by putting η= 2.084 assuming $\bar{\nu}$= 2.42. Indirect method
MOSTOVAYA et al. (11)	σ_f normalized to the averaged fission cross-section curve given in BNL 325 in the region 0.8-0.9 eV.
DE SAUSSURE et al. (12)	σ_f normalized by making the resonance integral $\int_{0.45\ eV}^{10\ eV} \sigma_f(E)\frac{dE}{E}$ equal to 127.9 barn (average of the results of SHORE and SAILOR and BOWMAN).
CAO et al. (13)	σ_f normalized to $\int_{8\ eV}^{10\ eV} \sigma_f(E)dE = 208.47$ barn eV obtained by SHORE and SAILOR.
BLONS et al. (14)	σ_f normalized to the integrated fission cross-section from 60-200 eV from MICHAUDON. Indirect normalization.

Table 2 COMPARISON OF FLUX DETERMINATION AND NORMALIZATION METHODS APPLIED IN THE QUOTED σ_f-MEASUREMENTS OF ^{235}U (AFTER 1970)

Authors	Neutron Flux Determination	Normalization	Corresponding $\sigma_f{}^*$ (barn)
De Saussure (15)	$^{10}B(n,\alpha)$	$\int_{7.8\ eV}^{11\ eV} \sigma_f(E)dE$ = 240 barn.eV (Deruytter and Wagemans, 16)	587.6
Deruytter and Wagemans (16)	$^{10}B(n,\alpha)$	$\int_{0.02060\ eV}^{0.06239\ eV} \sigma_f(E)dE$ = 19.27 ± 0 08 barn.eV (Deruytter et al., 1)	587.9
Silver et al. (17)	$^{10}B(n,\alpha)$	σ_f of De Saussure et al. (12) between 100 and 200 eV	577.1
Lemley et al. (18)	$^{6}Li(n,\alpha)$	σ [$^{6}Li(n,\alpha)$]	
Blons (19)	$^{10}B(n,\alpha)$	$\int_{100\ eV}^{200\ eV} \sigma_f(E)dE$ = 2103 barn.eV (De Saussure, 15)	587.6
Gayther et al. (20)	Calibrated boron-vaseline plug	$\bar{\sigma}_f$ = 2.349 barn in the interval 10-30 keV (Soverby, 32)	580.2
Perez et al. (21)	$^{10}B(n,\alpha)$	$\int_{100\ eV}^{200\ eV} \sigma_f(E)dE$ = 2103 barn.eV (De Saussure, 15)	587.6
Perez et al. (22)	$^{10}B(n,\alpha)$	$\int_{2\ keV}^{10\ keV} \sigma_f(E)dE$ = 31.643 barn keV (Perez et al., 21)	
Czirr et al. (23)	$^{6}Li(n,\alpha)$	σ_f = 585 4 barn	585.4
Wasson (24)	$^{6}Li(n,\alpha)$	$\int_{7.8\ eV}^{11\ eV} \sigma_f(E)dE$ = 238.4 barn eV	(583.5)
Gwin et al. (25)	$^{10}B(n,\alpha)$	σ_f of ENDF-B III between 0.02-0.4 eV	580.2
Wagemans and Deruytter (26)	$^{10}B(n,\alpha)$ [$^{6}Li(n,\alpha)$]	$\int_{7.8\ eV}^{11\ eV} \sigma_f(E)dE$ = 240 barn.eV	587.6
Czirr et al. (27)	$^{6}Li(n,\alpha)$	$\int_{0.02\ eV}^{0.1\ eV} \sigma_f(E)dE$ of Leonard (33)	585.4
Muradjan et al. (28)	$^{10}B(n,\alpha)$	$\int_{100\ eV}^{1000\ eV} \sigma_f(E)dE$ = 12 209 barn.eV	
Moore et al. (29)	$^{6}Li(n,\alpha)$	$\int_{7.8\ eV}^{11\ eV} \sigma_f(E)dE$ = 241 2 barn.eV	583.5
Wagemans et al. (30)	$^{10}B(n,\alpha)$ $^{6}Li(n,\alpha)$ *	$\int_{0.0206\ eV}^{0.06239\ eV} \sigma_f(E)dE$ = 19 26 ± 0.08 barn.eV (Deruytter et al , 1)	587.6
Corvi et al. (31)	$^{6}Li(n,\alpha)$	$\int_{7.8\ eV}^{11\ eV} \sigma_f(E)dE$ = 241.2 barn eV	583.5
This work	$^{6}Li(n,\alpha)$	$\int_{0.0206\ eV}^{0.06239\ eV} \sigma_f(E)dE$ = 19.26 barn eV	587.6

* up to 200 eV

in this table are peculiar and/or unreliable. Also for the more recent measurements reported in Table 2, only 6 out of 18 measurements are directly normalized in the thermal region.

For measurements not reaching the thermal region, the introduction of accurate secondary normalization integrals is very useful. Such integrals may also provide a link between absolute cross-section measurements at thermal and at higher neutron energies. In this context we proposed some years ago the fission integral $I_1 = \int_{7.8\,eV}^{11\,eV} \sigma_f(E)dE$, which is a rather favourable choice since it contains a large resonance, yielding a high counting rate and the signal to background ratio is good. Furthermore, since the cross-section values at its limits are small, this integral is not sensitive to bad resolution and small timing errors.

Another integral which may play a role as a secondary normalization integral is

$I_2 = \int_{0.1\,keV}^{1.0\,keV} \sigma_f(E)dE$, which should be especially useful for measurements not coming down to the eV-region.

Anyhow, these integrals should not be used blindly as is illustrated in Fig. 1. This figure shows the $^{10}B(n,\alpha)$ counting rate (for a constant time-of-flight channel width) in arbitrary units, as a function of the neutron energy (a) without an overlap filter, (b) with a cadmium overlap filter, (c) with a boron overlap filter. These data were obtained at the Geel linear accelerator GELINA. From this figure it is obvious that the neutron energy region from 100 to 1000 eV (I_2) is not suitable for normalization purposes for measurements using a Cd overlap filter, because of the presence of Cd transmission dips in this region. For measurements using a ^{10}B-overlap filter, the neutron flux in the eV-region is strongly reduced. In the example shown in Fig. 1c, about 85% of the 10eV-neutrons are absorbed in the overlap filter. So before normalizing such a measurement via I_1, one has to check the signal to background ratio in the 10eV energy region.

It is inherent to a good normalization that the final result does not depend on the normalization procedure used. E.g. normalizations via the integral I_1 or I_2 should be consistent. The large spread on the I_2-values reported in the literature (~7%) is problematic in this respect. One of the origins of these discrepancies is certainly the fact that most of the I_2 - values have been obtained via an indirect normalization procedure. Hence the first aim of a recently started series of experiments at the Geel linear accelerator was to determine I_1 and I_2 in one single experiment, directly normalized

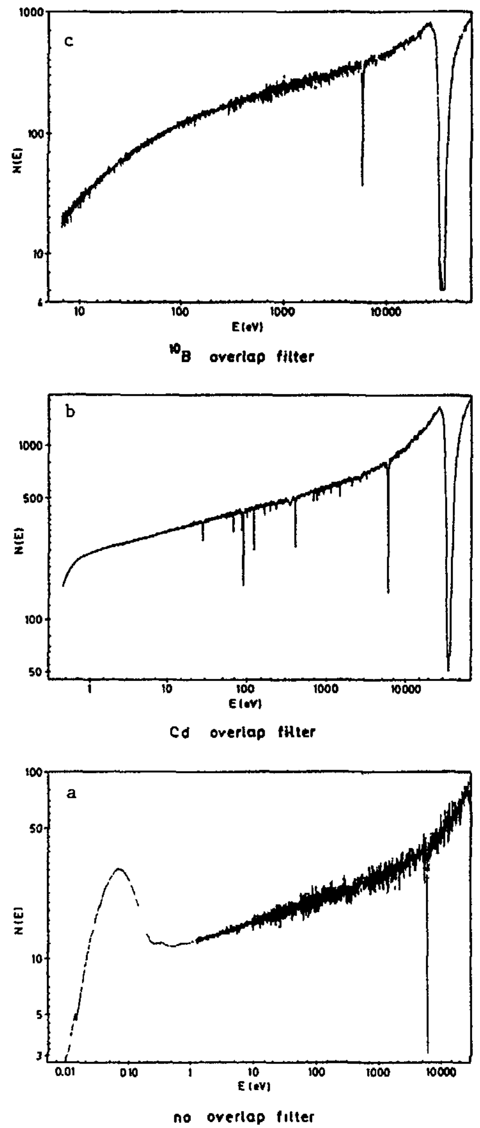

Fig. 1 : $^{10}B(n,\alpha)$ counting-rates as a function of the neutron energy (a) without overlap filter (b) with a cadmium overlap filter (c) with a boron overlap filter.

in the thermal region. The second goal was to cover the neutron energy region from 0.02 eV up to 30 keV in that same experiment, thus realizing a link between the thermal region and absolute measurements in the lowest part of the higher energy region (e.g. Szabo and Marquette, ref. 34).

EXPERIMENTAL CONDITIONS

No such measurement is available until now. The reason could be the rather exotic experimental conditions needed. One has indeed to cover a very large dynamic range with strongly different time of flight resolution requirements. At the Geel linear accelerator these requirements could be fulfilled by using a 4 ns time-coder with two million channels and an "accordeon" system (i.e. a variable t.o.f. channel width). The linac was operated at a repetition frequency of 100 Hz and a 4 ns pulse width.
The $^{235}U(n,f)$-fragments and the $^{6}Li(n,\alpha)t$ reaction products were simultaneously detected with surface barrier detectors from the same position in the neutron beam. In all our previous experiments a low detection geometry with the surface barrier detectors outside the neutron beam was used. In these experiments an almost 2π-geometry was realized by sandwiching the back-to-back ^{235}U and ^{6}Li foils between both surface barrier detectors; the whole system was placed into the collimated neutron beam. The thickness of the ^{6}LiF-target was 88 $\mu g/cm^2$. For the fission reaction, two independent measurements were performed respectively with a 100$\mu g/cm^2$ and a 500$\mu g/cm^2$ evaporated $^{235}UF_4$-layer.

The raw data are shown in Fig. 2. Typical $^{235}U(n,f)$ and $^{6}Li(n,\alpha)t$ counting-rate spectra (per 8 ns t.o.f. channel) are shown in the neutron energy region from 0.01eV up to 50 keV. The background has been determined with the black resonance technique and the data reduction was done as explained previously (e.g. ref. 30). The background was very low. A few typical background values for the $^{235}U(n,f)$ measurement with the 100$\mu g/cm^2$ sample are given within brackets: 0.0253eV (0.2%); 8.78eV resonance (0.15%); 11eV valley (5%); 30 keV (2%); 0.1 - 1 keV (between 1 and 5%). The fission cross-section was normalized to the fission integral $\int_{0.0206\,eV}^{0.06239\,eV} \sigma_f(E)dE = 19.26 \pm 0.08$ barn.eV as determined by Deruytter et al. (1). A check via a normalization procedure using a least square fit in the thermal region yielded a consistent normalization factor. Preliminary numerical values are given in Tables 3 - 6. These results will be discussed in the following chapter.

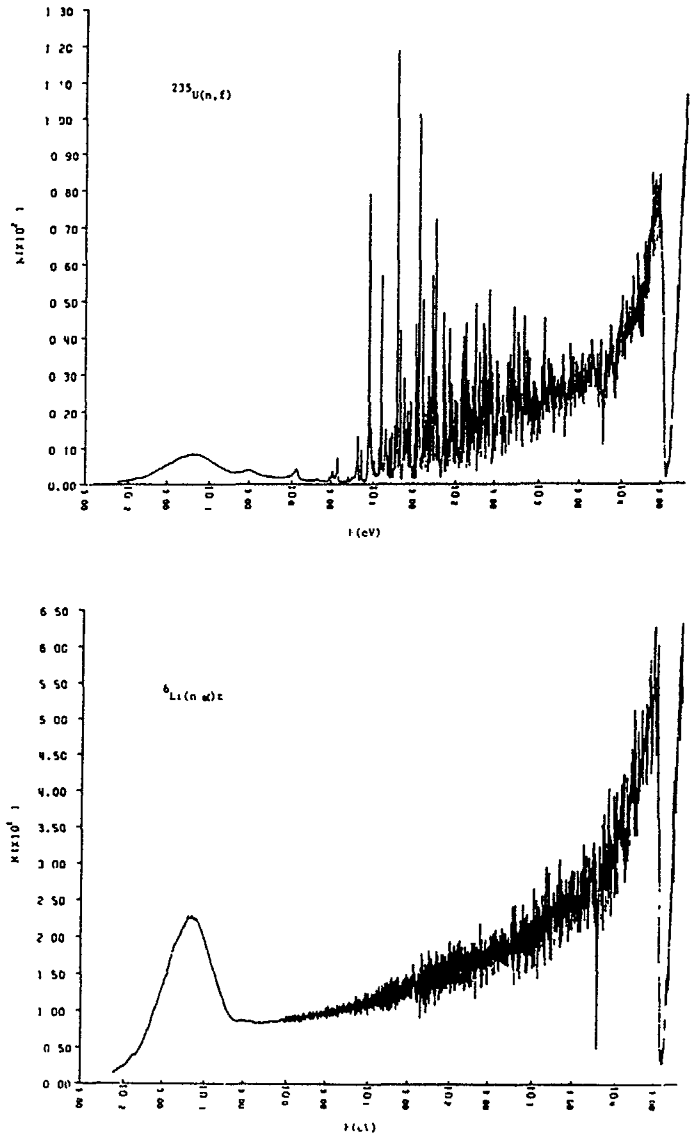

Fig 2 $^{235}U(n,f)$ and $^{6}Li(n,\alpha)t$ counting-rate spectra reduced to a constant 8 ns t.o.f. channel width

83 RESULTS AND DISCUSSION

A first group of results is given in Table 3, where the absolute fission cross-section data of Szabo and Marquette (34) are compared with the corresponding average fission cross-section values obtained from the present experiments. Obviously, both measurements agree within the experimental errors.

In Table 4 the average fission cross-sections obtained in the present measurements for a series of energy intervals are compared with other results. A first observation is that the results of the measurements with a 100 and with a 500 $\mu g/cm^2$ $^{235}UF_4$ sample are compatible. A second and more puzzling observation is that for intervals containing strong resonances (= high $\bar{\sigma}_f$-values) the present results are systematically lower than in most of the other data sets. This is especially true for the 10 - 20; 30 - 40 and 50 - 60 eV intervals. However, for intervals with $\bar{\sigma}_f \leqslant 30$ barn, the present results are quite plausible... A last observation is that the measurements relative to a $^6Li(n,\alpha)t$ flux monitor generally yield lower $\bar{\sigma}_f$-values than those made relative to a $^{10}B(n,\alpha)$-flux monitor.

In Table 5 a comparison is made of the fission integrals I_1 and I_2 relative to their thermal normalization values. For measurements with an indirect thermal calibration the σ_f°-value has been put within brackets. Also the I_1 and I_2-values obtained in the present experiments are somewhat surprizing: whilst the I_1/σ_f°-values are rather low, the I_2/σ_f°-values are in perfect agreement with the values of Gwin et al. (25) and Gzirr et al. (27), which are the only other measurements in which the I_2-integral was directly normalized in the thermal region. This confirms our previous observation, since the integral I_1 corresponds to a $\bar{\sigma}_f$-value of more than 70, whilst for I_2 $\bar{\sigma}_f \approx 13$ barn.

In Table 6 finally we compare the original values of the integrals I_1 and I_2 together with the neutron flux monitor used. By calculating the ratio of both integrals, the normalization constant is removed. Hence with consistent data sets only small fluctuations should occur. However, Table 6 reveals differences up to 10% between I_2/I_1-values. Another important observation is the apparent correlation between I_2/I_1 and the neutron flux monitor used. Measurements using a ^{10}B flux monitor systematically yield higher I_2/I_1-values than measurements relative to a ^6Li flux monitor, the exception being the present results which should, however, be considered cautiously in view of the surprisingly low I_1-values. Moreover, these low I_2/I_1-values in the Li-case are mainly a consequence of low I_2-values.

Table 3 Comparison of the absolute σ_f-data of Szabo and Marquette (ref.34) with the corresponding (preliminary) $\bar{\sigma}_f$-values of the present work.

E_n (keV)	σ_f (barn) (ref.34)	$\bar{\sigma}_f$ (barn)*
11.5 ± 3	2.76 ± 0.09	2.85
15.0 ± 3	2.50 ± 0.07	2.48
17.5 ± 3.5	2.15 ± 0.09	2.25
22.5 ± 2.5	2.20 ± 0.06	2.17
27 ± 3.5	2.10 ± 0.08	2.03

* average of the measurements with 100 and with 500 $\mu g/cm^2$

TABLE 4 THE (PRELIMINARY) AVERAGE CROSS SECTIONS (BARN) OBTAINED IN OUR MEASUREMENTS COMPARED WITH OTHER RECENT MEASUREMENTS, MAINTAINING THEIR ORIGINAL NORMALIZATION

INTERVAL / REF.	.02-.1 eV	.1-.5 eV	.5-1. eV	1-10 eV	10-20 eV	20-30 eV	30-40 eV	40-50 eV	50-60 eV	60-100 eV	.1-.2 keV	.2-.3 keV	.3-1. keV	1-10 keV	10-20 keV	20-30 keV
De Saussure (15)				40.14	52.95	36.27	57.06	33.33	61.99	24.34	21.03	20.86	11.58			
Ryabov (8)					46.09	35 05	52 12	32 21	51.10	24.23	21.39	20.83	11.69	4.41	2.98	2.51
Silver (17)										25.75	21.03	20.61	11.59	3.99	2.77	2.37
Lemley (18)										24.05	20.90	20.15	11.09	3.99	2.34	2.10
Blons (19)						34.28	57.31	34.00	64.47	25.15	21.03	20.77	11.71	4.38	2.54	2.20
Gayther (20)															2.53	2.17
Perez (21)					50.57	36 14	55 65	33 38	61.81	24.55	21.03	20.92	11.69	4.35		
Perez (22)															2.53	2.18
Czirr (23)											19.9	19.8	10.71		2.35	2.17
Wasson (24)											20.3	19.9			2.48	2.10
Gwin (25)	379.1	157 2	61.54							23.58	20.47	19.74	11.08	4.08	2.46	2.11
Wagemans (A)	384.1	159.1	60.64	40.64	52 62	38.08	59.02	34 57	64.59	25.40	21.25	20.91	11.53	4.41	2.64	2.22
(26) (B)											21.11	20.71	11.37	4.29	2.54	2.14
Czirr (27)	381.7	159	61.03							24.02	20.23	19.93	10.76			
Muradjan (28)											20.79	19.94	11.64	4.24	2.51	2.17
Moore (29)					52.35	37 36	55 19	33 11	60 14	23.85	20.73	19.53	10.80	3.87	2.52	
Wagemans (C)	384 7	162.9	63.44	41.58	53.64	37 76	58.19	33.66	63.73	25.24	21.43	21.29	11.81	4.31	2.59	2.22
(30) (B)											21.29	21.09	11.65	4.19	2.49	2.14
Biriukov (35)											21.88	20.87	11.62	4.29	2.49	2.09
Corvi (31)											20.37	20.16	11.19	4.16	2.46	2.10
This work (D)	384.0	162.7	66.3	41.1	50.7	37.2	52 8	33.3	59.0	23.9	20.4	20.0	11.3	4.27	2 56	2.10
(prelim.) (E)	384.7	161 4	65 4	40.5	49 8	36.9	52.5	32.9	58.4	24.2	19.8	19 6	11.2	4.24	2.47	2.10
ENDF-BV	382.4	159.7	62 4	41 93	54 54	38.07	56.73	34 35	63.01	23.95	20 54	20 15	11.22	4.20	2.48	2.12

(A) ORIGINAL DATA

(B) CORRECTED FOR NON 1/V 10B(n,α)-SHAPE

(C) REVISED DATA (SEE LIST OF REFERENCES)

(D) 500 $\mu g/cm^2$ ^{235}U target

(E) 100 $\mu g/cm^2$ ^{235}U target

Table 5 Comparison of the integrals I_1(7.8 eV, 11 eV) and I_2 (0.1 keV, 1keV) relative to their thermal normalization values.

Reference	σ_f^*(barn)	I_1(barn . eV)	I_1/σ_f^* (eV)	I_2(barn.keV)	I_2/σ_f^*(eV)
Shore & Sailor (4)	582	229.4	0.394		
Ryabov et al.(8)	582	217.8	0.374		
Michaudon et al. (6)	(582)	232.6	0.399		
		238.1	0.409		
Brooks et al. (10)	-	215.1	-		
Bowman et al. (9)	577.1	246.7	0.427		
De Saussure et al. (12)	(577.1)	236.7	0.410		
Mostovaya et al. (11)	-	255.6	-		
Cao et al. (13)	(582)	226.6	0.389		
Deruytter & Wagemans (16)	587.9	240.2	0.409		
Gwin et al. (25)	580.2	234.6	0.404	11.79	20.32
Czirr et al. (27)	585.4	244.7	0.418	11.54	19.71
Wagemans & Deruytter (26)	587.6	246.2	0.419		
This work (prelim.)	587.6	230.6 (a)	0.392	11.92	20.29
		226.3 (b)	0.385	11.78	20.05
Average			0.402		20.09
ENDF-BV	583.5	241.2	0.413	11.92	20.43

(a) 500 $\mu g/cm^2$ $^{235}UF_4$ target

(b) 100 $\mu g/cm^2$ "

TABLE 6 COMPARISON OF THE ORIGINAL VALUES OF THE SECONDARY NORMALIZATION INTEGRALS I_1 (7.8 EV, 11 EV) AND I_2 (0.1 KEV, 1 KEV)

REFERENCE	I_1(b.eV)	I_2(b.eV)	I_2/I_1	Φ
De Saussure et al.(12)	236.7	12.30	51.97	B
Gwin et al.(25)	234.6	11.79	50.26	B
Wagemans and Deruytter(26)	240.0*	12.29 (1)	51.20	B
		12.14 (2)	50.60	
Wasson (24)	238.4*	(11.68)	(48.99)	Li
Czirr et al. (27)	244.7	11.54	47.16	Li
Muradjan et al.(28)	-	12.21*		B
Moore et al.(29)	241.2*	11.59	48.05	Li
Wagemans et al.(30)	246.2	12.54 (1)	50.93	B
		12.39 (2)	50.31	
Biriukov et al.(35)	-	12.41		
Corvi et al. (31)	241.2*	11.88	49.25	Li
This work (Prel.)	230.6 (3)	11.92	51.69	Li
	226.3 (4)	11.78	52.05	
ENDF - BV	241.2	11.92	49.42	

* Normalization value

(1) Original value with a 1/v 10B(n,α)-shape adopted

(2) Corrected for non 1/v 10B (n,α)-shape

(3) 500 μg/cm^2 235 UF_4 target

(4) 100 μg/cm^2 235 UF_4 target.

CONCLUSIONS

The present measurements yield σ_f-data in the neutron energy region from 20 meV up to 30 keV directly normalized in the thermal region. In the keV-region these data are consistent with the absolute σ_f-measurements of Szabo and Marquette (34). For the secondary normalization integral I_2 values have been obtained in agreement with those of Gwin et al. (25) and Czirr et al. (27) which were also directly normalized in the thermal region.
For the I_1 integral, however, puzzling low values have been obtained. This was also the case for $\bar{\sigma}_f$ in neutron energy intervals containing strong resonances. Three additional measurements are planned to further investigate these observations: (i) maintaining the actual ~2π-geometry but using a ^{10}B-foil for the neutron flux detection (ii) using a low detection geometry with a ^{10}B- as well as a ^{6}Li-flux monitor. Only after these measurements definite conclusions on the I_1 and I_2 integrals can be formulated and final $\bar{\sigma}_f$-values can be released.

The present study also gives some evidence for a correlation between the integral I_2 and the neutron flux monitor used. The influence of a normalization via I_1 or I_2 on the final cross-section has been shown. The magnitude of possible normalization errors is illustrated.

Finally, since ^{235}U is expected to be an "easy" nucleus (low α-activity, high σ_f-values), there are some indications that the important discrepancies still present in ^{235}U(n,f) cross-section measurements might partially be due to errors in the neutron flux determination.

Acknowledgements

Mr. R. Barthélémy and Mr. J. Van Gils are acknowledged for their help during the experiments and their analysis. Thanks are also due to Dr. G. Coddens from the NEA Data Bank (Saclay) for providing us with integrated data from the files.

REFERENCES

(1) A.J. DERUYTTER, J. SPAEPEN, P. PELFER, Journ.Nucl.En. 27 (1973) 645

(2) O. WASSON, A. CARLSON, K. DUVALL, Nucl. Sc. and Engng. 80 (1982)282

(3) I. SZABO, J. LEROY, J. MARQUETTE, Neutron Standard Reference Data, IAEA Vienna (1974) 175

(4) F. SHORE and V. SAILOR, Phys. Rev. 112 (1958) 191

(5) A. MICHAUDON, Rep. CEA - R - 2552 (1964)

(6) A. MICHAUDON, H. DERRIEN, P. RIBON, M. SANCHE, Nucl. Phys. 69 (1965) 545

(7) K. IGNATIEV, I. KIRPICHNIKOV, S. SUKHORUCHKIN, Sov.At.En. 16 (1964) 121

(8) Y. RYABOV, S. DONSSIK, N. CHIKOV, N. YANEVA, Atomn. Energ. 24 (1968) 4; translated BNL - TR 219

(9) C. BOWMAN, G. AUCHAMPAUGH, S. FULTZ, M. MOORE, Proc. Conf. on Neutron Cross-Section Technology, Washington (1966), 2, 1004

(10) F. BROOKS, S. JOLLY, M. SCHOMBERG, M. SOWERBY, Rep. AERE - N - 1670 (1966)

(11) T. MOSTOVAYA and O. BESPALOV, Rep. INDC 152E (1967)

(12) G. DE SAUSSURE, L. WESTON, R. GWIN, R. INGLE, J. TODD, R. HOCKENBURY, R. FULLWOOD, A. LOTTIN, Proc. Conf. on Nuclear Data for Reactors, Paris (1967) 2, 233 and Rep. ORNL - TM - 1804

(13) M. CAO, E. MIGNECO, J. THEOBALD, J WARTENA, J. WINTER, J. Nucl. Energy 22, (1968)211

(14) J. BLONS, G. DEBRIL, J. FERMANDJIAN, A. MICHAUDON, Proc. Conf. on Nuclear Data for Reactors, Helsinki (1970), CN 26/60

(15) G. DE SAUSSURE (1971), private communication

(16) A.DERUYTTER and C. WAGEMANS, J. Nucl. Energy 25 (1971) 263

(17) E. SILVER, G. DE SAUSSURE, R. PEREZ, R. INGLE, Proc. Conf. on Neutron Cross-Section Techn., Knoxville (1971) 728

(18) J. LEMLEY, G. KEYWORTH, B. DIVEN, Nucl. Sci. Engn. 43 (1971) 281

(19) J. BLONS, Nucl. Sci. Engn. 51 (1972) 130

(20) D. GAYTHER, D. BOYCE, J. BRISLAND, Proc. Panel on Neutr. Stand. Ref. Data, Vienna (1972) 201

(21) R. PEREZ, G. DE SAUSSURE, E. SILVER, R. INGLE, H. WEAVER, Nucl. Sci. Engn. 52 (1973) 46

(22) R. PEREZ, G DE SAUSSURE, E SILVER, R. INGLE, H. WEAVER, Nucl. Sci. Engn. 55 (1974) 203

(23) J. CZIRR and G. SIDHU, Rep. UCRL - 77377 (1975)

(24) O. WASSON, Rep. ANL-76-90 (1976)183

(25) R. GWIN, E. SILVER, R. INGLE, Nucl.Sci.Engn. 59 (1976) 79

(26) C. WAGEMANS and A. DERUYTTER, Ann. Nucl. En. 3 (1976) 437

(27) J. CZIRR and W. CARLSON, Nucl. Sci. Engn. 64 (1977) 892

(28) G. MURADJAN, Y. ADAMCHUK, M. VOSKANJAN, L. PROKOFIEVA, Proc. Conf. on Neutron Physics, Kiev (1977) 3, 119

(29) M. MOORE, J. MOSES, G. KEYWORTH, J. DABBS, N. HILL, Phys. Rev. C 18 (1978) 1328

(30) C. WAGEMANS, G. CODDENS, A. DERUYTTER, Proc. Conf. on Nuclear Cross Sections for Techn., Knoxville (1979)961. The average cross-sections calculated from these measurements had to be slightly revised due to an error in the integration sub-routine. The corrected data are given in the present report (see Tables 4 - 6).

(31) F. CORVI et al., private communication (1982)

(32) M. SOWERBY, B. PATRICK, D. MATHER, Ann. Nucl. Sc. Engn., 1 (1974) 409

(33) B. LEONARD, D. KOTTWITZ, U. JENQUIN, K. STEWART, C. HEEB, Rep. EPRI-221 (1975)

(34) I. SZABO and J. MARQUETTE, Rep. ANL-76-90 (1976) 208

(35) S. BIRIUKOV, T. MOSTOVAYA, V. MOSTOVOI, A. OSSOCHNIKOV, A. SVETSOV, Proc. Conf. on Neutron Physics, Kiev (1980)

The 1982 INDC/NEANDC Nuclear Standards File - status and recommendations on the uranium 235 fission cross section and the californium 252 fission neutron spectrum

H Condé, National Defence Research Institute
P-I Johansson, The Studsvik Science Research Laboratory

1 Introduction

The Nuclear Standards Subcommittee of the International Nuclear Data Committee (INDC) has recommended the use of certain cross sections as standard cross sections for nuclear data measurements. The INDC Nuclear Standards File is under contineous review. In addition, the INDC Standards Subcommittee and the couterpart subcommittee of the Nuclear Energy Agency Nuclear Data Committee (NEANDC) exchange technical information on those standard terms which are common to the Standards Files of both Committees.

The objective of the file is to provide concise and readily used reference guidelines to essential nuclear standard quantities for a diversity of basic and applied endeavors.

The file consists of status summaries for fifteen nuclear data standards and data tabulations. The narrative summaries describe the current status of each of the standards, including references to recent relevant work and areas of continuing uncertainties. These brief reviews were prepared under the auspices of the INDC by outstanding specialists in the respective fields.

The large majority of the recommended numerical data for the standard cross section is taken from ENDF/B-V, produced by the US Cross Section Evaluation Working Group. The remainder of the numerical data is from evaluations undertaken by individuals or groups closely connected with nuclear data activities promoted by the INDC and NEANDC. Generally, the numerical data tables include quantitative definitions of the data uncertainties and some guidelines as to their appropriate usage.

The 1982 version of the INDC Nuclear Standards File will be published as an IAEA Technical Report. It summarizes the status of the individual nuclear standards as of the 12th meeting of the INDC in October 1981 with selective updating to May 1982.

The review responsibilities for the 1982 version of the file is shared among members of the INDC Standards Subcommittee and their delegates.

In particular the U-235 fission cross section has been reviewed by Prof Yankov, Kurchatov Institute of Atomic Energy, Moscow, the U-235 fission fragment anisotropy by Prof Kapoor, BARC, India and the Cf-252 fission spectrum by Dr Lemmel, IAEA and Prof Yankov in cooperation.

2 The U-235 fast fission cross section

The U-235 fission cross section is recommended as a standard between 0.1 to 20.0 MeV. The reference data are the ones of ENDF/B-V material number 1395.

The uncertainteis of the data are estimated to

100 keV to 150 keV	4.0 %
150 keV to 200 keV	3.0 %
200 keV to 400 keV	3.0 %
400 keV to 1 MeV	3.5 %
1 MeV to 2 MeV	2.5 %
2 MeV to 4 MeV	3.0 %
4 MeV to 10 MeV	3.5 %
10 MeV to 15 MeV	4.0 %
15 MeV to 20 MeV	6.0 %

Several new measurements of the fast fission cross section of U-235 were reported by Prof Yankov to the Subcommittee.

T Mostovaya et al (1) (I V Kurchatov Atomic Energy Institute, Moscow) measured the fission cross section using the time-of-flight method on the 60 MeV electron linac over the energy range of 0.1-100 keV with an accuracy of 1.5-2.0 %. The results are given i Table 2.1. They span the energy range that has long been uncertain. The value of the cross section over the energy interval of 0.09-0.1 MeV is 1.51±0.01 b; the corresponding ENDF/B-V value is 1.60 b.

F Corvi (2) (CES, JRC, Central Bureau for Nuclear Measurements, Geel) measured the fission cross section in the same energy range of 0.1-100 keV on the linac with a relative energy resolution of 0.27 %. The data were normalized to the ENDF/B-V value of the low energy fission integral betwen 7.8 and 11 eV, I=241.2 b eV. If the error of the standard is neglected the uncertainsties of the values given in Table 2.2 should not exceed ±2 % over the entire energy range.

E Zhagrov et al (3) (V G Khlopin-Radium Institute, Leningrad) determined the fission cross section at 46±7 keV and 120±9 keV. The neutron flux was measured by the $MnSO_4$ bath method. Their results were 2.08±0.08 b and 1.51±0.06 b, respectively. The latter value is in good agreement with the ENDF/B-V evaluation (1.52 b).

The fission cross section of U-235 reported by Arlt et al (4, 5, 6) has been determined employing the time correlated associated-particle technique. The measurements have been performed at E_n=2.6 MeV using the neutron generator at the Technical University of Dresden and at E_n=8.2 and 8.4 MeV using the 5 MV tandem generator of the CINR Rossendorf (GDR). The foils with U-235 have been prepared and calibrated at V G Khlopin Radium Institute, Leningrad.

As a result of two independent experiments (5) a value of 1.215+0.019 b at 2.56 MeV was obtained. The results at 8.2 MeV and 8.4 MeV were 1.741+0.057 b (4) and 1.801+0.043 b (6), respectively. These are in good agreement with the ENDF/B-V evaluation (1.78 b).

M Cancé et al (7) (Bruyères-le-Chatel) made a direct measurement of the ratio of fission to neutron-proton scattering cross sections with back-to-back deposits of U-235 and poyethylene. Two measurements have been made: the first at 2.5+0.04 MeV in order to check their experimental method, the second at 4.45+0.01 MeV. The cross section values are 1.26+0.03 b and 1.13+0.03 b, respectively; the corresponding value of the ENDF/B-V evaluation at 4.5 MeV is 1.11 b. The 2.6 MeV cross section value by Arlt et al (5) and the 2.5 MeV value by Cancé et al (7) are compared with the earlier values at similar energies in Fig 2.1. The numerical result of the ENDF/B-V evaluation is 1.25 b.

O A Wasson et al (8) (National Bureau of Standards, Washington) completed measurements at 14.1+0.01 MeV with a result of 2.080+0.030 b. They used the time correlated associated-particle technique with the $^3H(d,n)^4He$ reaction. This value is compared with the ENDF/B-V evaluation and some earlier values around 14 MeV in Figs. 2.2, 2.3 and 2.4. These results are consistent within the accuracy of about 1.5 %. The inspection of the figures suggests that the accuracy of this standard may be better than 1 % near 14 MeV.

A D Carlson (9) has reported that a precision measurement program over the energy range of 0.3-1.5 MeV is in progress at the National Bureau of Standards (USA). On the basis of these measuremnts, the ones noted above, and the values reported previously it can be concluded that the energy range from 3.0 to 6.0 MeV is likely to be the major one where uncertainties remain.

In addition, an experiment by A Bergman et al (10) is in progress to measure the fission cross section using a neutron spectrometer based upon the slowing-down technique over the enrgy range 0.1 to 50.0 keV to average accuracies of 1.5-2.0 %.

REFERENCES

1. T.A. Mostovaya, V.I. Mostovoi, S.A. Biriukov, A.A. Ossochnikov, A.V. Shvetsov. "Measurement of the fission cross section of ^{233}U and ^{235}U in the energy range 0.1-100 keV and of the ratio of the fission cross sections $^{233}U/^{235}U$ up to 2 MeV". Proc. 5th All-Union Conf. of Neutr. Phys., Kiev, 15-19 Sept. 1980. "Neutron Physics", part 3, p. 30, 1980, Moscow, INDC(CCP)-169/G.

2. F. Corvi. "Contribution for the updating of the ^{235}U (n,f) Standards File INDC-36/LN". Private Communication, 1981.

3. E.A. Zhagrov, Yu. A. Nemilov, A.V. Platonov, S.M. Solov'ev, V.E. Fominykh. "Fission cross section of ^{233}U, ^{235}U in the intermediate neutron energy range". (Reference same as for (1), page 45.)

4. R. Arlt, V. Grimm, M. Josch, G. Musiol, H.-G. Ortlepp, G. Pausch, R. Teichner, W. Wagner, I.D. Alkhazov, E.A. Ganza, L.V. Drapchinsky, V.N. Dushin, S.S. Kovalenko, O.I. Kostochkin, K.A. Petrzhak, A.V. Fomichev, V.I. Shpakov. "Absolute measurements of the ^{235}U fission cross-sections at incident neutron energies of 2.6 MeV and 8.2 MeV". (Reference same as for (1), page 192.)

5. R. Arlt, M. Josch, G. Musiol, H.-G. Ortlepp, R. Teichner, W. Wagner, L.V. Drapchinsky, V.N. Dushin, O.I. Kostochkin, S.S. Kovalenko, K.A. Petrzhak, V.I. Shpakov. "The Absolute Determination of the Fission Cross Section of ^{235}U at E_n = 2.56 MeV". Prog. Rep. German. Dem. Rep., INDC (GDR)-16/G, page 17, 1981. To be published in Kernenergie.

6. R. Arlt, M. Josch, G. Musiol, H.-G. Ortlepp, R. Teichner, W. Wagner, I.D. Alkhazov, L.V. Drapchinsky, O.I. Kostochkin, S.S. Kovalenko, K.A. Petrzhak, V.I. Shpakov. "Absolute Fission Cross Section Measurements on ^{235}U and ^{237}Np at E_n = 8.4 MeV". Prog. Rep. German Dem. Rep., INDC (GDR)-16/G, page 18, 1981. Proc. Int. Symp. on the Interaction of Fast Neutrons with Nuclei, Gaussig, 1980.

7. M. Cancé, G. Grenier, D. Gimat and D. Parisot. "Absolute neutron fission cross sections of ^{235}U at 2.5 and 4.45 MeV". Prog. Rep. Actinide, Bruyères-le-Chatel. NEANDC(E) 211 L', INDC(Fr)-41/L., page 14, 1981.

8. O.A. Wasson, A.D. Carlson, K.S. Duvall. "Measurement of the ^{235}U(n,f) Cross section at 14.1 MeV". BNL-NCS-29426, NEANDC(US)-210/U, INDC(USA)-86/L, page 104, 1981.

9. A.D. Carlson. "An Absolute Measurement of the ^{235}U(n,f) Cross Section from 300-1500 keV Neutron Energy". (Reference same as for (8), page 105.)

10. A.A. Bergman, A.G. Kolosovsky, S.P. Kuznetsov, A.N. Medvedev, A.E. Samsonov, V.A. Tolstikov. "Measurement of the ^{239}Pu and ^{235}U fission cross sections and their ratios in the energy range from 100 eV to 50 keV". (Reference same as for (1), page 49.)

Table 2.1 ^{235}U Fission Cross-Section (Reference 1)

E_1-E_2 keV	σ_f barn	E_1-E_2 keV	σ_f barn	E_1-E_2 keV	σ_f barn
0.1-0.2	21.88 ± 0.04	1 - 2	7.33 ± 0.02	10- 20	2.49 ± 0.01
0.2-0.3	20.87 ± 0.04	2 - 3	5.29 ± 0.02	20- 30	2.09 ± 0.01
0.3-0.4	12.97 ± 0.04	3 - 4	4.85 ± 0.03	30- 40	-
0.4-0.5	14.04 ± 0.06	4 - 5	4.34 ± 0.03	40- 50	1.84 ± 0.01
0.5-0.6	15.33 ± 0.06	5 - 6	3.95 ± 0.03	50- 60	1.82 ± 0.01
0.6-0.7	11.70 ± 0.06	6 - 7	3.45 ± 0.03	60- 70	1.74 ± 0.01
0.7-0.8	11.30 ± 0.06	7 - 8	3.28 ± 0.02	70- 80	1.67 ± 0.01
0.8-0.9	8.37 ± 0.05	8 - 9	3.00 ± 0.02	80- 90	1.60 ± 0.02
0.9-1.0	7.60 ± 0.05	9 - 10	3.09 ± 0.02	90-100	1.51 ± 0.01

Table 2.2 Average ^{235}U Fission Cross Section (Reference 2)

E_1-E_2 keV	σ_f barn	E_1-E_2 keV	σ_f barn	E_1-E_2 keV	σ_f barn
0.1-0.2	20.37	1 - 2	7.178	10- 20	2.460
0.2-0.3	20.16	2 - 3	5.231	20- 30	2.104
0.3-0.4	12.80	3 - 4	4.684	30- 40	1.975
0.4-0.5	13.18	4 - 5	4.157	40- 50	1.835
0.5-0.6	14.88	5 - 6	3.813	50- 60	1.781
0.6-0.7	11.24	6 - 7	3.235	60- 70	1.727
0.7-0.8	10.83	7 - 8	3.148	70- 80	1.652
0.8-0.9	8.051	8 - 9	2.937	80- 90	1.580
0.9-1.0	7.322	9 - 10	3.080	90-100	1.532

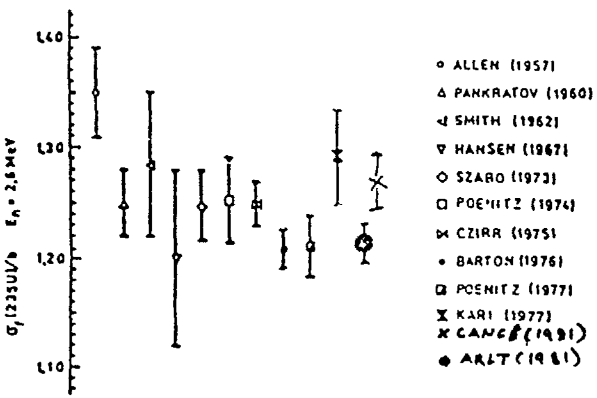

Figure 2.1 Comparison of the 1981 Arlt et al. (Ref 5) result at 2.6 MeV with previously reported values at similar energies.

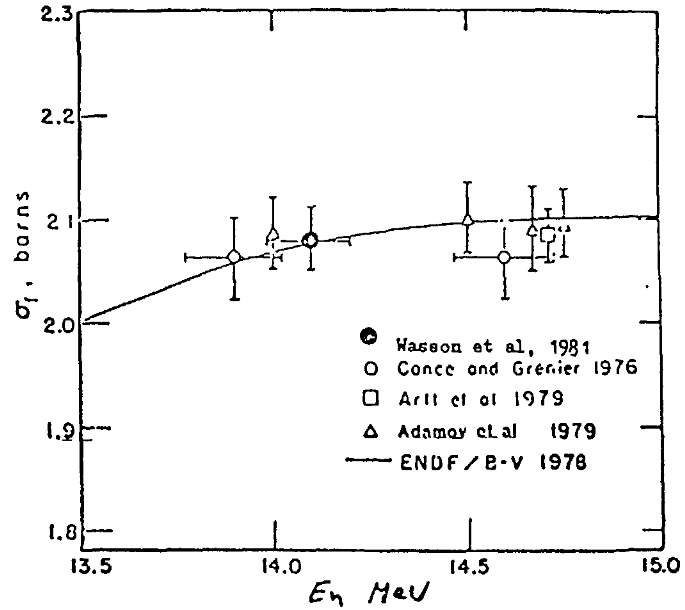

Figure 2.2

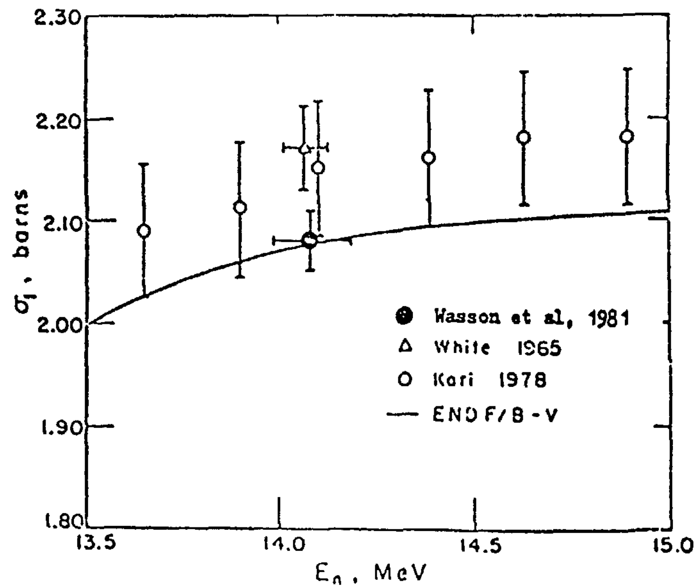

Figure 2.3

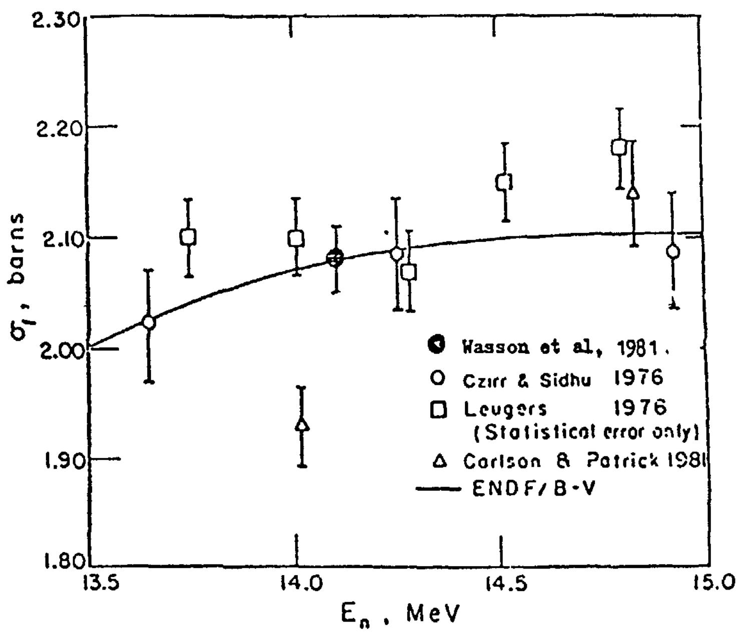

Figure 2.4

Figs. 2.2,2.3 and 2.4. Comparison of the 1981 Wasson et. al., (Ref 8) value with ENDF/B-V and some previously reported values in the 14 MeV range.

3 *The U-235 fission fragment anisotropies*

A knowledge of fission fragment anisotropies is important in the evaluation of experimental fission cross section measurements in which fission fragments are detected in a small range of angles. Fission fragment anisotropies also provide important information on the quantum states available at the saddle point of the fissioning nucleus which in turn provide a basis for theoretical understanding of the fission cross sections.

A first review of the status of the measured fragment anisotropies for different neutron energies for U-235 was presented by Prof. Kapoor to the Subcommittee.

In view of the scatter in data points from different measurements (Fig. 3.1) and our present inadequate knowledge of the Ko^2 versus E_x curve it is difficult to arrive at a set of the anisotropy values which one could recommed as the best set.

For the present, the solid line in Fig. 3.1 can serve as a recommended set of anisotropies, particularly in the energy range 1<E<5 MeV where the statistical theory is applicable and the uncertainties due to direct interaction effects and second chance corrections is minimal.

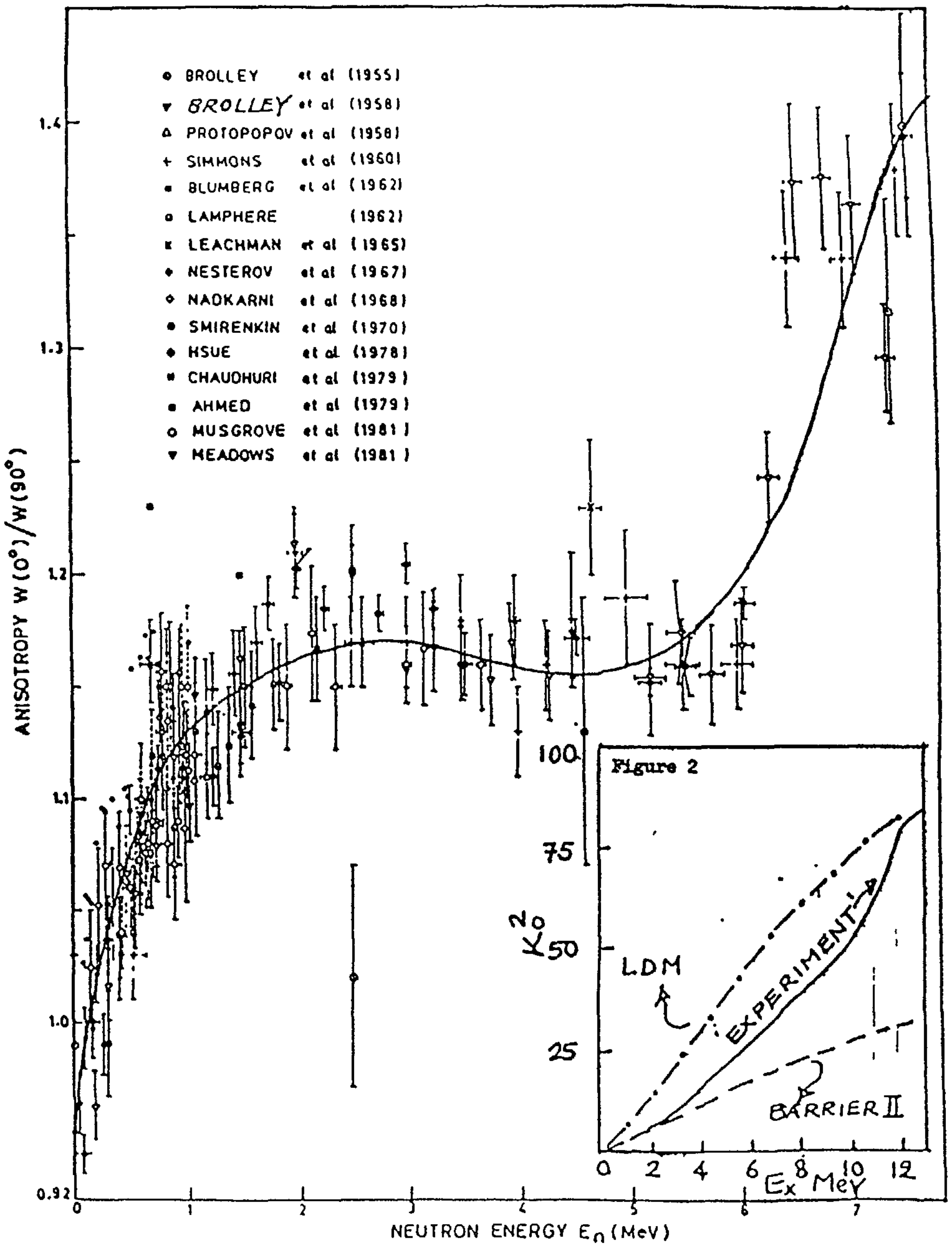

Figure 3.1

4 The prompt fission neutron spectrum of Cf-252

The Cf-252 fission neutron spectrum is employed as a basic reference in both microscopic and macroscopic measurements. The energy distribution impacts upon the determination of the essential nu-bar Cf-252 standard. The spectrum is also used as a relative flux standard in instrument calibration.

The spectrum has been measured with varying accuracies over a period of approximately 25 years. The history, as summarized by Blinov (1), is outlined in Table 4.1. Despite this wealth of information neither the shape nor average energy is known to an accuracy warranted by the importance of this standard spectrum.

Reviewing the available information, Blinov (1) concluded that the spectrum is maxwellian in shape. The conclusion was enforced by the results of a measurement also performed by Blinov (2). The observed spectrum was described by a Maxwellian with kT=1.42 MeV, with no significant deviation from this Maxwellian in the range from 1 keV to 3 MeV. The accuracy of the shape of the spectrum obtained in this work is essentially higher than that known from literature, especially for the region around 10 keV, where a 14 % (1σ) error is quoted (compared to 50-70 % in other measurements). The accuracy in the region from 100 keV to 4 MeV is better than $\pm$3 %.

Other recent experimental results of Boldeman (3) and of Bensch (4) are in agreement with the conclusions by Blinov.

The experimental definition of the spectrum is less accurate at low (<0.1 MeV) and at high energies (5 MeV) and in that regions uncertainties persist.

Starostov et al (5) measured the Cf-252 spectrum from 10 keV to 10 MeV. Contrary to the results of Blinov they obtained pronounced deviations from the Maxwellian form between 50 and 500 keV. Similar deviations have been reported in an earlier work of Meadows (6).

Mon Jiagnshen et al (7) measured the Cf-252 spectrum between 450 keV and 15 MeV. The observed spectrum was described by a Maxwellian with kT=1.416$\pm$0.023 MeV. At the high energy end between 11 and 15 MeV, the measured spectrum shows a structure exceeding the Maxwellian by a factor of 2. Similar deviations have been reported by Bensch (4) and by Maerten et al (8). Neither a Maxwellian nor a Watt spectrum seem to fit the data perfectly, but the deviations from a Maxwellian are small.

A measurement of the Cf-252 spectrum is in progress at ORNL by Spencer and Olsen. Semi-empirical calculation of the spectrum based on nuclear evaporation theory has been reported by Madland and Nix (9); the results slightly overestimate the high energy part of the spectrum compared to experiments.

Several important new experiments were reported at the International Conference on Nuclear Data for Science and Technology, Antwerp, September 1982; see Table 4.2. These data require a comprehensive review and evaluation.

It is recommended by the Subcommittee that the Maxwellian form of the Cf-252 spectrum with a temperature T=1.42 MeV be accepted as a comtemporary reference. This should be considered an interim status until the evaluation of the recent experiments becomes available.

The INDC Subcommittee on Standards will very much appreciate any steps this Consultants Meeting can take towards defining the accuracy of the Cf-252 spectrum presently achieved and towards defining work to be done in reaching an agreement on a spectrum to be used as a standard.

REFERENCES

1. M.V. Blinov, Proc. IAEA Consultants Mtg. on Neutron Source Properties, INDC(NDS)-114/GT (1980).
2. M.V. Blinov, IAEA Research Contract 2048, to be published.
3. J. Boldeman, Trans. Am. Nucl. Soc., 32, 733 (1979).
4. F. Bensch and H. Jansicek, INDC(AUS)-4 (1979).
5. B.I. Starostov et al., INDC(CCP)-164/L (1981).
6. J.W. Meadows, Phys. Rev., 157, 1076 (1976).
7. Mon Jiangshen et al., China I of Nucl. Phys. 3, 163 (1981).
8. H. Maerten, D. Seeliger and B. Stobinski, INDC(GDR)-17/L (1982).
9. D.G. Madland and J.R. Nix, Nucl. Sci. and Eng.,81,213(1982), and Proc. Int. Conf. on Nuclear Data for Science and Technology, Antwerp, 6-10 September 1982.
10. Papers presented at the Conf. on Nuclear Data for Science and Technology, Antwerp, 6-10 September 1982.

Table 4.1 Summary of Data on Fission Neutron Spectrum of ^{252}Cf through 1979. Compiled by Blinov (1)

Year	Authors	Neutron Energy Range (MeV)	Method of Neutron Detection	Results: $\bar{T}_{maxw}$ (MeV)(a)	Results: $\bar{E}$ (Mev)
1955	Hjalmar etc.(b)	2	Photoemulsion	1.40 ± 0.09	-
1957	Smith etc.	0.2 - 7.0	TOF, plast. scint.; photoemuls.	-	2.36
1961	Bonner	4	Integr. (Bramblett counter)	1.367 ± 0.030	-
1962	Bowman etc.	0.5 - 6.0	TOF, plast. scint.	-	2.34 ± 0.05
1965	Condé, During	0.07 - 7.5	TOF, ^{6}Li-glass, plast. scint.	1.39 ± 0.04	(2.09)
1967	Meadows	0.003 - 15	TOF, ^{6}Li-glass, liquid scint.	1.52	2.348
1969	Green	-	Integr. (Mn-bath)	1.39	(2.09)
1970	Zamjatnin etc.	0.005 - 6.0	TOF, ^{6}Li-glass, plast. scint.	1.48 ± 0.03	(2.22 ± 0.05)
1972	Jeki etc.	0.002 - 1.0	TOF, ^{6}Li-glass	1.57(1.3)	-
1972	Smith, Koster		Review	-	-
1976	Knitter		Review	-	-
1972	Werle, Bluhm	0.2 - 8.0	^{3}He-spectrometer, prop. counter	(1.42 ± 0.015)	2.155 ± 0.024 2.130 ± 0.022
1973	Green etc.	0.5 - 13	TOF, org. scint.	1.406 ± 0.015	2.105 ± 0.014
1973	Knitter etc.	0.15 - 15	TOF, org. scint.	1.42 ± 0.05	2.13 ± 0.08
1974	Spiegel	-	Integr. ("age")	-	2.21 ± 0.05
1974	Alexandrova etc.	2.04 - 13.2	Single-crystal spectrometer	1.42 ± 0.03	(2.13 ± 0.045)
1975	Kotelnikova etc.	0.5 - 7.0	TOF, liquid scint.	1.46 ± 0.02	(2.19 ± 0.03)
1975	Johnson	2.6 - 15	Single-crystal spectrometer	(1.42 ± 0.02)	2.13 ± 0.03)

Table 4.1 Summary of Data on Fission Neutron Spectrum of ^{252}Cf through 1979. Compiled by Blinov (1)
(Contd.)

Year	Authors	Neutron Energy Range (MeV)	Method of Neutron Detection	Results	
				T_{Maxw} (MeV) [a]	$\bar{E}$(MeV)
1976	Csikai, Dezsoa	2.5 - 15	Activation detector		
			(threshold reactions);	1.41 ± 0.02	(2.12 ± 0.03)
			"age" - method	1.48 ± 0.03	(2.22 ± 0.05)
1976	Batenkov etc.	0.02 - 2.0	TOF, ^{6}LiI-crystal	1.40	-
1976	Stewart etc.	-	Review	-	-
1975	Grundl etc.	0.25 - 8.0	Evaluation	(1.42)	2.13
1977	Blinov etc.	0.01 - 7.0	TOF, ^{6}LiI-crystal, ^{235}U-chamber	1.41 ± 0.03	2.12
1977	Djachenko etc.	<2	Amplitud., reaction ^{6}Li(n,α)T	1.18	-
1977	Nefedov etc.	0.01 - 10	TOF, metal. ^{235}U; ^{235}U - chamber	1.28	(1.92)
1978	Bertin	1 - 10	TOF, liquid scint.	(1.51)	2.27 ± 0.02
1978	Nefedov etc.	0.01 - 10	TOF, metal. ^{235}U, ^{235}U - chamber	1.43 ± 0.02	(2.15 ± 0.03)
1979	Blinov etc.	0.001 - 1	TOF, ^{6}LiI-crystal	1.42	-
1979	Boldeman etc.	0.6 - 15	TOF, plast. scint.	1.424 - 0.013	2.136 ± 0.020

[a]The values of T_{maxw} and $\bar{E}$ in brackets are taken not from the reference works, but calculated according to their data.

[b]References to above are explicitly given in Ref.

Table 4.2 Recent data (after 1979) on the Fission Neutron Spectrum of ^{252}Cf

Year	Authors	Ref.	Neutron Energy	Comments	Results	
					T_{maxw} (MeV)	$\bar{E}$ (MeV)
1979	Bensch et al	(4)	0.9–10	small deviations from Maxwellian	1.409 $\pm$ 0.05	(2.114)
1981	Mon Jiangshen etc.	(7)	0.45–15	small deviations from Maxwellian, excess neutrons above 11 MeV	1.416 $\pm$ 0.023	(2.124)
1982	Blinov et al	(10)	0.01–7	Maxwellian	1.418 $\pm$ 0.024	(2.127)
1982	Lajtai et al		0.025–1.2	(result not yet known)	?;	?!
1982	Poenitz et al	(10)	0.2–10	black neutron detector, small deviations from Maxwellian	1.439 $\pm$ 0.010	(2.159)
1982	Boettger et al	(10)	2–14	Maxwellian in the range of 3–13 MeV		
1982	Maerten et al	(8,10)	above 10	excess neutrons above 20 MeV		

SOME COMMENTS ON THE ^{235}U FISSION CROSS-SECTION DATA BASE ABOVE 1.5 MeV

D. B. Gayther and B. H. Patrick

Nuclear Physics Division, AERE, Harwell, Oxon., UK

Abstract

The main experimental requirements for making accurate fission cross-section measurements are presented and some of the most important experiments which form part of the ^{235}U data base above 1.5 MeV are critically examined in the light of these criteria. The examples discussed are taken entirely from the published literature.

Introduction

If we exclude the 14 MeV region, existing measurements of the ^{235}U fission cross-section exhibit some particularly large discrepancies at energies above 1.5 MeV. Several measurements differ in both the absolute value of the cross-section and its neutron energy-dependence (shape) by amounts which cannot be reconciled with the individual uncertainty assignments. It is our purpose to examine the data base in this region with the aim of finding, if possible, explanations for the discrepancies, and to suggest what further measurements, if any, should be made. The ^{235}U(n,f) data base used was that provided by the NEA Data Bank in October, 1982. Measurements in the 14 MeV region made with monoenergetic neutron sources will not be discussed since recent results are in reasonable agreement.

We begin by considering the following aspects of a fission cross-section measurement:

Neutron Source Characterization
Neutron Flux Determination
Fissile Sample Characterization
Fission Detection Efficiency
Documentation

These provide a framework for examining the main requirements of an accurate measurement and then assessing each entry in the $^{235}U(n,f)$ data base accordingly. Documentation is included in the list because, although not part of the actual measurement process, it is essentially the only medium through which the quality of the work can be judged.

The discussion is confined to differential cross-section measurements made with accelerator neutron sources. An integral cross-section which should be noted, however, is that for the $^{235}U(n,f)$ reaction averaged over the ^{252}Cf fission neutron spectrum. This quantity is currently known to about ±2% and its importance lies in the fact that if the $^{235}U(n,f)$ cross-section as a function of energy is folded with the ^{252}Cf spectrum, the result is very insensitive to uncertainties in the shape of the fission neutron spectrum. It thus provides a useful absolute value for normalizing shape measurements of the differential cross-sections.

Neutron Source Characterization

The main features which have to be considered are summarized below, separating measurements made with mono-energetic neutron sources from those made with "white" neutron sources such as linacs.

INCIDENT NEUTRON ENERGY (E_n)

Mono	*White*
Charged particle energy - accuracy of measurement - reproducibility - calibrate with resonances and reaction thresholds	Measurement of flight time and effective flight path length. Possible dependence of effective flight path on E_n.

Calibrate E_n with standard neutron resonances

NEUTRON ENERGY RESOLUTION (ΔE_n)

Mono	*White*
Target thickness - weigh - observe energy loss from small alpha-emitting deposit	Neutron source pulse shape - calculate - measure with narrow neutron resonances - dependence on E_n - possible room-return effects
E_n - calculate - measure by neutron time-of-flight (if available) - effect of angular spread at the detector of the source neutrons	Detector time response - measure - possible room-return effects

PRESENCE OF UNWANTED E_n

Mono	*White*
Effect of collimators if present	Effect of collimators and flight tubes

Room return

Target contamination - how checked? (especially for deuteron beams)	Background determination by 'notch' filter - accuracy?
Background determination - effectiveness of shadow bars - time-of-flight/pulsed accelerator	How determined for E_n > 1 MeV?

Neutron Flux Determination

It is preferable to record the incident neutron fluence at the sample and the yield of fission events simultaneously. In measurements where this is not possible it will be necessary to use an independent means of monitoring the neutron output during each experimental run, so introducing additional errors in the measured cross-section.

METHOD USED

Reference to primary standard cross-section

Associated particle/activity (Mono only)

The time-correlated associated particle technique effectively removes background in the fission counter caused by scattered neutrons or neutrons arising from other reactions

Detector designed to have an efficiency independent (or nearly independent) of E_n

Calculated efficiency should be verified experimentally

When only the shape of the flux detector efficiency is known and not its absolute value, it will be necessary to consider the use of the detector in a neutron energy region suitable for normalizing the fission cross-section.

GEOMETRICAL EFFECTS

If the neutron fluence and fission yield are not measured in the same geometry with respect to the neutron source, problems can arise:

e.g. Background effects may be very different in each detector and if not accurately accounted for can produce systematic errors.

For a white neutron source, if the flux and fission detector are at different flight path lengths they may "see" each region of the source with different weights with the possible effect that different neutron spectra will be observed.

If the fissile material is not deposited uniformly across the sample, it will be necessary either to confirm that the incident neutron beam is uniform across the sample, or, measure the intensity distribution of the incident neutrons across the sample in addition to determining the variation in fissile deposit thickness.

ELECTRONIC EFFECTS

The effects of dead-time and pile-up receive scant attention in the literature. They can be very important, and correct allowance for them should be validated.

Experimenters using electron linacs at high E_n (and thus short flight times) need to demonstrate that their detectors have fully recovered from the effects of the gamma-flash.

Fissile Sample Characterization

The assumption is made that precision measurements of the fission cross-section must rely on detecting the fission fragments. Fission neutron detection is unsuitable at high E_n, and fission gamma-ray measurements are difficult to interpret. Sample characterization thus means assaying a thin fissile deposit, and the main features which have to be considered are listed below.

Isotopic purity (S,A)* - accuracy of mass-spectrometry has to be specified

Mass assay (A) - in alpha-assay, the uncertainties in the half-lives required will limit the accuracy to ~½%

comparison with standard foil?

International intercomparisons show that small deposits can be measured to ~½%

destructive assay to validate results?

Uniformity of deposit (S,A) - if required can use:

autoradiograph,
alpha-counting,
fission counting with pencil beam of thermal neutrons

Stability of deposit (A) - it is crucial to establish that no loss of fissile material or any deterioration in the deposit occurs throughout the course of the measurements

*S - relevant to a shape measurement of the cross-section
A - relevant to an absolute measurement of the cross-section

Fission Detection Efficiency

In the ideal fission detector, one fragment at least is observed for every fission event occurring in the fissile deposit. The practical detector rarely achieves an efficiency >99% because count rate considerations generally dictate 2π-geometry and deposit thicknesses $\gtrsim$100 $\mu g/cm^2$. The most serious loss of events arises from absorption of fragments within the deposit, and this and other effects are now considered.

DETERMINATION OF EFFICIENCY

Fragment absorption in deposit (A)	- calculation of effect is simple, but magnitude depends on fragment range which may not be known accurately. For precision measurements, self-absorption must not therefore exceed one or two %.
Extrapolation of observed pulse-height distribution to zero (A)	- a discriminator level has to be imposed to reject small background pulses. Extrapolation below this level (ETZ) can only be made with confidence if the observed distribution can be reproduced by calculation. For a thin deposit and well-designed chamber, the ETZ will be $\sim$1%, and the uncertainty in the detection efficiency will be $\sim\frac{1}{4}$%.
Fragment angular distribution effects (S,A)	- the forward peaking produced by the momentum of the incident neutron is simply removed by repeating the measurements with the plane of the deposit rotated through 180° with respect to the beam. The effect of the angular distribution inherent in the fission process requires a knowledge of deposit thickness, fragment range and the distribution itself. For ^{235}U at present energies and a deposit of $\sim$100 $\mu g/cm^2$ this effect introduces an uncertainty of <0.1%.
Neutron scattering (S,A)	- the effect on efficiency of scattering of the incident neutrons in deposit backings, support struts and the chamber body can be made small in the fast neutron energy region by suitable design.

CALIBRATION WITH THERMAL NEUTRONS

The measurement of the efficiency with a beam of thermal neutrons of known flux may not achieve the required accuracy because of uncertainties in determining the effect of neutron scattering in the chamber structures.

GEOMETRICAL AND ELECTRONIC EFFECTS

The remarks in the section on the determination of neutron flux also apply here.

Documentation

For a measurement to be properly evaluated, detailed information on the various points raised in the previous sections must be available. Some journals will find such detail unacceptable, in which case an alternative or additional outlet must be found. The reports issued by national laboratories provide an ideal form of publication, although some would argue that refereeing is not as stringent as in the well-known journals. Reliance on presenting the information in a Ph.D. thesis is undesirable as these are often difficult to obtain.

In recent years, the sophistication of evaluation techniques has increased to the point where, for the most accurate standards, covariance information can be taken into account. Although it can be difficult to assign covariances to published measurements, it may be necessary to estimate values for inclusion in evaluations. It is now almost essential for covariances to be provided in future publications.

Additional Comments on the ^{235}U Data Base

A list of the most important measurements on the ^{235}U fission cross-section above $\sim$1.5 MeV is shown in Table 1 for mono-energetic sources and in Table 2 for white spectrum sources. The data from the measurements listed in the tables are shown in Fig. 1 from 2 to 6 MeV and in Fig. 2 from 6 to 10 MeV. Only measurements made since 1965 have been included as it is thought that, generally speaking, the errors in older measurements are such that they make little contribution to the accurate determination of the cross-section. In addition, measurements by Brown et al (1966) and Seeger (1970) using nuclear devices as a source of neutrons, are not considered to be sufficiently accurate to make a significant contribution and, for the same reason, the measurement of Osterhage (1978) done on a linac, was also rejected. Measurements of other cross-sections, which are not primary standards, made relative to ^{235}U have been omitted as they give information on the other cross-section rather than on $^{235}U(n,f)$.

It can be seen from Figs. 1 and 2 that there is a spread of up to 10% in the measured values in the energy range from 2 to 7 MeV and there are also differences in shape. These discrepancies are often considerably larger than the estimated errors would suggest they should be and this would seem to indicate that unknown systematic errors are present in at least some of the measurements. Tables 1 and 2 contain a few comments on each measurement and some additional comments are now offered. If these are solely directed at the white source measurements, it is because that is where most of the experience of the authors of this paper lies.

In the measurement by Czirr and Sidhu (1975a), the fractional background in the proton-recoil flux detector shows a strong and fluctuating dependence on the neutron energy whereas in a similar measurement by Carlson and Patrick (1978), no variation was observed (see Fig. 3). This difference is rather puzzling, as the two measurements were carried out using somewhat similar arrangements, and gives rise to some concern.

Fig. 4 shows the proton-recoil detector time walk as a function of proton energy as determined by Czirr and Sidhu (1975a). A correction for this effect must be applied to the neutron time-of-flight before calculating the neutron energy for the flux detector. A similar correction was found to be necessary in the experiment of Carlson and Patrick (1978). As the correction is a relative one it is necessary to adjust the zero of the time walk axis to give the correct value for some well-known neutron energy, usually a resonance in ^{12}C observed by placing a slab of graphite in the neutron beam while making a measurement of the flux. This is a perfectly satisfactory arrangement if one can be sure that the time walk is exactly as measured. But the way in which the measurement is done throws some doubts on this. The walk is determined either by using a pulser or with an alpha-particle source and an amplifier, the gain of which is varied, to simulate the desired proton energy range. The question that arises is to what degree these simulations are a true representation of the pulses produced by protons in the Si(Li) detector used. The protons will penetrate the Si(Li) detector to a distance determined by their energy and therefore the pulse shape may change as a function of proton energy. However, in the simulations, no such change in shape occurs and since the time walk may be dependent on the shape, errors may arise. A measurement with a graphite slab in the beam allows the energy scale to be checked up to ~6 MeV using well defined features in the total cross-section of carbon but above that energy no such checks have been carried out and, indeed, sufficiently sharp features may not exist in any cross-section to allow this method to be used. Until such checks have been performed, the energy scales determined in this way must be suspect unless it has been shown that they give correct values for known energy features.

The accurate determination of the neutron flux is clearly of prime importance in any measurement of the ^{235}U fission cross-section. In this respect, it might be instructive to look closely at the detectors used by Leugers et al (1976) and by Kari (1978). Both of these measurements apparently used the same device which is illustrated in Fig. 5. The device consists of two separate detectors, each with a thin radiator foil in a gas scintillation counter system. In the neutron energy region from 1-6 MeV, a single gas scintillation chamber viewed by three photomultipliers (only one is shown) is used and this is shown as detector II in Fig. 5. For energies above 5 MeV, protons from a radiator foil are identified by coincidence in three different scintillation chambers, this arrangement being detector I shown in Fig. 5. In the low energy detector, protons corresponding to a given neutron energy will emerge from the radiator with all energies from zero to the maximum and, in theory, the detector response should be an essentially flat pulse height distribution with a sharp cut-off at the maximum energy. The measured response for several neutron energies is shown in Fig. 6a where it can be seen that the shape is far from ideal. In particular, the low pulse height ends of the spectra show a distinct threshold. This cannot arise from the kinematics of the H(n,p) reaction but must be a consequence of the inability of the photomultipliers to respond to low energy protons or of the electronics which handle the pulses. Either way, it is difficult to see how the response can be calculated with sufficient accuracy to enable the device to be used to measure the absolute value of the flux as a function of neutron energy.

The response of the detector used for higher energy neutrons is easier to understand. The coincidence requirement from the three gas scintillator sections ensures a restricted range of proton energies for a given neutron energy, giving rise to a peak in the pulse height spectrum as illustrated in Fig. 6b.

Conclusions

Between 2 and 8 MeV, the spread in the measured data is $\gtrsim$10%. However, some measurements may contain significant systematic errors which could lead to their being downweighted. This could have a considerable effect on the data base, leaving it rather sparse, particularly where shape measurements are concerned.

In the range 8-20 MeV (excluding the 14 MeV region) the existing data base consists of only three shape measurements, all of which may suffer from systematic errors.

If the requirements are for the ^{235}U fission cross-section to be known to 1-2% accuracy, then the data base in the region 2-20 MeV is inadequate.

Recommendations

1. Accurate shape measurements are required between 1 and 20 MeV.
2. Further mono-energetic absolute cross-section measurements are required in the range 3 to 8 MeV.
3. Documentation of measurements must give full experimental details of the type discussed in this paper in a readily accessible form.

References

Arlt R. et al (1980) Proc. Conf. Nucl. Cross Sections and Technology (Knoxville) NBS Special Publication, Vol. 594, p.990.

Barton D. M. et al (1976) Nucl. Sci. Eng. 60, 369.

Brown W. K. et al (1966) Proc. Conf. on Neut. Cross Sections and Technology, Washington, D.C., p.971.

Cancé M. and Grenier G. (1978) Proc. Conf. Neut. Phys. and Nuc. Data, Harwell, p.864.

Carlson A. D. and Patrick B. H. (1978) Proc. Conf. Neut. Phys. and Nuc. Data, Harwell, p.880.

Czirr J. B. and Sidhu G. S. (1975a) Nucl. Sci. Eng. 57, 18.

Czirr J. B. and Sidhu G. S. (1975b) Nucl. Sci. Eng. 58, 371.

Kari K. (1978) Karlsruhe report KFK-2673.

Kuks I. M. et al (1973) Proc. Conf. on Neut. Physics, Kiev, Vol. 4, 18.

Leugers B. et al (1976) Proc. NEANDC/NEACRP Specialists Meeting on Fast Neutron Fission Cross Sections, Argonne Nat. Lab., ANL-76-90, p.246.

Osterhage W. W. et al (1978) J. Phys. G: Nucl. Phys. 4, 587.

Poenitz W. P. (1974) Nucl. Sci. Eng. 53, 370.

Poenitz W. P. (1977) Nucl. Sci. Eng. 64, 894.

Seeger P. A. (1970) Los Alamos report LA-4420.

Szabo I. and Marquette J. P. (1976) Proc. NEANDC/NEACRP Specialists Meeting on Fast Neutron Fission Cross Sections, Argonne Nat. Lab., ANL-76-90, p.208.

White P. H. (1965) J. Nucl. Ener. 19, 325.

TABLE 1

^{235}U Fission Cross-section Data Base Above ∿1.5 MeV

Mono-energetic sources

Authors	Date	Energy Region (MeV)	Flux Measurement For E_n > 1.5 MeV	Comments
White	1965	0.04-14	H(n,p) + Si det. for $E_n \geq 1$ MeV. Assoc. particle at 14.1 MeV	Very comprehensive measurements. Well documented. No coinc. for assoc. particle.
Kuks et al	1973	2.5	Assoc. particle with gas counter	Mica fission detector. 10% ^{238}U in fission foil.
Poenitz	1974	0.035-3.5	Grey and black detectors	Relative measurements normalised to absolute measurement at 3.5 MeV. Very comprehensive and well documented.
Barton et al	1976	1-6	H(n,p) + Si det.	Pulsed VdG. High accuracy claimed. Comprehensive and well documented.
Szabo et al	1976	up to 5.5 MeV	Calibrated long counter	Pulsed VdG. Comprehensive set of measurements. Early data suffered from loss of fissile material.
Poenitz	1977	0.2-8.2	Black detector	Pulsed VdG. Fission chamber and BND subtend different solid angle at source. Up to 15% correction for flux anisotropy.
Cancé et al	1978	2.5	H(n,p) + Si and directional long counter of Szabo	Preliminary data.
Arlt et	1980	2.6-14.7	Time correlated assoc. particle	Comprehensive set of measurements claiming high accuracy, except at 8.2 MeV due to poor statistics.

TABLE 2

^{235}U Fission Cross-section Data Base Above ∿1.5 MeV

White spectrum sources

Authors	Date	Energy Region (MeV)	Flux Measurement For E_n > 1.5 MeV	Comments
Czirr and Sidhu	1975a	3-20	H(n,p) + Si	Fission rate and flux measured at very different distances from source and in different geometries. Considerable variation in flux background with neutron energy. Effect of gamma-flash on flux detector not checked. Attempt made to measure time walk of flux detector.
Czirr and Sidhu	1975b	0.8-4	H(n,p) + Si	Same technique as above.
Leugers et al	1976	1.2-20	H(n,p) + gas scintillators	Inadequate documentation makes quality of flux measurement difficult to assess. Both fission fragments measured in coincidence in gas scintillators. Flux and fission measurements done at essentially same distance from source and in same geometry.
Kari	1978	1-20	H(n,p) + gas scintillators	Very similar to measurement by Leugers et al, but fission and flux measured at very different distances from source and in different geometries. Small statistical errors.
Carlson and Patrick	1978	1-20	H(n,p) + Si	Similar measurement to Czirr and Sidhu but with flux and fission counting done at essentially same distance and same geometry. Much less variation in flux background. Checks on effect of gamma-flash on detector efficiencies. Only data up to 6 MeV released so far.

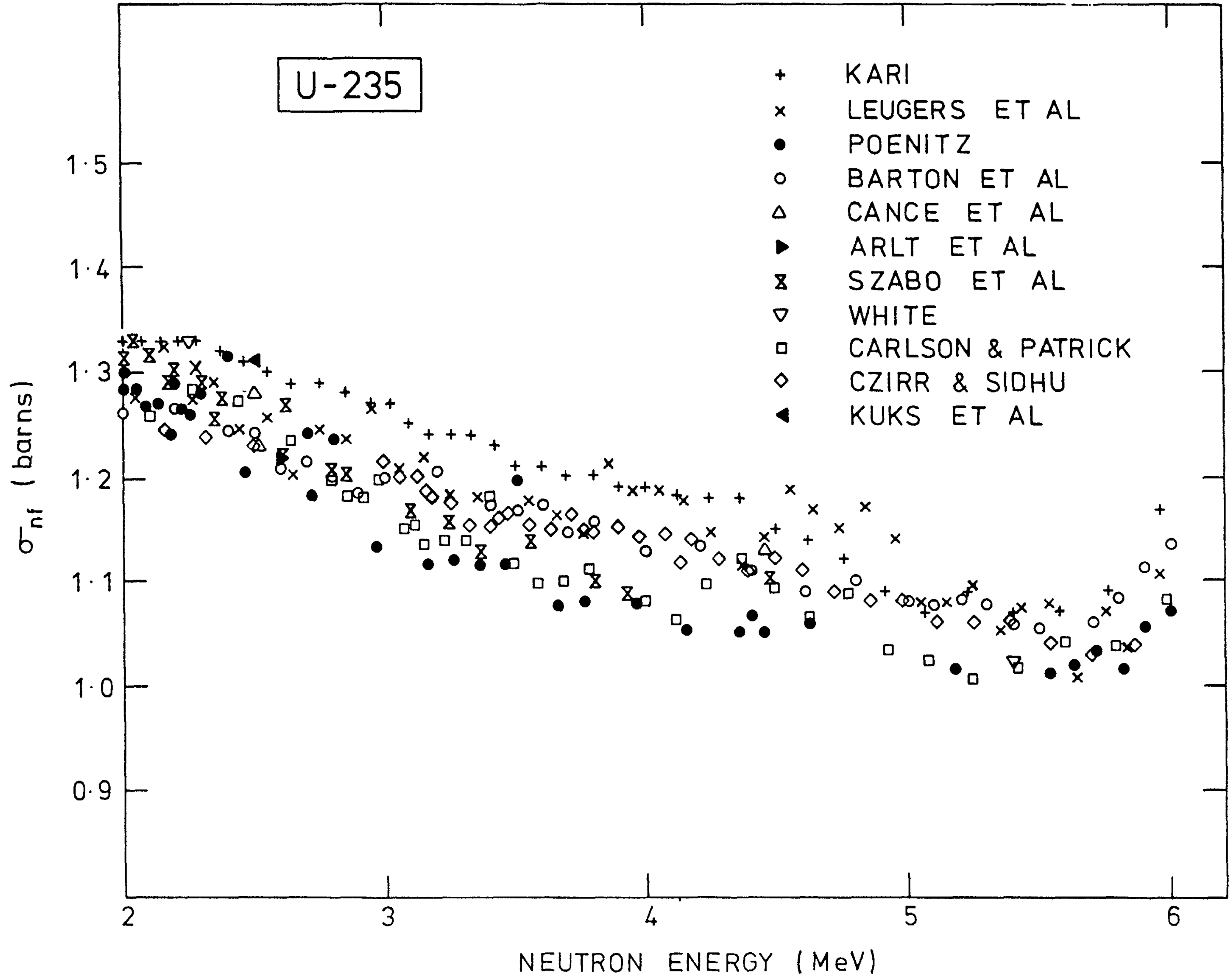

Fig. 1. Measurements of the ^{235}U fission cross-section between 2 and 6 MeV.

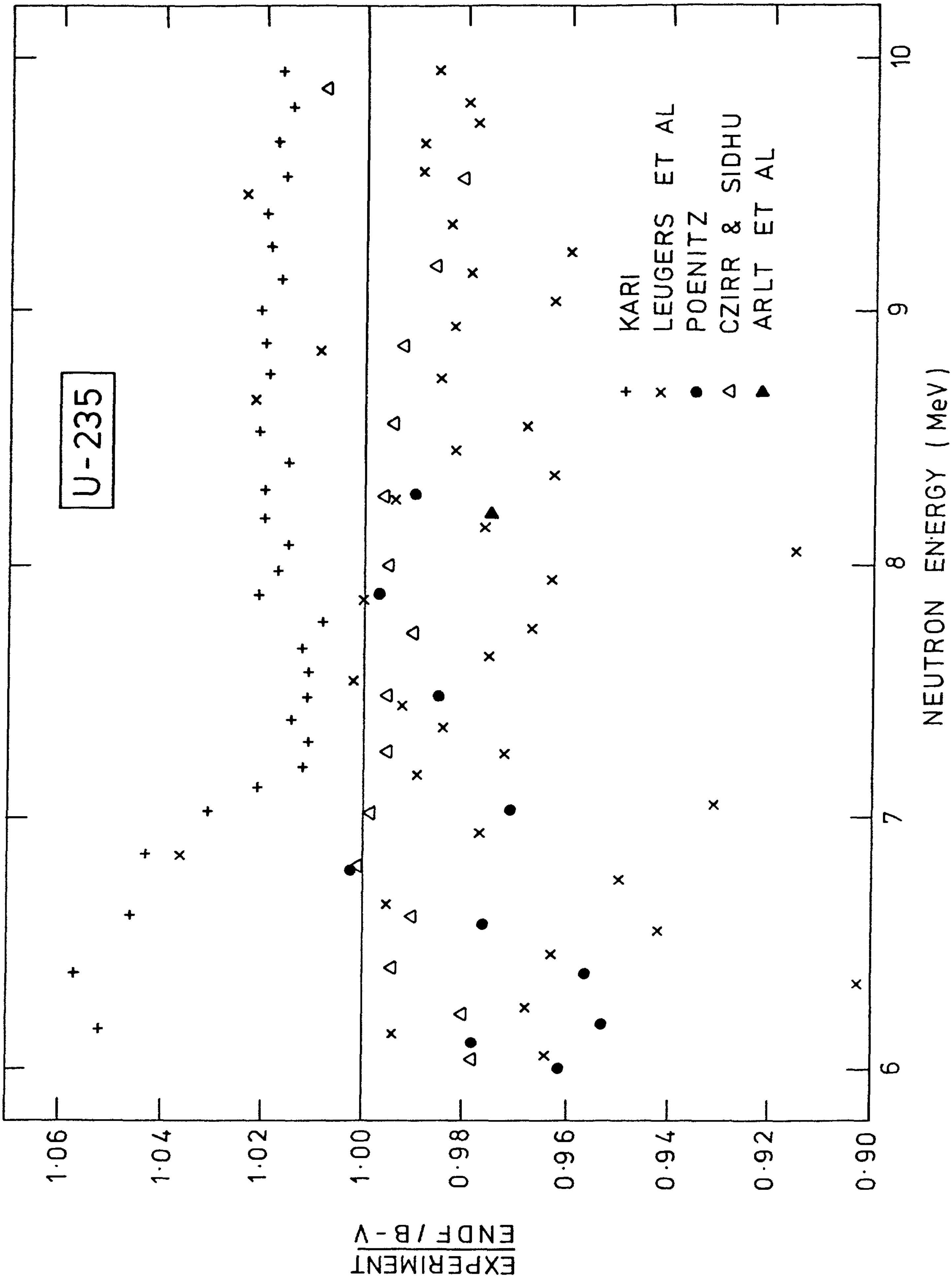

Fig. 2. Measurements of the ^{235}U fission cross-section between 6 and 10 MeV relative to the ENDF B-V evaluation.

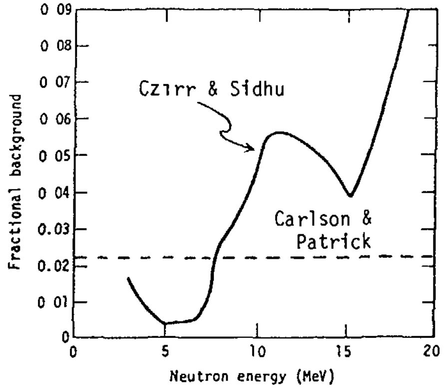

Fig. 3. The fractional background in the proton-recoil flux detector as a function of neutron energy for the measurements by Czirr and Sidhu (1975a) and Carlson and Patrick (1978).

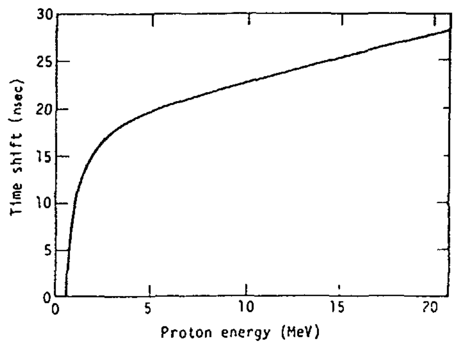

Fig. 4. The proton recoil detector time-walk as a function of proton energy as measured by Czirr and Sidhu (1975a).

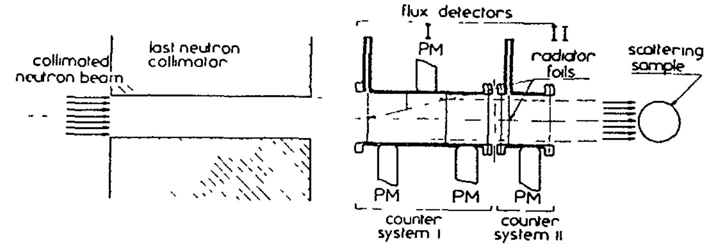

Fig. 5. Schematic experimental arrangement used by Leugers et al (1976) and Kari (1978) for the measurement of absolute neutron flux.

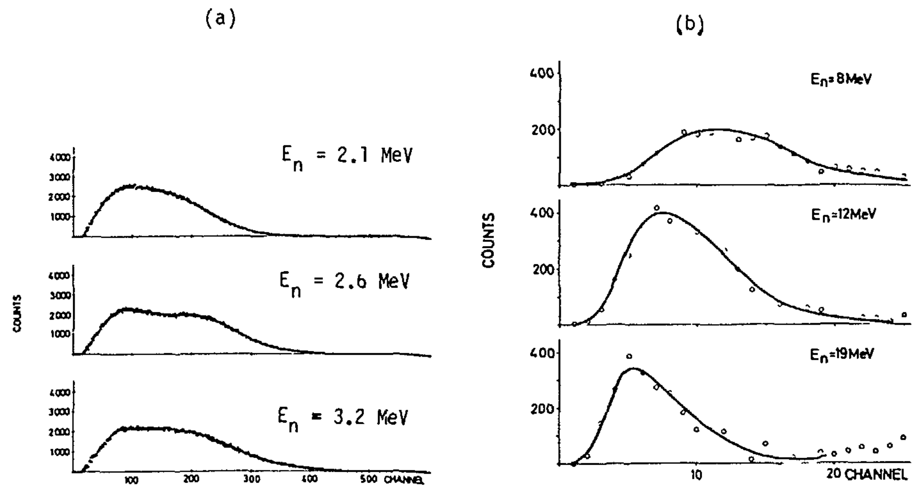

Fig. 6. (a) Proton recoil spectra as measured by detector II (Fig. 5) for several incident neutron energies.

(b) Proton recoil spectra as measured by detector I (Fig. 5) for several incident neutron energies.

CURRENT PROBLEMS IN THE DATA BASE FOR A REEVALUATION OF THE ^{235}U FISSION CROSS SECTION IN THE FAST NEUTRON ENERGY REGION

V.G. Pronyaev, D.E. Cullen, H.D. Lemmel
IAEA, Vienna

Abstract

Recent measurements of the ^{235}U fission cross section are compared over three energy ranges extending from 0.1 to 20 MeV. New absolute measurements at 2.5, 8.5 and 14 MeV indicate that the cross section is now known with an accuracy of 1% near the 14 MeV point and with an accuracy not better than 2-3% for the other two energies. Comparison of the latest shape measurements shows disagreement in shape by about 3-4%.

Requirements on the accuracy of the U-235 fission cross section

At present the World Request List for Nuclear Data (WRENDA) contains 8 high priority requests for the ^{235}U fission cross section in the fast energy region, with accuracy requirements ranging from 1 to 2%. These requirements are based on fast breeder sensitivity calculations as well as on the fact that the ^{235}U fission cross section is extensively used as a standard for other important neutron cross section measurements. For example one request can be summarized as follows: L.N. Usachev requests an accuracy of 1.1% for 0.1-0.8 MeV, 1.4% for 0.8-4.5 MeV and 2% above 4.5 MeV. These requests relate to evaluated data, the accuracy achieved in individual experiments may be lower. M.N. Nikolaev with regard to WRENDA requests on the ^{235}U fission cross section formulated that "a request may be considered fulfilled, when at least three measurements using different methods agree within the requested accuracy".

The current U-235(n,f) standard and other evaluations

Currently the ENDF/B-V $^{235}U(n,f)$ cross section is being widely used as a standard for other neutron reaction cross section measurements. The ENDF/B-V ^{235}U evaluation (MAT No. 6395) was compiled by M.R. Bhat in 1979. The documentation for the ENDF/B-V $^{235}U(n,f)$ cross section states that in the energy range 0.1 to 20 MeV the evaluation of Poenitz [1] was used. However, comparison of the numerical values indicates that the ENDF/B-V values are actually about 1% higher than Poenitz [1] values. In fact ENDF/B-V contains a preliminary version of Poenitz's evaluation; the preliminary version was based on consideration of microscopic data published up to 1978. Consideration of integral data, such as ^{235}U fission averaged over the ^{252}Cf fission neutron spectrum, caused Poenitz to lower his final evaluation at about 1% [1].

Fig. 1 compares the ENDF/B-V and Poenitz evaluations: the solid line represents the ENDF/B-V data and the dash line those of Poenitz [1]. Poenitz's evaluation considered all data available up to the time of the

1978 Harwell Conference on Neutron Physics. Since the Harwell Conference a number of other evaluations have been performed, probably using essentially the same data base as that used by Poenitz for his evaluation. These evaluations include the ^{235}U evaluations in the UKNDL, JENDL-2, ENDL82 libraries and the evaluation of V.A. Konshin and co-workers [6]. All of these are presented in Fig. 1; from this figure we can see that 2% discrepancies are rather typical. The UKNDL evaluation presented in Fig.1 is rather old since it was published in 1972 and is given here only from the point of view of completeness of intercomparison.

Recent measurements

Since the completion of the ENDF/B-V evaluation, there have been a number of measurements of the ^{235}U fission cross section in the energy range up to 20 MeV. These include - shape measurements carried out by Kari and Cierjacks (1978), and a few high precision absolute measurements at 14 MeV by Cance et al. (1978), Wasson et al. (1981), Mahdavi et al. (1982), Arlt et al. (1981), Li Jingwen et al. (1982), at 8.4 MeV by Arlt et al. (1981) and at 2.5 MeV by Cance et al. (1980) and Arlt et al. (1980). All of these results, together with the ENDF/B-V ^{235}U fission cross section are shown in Fig. 2.

In the following figures we shall consider all data available through the international library of the experimental neutron cross sections (EXFOR). These data were supplemented by results of later measurements which are not yet available in EXFOR. Only data measured after 1970 were considered.

In this paper the energy range from 100 keV to 20 MeV has been sub-divided into three energy regions: from 100 keV to about 1 MeV, from 1 MeV to 5 MeV and from 5 MeV to 20 Mev; the reason for this sub-division will become clear later in this paper. Below we shall consider the status of the available data for these energy regions.

Energy region from 100 keV to 1 MeV

1. Most data presented in Fig. 3 show good agreement (within the limits of 2%) with each other. Some new measurements carried out with low accuracy have not been considered.

2. There appears to be some structure in the fission cross section below 350 keV that ought to be taken into account during the evaluation process.

3. Measurements which used the $^{6}Li(n,t)$ reaction as a neutron flux monitor may contain some systematic error in the energy region 200-350 keV because of the error in the magnitude and especially in the position of the resonance in the $^{6}Li(n,t)$ cross section in this energy region.

4. It seems that after renormalization and statistical treatment of the data a 1-2% accuracy can be achieved for the ^{235}U evaluated fission cross section in the energy range 0.1-1 MeV.

5. By examining the latest experimental data (as in Fig. 3) there are indications that a new evaluation would be about 1-2% lower than the existing ENDF/B-V evaluation, i.e. in the direction of the evaluation published by Poenitz [1].

Energy region from 1 to 5 MeV

1. The results of many measurements for this energy region presented in Fig. 4 differ from each other by more than the experimental uncertainties. Also there is a strong discrepancy in the energy dependence between the results of several shape measurements; it is not possible to remove this discrepancy by simple renormalization of the data.

2. Fig. 5 shows the results of the latest absolute measurements at E_n= 2.5 MeV (separate symbols) and shape measurements using the normalization presented by the authors (symbols connected by straight lines). The absolute cross section measurements near 2.5 MeV carried out by different authors, e.g. Cance et al. (1980), Arlt et al. (1980) and based on different methods, give rather conflicting results covering a cross section range between 1.2 and 1.3 barn.

3. Considering the available experimental data it appears that it would be currently difficult for an evaluation in this energy region to achieve an accuracy of 1-2%.

Energy region from 5 to 20 MeV

1. The general picture of ^{235}U fission cross section data in the 5-20 MeV energy range is shown in Fig. 6. Absolute measurements in this energy region have been made in two narrow energy intervals near 8 and 14 MeV and are shown separately in Figs. 7 and 8 together with the same shape measurements. It seems that the ^{235}U fission cross section value for the 14 MeV energy point is well known (1%) and could be used for normalization of shape measurements.

2. The two shape measurements covering the range from 1 to 20 MeV carried out by Czirr and Sidhu (1975) and Kari and Cierjacks (1978) predict different energy dependences of the cross section. To show this more clearly the results of these measurements have been renormalised to the value of 1.25 barn at E_n=2.5 MeV and are presented in Fig. 9, together with the results of the last absolute measurements as well as the ENDF/B-V evaluation. Good agreement among all data at 14 MeV can be seen, but disagreement in the 5 to 11 MeV energy range reaches 5-6%.

3. The existing data at neutron energies higher than 15 MeV are so discrepant that it is difficult to expect a high accurate evaluation in this energy range.

Future Measurements

The available experimental data do not yet reach the required accuracy except for the 14 MeV point ($\sim$1%). If the origin of the experimental discrepancies cannot be identified, new measurements are required, specifically absolute measurements at 2.5 and 8 MeV energies, designed to achieve an accuracy comparable to that currently achieved for 14 MeV energy point ($\sim$1%). The values of the cross section at these three energies can be used both for normalization of those shape measurements which were performed over narrow energy intervals near one of these base points, as well as to check shape measurements which extend over energy ranges which include two or more of these points. More attention has to be paid to the analysis of the energy dependent corrections in the shape measurements, having in mind, that the energy independent corrections could be introduced by a simple renormalization to the values of the cross sections evaluated at the base points.

Conclusion

The results of recent ^{235}U fission cross section measurements were compared from the point of view of a possible re-evaluation of the ENDF/B-V standard curve. The conclusions of this comparison are as follows,

- based on existing experimental data a 1-2% accuracy cannot be achieved over the entire 0.1-20 MeV energy range;

  measurements should be performed near 2.5 and 8 MeV in an attempt to achieve 1% accuracy;

  the accuracy requirements formulated in WRENDA have not yet been met. The requests in WRENDA should be carefully reviewed in particular toward justifying new measurements.

References

[1] W.P. POENITZ, ANL/NDM-45 (1979)

[2] A.D. CARLSON, J.W. BEHRENS, Proceedings of the International Conference on "Nuclear Data For Science and Technology", Antwerp, Belgium, September 1982, p. 456 (1982)

[3] R. ARLT et al., ZFK-459, 35 (1981)

[4] Li JINGWEN et al., see [2], p. 55 (1982)

[5] M. MAHDAVI, G.F. KNOLL, J.C. ROBERTSON, see [2], p. 58 (1982)

[6] V.A. KON'SHIN, V.G. ZHARKOV, E.SH. SUKHOVITSKIJ, INDC(CCP)-148/L (1980)

[7] V.M. ADAMOV et al., Proceedings of the International Conference on "Nuclear Cross Section for Technology", Knoxville, USA, October 1979, p. 995 (1979)

Figures

FIG. 1 Comparison of the ^{235}U fission cross section evaluations carried out in the last years: ENDF/B-V current standard (solid line), W.P. Poenitz's evaluation [1] (dashed line), UKNDL (dotted line). V.A. Kon'shin et al. evaluation [6] (dashed-dotted line), JENDL-2 Library (crosses), ENDL-82 Library (open circles).

FIG. 2 Comparison of the results of measurements carried out after 1978 and the current ^{235}U fission cross section standard (solid line). The entry number from the EXFOR library is given after the name of the author or first author.

FIG. 3 The ^{235}U fission cross section in the 0.1-1 MeV energy range. The entry (and sometimes subentry) number from the EXFOR Library is given after the name of the author or first author.

FIG. 4 The ^{235}U fission cross section in the 1.0 to 5.0 MeV energy range. The entry number of the data set from EXFOR Library is given after the name of the author or first author.

FIG. 5 Comparison of the results of some shape measurements as given by authors (symbols connected by lines) and absolute cross section measurements (separate symbols) for ^{235}U fission cross section near 2.5 MeV.

FIG. 6 ^{235}U fission cross section in the 5 to 20 MeV energy range. Entry numbers of the data set from EXFOR Library are given after the name of the author or first author.

FIG. 7 Comparison of the results of some shape measurements as given by authors (symbols connected by lines) and absolute measurements (separate symbols) for ^{235}U fission cross section near 8 MeV.

FIG. 8 Same as Fig. 7 but for E_n = 14 MeV.

FIG. 9 The ^{235}U fission cross section in the 1-20 MeV energy region after renormalization of the shape measurements as described in the text. The solid line presents the ENDF/B-V values.

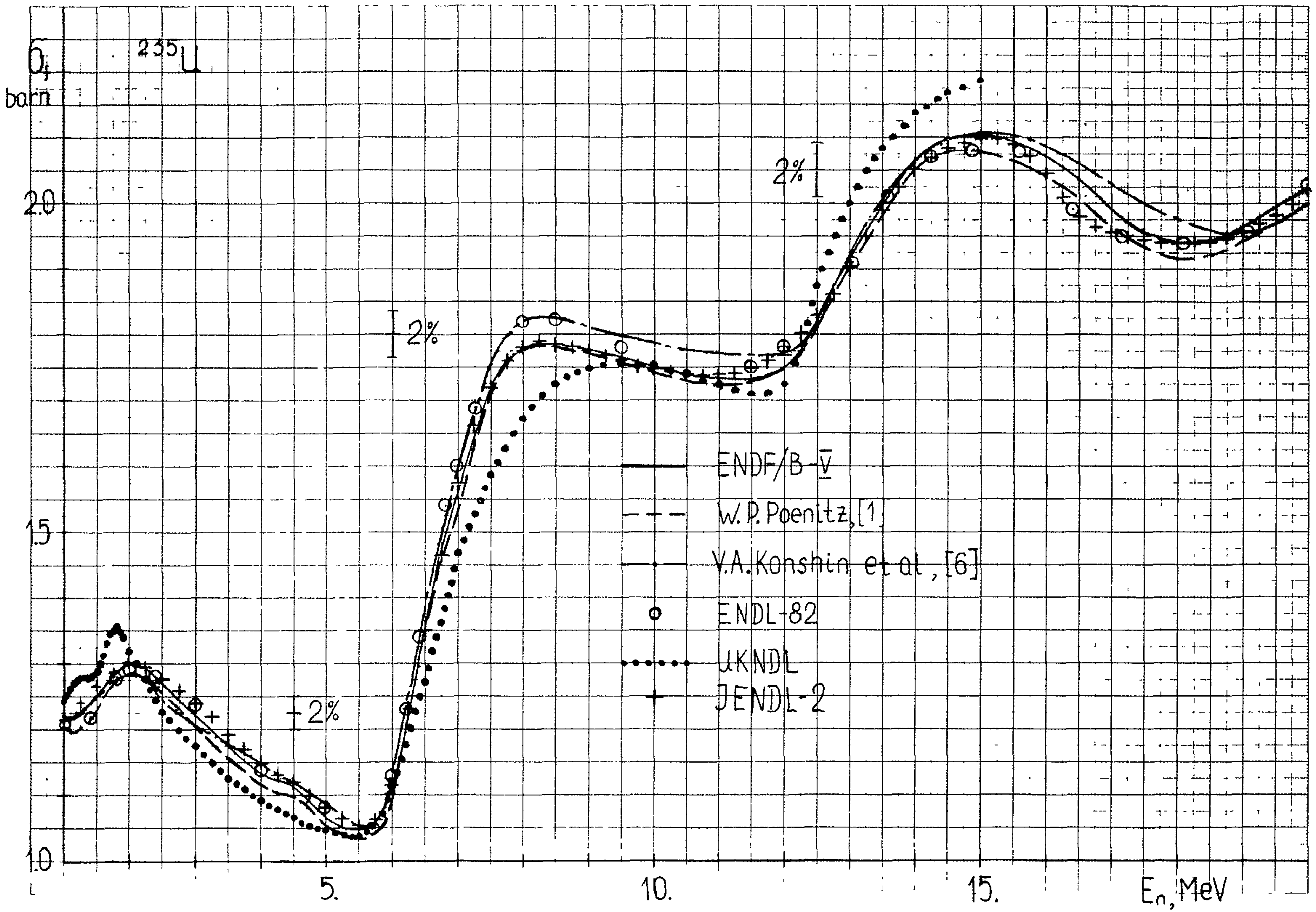

σf barn
235U
2.0
1.5
1.0
5.
10.
15.
En, MeV
2%
2%
2%
ENDF/B-V
W.P.Poenitz,[1]
V.A.Konshin et al, [6]
ENDL-82
UKNDL
JENDL-2

Fig. 1

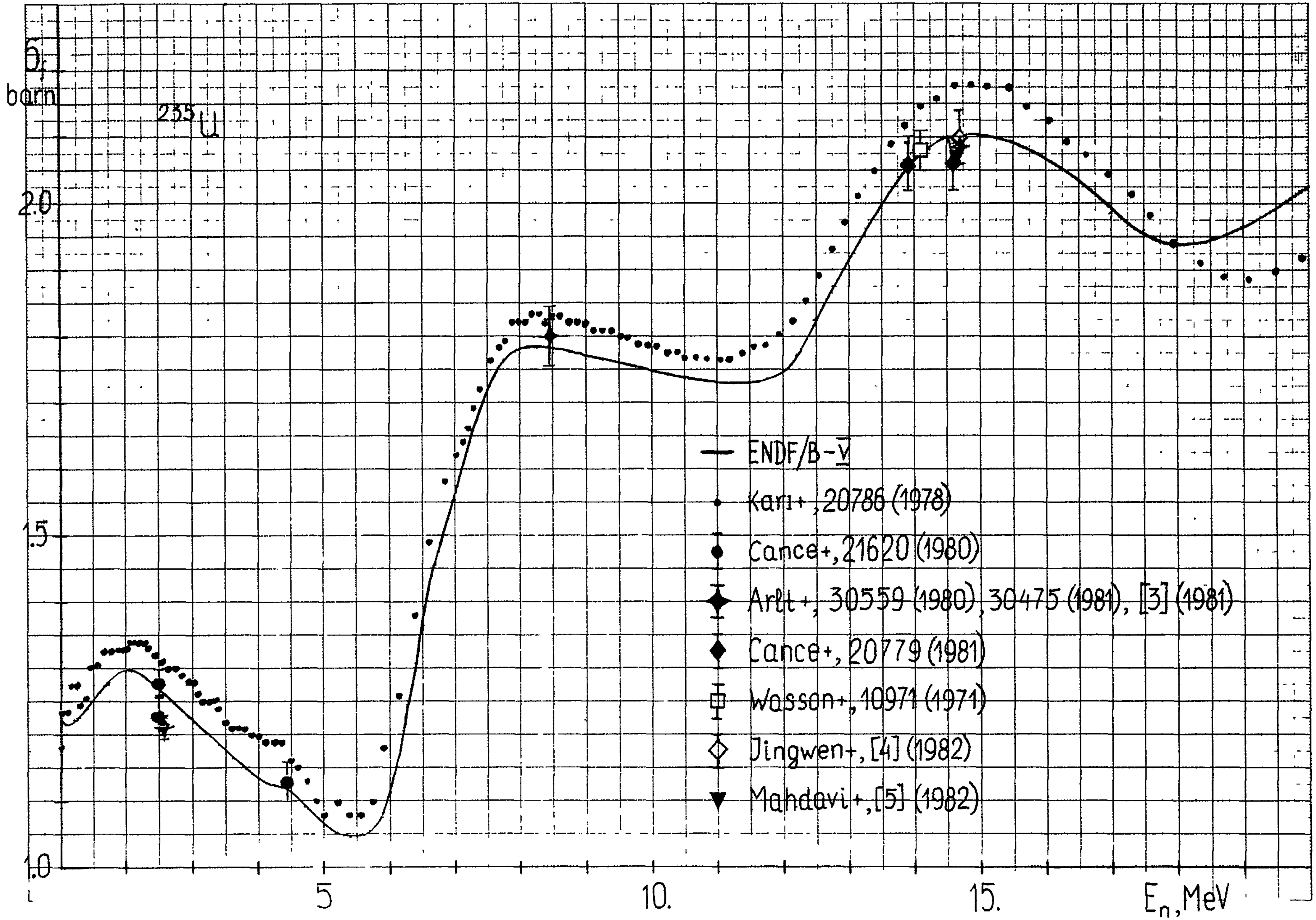

σ
barn
235U
2.0
1.5
1.0
5
10.
15.
En,MeV
ENDF/B-V
Kari+, 20786 (1978)
Cance+, 21620 (1980)
Arlt+, 30559 (1980), 30475 (1981), [3] (1981)
Cance+, 20779 (1981)
Wasson+, 10971 (1971)
Jingwen+, [4] (1982)
Mahdavi+, [5] (1982)

Fig. 2

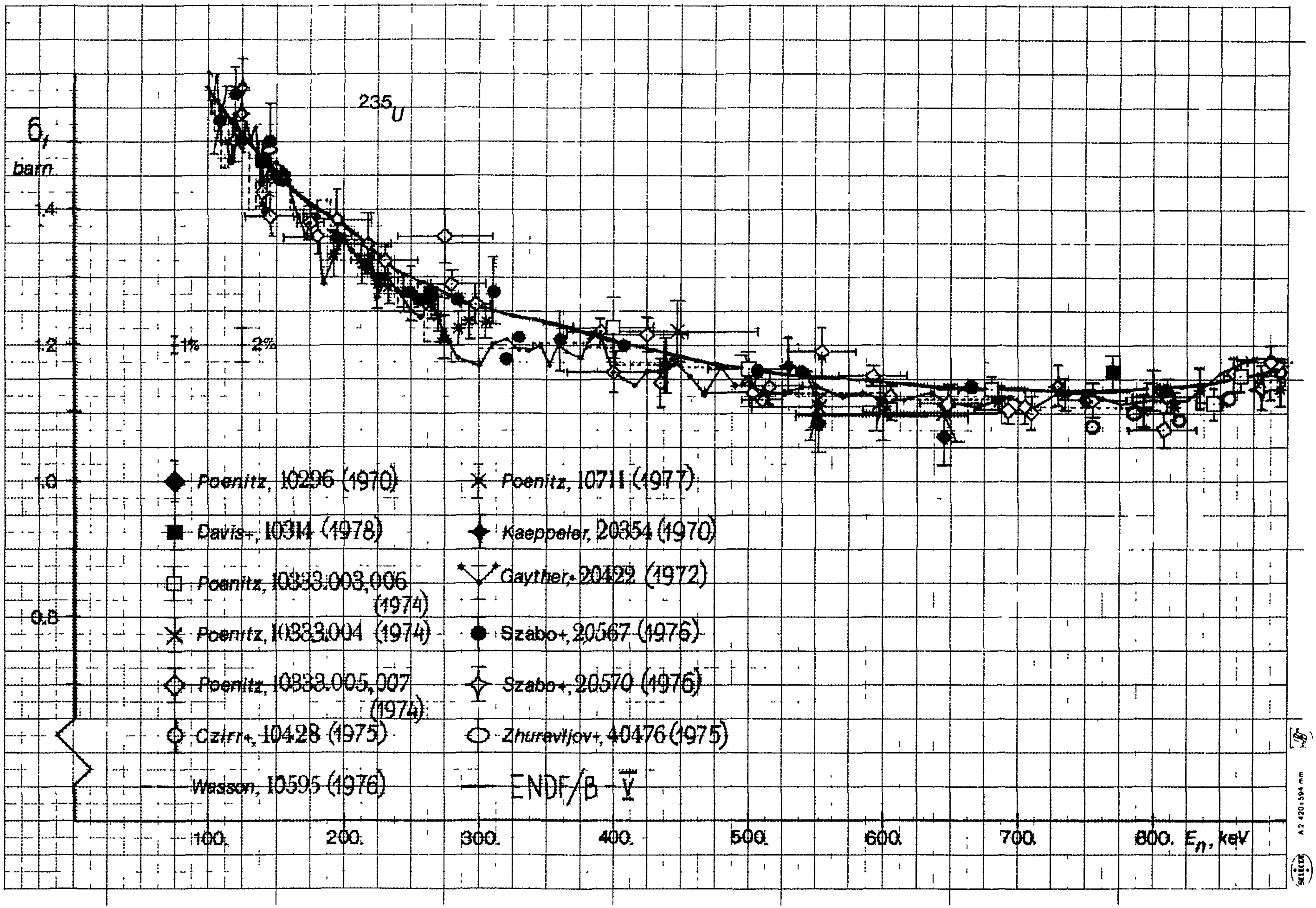

σ_f
barn
^{235}U
1.4
1.2
1.0
0.8
1%
2%
Poenitz, 10296 (1970)
Poenitz, 10711 (1977)
Davis+, 10314 (1978)
Kaeppeler, 20354 (1970)
Poenitz, 10333.003,006 (1974)
Gayther+ 20422 (1972)
Poenitz, 10333.004 (1974)
Szabo+, 20567 (1976)
Poenitz, 10333.005,007 (1974)
Szabo+, 20570 (1976)
Czirr+, 10428 (1975)
Zhuravljov+, 40476 (1975)
Wasson, 10595 (1976)
ENDF/B-V
100.
200.
300.
400.
500.
600.
700.
800. E_n, keV

Fig. 3

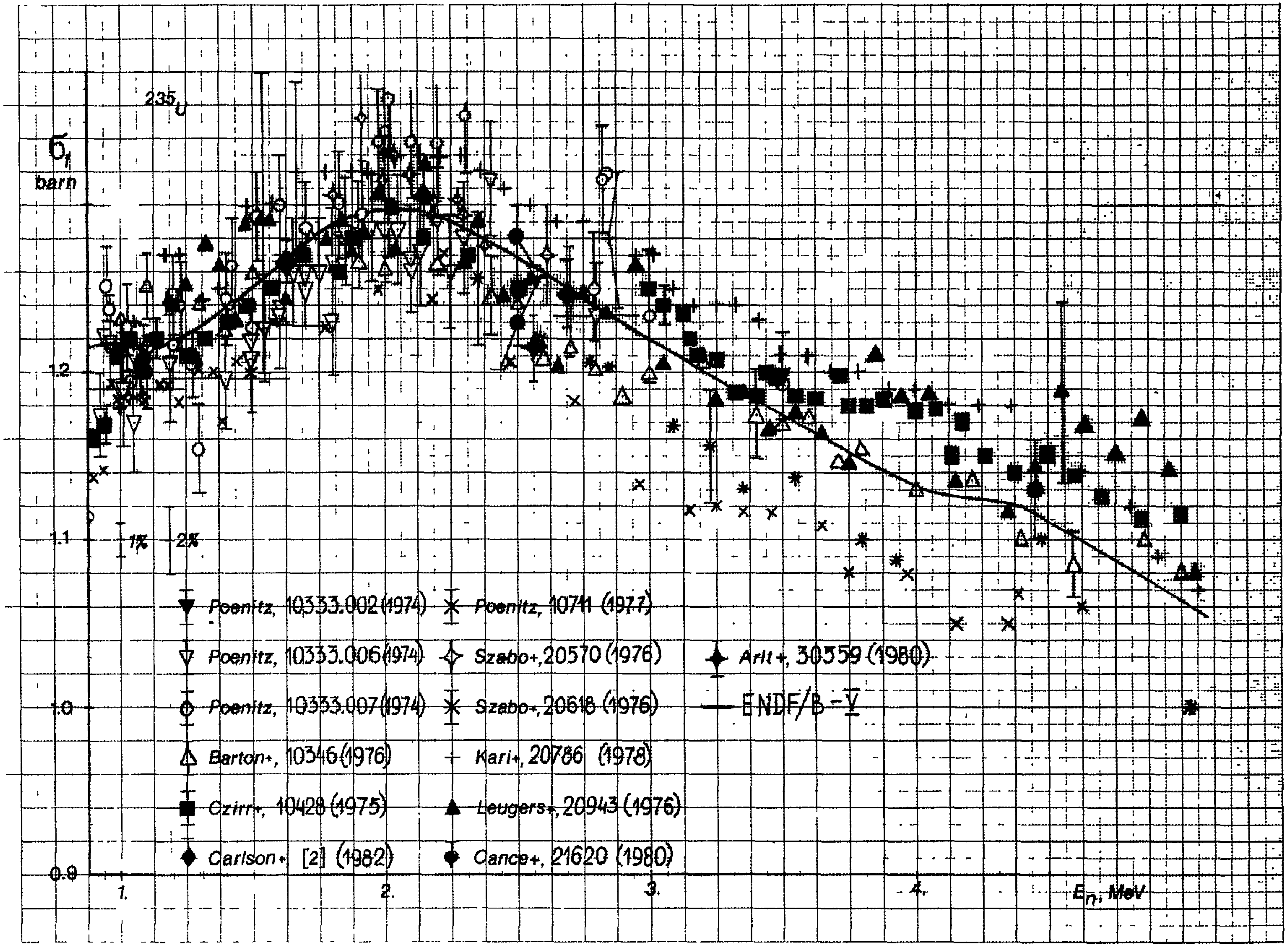

235U
σf
barn
1.2
1.1
1.0
0.9
1%
2%
1.
2.
3.
4.
En, MeV
Poenitz, 10333.002 (1974)
Poenitz, 10333.006 (1974)
Poenitz, 10333.007 (1974)
Barton+, 10346 (1976)
Czirr+, 10428 (1975)
Carlson+ [2] (1982)
Poenitz, 10741 (1977)
Szabo+, 20570 (1976)
Szabo+, 20618 (1976)
Kari+, 20786 (1978)
Leugers+, 20943 (1976)
Cance+, 21620 (1980)
Arlt+, 30559 (1980)
ENDF/B-V

Fig. 4

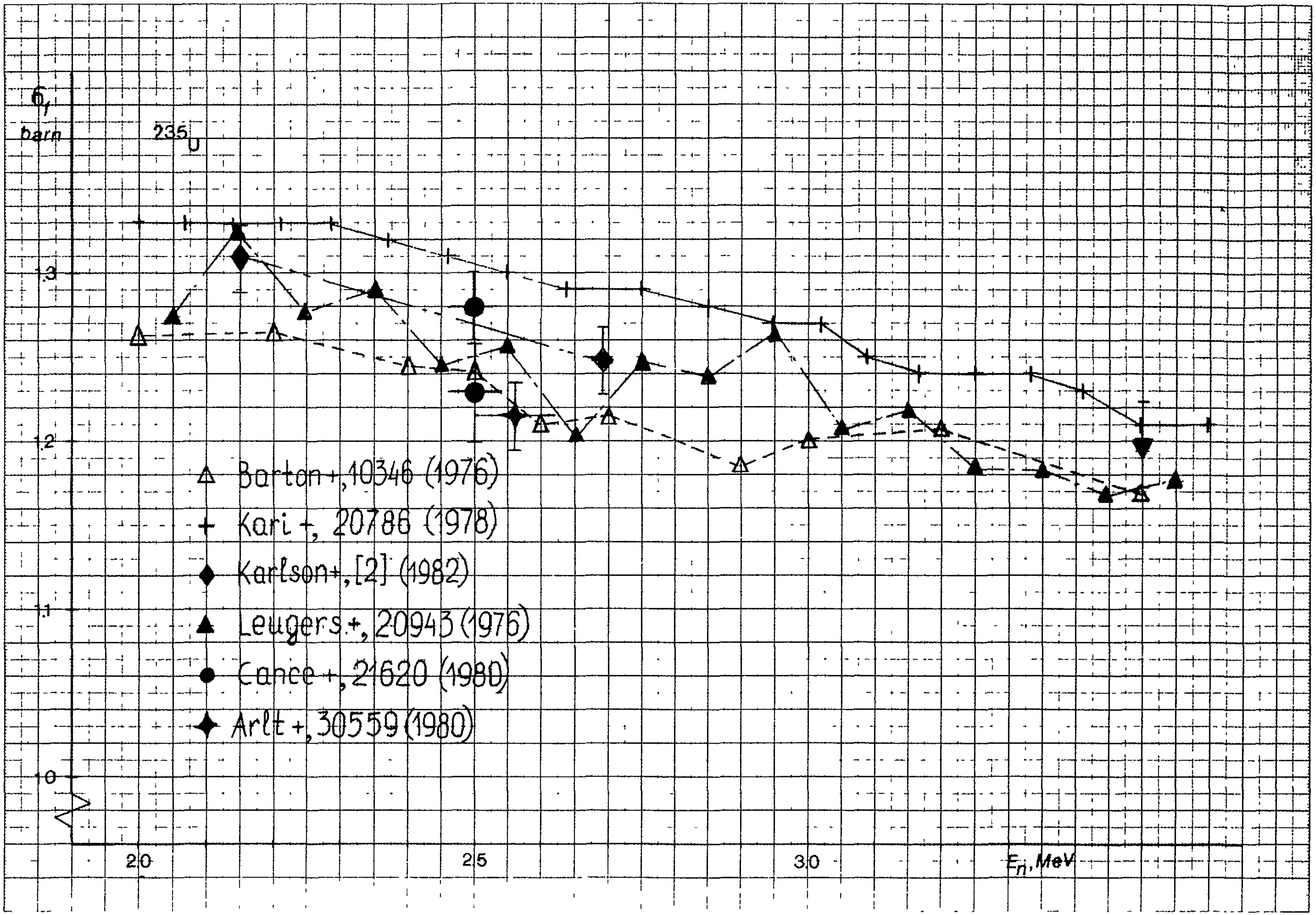
σf
barn
235U
1.3
1.2
1.1
1.0
2.0
2.5
3.0
En, MeV
Barton+, 10346 (1976)
Kari+, 20786 (1978)
Karlson+, [2] (1982)
Leugers+, 20943 (1976)
Cance+, 21620 (1980)
Arlt+, 30559 (1980)

Fig. 5

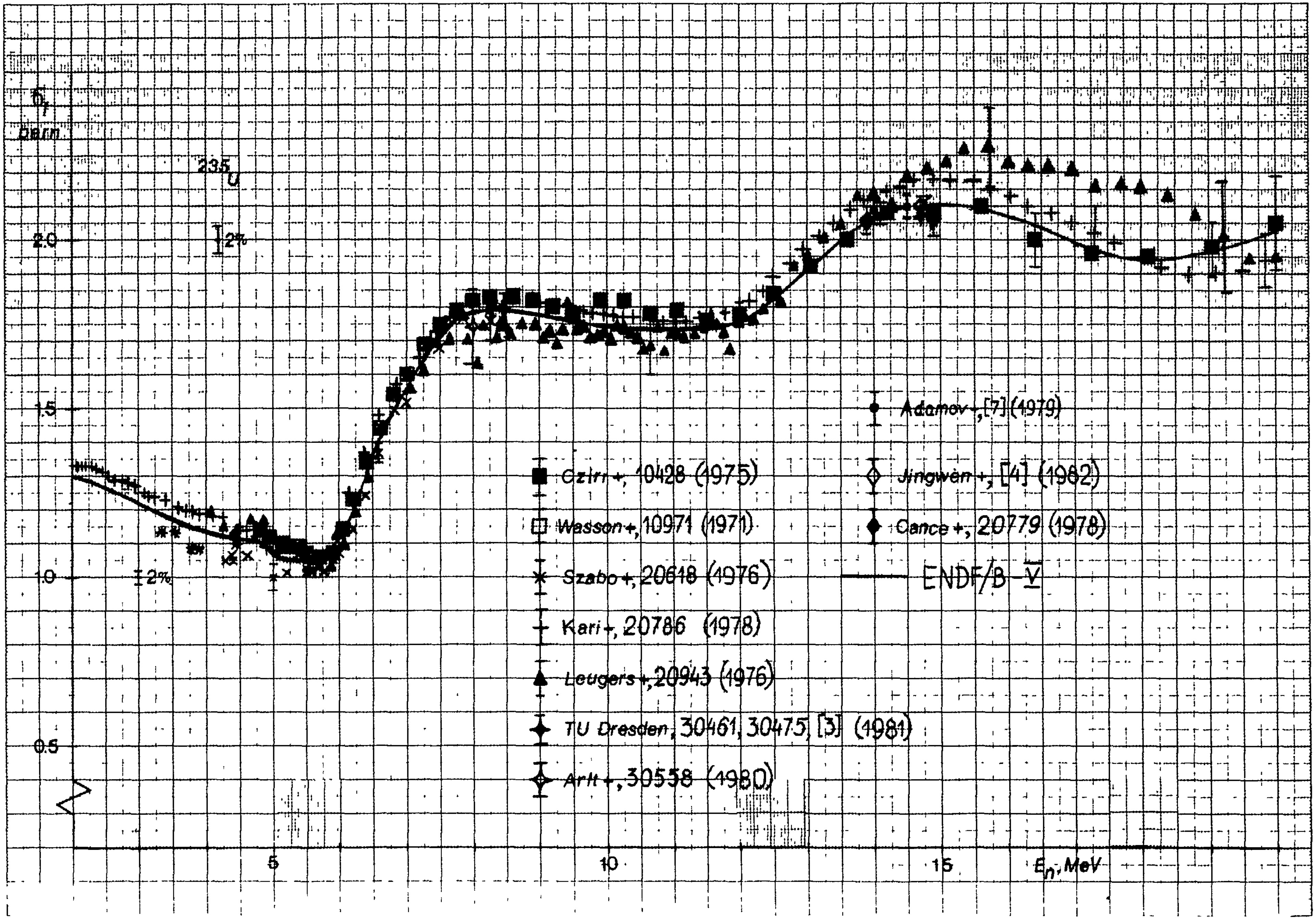

σ_f barn
^{235}U
2%
2%
2.0
1.5
1.0
0.5
5
10
15
E_n, MeV
Czirr +, 10428 (1975)
Wasson +, 10971 (1971)
Szabo +, 20618 (1976)
Kari +, 20786 (1978)
Leugers +, 20943 (1976)
TU Dresden, 30461, 30475, [3] (1981)
Arlt +, 30558 (1980)
Adamov +, [7] (1979)
Jingwen +, [4] (1982)
Cance +, 20779 (1978)
ENDF/B-V

Fig. 6

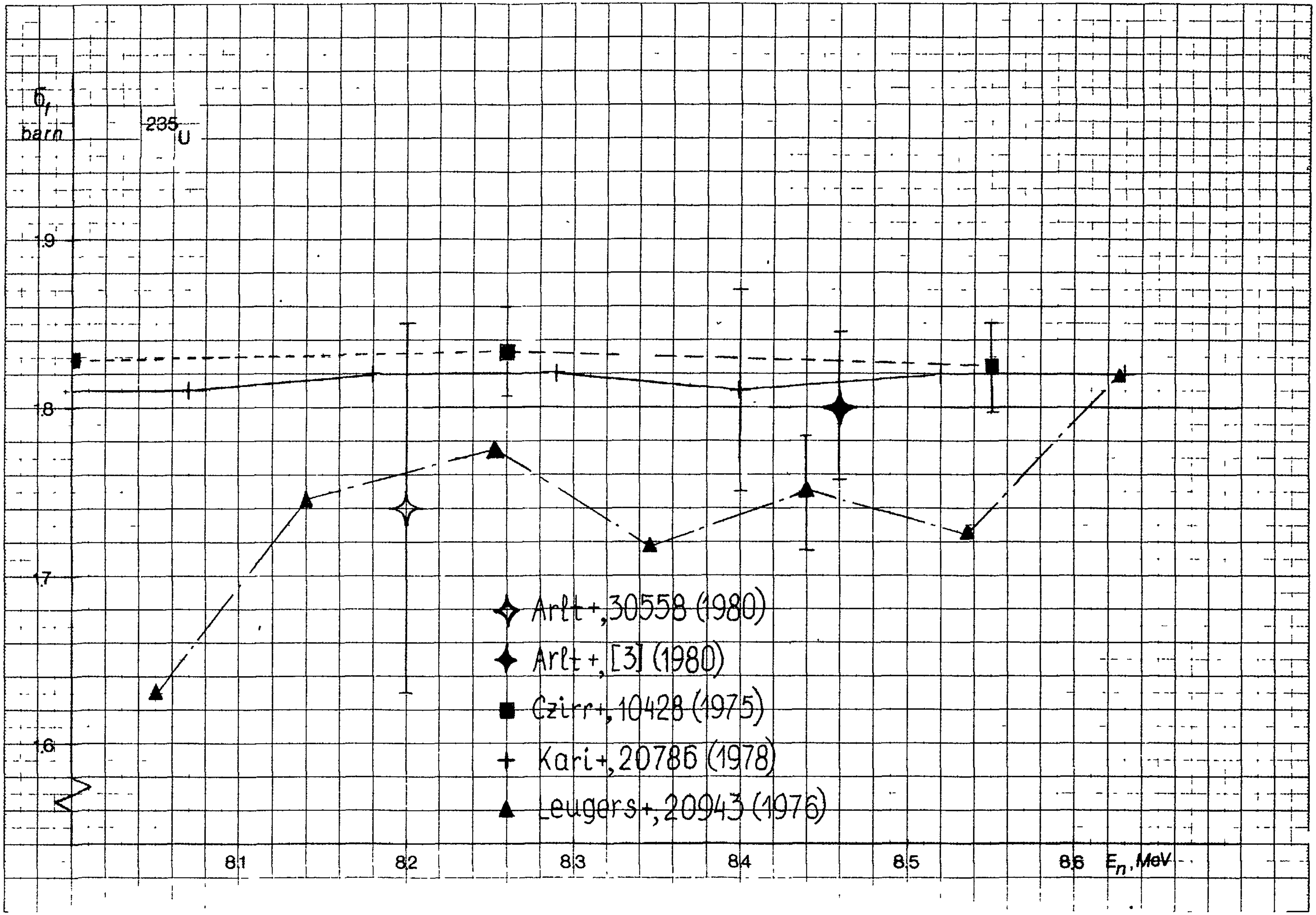
σf
barn
235U
.9
.8
.7
.6
8.1
8.2
8.3
8.4
8.5
8.6
En, MeV
Arlt+,30558 (1980)
Arlt+,[3] (1980)
Czirr+,10428 (1975)
Kari+,20786 (1978)
Leugers+,20943 (1976)

Fig. 7

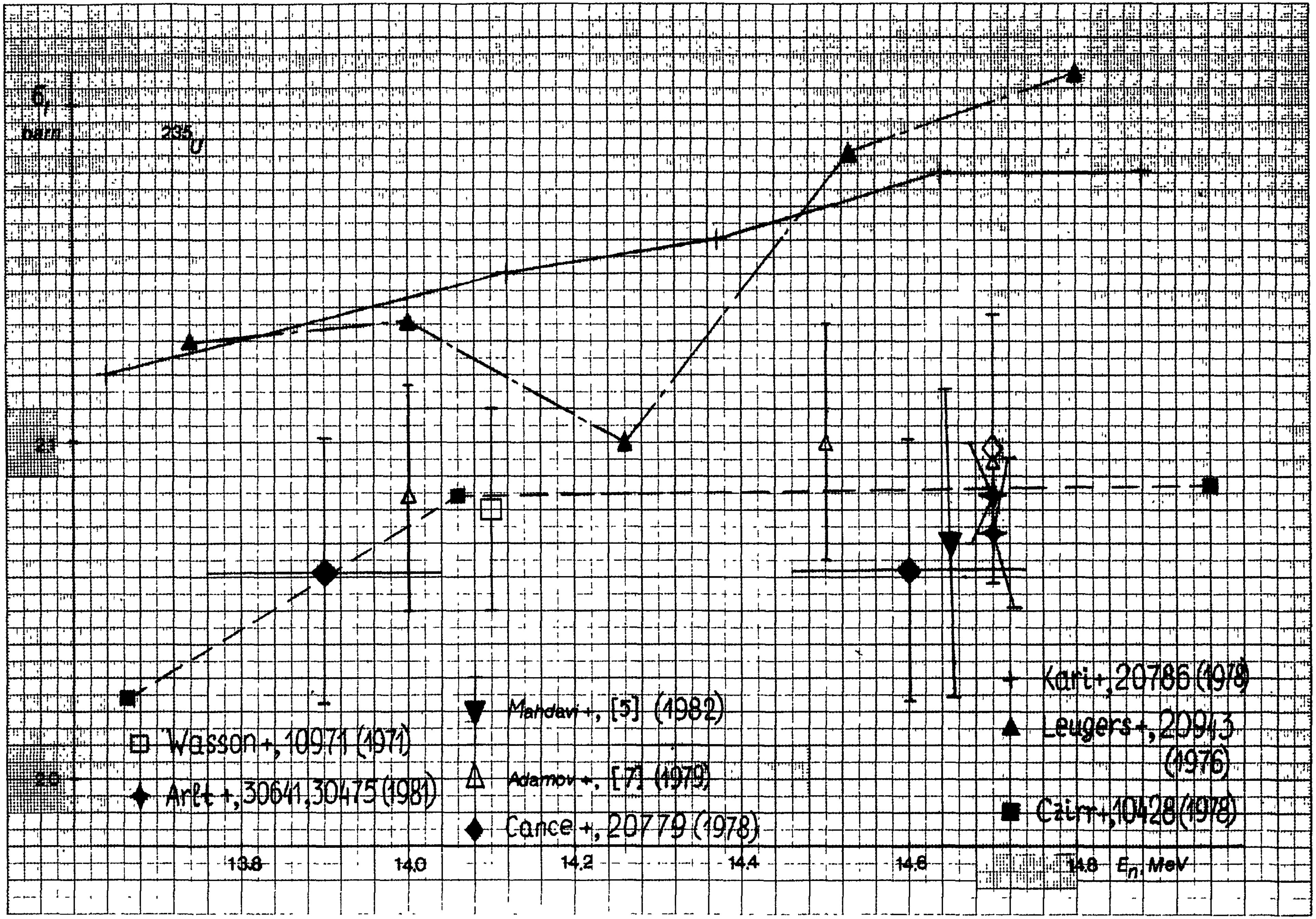
σ, barn
235U
21
20
13.8
14.0
14.2
14.4
14.6
14.8 En, MeV
Wasson+, 10971 (1971)
Arlt+, 30641, 30475 (1981)
Mahdavi+, [5] (1982)
Adamov+, [7] (1979)
Cance+, 20779 (1978)
Kari+, 20786 (1978)
Leugers+, 20913 (1976)
Czirr+, 10428 (1978)

Fig. 8

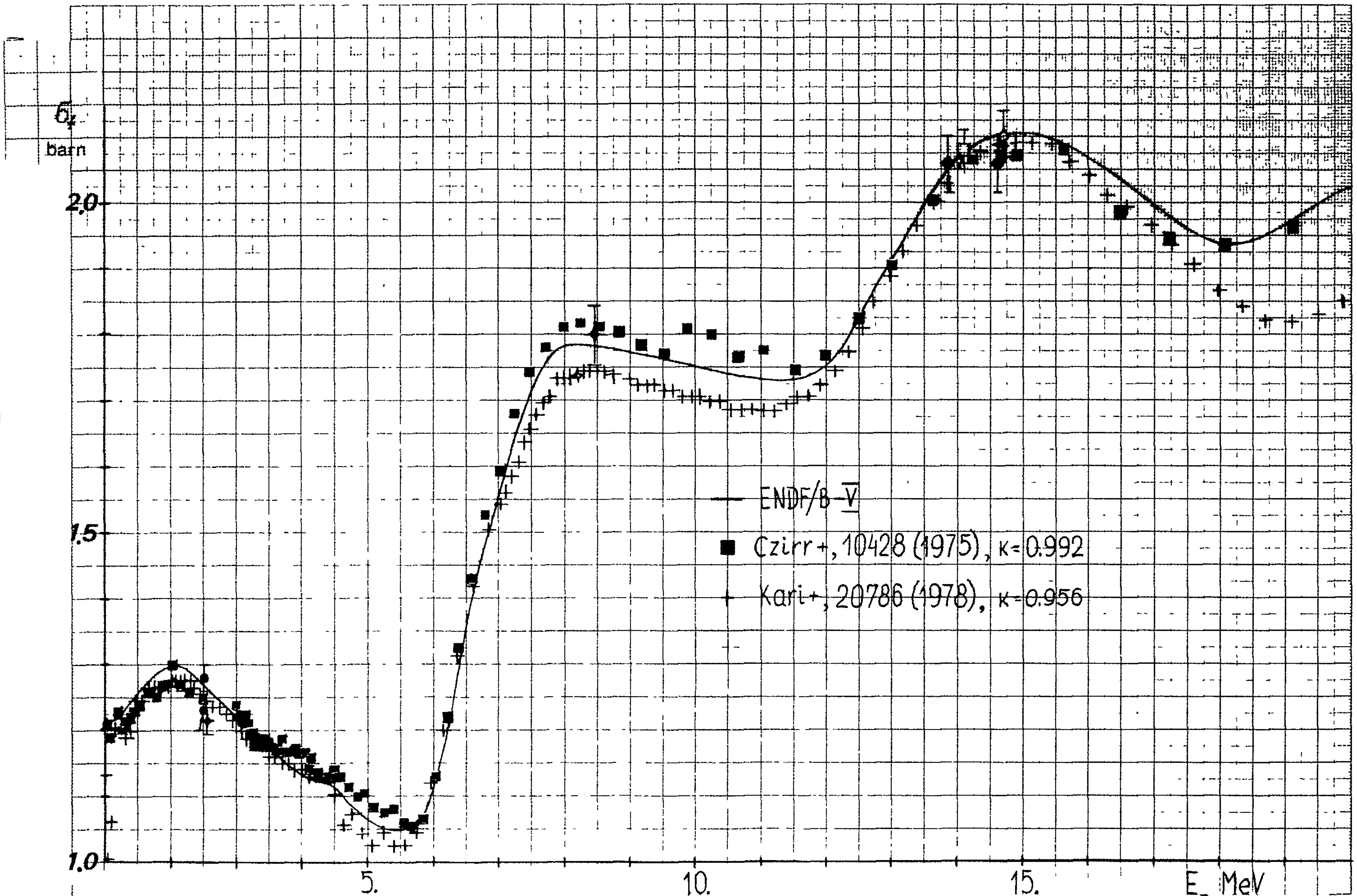

σ_t
barn
2.0
1.5
1.0
5.
10.
15.
E_n, MeV
ENDF/B-V
Czirr+, 10428 (1975), κ=0.992
Kari+, 20786 (1978), κ=0.956

Fig. 9

A Preliminary Evaluation of the $^{235}U(n,f)$ Cross-Section from 100 keV to 20 MeV

M. R. Bhat

National Nuclear Data Center
Brookhaven National Laboratory
Upton, NY 11973 USA

ABSTRACT

A preliminary evaluation of the fission cross-section of ^{235}U from 100 keV to 20 MeV is described. Variance-covariance matrices for a number of experimental data sets were constructed and used to evaluate the fission cross-section following a Bayesian procedure. The evaluated fission cross-section is compared with experimental data including the ^{252}Cf fission neutron spectrum averages and some of the problems encountered in carrying out the fit are discussed.

INTRODUCTION

The fission cross-section of ^{235}U from 100 keV to 20 MeV is used as a primary cross-section standard and has to be evaluated using the experimental data available in this energy region. The evaluation methods are based on the least-squares criterion of Gauss [1] extended to the full variance-covariance matrix of experimental data by Aitken [2] and to the recursive algorithm for the step-wise inclusion of new data by Swerling [3]. The recursive method of Swerling may also be interpreted as a Bayesian procedure where starting from a prior, it is modified by using new experimental data to give a new best estimate and its variance-covariance matrix [4]. Use of these methods for the adjustment and error evaluation of neutron cross-section data was initiated by Dragt et. al. [5] and a further discussion of these procedures may be found in Refs. 6, 7. The evaluation method used here is a Bayesian procedure and follows the treatment of Dragt et. al. [5]. Similar methods have also been used by Perey [8], Hetrick and Fu [9] and by Larson [10].

EVALUATION PROCEDURE

The prior cross-section is specified by a column vector T containing n_t elements and a variance-covariance matrix M of order $(n_t x n_t)$. The n_t elements are the fission cross-sections given on a convenient energy grid. The new experimental data are given as a vector R of n_r elements and a covariance matrix V of order $(n_r x n_r)$. If the corresponding quantities calculated from the prior T are $\overline{R}(T)$, the new "best" estimate T' may be found as the vector that minimizes

$$q^2 = (T'-T)^t M^{-1}(T'-T)+(\overline{R}'-R)^t\ V^{-1}(\overline{R}'-R) \tag{1}$$

where t indicates transpose and $\overline{R}'$ corresponds to the new T' and is given by

$$\overline{R}' = \overline{R} + G\ (T'-T) \tag{2}$$

where G is a $(n_r x n_t)$ sensitivity matrix

$$G = \frac{\delta\overline{R}}{\delta T} \tag{3}$$

The new vector T' and its variance-covariance matrix M' may be found as shown by Dragt from

$$T' = T + AX \qquad \text{and} \tag{4}$$

$$M' = M - AWA^t \tag{5}$$

where

$$A = MG^t \tag{6}$$

and the vector X is a solution of

$$(N+V)\ X = R-\overline{R} \tag{7}$$

and

$$N = GMG^t \tag{8}$$

and

$$W = (N+V)^{-1} \tag{9}$$

To implement these equations a program BFIT (for Bayesian FIT) was written and has been used in this work. In actual practice, a type of "scaling" was used in solving these equations. Thus the vector T is set,

$$T = S_T T_S \tag{10}$$

where S_T is a diagonal matrix with diagonal elements t_1, t_2 ---- t_{n_t} and T_S indicates the "scaled" T vector.

Similarly, the vectors R, $\overline{R}$, $\overline{R}'$ are scaled using a diagonal scaling matrix S_R with diagonal elements $\overline{r}_1$, $\overline{r}_2$ ---- $\overline{r}_{n_r}$. The (i,j)-th element of the scaled sensitivity matrix G_S may be written as

$$(G_S)_{ij} = \frac{t_j}{r_i} G_{ij} \qquad (11)$$

where G_{ij} are the elements of the sensitivity matrix G defined by equation (3). The remaining equations (4) - (9) have exactly the same form as above provided each matrix is replaced by its "scaled" counterpart transformed by the scaling matrices S_T and S_R. Working with the scaled vectors T_S, R_S corresponds physically to using ratios of the cross-sections divided by the corresponding cross-sections given by the prior. Or in other words, the "gross" energy dependence of the cross-section is removed and the program uses ratios centered around the value 1.0 and any deviations from 1.0 are used to modify the prior.

In practice, this gives a certain amount of numerical stability to the program and the evaluation procedure.

DATA USED IN THE EVALUATION

The program BFIT can handle a prior vector T of maximum number of points equal to 150. Absolute ^{235}U (n,f) data were plotted and a smooth curve drawn through them and the cross-section values corresponding to the energy grid of the ENDF/B-V ^{235}U fission cross-section from 100 keV-20 MeV were read off from it. This is indicated by the MAT/MT/MF numbers as 5500/3/18 in the ENDF/B notation. The variance matrix M of the prior was arbitrarily set to have 3% error along the diagonal and a constant correlation coefficient ρ=0.5 for the off-diagonal elements. The experimental data used in this fit are given in Table I with references and the energy ranges covered by them. Two of these data sets [26,28] give ^{252}Cf fission spectrum averaged values of the ^{235}U fission cross-section.

The variance-covariance matrices of each of these data sets were formed using the procedures discussed by Perey [29] and by Mannhart [30]. All available information about a measurement obtained either from the publication, X-4 data files or private communication with the authors was used. The experimental errors were divided into statistical and a number of components of systematic errors. The correlation coefficient between the i-th component of systematic errors at two different energies was assumed to be constant and equal to 1.0 unless specifically stated by the author to be otherwise. It is quite possible that these correlation coefficients are energy dependent with different ranges of correlation. Guidance on this can only be provided by the data measurer and was unavailable in most cases. Error in the energy scale ΔE_n and the effect of finite resolution on the data were included by estimating additional data uncertainty due to these and increasing the errors. Data uncertainty due to fluctuations in the data below 350 keV were included using the results of Bowman et. al. [31]. In using the ^{252}Cf fission neutron spectrum averaged cross-sections it was assumed that the Californium spectrum could be represented by a Maxwellian with θ = 1.42 MeV. This may not be the best representation of experimental data. Further, the variance-covariance matrix of the Californium spectrum is not available. These pieces of information are essential for an effective use of this integral measurement in data evaluation.

Amongst the data sets given in Table I, Nos. 1-8 were treated as shape data which could be arbitrarily normalized. The corresponding normalization constants were determined as part of the fitting procedure by extending the T vector and its covariance matrix M to include these.

RESULTS AND CONCLUSION

The result of this evaluation procedure is shown in Figs. 1-4 plotted against the experimental data used. The ENDF/B-V evaluation is also shown for comparison. It is noted that from 0.1-0.7 MeV, the present evaluation is systematically lower on an average by 1.6% (maximum deviation-3.5%) than the ENDF/B-V evaluation, from 0.7-4.0 MeV it is lower on an average by 1.2% (maximum deviation-2.8%). From 4.0-6.5 MeV, the BFIT result is lower than ENDF/B-V on an average by 0.2% and from 6.5-13.5 MeV higher by 0.8%. Above 15 MeV the present evaluation follows Kari data whereas ENDF/B-V cross-section follows the Czirr data. The ^{252}Cf spectrum average over a Maxwellian spectrum with θ = 1.42 MeV is found to be 1.217 b without including the Grundl [28] and Adamov [26] data, and equal to 1.218 b if they are included. It is noted that the final evaluated curve shows a non-smooth behaviour due to the statistical fluctuations in the input data and is quite consistent with them. A smoothing of the final result with a corresponding transformation of its variance-covariance matrix could be done to obtain a smooth curve. A "goodness-of-fit" for the whole evaluation was obtained as follows. Starting from a prior, in the first iteration the effect of each data set was incorporated into its prior. In a second iteration a "chi-square" defined by

$$\chi_i^2 = (R-\overline{R})^t \; (N+V)^{-1} \; (R-\overline{R}) \qquad (12)$$

is calculated for the i-th data set. In the above equation $R, \overline{R}$, N and V refer to this data set and have been defined before. In this iteration the evaluated curve obtained in the first iteration is not altered, thus χ_i^2 for each data set is calculated comparing it with the same final curve obtained in the first iteration. Using these a global χ^2 /Degree of Freedom defined as

$$\text{Global } \frac{\chi^2}{D.F} = \frac{\sum_i \chi_i^2}{(N_{tot} - N_{par})} \qquad (13)$$

is calculated. Here the summation is over all the data sets and N_{tot} is the total number experimental points and N_{par} the number of parameters (number of points + normalizing constants) determined from the fit. For the fit shown here this global χ^2 /D.F. was found to be equal to 0.85 indicating a reasonable fit to the data. The diagonal elements of the variance-covariance matrix of the evaluated curve showed errors ranging from 0.5 - 2.0%. These low error estimates of the evaluated curve have to be reconciled with the spread in experimental data shown in Figs. 1-4 by further studies of the fitting procedure.

REFERENCES

1. K. F. Gauss, Werke, 4, 1-93 (1809), See also NBS. Sp. Pub. 300 Vol.1, p. 265 (1969).

2. A. C. Aitken, On least squares and linear combination of observations, Proc. Roy. Soc. Edinb. A55, 42 (1935).

3. P. Swerling, First order error propagation in a stagewise smoothing procedure for satellite observations, J. Astronautical Sci. 6, 46 (1959).

4. N. Morrison, Introduction to sequential smoothing and prediction, McGraw-Hill Book Co. (1969).

5. J. B. Dragt. et. al., Methods of adjustment and error evaluation of neutron capture cross-sections; application to fission product nuclides, Nuc. Sci. Eng. 62, 117 (1977).

6. B. A. Magurno and S. Pearlstein (Eds.), Proc. of the conference on nuclear data evaluation methods and procedures, Vols. 1,2, BNL-NCS-51363 (1981).

7. R. W. Peelle, Uncertainty in the nuclear data used for reactor calculations, Advances in Nuc. Sci. and Technology 14, 11 (1982) Plenum Pub. Corp.

8. F. G. Perey, Contributions to few-channel spectrum unfolding, ORNL/TM-6267 (ENDF-259) (1978).

9. D. M. Hetrick and C. Y. Fu, GLUCS: A generalized least-squares program for updating cross-section evaluations with correlated data sets ORNL/TM-7341 (ENDF-303) (1980).

10. N. M. Larson, User's Guide for BAYES: a general-purpose computer code for fitting a functional form to experimental data, ORNL/TM-8185 (ENDF-323) (1982).

11. A. D. Carlson and B. H. Patrick, Measurements of the ^{235}U fission cross-section in the MeV region, Proc. of an international conf. on neutron physics and nuclear data for reactors, Harwell (1978) and private communication.

12. O. A. Wasson et. al., Absolute measurement of the U-235 fission cross-section from 0.2 to 1.2 MeV, Nuc. Sci and Eng. 81, 196 (1982).

13. J. B. Czirr and G. S. Sidhu, Fission cross-section of U-235 from 3 to 20 MeV, Nuc. Sci. and Eng. 57, 18 (1975) and Fission cross-section of U-235 from 0.8 to 4 MeV, Nuc. Sci. and Eng. 58, 371 (1975).

14. W. P. Poenitz, Relative and absolute measurements of the fast-neutron fission cross-section of U-235, Nuc. Sci. and Eng. 53, 370 (1974).

15. W. P. Poentiz, Additional measurements of the ^{235}U (n,f) cross-section in the 0.2 to 8.2 MeV range, Nuc. Sci. and Eng. 64, 894 (1977).

16. I. Szabo and G. P. Marquette, Measurements of the neutron induced fission cross-sections of U-235 and Pu-239 in the MeV energy range, ANL-76-90, 208 (1976).

17. D. B. Gayther et. al., Proc. 2nd IAEA panel on neutron standard reference data, p. 207 (1974).

18. D. M. Barton et. al., Measurement of the U-235 fission cross-section over the neutron energy range 1 to 6 MeV, Nuc. Sci. and Eng. 60, 369 (1976).

19. K. Kari, KFK-2673 (1978).

20. O. A. Wasson et. al., Measurement of the ^{235}U neutron-induced fission cross-section at 14.1 MeV, Nuc. Sci. and Eng. 80, 282 (1982).

21. M. C. Davis et. al., Absolute measurements of ^{235}U and ^{239}Pu fission cross-sections with photo neutron sources, Ann. of Nuc. Energy, 5, 569 (1978).

22. P. H. White, Measurements of the ^{235}U neutron fission cross-section in the energy range 0.04 - 14 MeV, Journ. of Nuc. Energy A/B 19, 325 (1965).

23. M. Cance' and G. Grenier, Absolute neutron fission cross-sections of ^{235}U, and ^{238}U and ^{239}Pu at 13.9 and 14.6 MeV, Nuc. Sci. and Eng. 68, 197 (1978).

24. M. Cance' and G. Grenier, CEA-N-2194 (1981).

25. I. M. Kuks, Kiev 4, 18 (1973).

26. V. M. Adamov et. al., Absolute measurements of induced fission cross-sections of heavy nuclides for both ^{252}Cf fission spectrum neutrons and 14.7 - MeV neutrons, NBS Sp. Pub. 594, 995 (1980).

27. R. Arlt et. al., Kernenergie, 25, 199 (1982), ZFK-459, 35 (1981), Kernenergie, 24, 48 (1981).

28. J. Grundl et. al., Private communications (1982).

29. F. G. Perey, Covariance matrices of experimental Data, Proc. of an international conf. on neutron physics and nuclear data for reactors, Harwell (1978) p. 104.

30. W. Mannhart, A small guide to generating covariances of experimental data, PTB-FMRB-84 (1981).

31. C. D. Bowman et. al., Structure limitations on accuracy of U-235 fission cross-section measurements, 270, ANL-76-90 (1976).

TABLE I

^{235}U (n,f) Data Sets Used in the Fit

No	Author	Ref.	Energy Range (keV)	Comments
1	Carlson and Patrick	11	1.171+3 - 6.203+3	Preliminary
2	Wasson et. al.	12	9.9+1 - 7.5+2	
3	Czirr and Sidhu	13	7.54+2 - 2.01+4	
4	Poenitz	14	3.99+2 - 2.803+3	BND Shape data normalized at 800 keV
5	Poenitz	14	8.4+1 - 3.5+3	GND Shape data normalized at 3.5 MeV
6	Poenitz	15	2.15+2 - 3.05+2	TOF Shape Data
7	Szabo	16	7.25+1 - 1.01+3	White Counter
8	Gayther	17	7.1086+1 - 1.0039+3	
9	Barton	18	1.0+3 - 6.0+3	
10	Kari	19	1.0+3 - 2.075+4	
11	Wasson et. al.	12	2.44+2 - 1.196+3	
12	Wasson et. al.	20	1.41+4	TCAP
13	Davis et. al.	21	1.4+2 - 9.64+2	
14	Poenitz	14	3.5+3	Large BND
15	Poenitz	14	8.0+2	Small BND
16	Poenitz	14	4.48+2 - 6.44+2	Assoc. activity
17	Poenitz	14	4.98+2	Vanadium bath
18	Poenitz	15	1.93+2 - 2.93+2	

Table I (cont'd)

No	Author	Ref.	Energy Range (keV)	Comments
19	Poenitz	15	6.84+2 - 4.449+3	
20	Poenitz	15	4.396+3 - 8.275+3	
21	Szabo	16	7.8+1 - 1.99+2	Knoxville '71
22	Szabo	16	7.1+1 - 2.61+3	Kiev '73
23	Szabo	16	2.35+3 - 5.53+3	
24	White	22	1.27+2 - 1.41+4	
25	Cance' & Grenier	23	1.39+4 - 1.46+4	
26	Cance' & Grenier	24	2.5+3 - 4.45+3	
27	Kuks	25	2.5+3	
28	Adamov et. al.	26	1.48+4	Revised '77 datum
29	Adamov et. al.	26	1.4+4 - 1.47+4	TCAP
30	Arlt et. al.	27	2.56+3 - 1.47+4	TCAP
31	J. Grundl et. al.	28	Cf-252 Avg.	$<\sigma_f>=1.216\pm0.019$b
32	Adamov et.a l.	26	Cf-252 Avg.	$<\sigma_f>=1.241\pm0.019$b

FIGURE CAPTIONS

FIG. 1. ^{235}U (n,f) Experimental Data with BFIT and ENDF/B-V Evaluations from 100-700 keV.

Fig. 2. ^{235}U (n,f) Experimental Data with BFIT and ENDF/B-V Evaluations from 0.2-3.2 MeV.

Fig. 3. ^{235}U (n,f) Experimental Data with BFIT and ENDF/B-V Evaluations from 0.6-6.6 MeV.

Fig. 4. ^{235}U (n,f) Experimental Data with BFIT and ENDF/B-V Evaluations from 6-20 MeV.

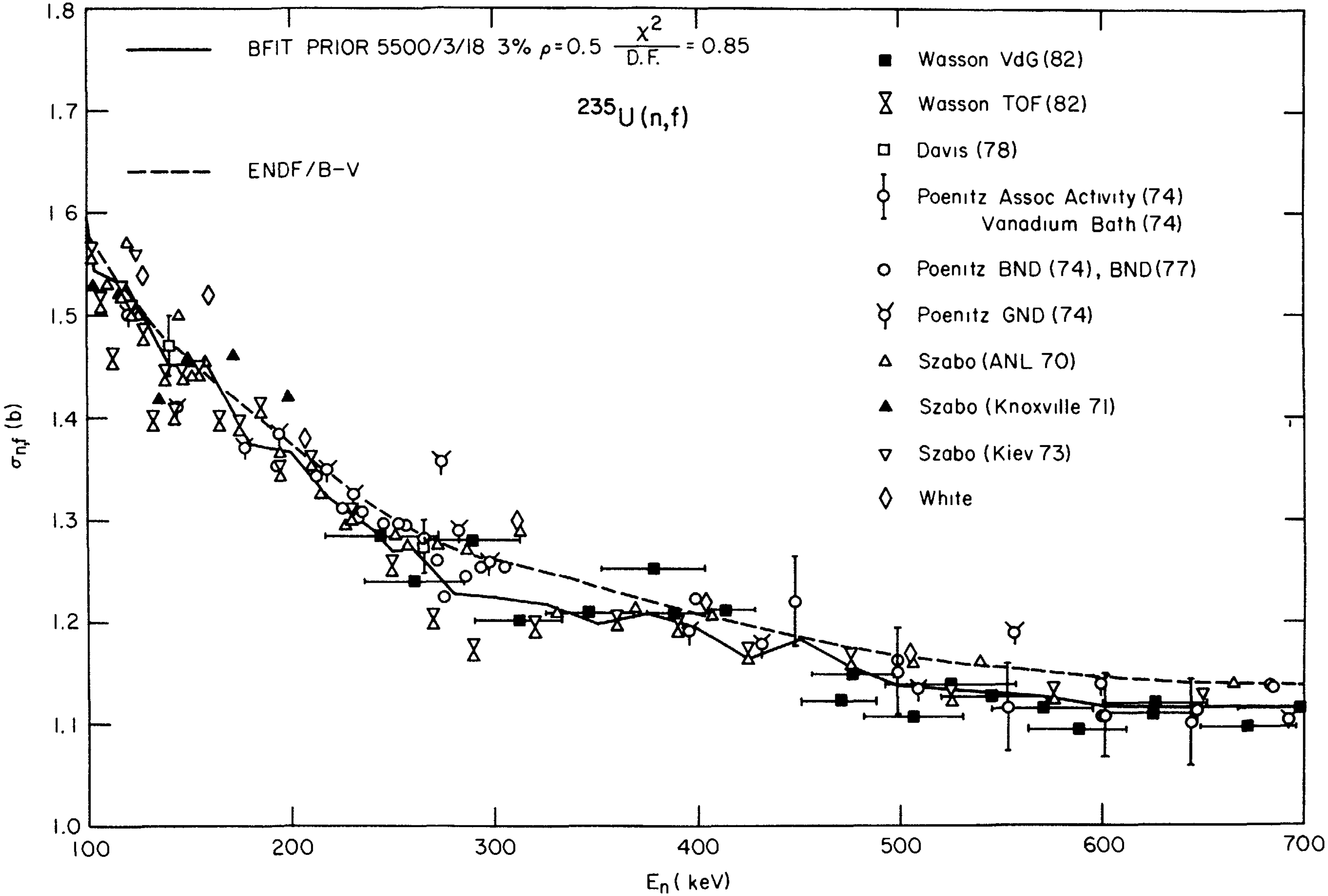

FIG. 1. ^{235}U(n,f) Experimental Data with BFIT and ENDF/B-V Evaluations from 100-700 keV

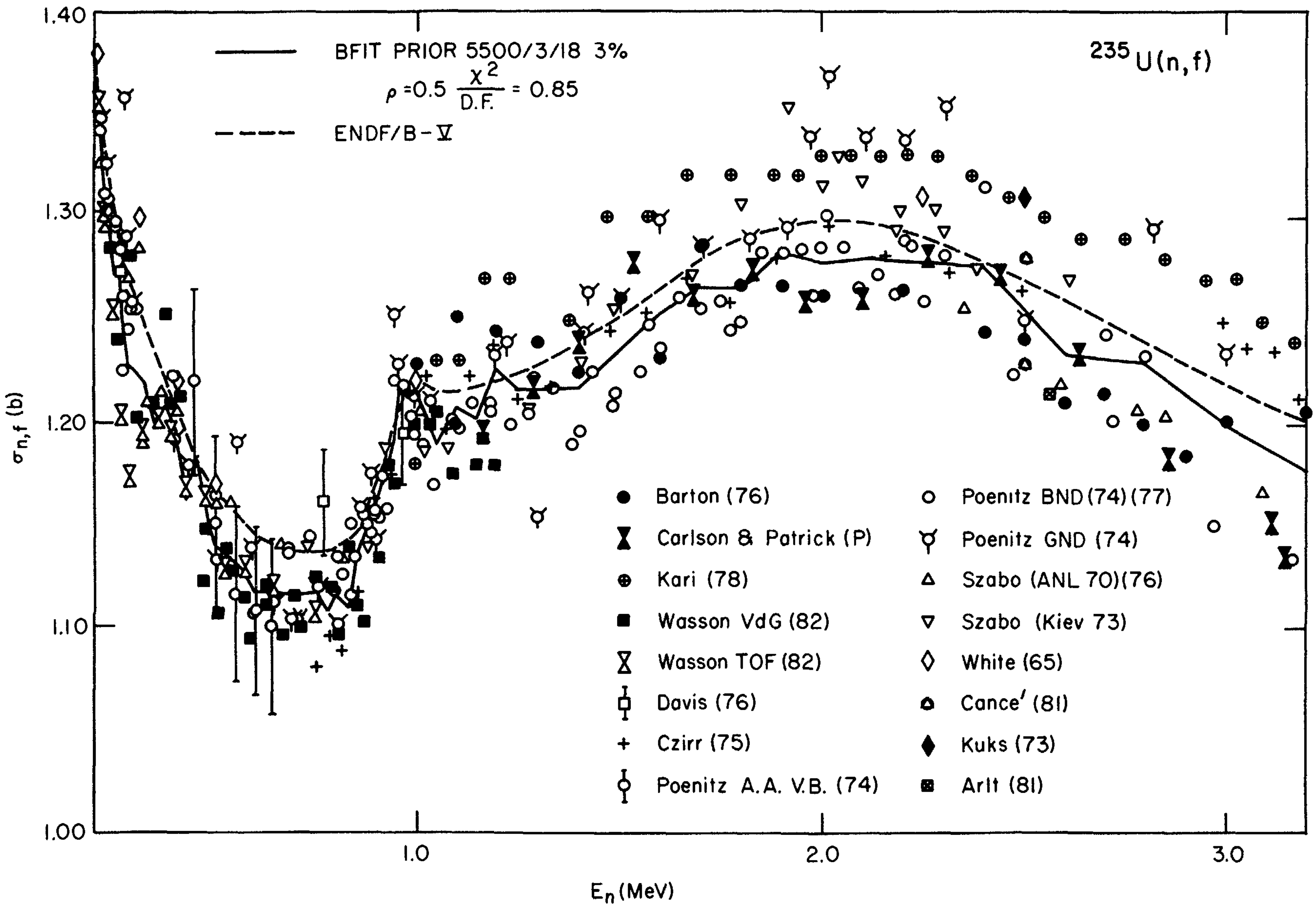

FIG. 2. $^{235}U(n,f)$ Experimental Data with BFIT and ENDF/B-V Evaluations from 0.2–3.2 MeV.

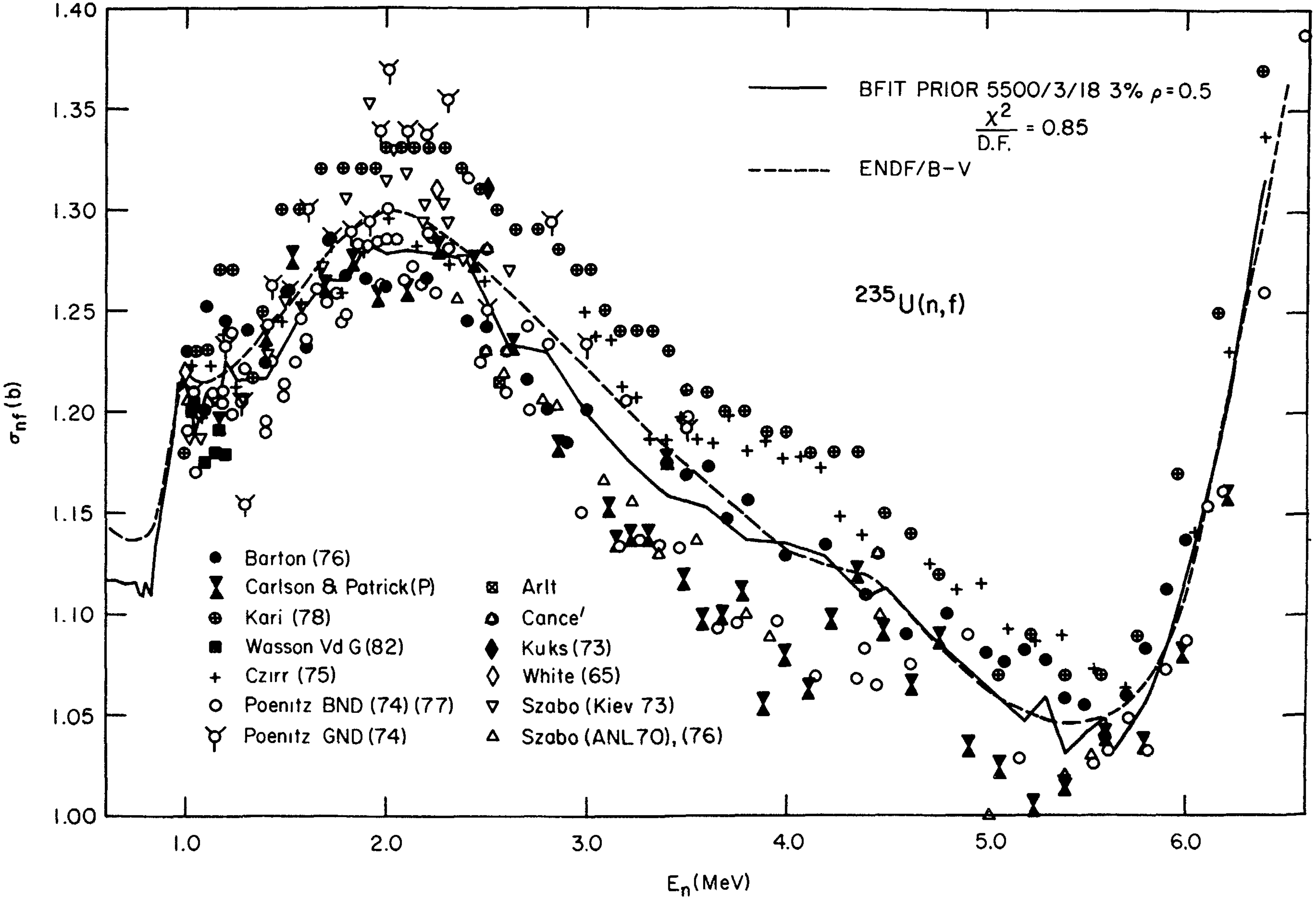

FIG. 3. ^{235}U(n,f) Experimental Data with BFIT and ENDF/B-V Evaluations from 0.6-6.6 MeV.

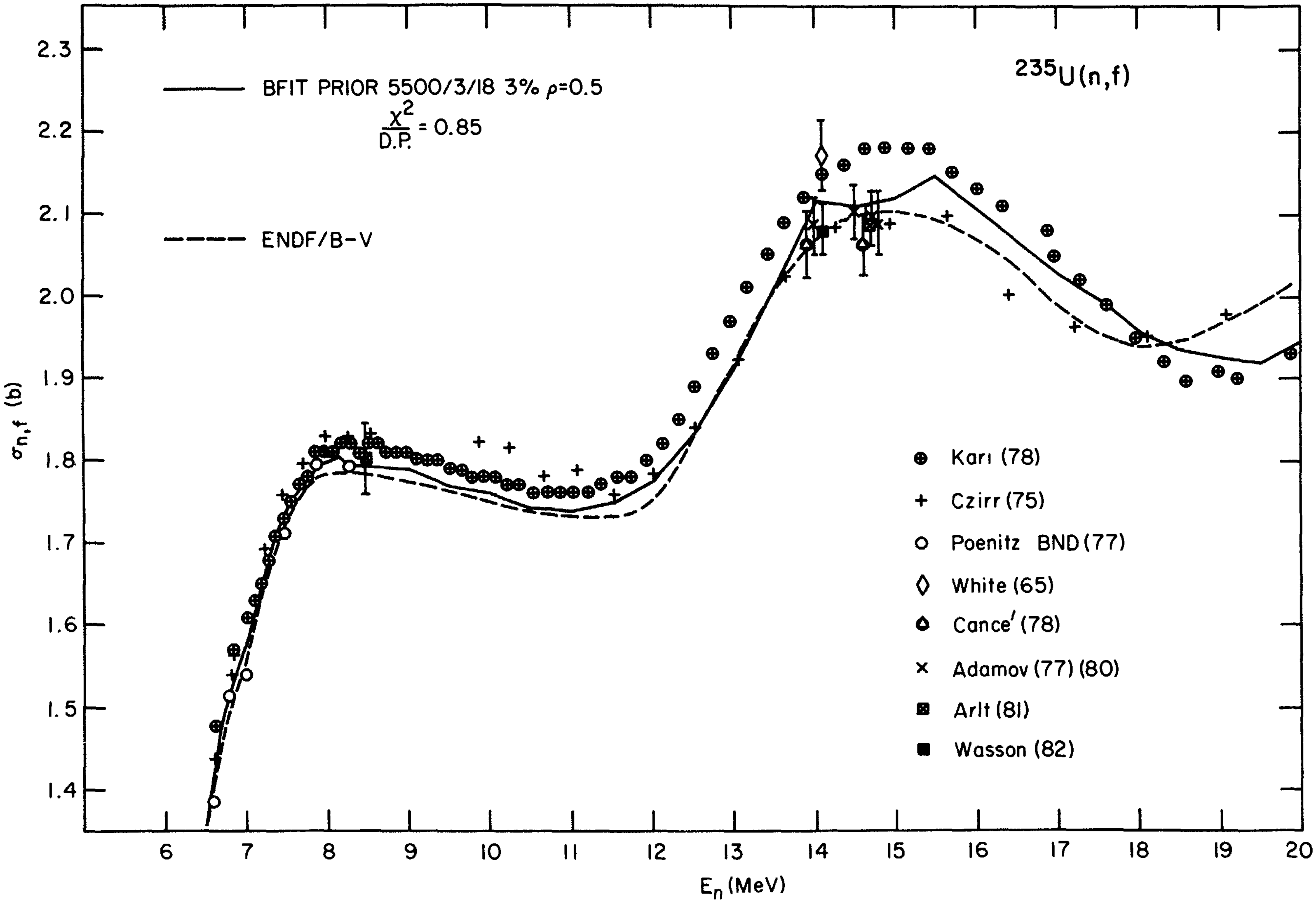

FIG. 4. ^{235}U(n,f) Experimental Data with BFIT and ENDF/B-V Evaluations from 6–20 MeV.

INVESTIGATION OF FISSION LAYERS FOR PRECISE FISSION CROSS SECTION MEASUREMENTS WITH A GRIDDED IONIZATION CHAMBER

C. Budtz-Jørgensen and H.-H. Knitter
Commission of the European Communities
Joint Research Centre
Central Bureau for Nuclear Measurements
Geel, Belgium

ABSTRACT

An ionization chamber with Frisch-grid is used to determine both the energy (E) of the charged particles emitted from the source positioned coplanar with the cathode, and the cosine of the emission angle (ϑ) with respect to the normal of the cathode. In the plane determined by the variables cos ϑ and E it is possible to identify an area which is unaffected by backscattering and selfabsorption. Events belonging to this area show an isotropic angular distribution for alpha particles and also for fission fragments induced by thermal neutrons, which, extrapolated to 90°, yields the absolute number of events.

The capabilities of this technique are demonstrated by the investigation of four evaporated $^{235}UF_4$ layers and one suspension sprayed $^{235}U_3O_8$ layer. For the UF_4 layers the alpha particle source strengths were determined, and agreement was found within 0.3% with values independently measured by low geometry alpha counting.

The same method was applied also to fission events induced by thermal neutrons. An accuracy for the determination of the total number of fission events of better than 0.5% is reached. The longstanding doubts on the magnitudes of fragment absorption and scattering are in principle circumvented by the present method and therefore no assumptions on fragment ranges and scattering cross-sections are needed.

It is also emphasized that the present method, within reasonable limits, is insensitive to source shape and thickness homogeneity.

1. INTRODUCTION

The neutron induced fission cross section of ^{235}U is requested for technological purposes with an accuracy of 1 % (1) and for neutron metrological application an even higher precision is desirable. As a result of the workshop on the absolute ^{235}U fission cross section held at Argonne National Laboratory, U.S.A., it was stated that this cross section is determined with an accuracy of ± 3 % in the neutron energy range from 100 keV to 20 MeV, but for some local regions below 1 MeV and above the second chance fission threshold. In these regions the uncertainty should be increased to a ± 5 % band (2,3). This situation makes it evident, that new experimental data can add significant information only when their total accuracy is well below this ± 3 % limit. For future experiments Poenitz (3) concludes as a result of his analysis and evaluation of ^{235}U fission cross section measurements, that the preferable techniques will be those involving the determination of absolute masses and detection efficiencies rather than the reliance on shape measurements and normalization at low neutron energies. If one follows this suggestion then one must concentrate on reducing the errors made in the determination of these two most important quantities.

The masses of fission layers were determined in the past, surely to not better than 1 % as is e.g. reflected in table 2 of Poenitz (3) comparative fission foil studies. The mass determination can be improved in several ways, but also by the precise alpha counting method which is described in the present paper. With this method, which is absolute in its own, an accuracy for the alpha source strength determination of 0.25 % is reached. This yields an error on the fission foil mass of 0.35 % if an error of the alpha half life of ^{234}U of 0.24 % is assumed as given in ref. (4).

Even more important is a reduction of the error in the determination of the absolute number of fission events induced in the fission layer. Here usually two corrections are applied, the extrapolation towards zero pulse height and the correction for events lost in the foil. Both corrections, when 2π-geometry must be used, are very uncertain, since no or crude considerations are made e.g. about the pulse height mass defect when extrapolating spectra, scattering of fragments in the sample, "average" ranges of fission fragments in the layer material, inhomogeneities or grain sizes in samples painted or made by electrospraying of suspensions etc. All these effects can result in uncertainties as large as the corrections themselves.

The grain size in fission layers of nominal thicknesses of 100 $\mu g/cm^2$ to 200 $\mu g/cm^2$ can e.g. become so large that a determination of the fission fragment detection efficiency is even not possible.

In the present work an ionization chamber with Frisch-grid (5) is used to investigate the alpha and also the fission fragment emission from evaporated $^{235}UF_4$ layers of four different thicknesses and of one layer prepared by electrospraying of a suspension of $^{235}U_3O_8$. The simultaneous measurement of both the cosine of the emission angle ϑ with respect to the normal of the fission layer, which is coplanar with the chamber cathode, and the charged particle energy permits a determination of the alpha source strength with an accuracy of less than 0.3 % and of the absolute number of fission events with an accuracy of less than 0.5 %. The method circumvents the above mentioned problems in absolute alpha and fission event counting, and within reasonable limits, it is insensitive to layer shape and thickness homogeneities.

2 DESCRIPTION OF THE METHOD

The present investigations were based on a gridded ion chamber where signals from the anode and the cathode are used to derive both the energy of the ionizing particle and the cosine of its emission angle with respect to the normal of the electrodes. This type of chamber has been studied (5) at our laboratory for some time and has successfully been used in several angular distribution measurements (6-8) of neutron induced nuclear reactions. The main objective of this work is to investigate the possibility to use such chambers in accurate charged particle counting measurements. The working principle and the data processing procedures used in connection with these chambers are described in ref. (5-8). However, some points essential for the present purpose will be repeated here.

Consider a fast-parallel-plate ion chamber with a grid inserted between the anode and cathode at a distance d from the cathode. It is assumed that the electron capture is negligible and that the amplifier time constants are long compared to the electron transit time but very short compared to the positive ion transit time. An ionizing particle originating from the cathode will then give rise to a signal at the cathode, which after amplification is

$$q_c = G_c \cdot N \cdot [1 - (\bar{X}(E)/d) \cdot \cos\vartheta] \qquad (1)$$

where G_c is proportional to the cathode amplifier gain. N is the number of ion pairs formed and $\bar{X}(E)$ is the distance from the origin of the track to the center of the ionization charge. E is the initial energy of the ionizing particle and ϑ is the angle of the track with respect to the normal of the electrodes. Since the induction effects of the positive ions are eliminated by the grid the magnitude of the anode signal is

$$q_a = G_a \cdot N \propto E \qquad (2)$$

where G_a is dependent on the gain in the anode amplifier and contains other factors that are also common to G_c. The value of cos ϑ associated with any ionizing particle can then be found from the two signals forming the quantity

$$\cos\vartheta = \frac{1 - (q_c/q_a) \cdot (G_a/G_c)}{\bar{X}(E)/d} \qquad (3)$$

From eq. (3) it is obvious that a correct determination of cos ϑ, especially for $\vartheta \cong 90°$, requires a precise knowledge of the gain ratio G_a/G_c of the two amplifier chains. This ratio can be determined converting the detector into a non-gridded ion chamber. The anode and the grid are then connected together and the charge signals induced by the ionization on the cathode and anode have identical magnitudes. The pulse height ratio of the amplified signals is therefore equal to the gain ratio of the amplifiers.

The quantity $\bar{X}(E)$ depends on the particle type and energy and can be determined either from calculation using the particle electronic stopping powers in the counter gas, or experimentally from the distribution of the nominator in the right hand side of eq. (3) which extends from 0 (cos ϑ = 0) to $\frac{\bar{X}(E)}{d}$ (cos ϑ = 1).

In the derivation of eq. (3) it was assumed that the anode is completely shielded from the induction of the positive ions. Actually a fraction σ of the lines of force passes through the grid and ends on the anode. The cathode signal is not affected but the anode signal amplitude becomes

$$q_a = G_a \cdot N \cdot [1 - \sigma \cdot (\bar{X}(E)/d) \cdot \cos\vartheta] \qquad (4)$$

The dependence of σ on chamber dimensions is discussed in ref. (6) and is in most designs of the order of a few percent. The correction term in eq. (4) can readily be found from the measured anode and cathode pulse heights since

$$\sigma \cdot \frac{\bar{X}(E)}{d} \cdot \cos\vartheta \cong \sigma\,[1 - (q_c/q_a) \cdot (G_a/G_c)] \qquad (5)$$

Applying this correction to the anode pulse height ensures that eq. (2) is fulfilled.

From the cos ϑ values determined by the above procedure one can generate the distribution of cos ϑ for all particles leaving the sample. In the case of angular isotropy the distribution has a rectangular shape, however the distribution is distorted for cos ϑ values close to cos ϑ = 0 (ϑ = 90°) due to scattering and selfabsorption effects, and an integration of the distribution will not yield the true sample activity. But for samples with a thickness small compared to the particle range, these disturbing effects become negligible above a certain cos ϑ value, such that the sample activity can be determined from this undisturbed part of the cos ϑ distribution. This is in principle the same method as used in conventional low geometry counting. However, the simultaneous registration of E and cos ϑ permits that the solid angle on which the source strength determination is based in most cases can be chosen large such that a high counting efficiency can be maintained. The method gives also a measure of the quality of the investigated samples. This will be illustrated in the following chapters.

3. EXPERIMENTAL DETAILS FOR UF_4 SOURCE MEASUREMENTS

Alpha particle counting was performed on four $^{235}UF_4$ samples vacuum evaporated on highly polished stainless steel disks. The layers had an active diameter of 1.27 cm and nominal thicknesses of 15, 75, 300 and 500 $\mu g.cm^{-2}$ The isotopic composition of the sample material as determined by mass spectrometry at our laboratory was ^{234}U : 0.1763 at.%, ^{235}U : 99.3608 at.%, ^{236}U : 0.0297 at.% and ^{238}U : 0.4332 at.%. Only the decay of ^{234}U and ^{235}U play a significant role. The measurements of the alpha activity were made with a gridded chamber using CH_4 at 1.5 bar pressure as counter gas. The distance between cathode and grid was 3.2 cm and the grid to anode distance was 0.6 cm. The grid was constructed of 0.1 mm thick stainless steel wires spaced 1 mm apart. The wires were welded on a stainless steel ring, 1 mm thick, and with an inside and outside diameter of 9 cm and 12 cm respectively. The anode and the cathode, which contained the sample, had also a diameter of 12 cm. From these dimensions the value of σ was calculated (6) to be 0.032. The chamber was operated with + 3.5 kV on the anode, + 2.2 kV on the grid and 0 kV on the cathode. These voltage settings fulfill the requirement for complete collection of the ionization electrons. The cathode and anode signals were amplified with two charge sensitive preamplifiers Ortec model 142 A and further amplified with two highly linear spectroscopic amplifiers Ortec model 450. The pulses were digitized to 8192 channels each and sent to an on-line computer system, Nuclear Data 6660, which stored them sequentially on magnetic tape. All data processing was done off-line.

The alpha counting of each of the sources was preceded by a determination of the ratio between the cathode and anode amplifier gains. The grid was temporarily connected to the anode and the ratio between the amplified anode and cathode pulses was measured in this parallel plate configuration. Due to the amplifier noise the ratio gave a Gaussian distribution with a relative width (FWHM) of ~ 0.5 %. However, the mean of this distribution, which gives the gain ratio, was readily determined to better than 0.1 %.

The source measurements were done with the chamber in the gridded version. Each of the samples was counted in several runs with about $5 \cdot 10^5$ counts.

4. ANALYSIS OF SOURCE STRENGTH FROM BI-PARAMETRIC ALPHA SPECTRA

The upper part of fig. 1 shows the pulse height distribution of the anode signals obtained from the 75 $\mu g.cm^{-2}$ thick UF_4 sample. The two main alpha lines from the decay of ^{234}U and ^{235}U are only partly separated and a low energy tail due to selfabsorption and scattering is visible.The lower part of fig. 1 shows the pulse height distribution of the cathode signals which is broadened due to the cos ϑ dependence. The upper part of fig. 2 is a plot of the bi-parametric distribution of the number of alpha events versus the anode signal and versus the ratio of cathode to anode signal. This ratio is for a single alpha line distributed between (1 - $\bar{X}(E)/d$) and 1; see equations (1) and (2). The value of $\bar{X}(E)/d$ can therefore be found directly from the figure as indicated for the ^{234}U 4.77 MeV alpha line. In order to determine $\bar{X}(E)/d$ also at lower energies, the energy dependence of $\bar{X}(E)$

was calculated using the stopping power values of CH_4 for alpha particles (7). The $\bar{X}(E)/d$ values were entered in the analyser routine and the cos ϑ value for each event could then be determined according to eq. (3).

The ratio q_c/q_a is at low alpha particle energies peaked close to $q_c/q_a = 1$. Events giving small anode pulse heights stem from alpha particles which are emitted at grazing angles close to $\vartheta = 90°$, where they have lost part of the energy in the sample. Since the range of the alpha particles in the gas and therefore also $\bar{X}(E)$ decrease with decreasing energy it follows from equations (1) and (2) that the ratio q_c/q_a converges towards G_c/G_a as the energy approaches zero. Fig. 3 shows a plot of the centroids of the q_c/q_a distributions as function of energy below 3 MeV. A linear extrapolation of the ratio to zero energy yields a value which agrees to better than 0.05 % with the gain ratio, G_c/G_a, found by the previously described parallel plate method. The agreement between the two methods demonstrates also that capture of ionization electrons in the gas or by the grid must be negligible, since electron losses would result in the strongest reduction of the anode pulse heights when the chamber is operated in the gridded mode. The lower part of fig. 2 gives the bi-parametric distribution of cos ϑ and E for the 75 $\mu g.cm^{-2}$ sample. The cos ϑ distributions are, even for the rather thin samples, strongly influenced by the sample thickness. The low energy tail is mainly distributed close to cos $\vartheta = 0$. This is further illustrated in fig. 4, where the energy distributions are displayed with high resolution and cos ϑ intervals are given in steps of 0.1. It is seen how the alpha peaks become broader as the average path of the alpha particles through the sample layer becomes longer with increasing value of cos ϑ. The peaks are completely washed out near cos $\vartheta = 0$. However, for larger cos ϑ values, all the energy spectra show well defined peaks with very little low energy tailing. This is important, since it means that only the lowest cos ϑ intervals (cos $\vartheta < 0.2$) are influenced by backscattering and losses due to selfabsorption. The fraction of counts found in the low energy tails below 3 MeV for the 75 $\mu g.cm^{-2}$ and 500 $\mu g.cm^{-2}$ samples is given as function of cos ϑ in fig. 5. This fraction decreases rapidly with increasing cos ϑ. For an angular cone such that cos $\vartheta > 0.3$ the tails contain only 0.07 % and 0.2 % of all alpha particles emitted into the active volume of the chamber for the two samples respectively. It is believed that the low energy signals originate from alpha particles which have lost an appreciable amount of energy in the sample ($\vartheta \sim 90°$) or in the backing ($\vartheta > 90°$) and then made a large Rutherford scattering out into the active volume of the detector. Therefore these events do not initially belong to the selected angular cone. It was decided not to include the content of the low energy tails in the determination of the sample strength. However, this point needs further clarification and at present the tail content is treated as part of the systematic error. Of course, this error can be made negligible by choosing a high limit for cos ϑ.

The determination of the source strength is based on the cos ϑ distribution integrated over all alpha lines in the energy spectrum. Fig. 6 displays this distribution for the 75 $\mu g.cm^{-2}$ sample. The distribution has a rectangular shape as expected from an isotropic angular distribution. However a small top is visible close to cos $\vartheta = 0$. This is very likely due to backscattered alpha particles, which, because of the strongly foreward peaked Rutherford scattering law, will leave the sample with angles close to $\vartheta = 90°$. According to the discussion above, a lower limit $(\cos\vartheta)_{min}$ can be found such that the effects of backscattering and selfabsorption are negligible for $\cos\vartheta > (\cos\vartheta)_{min}$. Therefore the height, N, of the plateau in the cos ϑ distribution above $(\cos\vartheta)_{min} = 0.3$ has the same value as it would have in the ideal case where no scattering or selfabsorption were present. The true source strength Φ can be determined from

$$\Phi = 2 \cdot \int_0^1 N \cdot d(\cos\vartheta) = 2 \cdot (A + \Delta A) \tag{4}$$

where A is the number of counts summed above $(\cos\vartheta)_{min}$ and $\Delta A = N \cdot (\cos\vartheta)_{min}$ is the extrapolation from $(\cos\vartheta)_{min}$ down to $\cos\vartheta = 0$.

Compared to conventional low geometry counting techniques the error sources of the present method originate from the detector associated electronics instead of geometrical uncertainties. The extrapolation depends of course critically on a precise definition of the cos $\vartheta = 0$ value, or, which is the same, on an accurate determination of the gain ratio G_c/G_a. As described previously, two independent methods were used to determine this ratio yielding results which agreed within 0.05 %. However, during the measurement period (~ 1 week) this ratio varied by up to 0.15 % due to drifts in the amplifier chains. This value was assumed to be a conservative estimate of the maximum amplifier drift during a single run (~ 10 h). The linearity of the electronic chains was checked with a precision pulse generator and the non-linearity was found to be less than 0.1 %. This high degree of linearity was also reflected in the constancy of the plateau of the cos ϑ distributions. Least square fits of the P(cos ϑ) distribution to a polynomial expression yielded typically :

$P(\cos\vartheta) = N [1 + (0.003 \pm 0.005) \cdot \cos\vartheta]$ which results in an uncertainty of 0.09 % for the extrapolation. Table I lists the error sources and their contribution to the uncertainty of the measured sample activities. The first column of table II gives the activities of the four samples as determined from the cos ϑ distributions. The second column gives the activities for the three most active samples as independently measured by conventional low geometry counting (8). The results of the two methods agree within the stated uncertainties of ~ 0.3 %. The accuracy as given in table I is sufficient for our present needs. However, the error contributions from the gain drift, the non-linearity and the dead time can certainly be considerably reduced, such that the total systematic error would be less than 0.2 %. It should be emphasized that the present technique has a detection efficiency which is about one order of magnitude larger than in the low geometry counting. The method has also the advantage that it is independent of sample shapes and thickness inhomogeneities as long as these quantities stay within reasonable limits.

5. SAMPLE THICKNESS AND ALPHA BACKSCATTERING EFFECTS.

The third column of table II contains the count rates measured in 2π geometry using the anode pulse height spectra as displayed in fig. 1. The ratio $N^{2\pi}/N^{\cos}$ between the results of the 2π counting and the cos ϑ method is plotted in the upper part of fig. 7 as function of sample thickness. This ratio differs from 1 since the 2π counting is affected by backscattering of alpha particles and losses due to selfabsorption in the sample layers. The losses can be calculated from the simple equation

$$\Delta_{sample} = \frac{t}{2\,R_{UF_4}} \qquad (7)$$

where t is the sample thickness. The range R_{UF_4} was calculated for the UF_4 compound using the equation :

$$\frac{1}{R_{UF_4}} = \frac{W_F}{R_F} + \frac{W_U}{R_U} \qquad (8)$$

where W_F and W_U are the weight fractions of fluor and uranium in UF_4 and the ranges R_F and R_U in pure fluor and pure uranium were taken from ref. (7). It is seen that the dependence of the measured ratio $N^{2\pi}/N^{\cos}$ on sample thickness is stronger than calculated according to eq. (7). This is in qualitative agreement with the results of ref. (9) where scattering and absorption corrections for uranium oxide layers were studied. They concluded that the relative number of backscattered particles decreases with increasing sample thickness, becoming nearly negligible for $t/R > 0.1$, a dependence which has to be added to the selfabsorption described by eq. (7). Another explanation for part of the strong sample thickness dependence of the $N^{2\pi}/N^{\cos}$ ratio was found from a simultaneous investigation of the energy loss the alpha particles suffered when passing through the sample. This energy loss could be determined as a function of cos ϑ from the width, FWHM of the 4.77 MeV ^{234}U alpha line belonging to a given cos ϑ interval. The analysis was based on the type of spectra displayed in fig. 4. Fig. 8 displays in a lorarithmic plot the widths found for the four samples. Here cos ϑ intervals of 0.05 have been chosen and the contribution from electronic noise ~ 16 keV was quadratically subtracted. The energy losses are for the three thicker samples inversely proportional to cos ϑ and are thus proportional to the path length of the alpha particles in the layers. The widths of the alpha peaks measured for the 15 $\mu g/cm^2$ sample do not fulfill this relation for cos ϑ approaching 1, since the intrinsic resolution of the detector is comparable in magnitude to the sample energy-loss $\Delta E_\perp$ for alpha particles leaving the sample with directions perpendicular to the surface. However, the vertical energy losses for all samples were found from linear extrapolation to cos ϑ = 1 as indicated in fig. 8. The energy losses $\Delta E_\perp$ are in the lower part of fig. 7 compared to calculations, where the stopping power for alpha particles in the UF_4 compound was determined using the Bragg additivity rule and the stopping power data of ref. (7) for alpha particles in pure uranium and pure fluor. Although the measured energy losses follow a linear dependence with respect to the sample thickness, it is seen that the energy loss in the sample material is ~ 15 % larger than the values obtained from the calculations. A possible explanation could be that the sample material contains chemical impurities or that the stoichiometric composition differs from the assumed UF_4, such that the samples are thicker with respect to stopping compared to the thickness as determined from the sample alpha activities. This explanation is also supported by the above discussions on the sample selfabsorption losses.

6. FISSION FRAGMENT COUNTING

The proposed method for absolute charge particle counting was investigated with respect to fission fragment counting. The measurements were made with the previously described UF_4 samples but included also a sample prepared by electrospraying of a U_3O_8 suspension. The latter sample had a diameter of 2.8 cm and a nominal thickness of 100 $\mu g/cm^2$. The detector was mounted in front of a CBNM Van de Graaff beam line and neutrons were produced using the $^7Li(p,n)$ reaction. The neutrons were "thermalized" in blocks of paraffin in order to insure that the neutron induced fission events gave an isotropic angular distribution of the fission events. The distance between the cathode and the grid had been reduced to 2.5 cm and the chamber was operated at 1 bar pressure which was sufficient to stop the fragments in the active volume between the cathode and the grid. The upper part of fig. 9 displays the anode pulse height spectrum of fission fragments measured with the 75 $\mu g/cm^2$ UF_4 sample.

Besides the light and heavy fragment peaks low energy events due to selfabsorption are visible. The bias was set above the alpha peak and the 2π counting was made in the usual way extrapolating linearly to zero pulse height. This extrapolation which amounted to 2.56% for the 500 $\mu g/cm^2$ UF_4 sample may underestimate the number of fission events falling under the alpha peak due to the ionization defect of ~ 5 to 7 MeV (13) for fission fragments. However, very little is known about the pulse height defect for fission fragments even in the most commonly used counter gases. The lower part of fig. 9 shows the cathode pulse height spectrum where the separation between light and heavy fragment pulses is distorted due to the cos ϑ dependence. The upper part of fig. 10 shows the biparametric distribution of q_c/q_a. The ratio q_c/q_a is for a given energy E distributed between $1 - \bar{X}(E)/d$ and 1 and the quantity $\bar{X}(E)$ was found for all fission fragment energies in a similar manner as depicted in fig. 2. The cos ϑ value belonging to each fission fragment was then calculated using eq. (3). The lower part of fig. 10 displays the biparametric distribution of cos ϑ and the fragment energy. Again it is seen that energy degradation of the fragments occurs for cos ϑ approaching zero. However, in this case there is also a high energy tail (barely visible in the figure) distributed close to cos ϑ = 0. This tail stems from fission events where the fragment initially emitted downwards into the backing is scattered out in the detector volume where its ionization charge is added to the ionization of the unscattered fragment. Due to the strongly foreward peaked scattering cross section this only happens, as observed, close to cos ϑ = 0. As it was the case for the alpha particles a cos ϑ value $(\cos\vartheta)_{min}$ can be found such that the fission spectra have no tailing for $\cos\vartheta > (\cos\vartheta)_{min}$. This is illustrated in the upper part of fig. 11, which is a plot of the integrated fission fragment energy spectrum for cos ϑ > 0.5 measured with the 75 $\mu g/cm^2$ UF_4 sample. However, a similar improvement was not found for the 100 $\mu g/cm^2$ suspension sprayed U_3O_8 sample for which the energy spectrum in the same cos ϑ interval is given in the lower half of fig. 11. The valley between the light and heavy fragment peaks is filled and an appreciable low energy tail is observed. The difference between the two types of samples is further illustrated in fig. 12 which shows the fraction of events falling in the low energy tail between 10 and 35 MeV as function of cos ϑ, whereas the tail content for the evaporated UF_4 sample decreases rapidly with cos ϑ becoming negligible for cos ϑ > 0.3. The tail content for the sprayed sample changes weakly with cos ϑ and amounts to 0.4% in the cos ϑ interval from 0.9 to 1. This means that even fission fragments emitted with a direction perpendicular to the sample can encounter appreciable energy losses and it is certainly a possibility that some of these fragments can be stopped completely in the sample. Although the nominal sample thickness ~ 100 $\mu g/cm^2$ is small compared to the fission fragment ranges the sample must contain grains which individually can have sizes larger than the fission fragment ranges. This makes it extremely difficult to correct for selfabsorption in the sample, since correction formulas like eq. (7) are no longer valid. This is the more serious since suspension sprayed or painted samples often have been used in fission cross section measurements, especially with more exotic samples where the material losses in connection with vacuum evaporation can not be tolerated. For fast neutron induced fission cross section measurements, lacking or incorrect absorption corrections can lead to a wrong determination of the cross section shape due to the energy dependence of the fission fragment angular distributions.

Fig. 13 displays the cos ϑ distributions for all the four evaporated UF_4 samples. It is clearly seen how the selfabsorption increases with sample thickness. The true number, N^{cos}, of neutron induced fission events was determined in the same way as described in the section on alpha particle counting. However due to the shorter range of the fission fragments it was necessary to increase $(\cos \vartheta)_{min}$ up to $\cos \vartheta = 0.6$ for the thickest of the samples in order to assure that there were no fission events with energies lower than the bias level. The ratios $N^{2\pi}/N^{cos}$ between the 2π counting and the intensities found from the cos ϑ distributions are plotted in fig. 14. For the four UF_4 samples this ratio has a linear dependence with sample thickness which extrapolated to zero thickness yields a value $N^{2\pi}/N^{cos} = 1.000 \pm 0.002$. Backscattering will not increase the counting in a 2π detector since this will result in one sum pulse from the two fragments. The inefficiency, $1 - N^{2\pi}/N^{cos}$, of the 2π counting is for the UF_4 samples given by :

$$(9) \qquad \Delta_{UF_4} = (10.5 \pm 0.7) \times t \ \%,$$

where the thickness t is given in mg/cm^2 of UF_4. It should be remembered that the 2π counting is affected both by selfabsorption and by the extrapolation of the fragment spectrum down to zero pulse height. The layer absorption was calculated according to eq. (7) using an average fission fragment range determined with the help of eq. (8). The ranges of an average fission fragment in pure uranium and pure fluor were taken from the range tables of ref. (14). It must be noted that the ranges of heavy ions in matter probably are not known to better than 20 % (14). The calculated absorption is shown in fig. (14) as a dashed line and has a somewhat weaker thickness dependence than experimentally observed. Neglecting the uncertainties with respect to the fission fragment ranges and the extrapolation of the 2π spectra to zero pulse height this is consistent with the results found for the absorption of alpha particles in the samples and supports the conclusion that the sample material might contain chemical impurities or that the stoichiometric composition differs from the assumed UF_4.

Also given in fig. 14 is the $N^{2\pi}/N^{cos}$ ratio obtained from the sprayed U_3O_8 sample. As discussed previously the biparametric distribution of cos ϑ and E measured on this sample showed that there did not exist a cos ϑ value above which there was no selfabsorption. Therefore the cos ϑ distribution for this sample can only be used to determine a lower limit for the loss of fission fragments in the sample. However this limit $\Delta_{U_3O_8} = 3.7 \pm 0.3$ % is about a factor of three more than expected for an evaporated UF_4 sample of similar thickness, see eq. (9). Again confirming that this type of sample due to its selfabsorption problems should not be used in fission cross section measurements.

7 CONCLUSIONS

The here presented bi-parametric method of measuring both the energies of the charged particles and their emission angles with respect to the normal of a plane source gives a clear and vivid picture of the process which these particles experience on their different ways out from the source layer into the directly faced counter gas. In the two-parametric spectra it is clearly seen in which parameter range they are undisturbed. This information permits then in the case of the alpha particles an analysis of the source strength and in that of the fission fragments, a determination of the absolute number of fission events with an accuracy of better than 0.3 % and 0.5 % respectively. The error sources of earlier methods like backscattering, absorption processes and source inhomogeneities are circumvented by the present method. The strength of the present method lies in the very large geometry factor and its clear distinction between disturbed and undisturbed events.

REFERENCES

1) WRENDA 81/82, IAEA-INDC(SEC) 78/URSF (1981).

2) W. Poenitz and A.B. Smith,
ANL-76-90, page 450 (1976).

3) W.P. Poenitz, J.W. Meadows, R.J. Armani,
Proc. of the Int. Conf. on Nucl. Cross-Sections and Technology,
Knoxville, Oct. 1979, NBS Special Publ. 594 p. 483.

4) Proposed recommended list of heavy element radio nuclide decay data,
IAEA INDC(NDS)-127/NE, Editor : A. Lorenz, Vienna (Dec. 1981).

5) H.-H. Knitter and C. Budtz-Jørgensen,
Proc. of the International Conference on Nuclear Cross Sections for
Technology, Knoxville, USA, Oct. 1979, NBS Spec. Publ. 594, p. 947 (1980).

6) H.-H. Knitter, C. Budtz-Jørgensen, D.L. Smith and D. Marletta,
Nucl. Sci. Eng. 83, 229 (1983).

7) J.W. Meadows and C. Budtz-Jørgensen,
Proc. Intern. Conf. on Nuclear Data for Science and Technology,
Antwerp, Sept. 1982, page 740, D. Reidel Publ. Company, Dordrecht, NL.

8) C. Budtz-Jørgensen and J.W. Meadows,
Lecture Notes in Physics Vol. 158, 111 (1982).

9) O. Bunemann, T.E. Cranshaw and J.A. Harvey,
Can. J. Res. 27A, 191 (1949)

10) J.F. Ziegler,
Handbook of Stopping Powers and Ranges in all Elemental Matter,
Vol. 4, Pergamon Press.

11) B. Denecke,
Private Communication (1983).

12) L.L. Lucas and J.M.R. Hutchinson,
Intern. Journ. of Applied Radiation and Isotopes 27, 35 (1976).

13) H.W. Schmitt and R.B. Leachman,
Phys. Rev. 102, 183 (1956).

14) U. Littmark and J.F. Ziegler,
Handbook of Stopping Powers and Ranges of Ions in Matter, Vol. 6,
Pergamon Press, New York (1980).

Table I : Error sources and their typical contribution to the error of the source strength

Error source	Error [%]
Statistics	0.1 - 0.2
Gain drift	0.15
Electron capture	0.10
Non-linearity	0.09
Dead time	0 - 0.1
Low energy tailing	0.07- 0.20
Tot. systematic error	0.21- 0.30

Table II : Strengths of the four UF_4 alpha sources as determined by the present method "cos ϑ", the low geometry counting, and by the 2π-counting.

Sample	"cos ϑ" [s^{-1}]	Low geometry [s^{-1}]	"2π" [s^{-1}]
25A - 27	8.89 ± 0.03		9.11 ± 0.03
25A - 36	44.03 ± 0.11	44.16 ± 0.13[a]	44.65 ± 0.04
25A - 93	165.24 ± 0.51	165.35 ± 0.26[a]	163.36 ± 0.21
25A - 96	273.26 ± 0.98	272.60 ± 0.41[a]	264.54 ± 0.44

a) values obtained from ref. (8)

FIGURE CAPTIONS

Fig. 1
The pulse height distributions for the anode and cathode signals are plotted in the upper and lower part of the figure respectively.

Fig. 2
The upper part shows a biparametric distribution of the number of alpha events versus the anode signal and versus the ratio of cathode to anode signal. The lower part shows the number of alpha events versus the alpha energy and versus the cos ϑ with high resolution in the cos ϑ-parameter. Both spectra are measured with the 75 $\mu g/cm^2$ sample.

Fig. 3
The ratios $< q_c/q_a >$ measured with the gridded chamber are plotted for anode pulse heights between 1 and 3 MeV together with their errors. The full line represents the results of a least squares fit through the experimental points. The extrapolated value at zero pulse height is compared with the parallel plate value.

Fig. 4
Biparametric distributions are shown versus cos ϑ and versus the alpha energy, for two different samples with high resolution in the energy parameter.

Fig. 5
The fraction of events in percent of the total which were found in a cos ϑ-interval of 0.1 and below 3 MeV energy is plotted versus cos ϑ.

Fig. 6
The cos ϑ-distribution measured for the 75 $\mu g/cm^2$ sample and integrated over all alpha lines is shown.

Fig. 7
The measured energy loss of the 4.77 MeV alpha particles is plotted in the lower part versus the source thickness obtained from the source strength assuming a pure UF_4 deposit. The dotted line represents the energy loss calculated from the stopping power of 4.77 MeV alphas in UF_4 $dE/dX = 0.354$ keV $\mu g^{-1} cm^2$ The upper part shows the 2π-countrate divided by half the source strength versus the source thickness. The dotted line shows the correction for alphas lost in the source layer.

Fig. 8
The full widths at half the maxima (FWHM) of the alpha peaks for all the sources are plotted as function of cos ϑ in a double logarithmic scale. On the right hand side the vertical energy losses are indicated.

Fig. 9
The pulse height distributions of fission fragments from the thermal neutron induced fission of ^{235}U for the anode and cathode signals are plotted in the upper and lower part of the figure respectively. The measurements were made with the 75 $\mu g/cm^2$ vacuum evaporated UF_4 sample.

Fig. 10
The upper part shows a bi-parametric distribution of the number of fission fragments versus the energy and versus the ratio of cathode to anode signal. The lower part shows the number of fission fragments versus the fragment energy and versus cos ϑ with high resolution in the cos ϑ parameter. Both spectra are measured with the 75 $\mu g/cm^2$ vacuum evaporated UF_4 sample.

Fig. 11
Fission fragment energy spectra for cos $\vartheta > 0.5$ are shown for the 75 $\mu g/cm^2$ vacuum evaporated UF_4 sample and for the 100 $\mu g/cm^2$ U_3O_8 suspension sprayed sample in the upper and lower part of the figure respectively.

Fig. 12
The fraction of fission events in percent of the total which were found in cos ϑ intervals of 0.1 in the fission fragment energy range between 10 MeV and 35 MeV are plotted versus cos ϑ for the 75 $\mu g/cm^2$ vacuum evaporated UF_4 sample and for the 100 $\mu g/cm^2$ U_3O_8 suspension sprayed sample with a thick and thin histogram line respectively.

Fig. 13
The cos ϑ distributions of the fission fragments for the four UF_4 vacuum evaporated samples are plotted in ascending order with their thickness. The $(\cos \vartheta)_{min}$ values are indicated by vertical lines.

Fig. 14
The ratio of the 2π-countrate and the total number of fission events determined from the cos ϑ distribution is plotted versus the sample thickness. The full circles and the triangle represent the measurements with the vacuum evaporated UF_4 samples and the U_3O_8 suspension sprayed samples respectively. The meaning of the full and the dashed line is explained in the text.

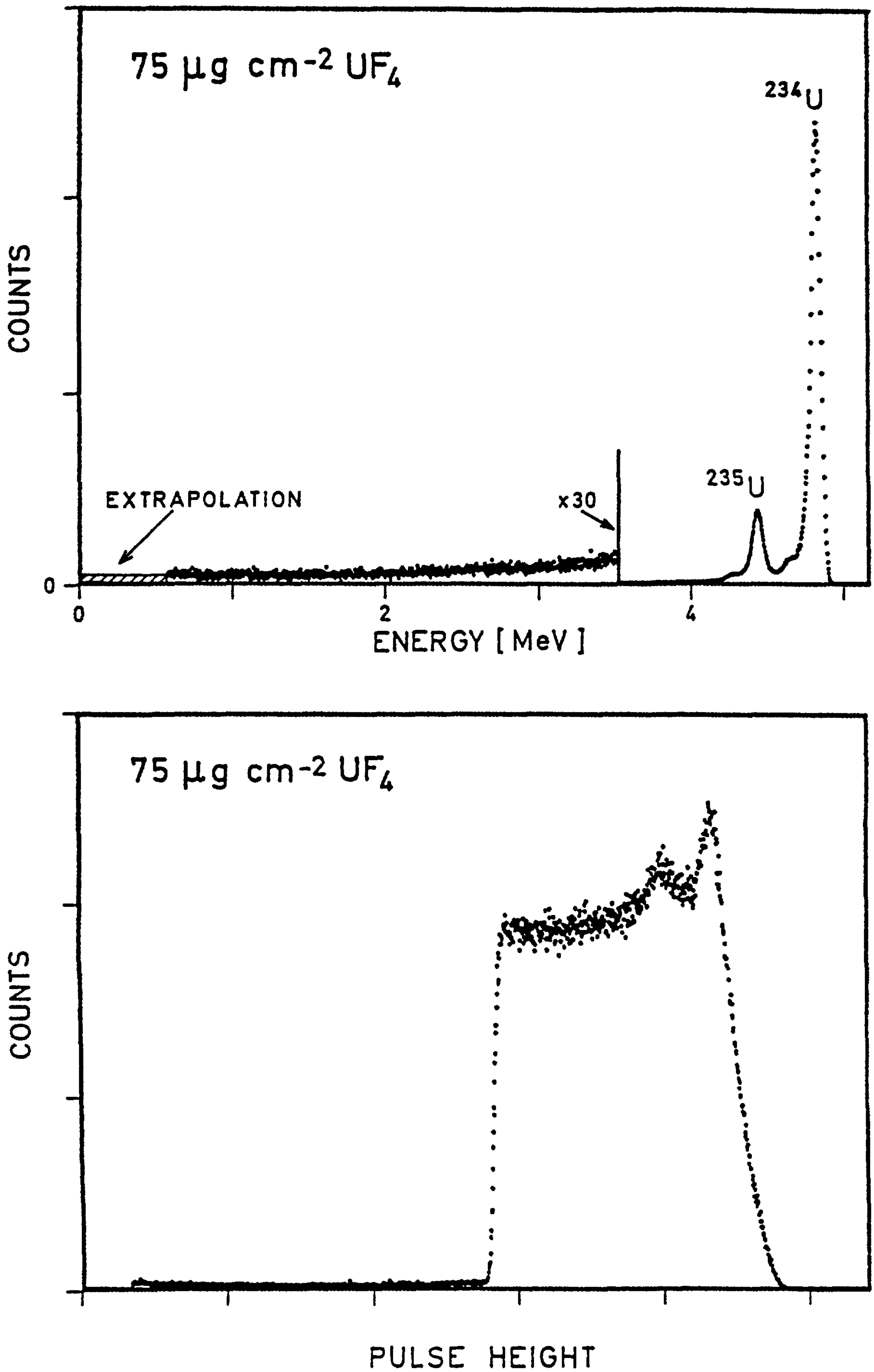
75 µg cm-2 UF4
234U
235U
EXTRAPOLATION
x30
COUNTS
0
0
2
4
ENERGY [MeV]
75 µg cm-2 UF4
COUNTS
PULSE HEIGHT

FIG. 1

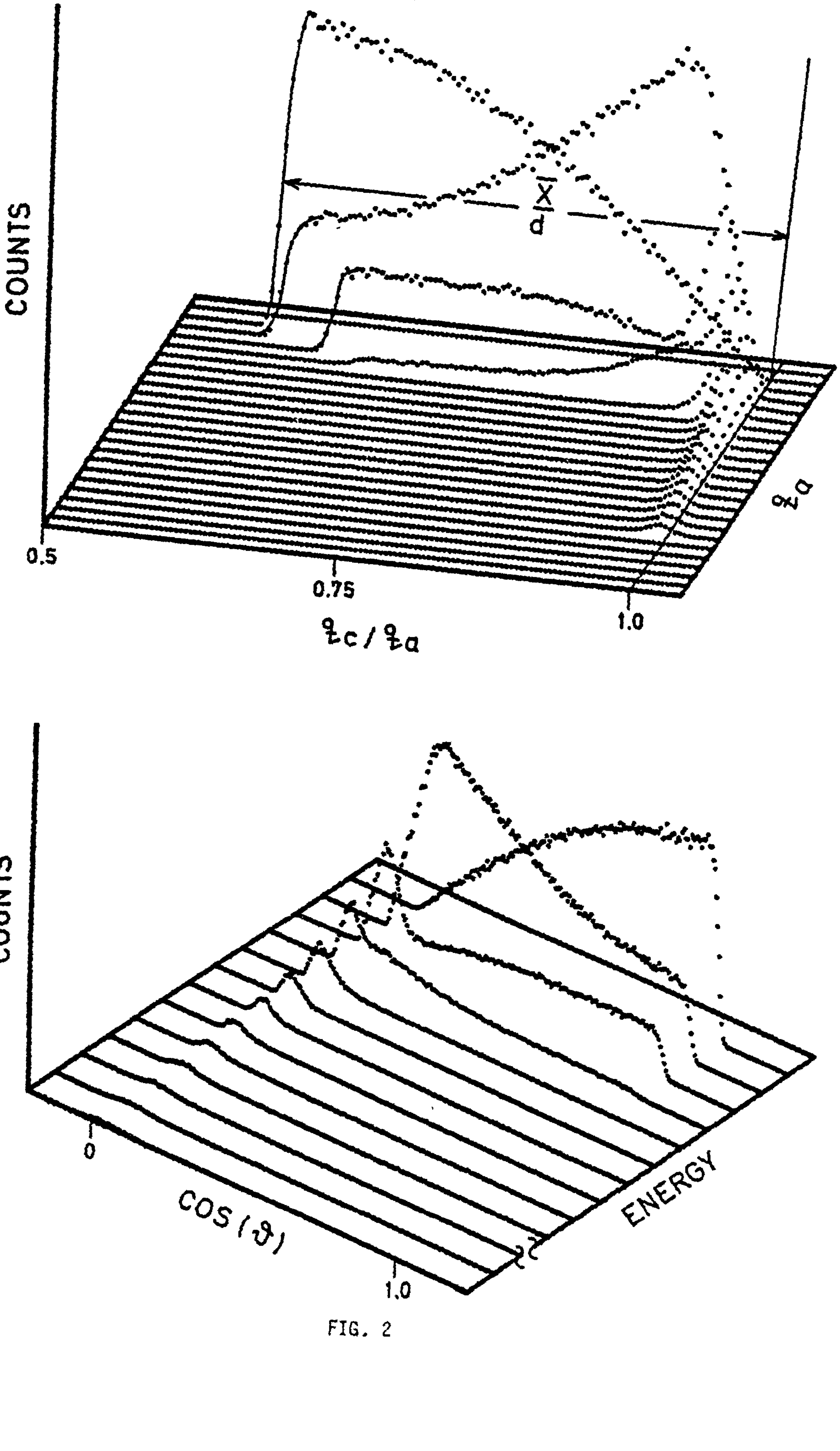

FIG. 2

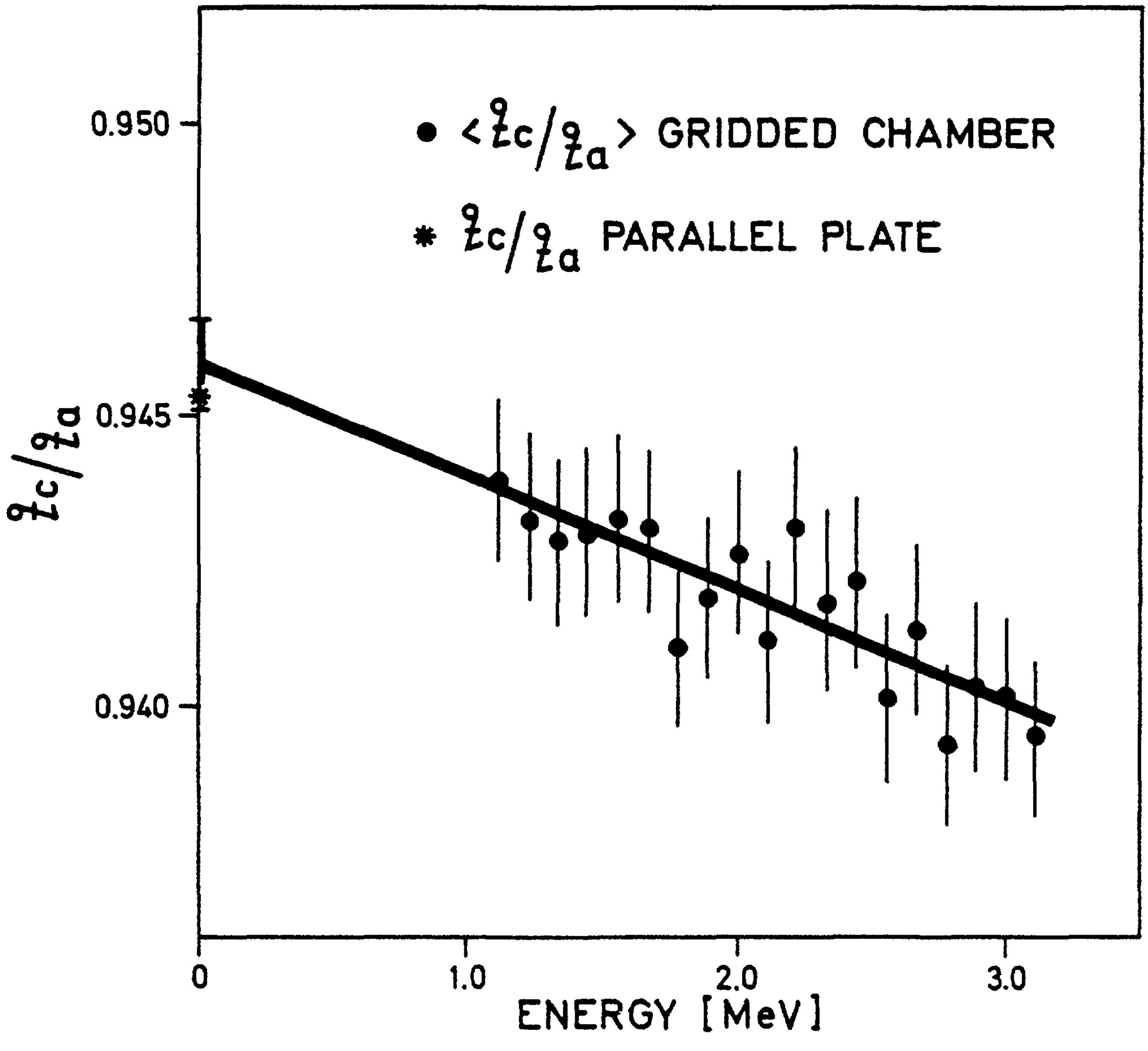

● ⟨q_c/q_a⟩ GRIDDED CHAMBER
✱ q_c/q_a PARALLEL PLATE
q_c/q_a
0.950
0.945
0.940
0
1.0
2.0
3.0
ENERGY [MeV]

FIG. 3

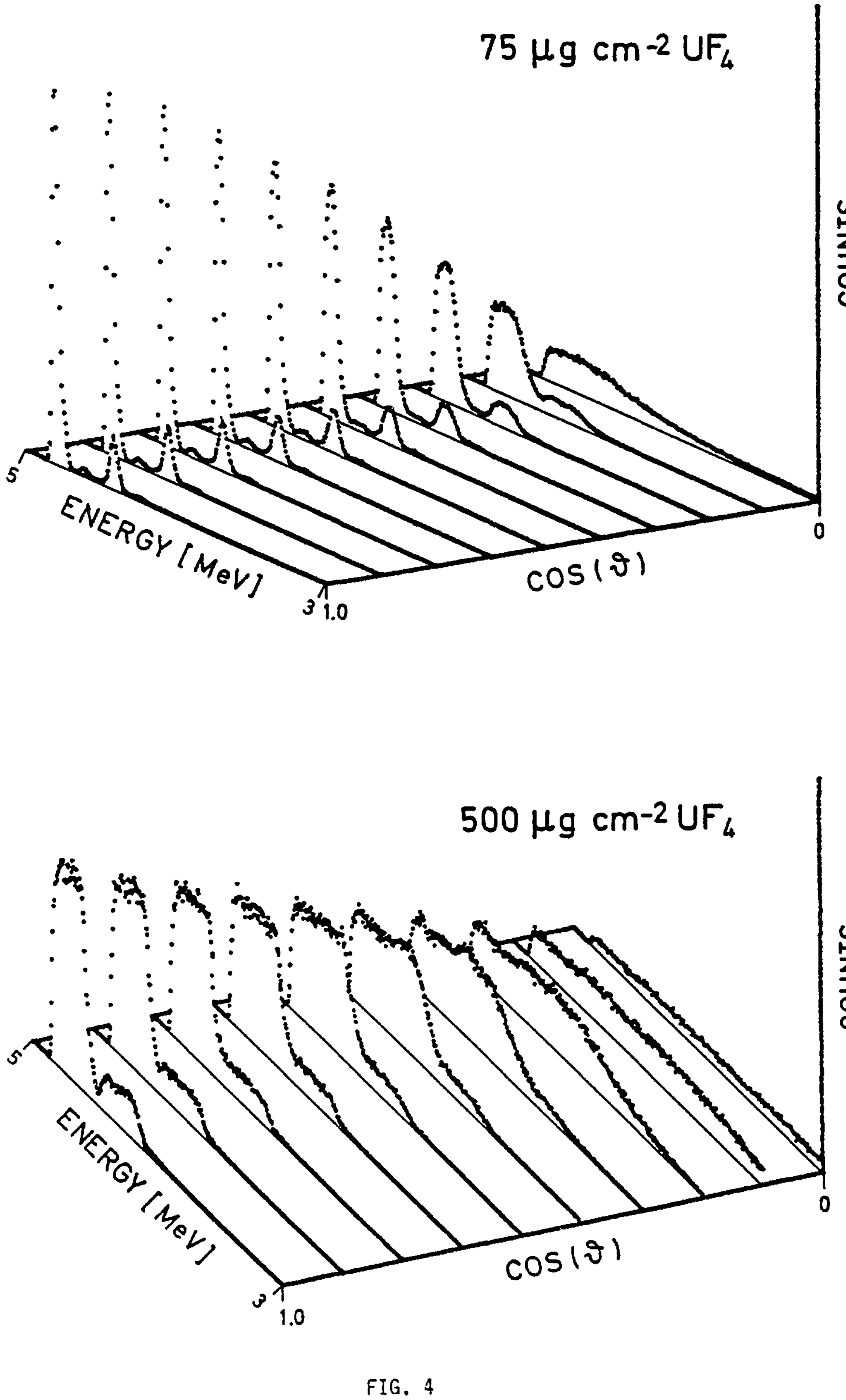
75 µg cm-2 UF4
COUNTS
5
ENERGY [MeV]
3
1.0
COS (ϑ)
0
500 µg cm-2 UF4
COUNTS
5
ENERGY [MeV]
3
1.0
COS (ϑ)
0

FIG. 4

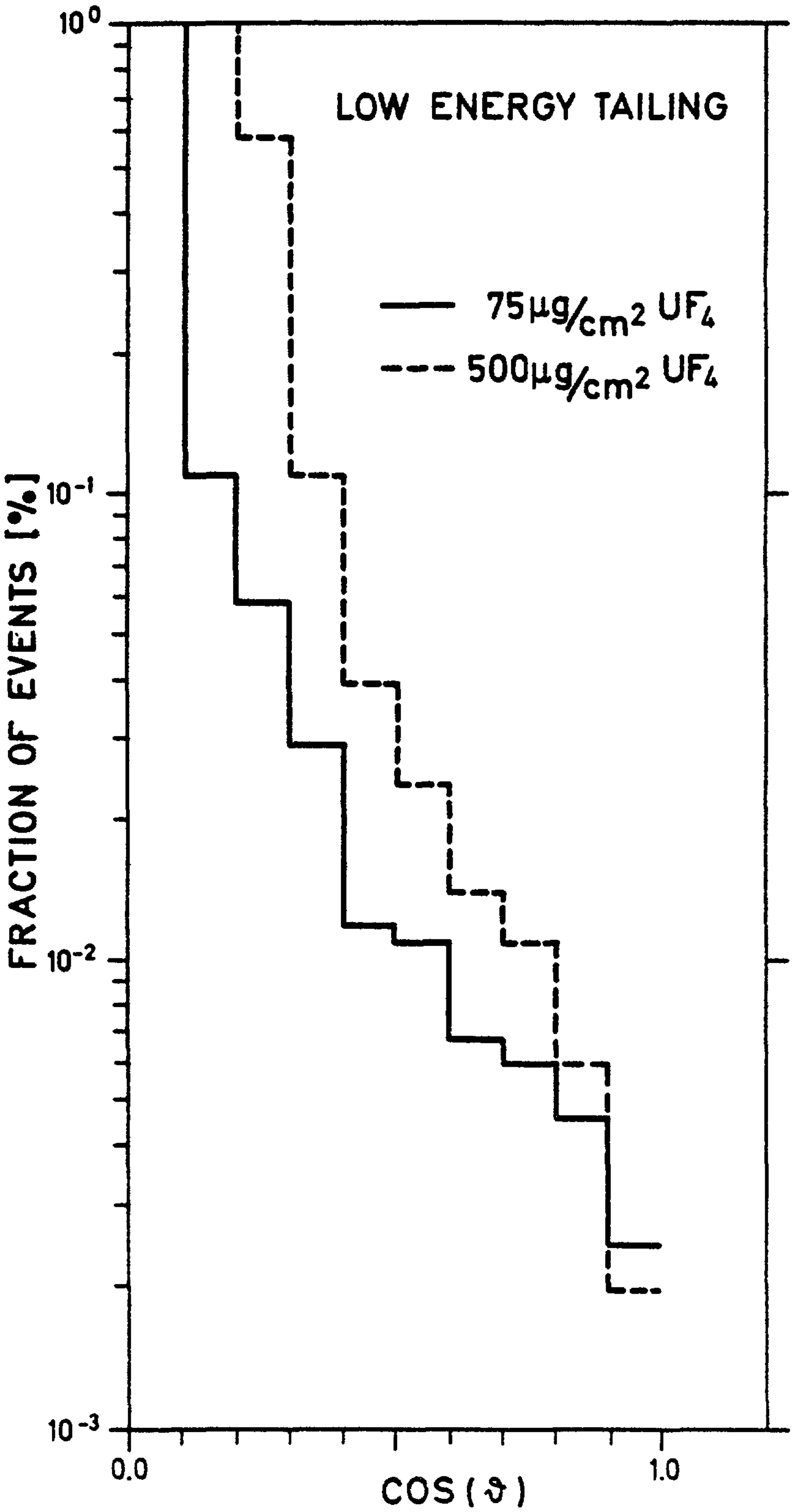
LOW ENERGY TAILING
75μg/cm2 UF4
500μg/cm2 UF4
FRACTION OF EVENTS [%]
10^0
10^-1
10^-2
10^-3
0.0
1.0
COS (ϑ)

FIG. 5

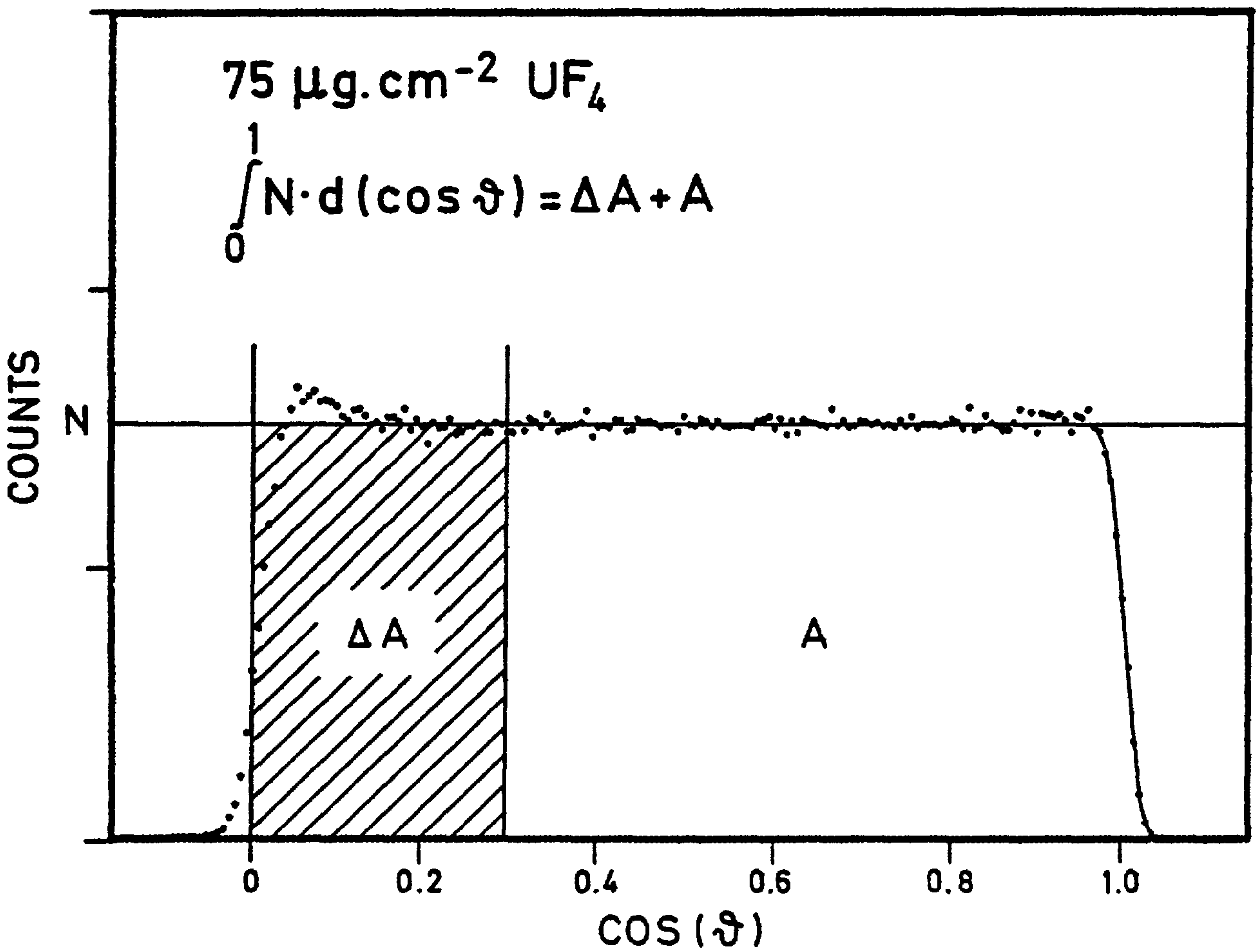

75 µg.cm^{-2} UF$_4$
$\int_0^1 N \cdot d(\cos\vartheta) = \Delta A + A$
COUNTS
N
ΔA
A
0
0.2
0.4
0.6
0.8
1.0
COS (ϑ)

FIG. 6

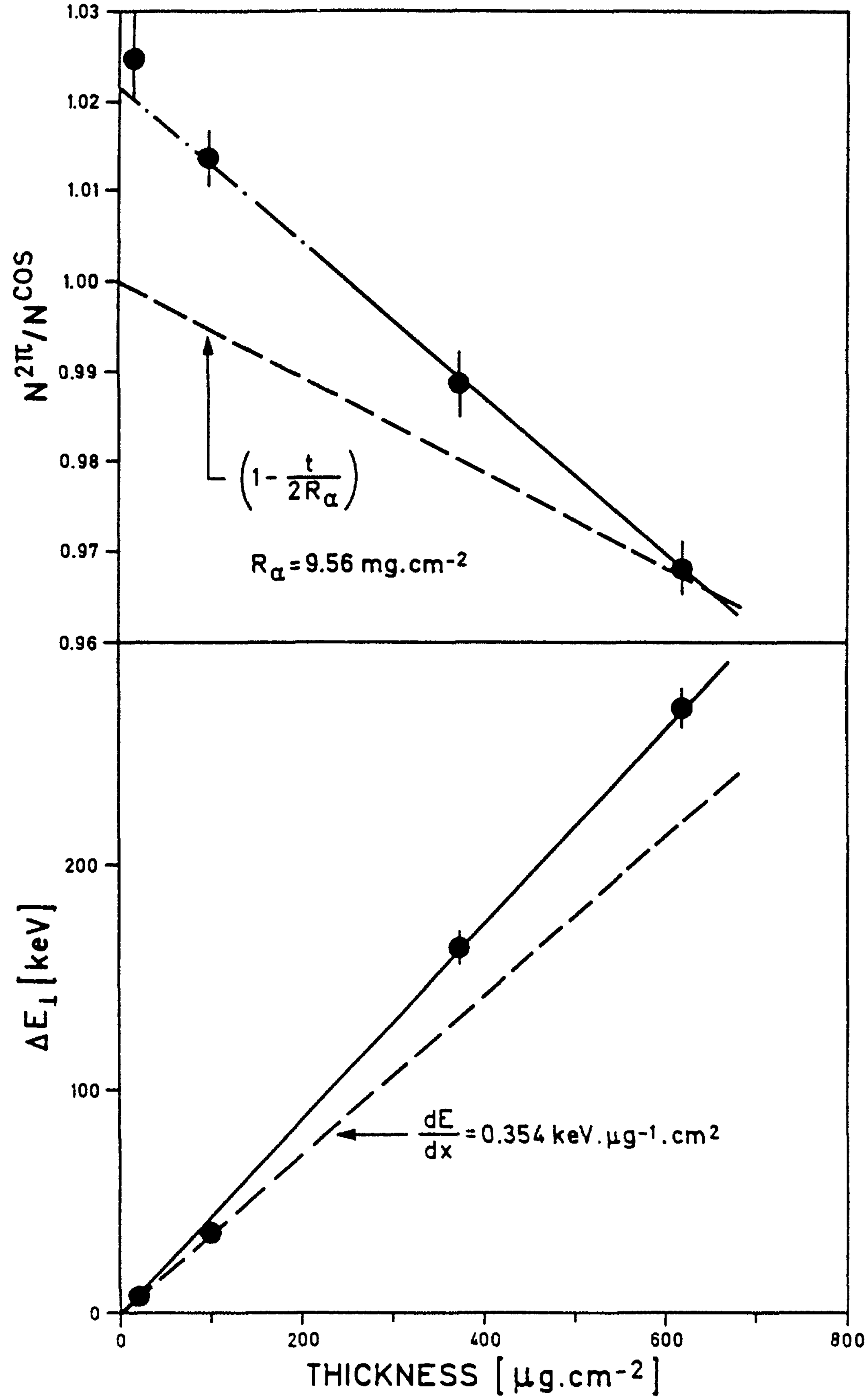
1.03
1.02
1.01
1.00
0.99
0.98
0.97
0.96
$N^{2\pi}/N^{COS}$
$\left(1-\frac{t}{2R_\alpha}\right)$
$R_\alpha = 9.56$ mg.cm^{-2}
0
100
200
$\Delta E_\perp$ [keV]
$\frac{dE}{dx} = 0.354$ keV.μg^{-1}.cm^2
0
200
400
600
800
THICKNESS [μg.cm^{-2}]

FIG. 7

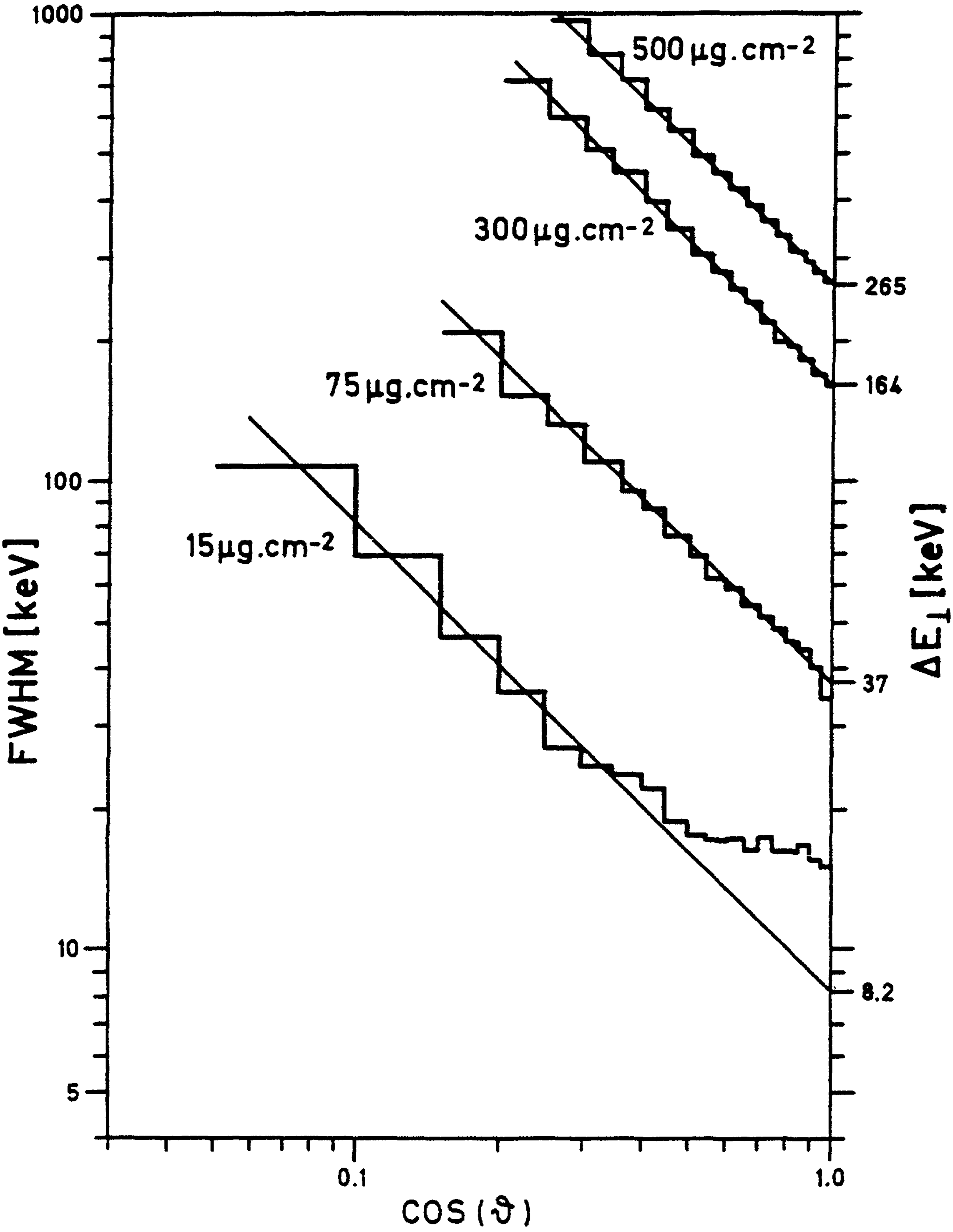

1000
100
10
5
500 µg.cm-2
300 µg.cm-2
75 µg.cm-2
15 µg.cm-2
265
164
37
8.2
FWHM [keV]
ΔE⊥ [keV]
0.1
1.0
COS (ϑ)

FIG. 8

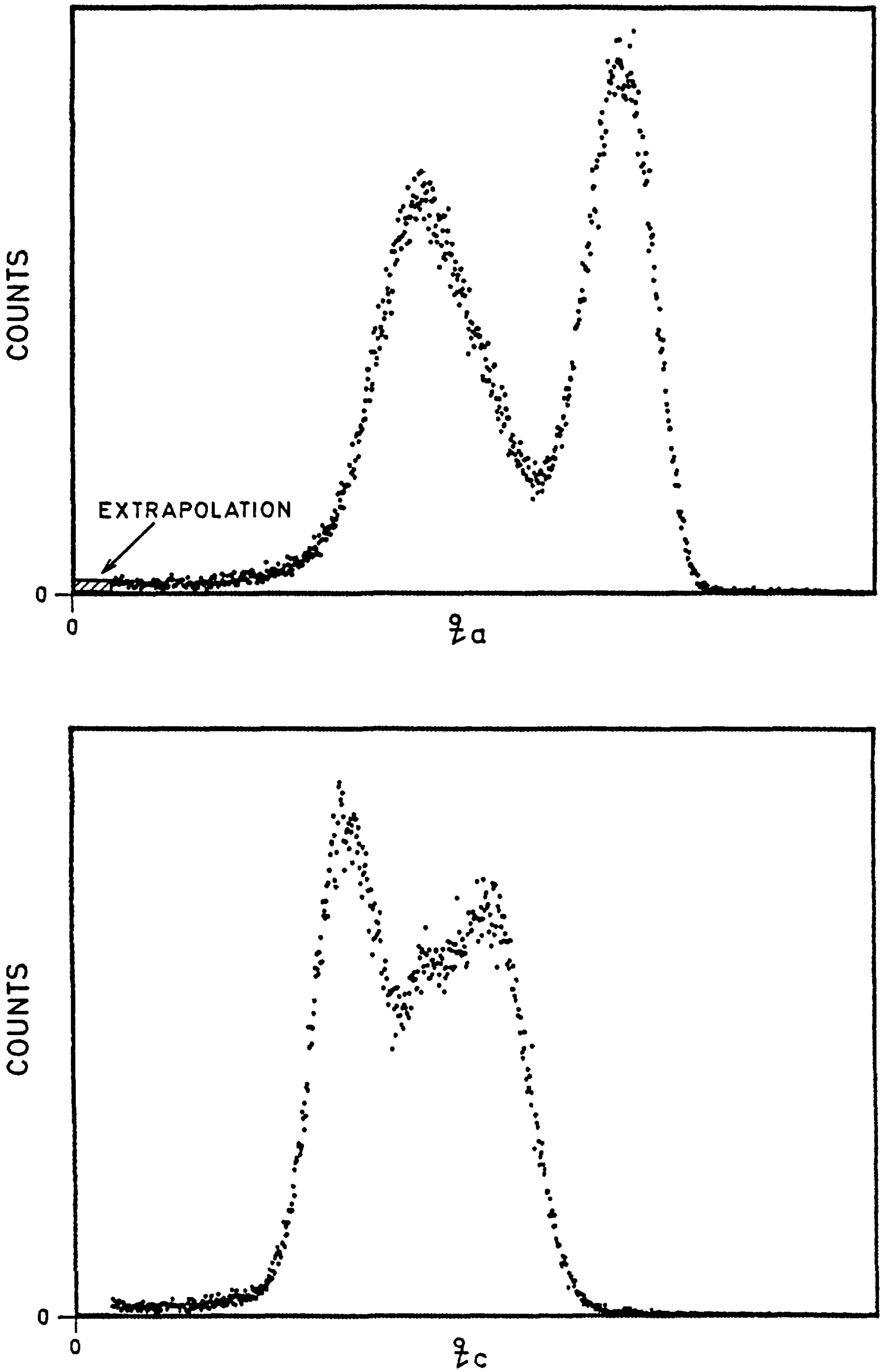

FIG. 9

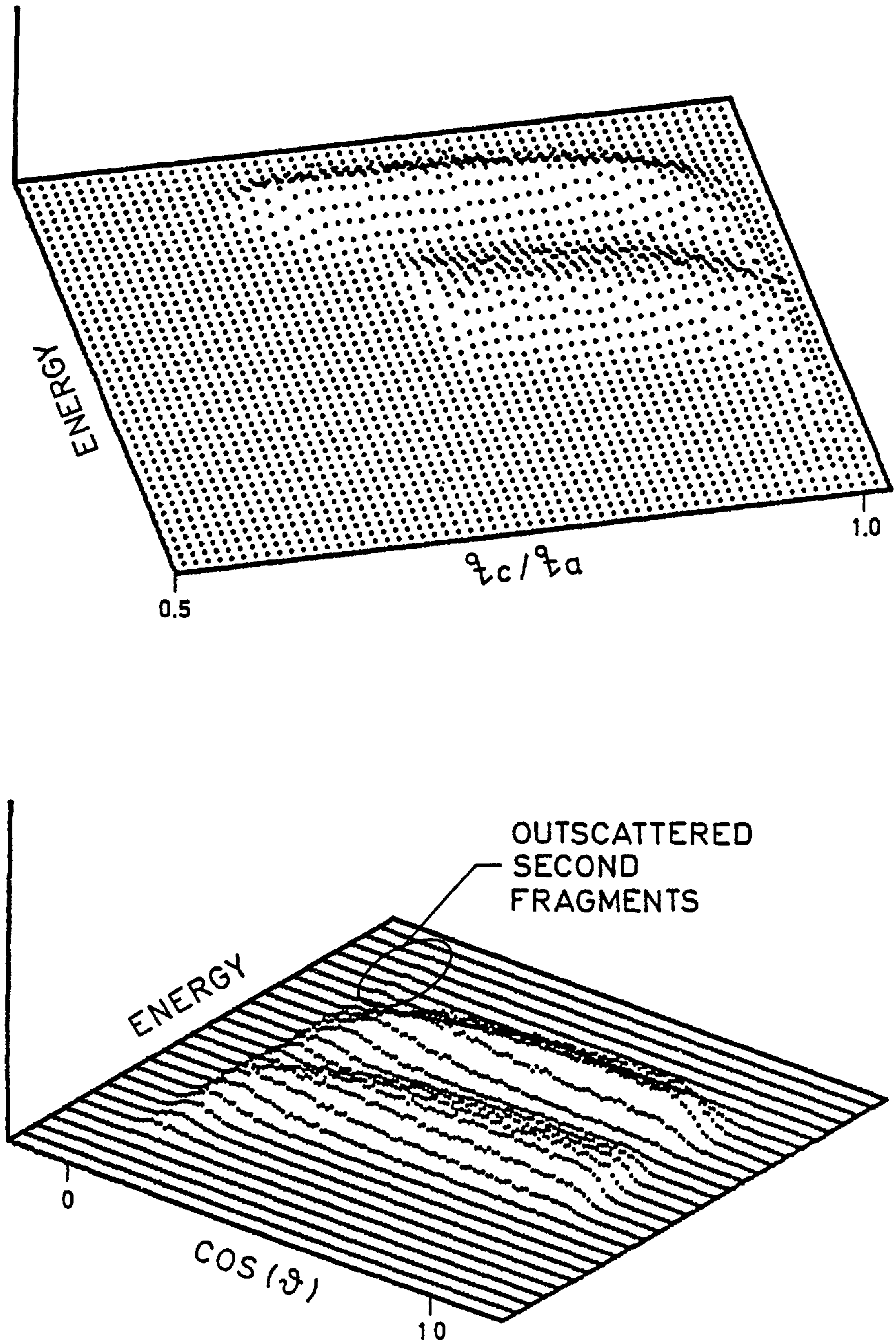
ENERGY
q_c/q_a
0.5
1.0
OUTSCATTERED
SECOND
FRAGMENTS
ENERGY
0
COS (ϑ)
1 0

FIG. 10

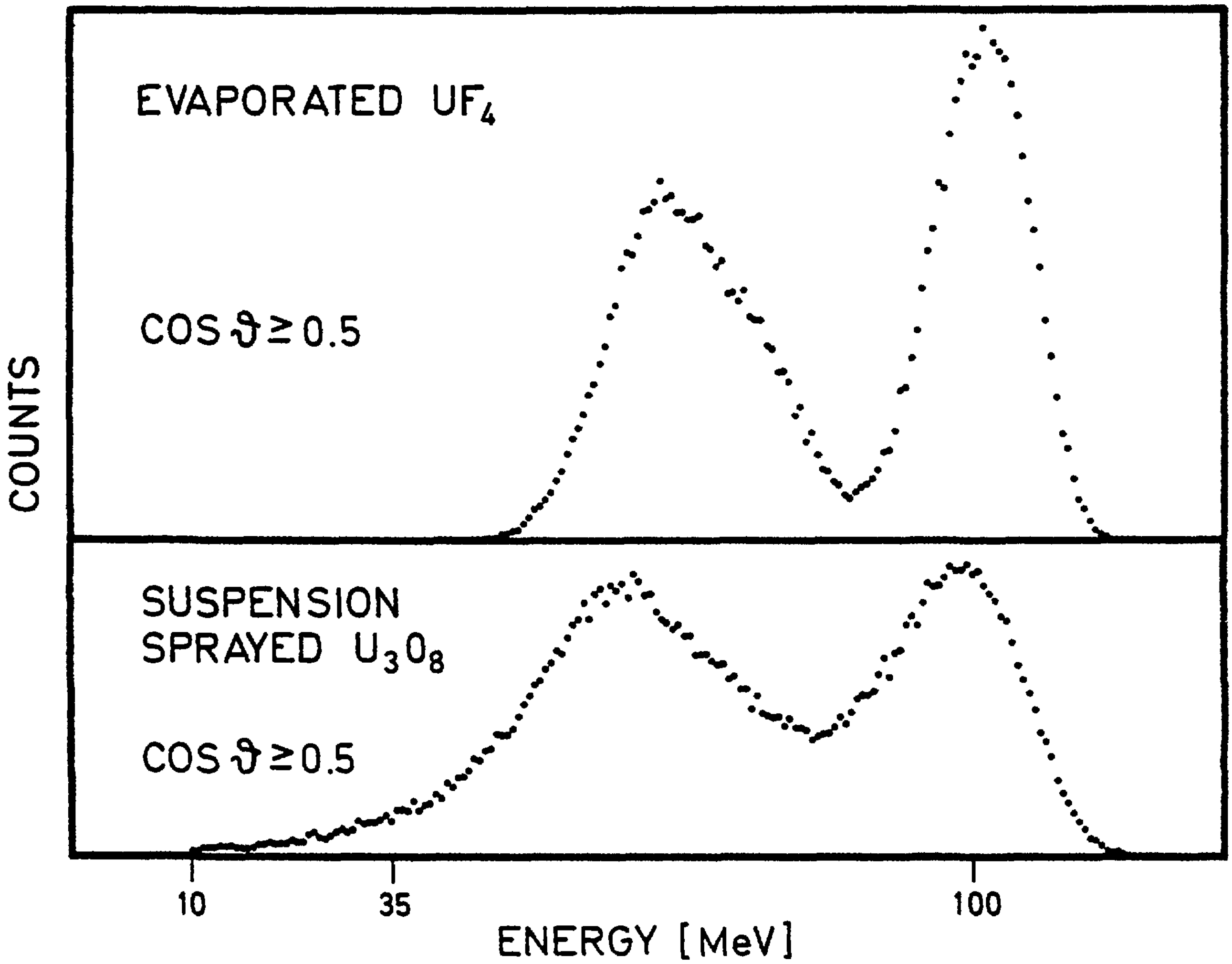
EVAPORATED UF_4
$\cos\vartheta \geq 0.5$
COUNTS
SUSPENSION
SPRAYED U_3O_8
$\cos\vartheta \geq 0.5$
10
35
100
ENERGY [MeV]

FIG. 11

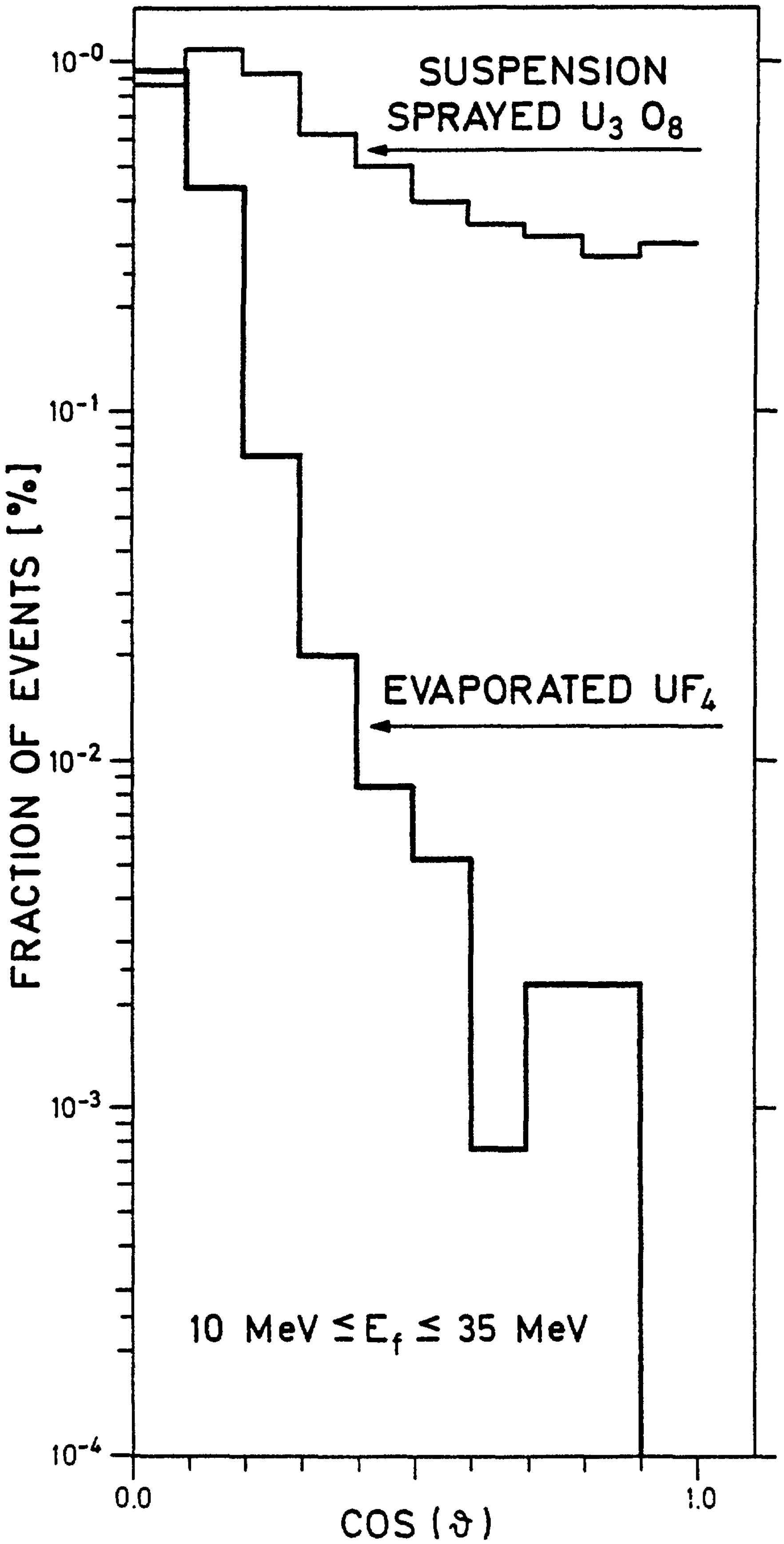

SUSPENSION SPRAYED U_3O_8
EVAPORATED UF_4
10 MeV ≤ E_f ≤ 35 MeV
FRACTION OF EVENTS [%]
COS (ϑ)
10^{-0}
10^{-1}
10^{-2}
10^{-3}
10^{-4}
0.0
1.0

FIG. 12

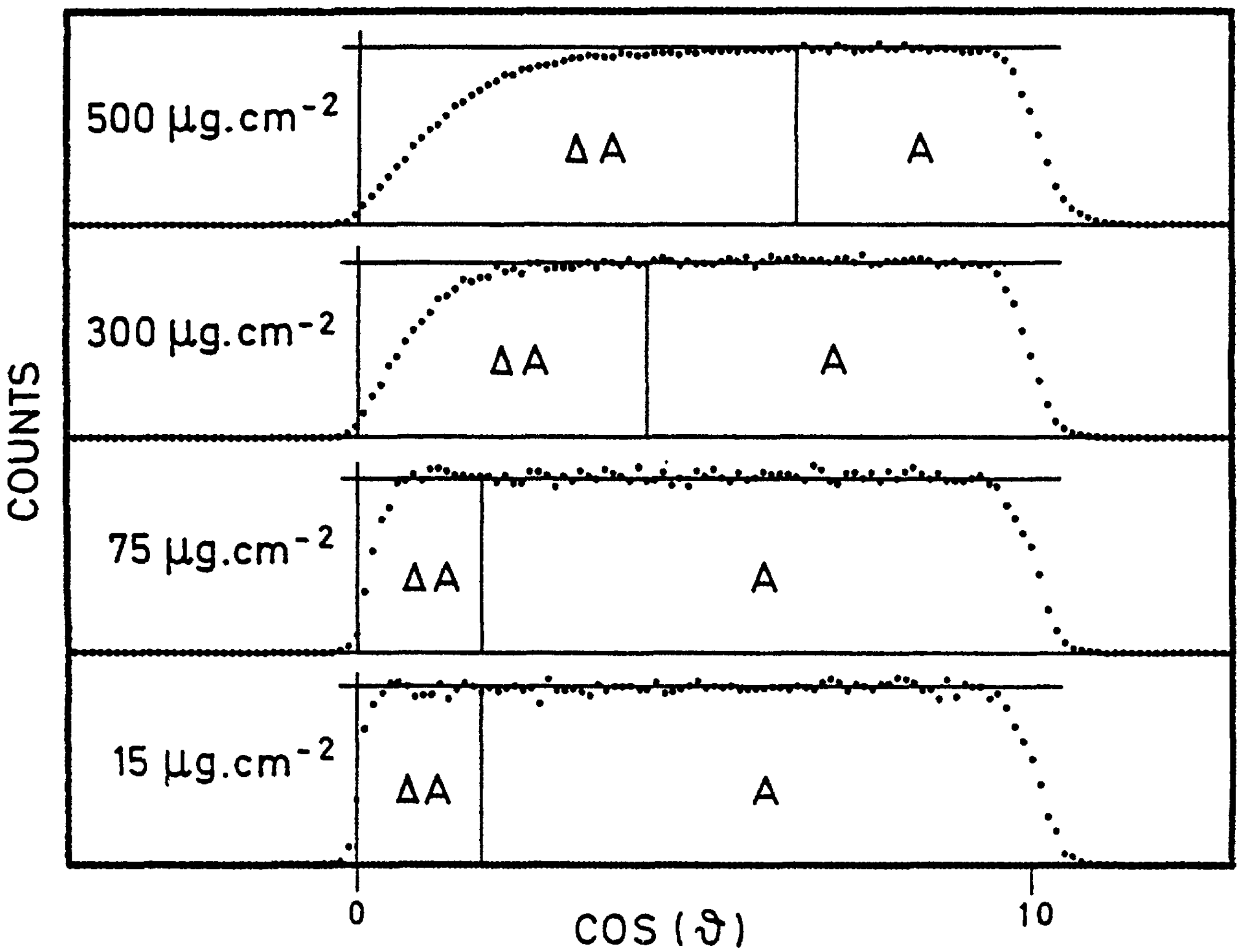
500 µg.cm⁻²
ΔA
A
300 µg.cm⁻²
ΔA
A
75 µg.cm⁻²
ΔA
A
15 µg.cm⁻²
ΔA
A
COUNTS
0
10
COS (ϑ)

FIG. 13

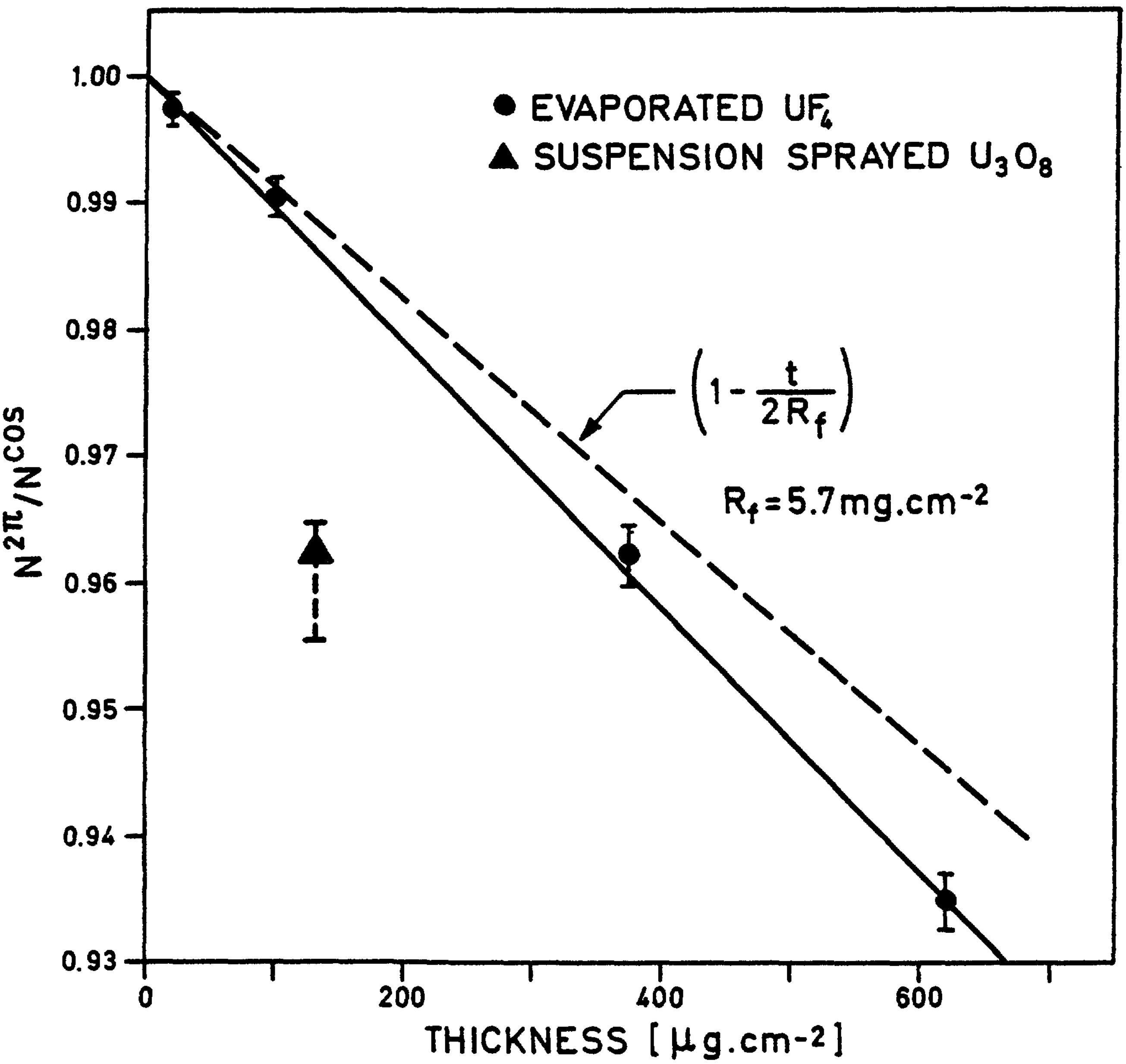
1.00
0.99
0.98
0.97
0.96
0.95
0.94
0.93
$N^{2\pi}/N^{cos}$
● EVAPORATED UF_4
▲ SUSPENSION SPRAYED U_3O_8
$\left(1-\frac{t}{2R_f}\right)$
$R_f = 5.7 mg.cm^{-2}$
0
200
400
600
THICKNESS [μg.cm-2]

FIG. 14

Analysis of the Uncertainties of the RIL-TUD Fission Cross Section Measurement employing the TCAPM

R Arlt and H G Ortlepp

Technical University of Dresden, GDR

1 Introduction

Absolute fission cross-section measurements at fixed neutron energies of 2 6, 8 5 and 14 7 MeV are being performed at the Radiuminstitute Leningrad (RIL) and the Technical University of Dresden (TUD) employing the time correlated associated particle method (TCAPM) [1] The number of neutrons reaching the fission target is determined by counting the charged particles (N_{AP}) associated with these neutrons due to the kinematics of the neutron producing reactions [D(d,n)^{3}He or T(d,n)^{4}He] The fission events (N_f) are counted in coincidence with the associated particles only, since more neutrons than the associated paticles reach the fissile layer (Fig. 1) The fission cross section is given by the formula

$$\sigma_f = \frac{N_f}{N_{AP} \cdot n}$$

where n is the number of fissile nuclei per cm^2. The sources of uncertainties in N_f and n are common with these of other methods of fission cross-section measurements, where fast fission chambers are used. The uncertainty of N_{AP}, however, is connected with the special conditions of the TCAPM

2 Uncertainties Common With Other Methods

2 1 The Fission Chamber Inefficiency

A certain inefficiency of the fission chamber is caused by fission fragments which were absorbed in the foil or did not leave it with suffi-

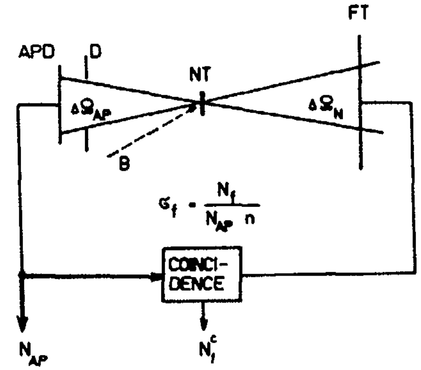

Fig. 1 Scheme of the TCAPM
B-deuteron beam, NT-neutron producing target, D-aperture, APD-charged particle detector, FT-fission target.

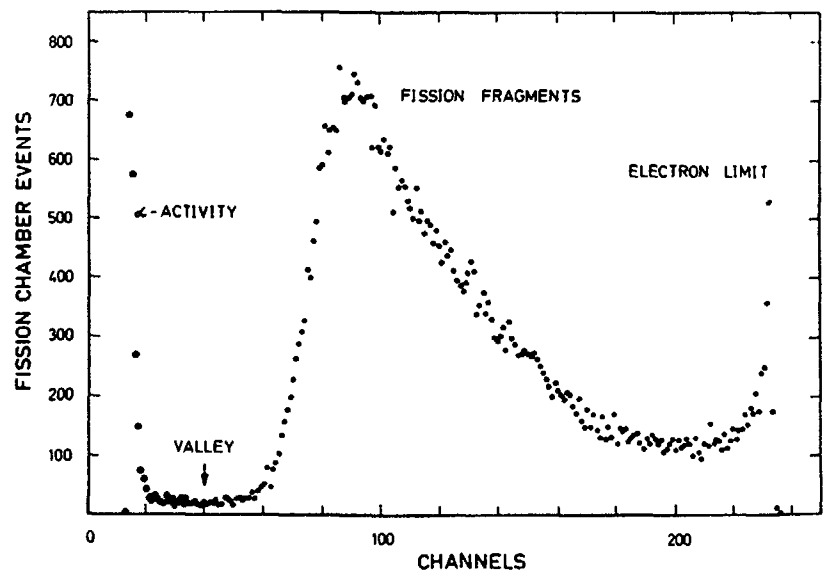

Fig. 2· Amplitude distribution of the fission chamber current pulses, obtained with the help of a fast stretcher.

cient residual energy to be accounted for. A straightforward procedure for the calculation of the fraction of lost events is commonly used.

The low-energy tail of the fission chamber pulse height spectrum caused by near plane events is extrapolated to zero pulse height. Afterwards, the total absorption considering the

$$\frac{t}{2R} \text{ - factor}$$

(t is the thickness of the deposit, R the range of the fission products), the anisotropy and the momentum transfer is calculated [2]. The low energy tail of the pulse height spectrum cannot be measured down to zero pulse height due to the alpha activity of the deposit. Therefore assumptions have to be made for the part superimposed by the alpha spectrum. White [3], for example, obtained a linear increasing tail in a full energy absorption chamber. In the TUD and RIL measurements, ΔE fission chambers are used and flat tails are observed (Fig. 2). A theoretical estimation of the residual energy distribution of near-plane fragments, assuming a proportionality of the energy losses,

$$\frac{dE}{dx}$$

to the square root of the energy (E)

$$\frac{dE}{dx} \sim \sqrt{E}$$

for fragments with *mean mass and energy values is shown in Fig. 3. In* ΔE chambers a smaller fraction of the tail is recorded than in the full energy chambers. Thus the difference in the slope can be understood. The systematical *error* of a linear extrapolation of the tail to *zero* can be estimated to be less than 0.5% for a 0.3 mg/cm^2 foil for the experimental conditions of the RIL-TUD experiments. The $\sqrt{E}$-law, however, is a poor description of the fission fragment stopping power, especially in the last part of the fission products path. It can be shown that when

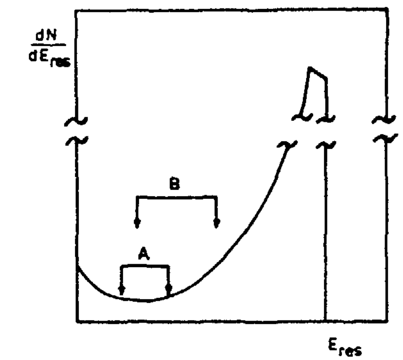

Fig. 3: Qualitative estimate of the residual energy distribution of fragments of same energy and mass, emitted isotropically from an ideally flat layer of t = 0.05 R thickness. A - fraction, appearing in a differential chamber as plateau, B - plateau region for a full energy chamber

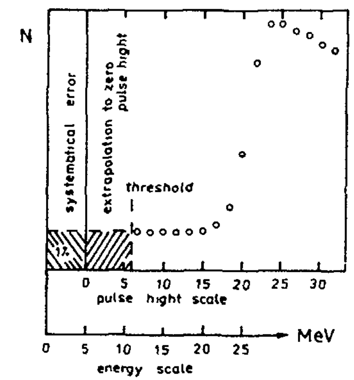

Fig. 4: Possible systematical error due to the ionisation defect.

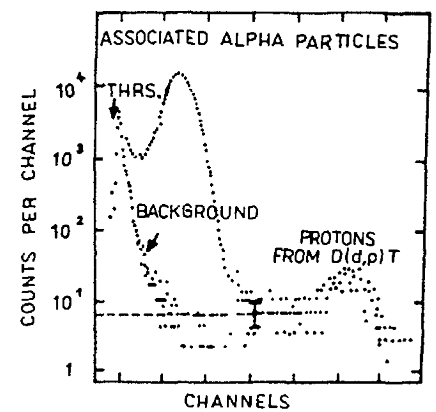

Fig. 5: Pulse height spectrum of the AP-channel in the 14.7 MeV experiment. The background was taken with a non-tritium loaded target

employing a more realistic expression for the stopping power[6], the systematical error of the linear extrapolation should become less

It has to be stressed that the measured pulse height distribution depends not only on the chamber design but also on the method of the analogue processing of the spectrometric pulses Several open questions are connected with the total absorption correction The mean fission fragment range depends on the chemical composition of the layer which is not exactly known in many cases A difference of 0 2% in the absorption correction can be estimated for an $h = 0{,}3\ mg/cm^2$ foil thickness between UO_2[4] and U_3O_8[3] The usually unknown surface roughness leads to an increase of the absorption loss too Using the notation used in [3], the absorption loss increases by 0 5% for a foil of 0 3 mg/cm^2 if a "roughness" of 0 5 h is introduced

The ionisation defect is an additional effect which may lead to an inrease of the inefficiency In the last part of the flight path the fragments are slowed down mainly by nuclear collisions without ionisation Therefore the pulse height scale is shifted, compared with the energy scale, by about 5 MeV [5] A rough estimation assuming the ionisation to be switched out and the nuclear stopping switched on at 5 MeV residual fragment energy gives a 1% efficiency loss for this worst case estimation (Fig 4). The nuclear stopping exceeds the ionisation loss only below about 2 MeV[6] but is present up to about 20 MeV As a result the energy scale is contracted up to about 20 MeV, thus increasing the plateau height Therefore the above mentioned systematical error due to the ionisation defect should be compensated partially because for the extrapolation to zero pulse height a higher number of events per channel is used A proper theoretical calculation and experimental investigation of all effects determining the inefficiency seems to be a rather complex problem Consequently, besides the detailed treatment of all these effects, direct measurements of the total inefficiency employing different methods so as coincident fission product - neutron counting, angular distribution analysis or mixed source alpha/fission product counting are strongly suggested

2.2 Alpha-Counting of the Foils

The TCAPM requires the areal density of the fissile layer only, but not its total mass Determinations of the areal density are carried out at the RI Leningrad with an uncertainty of 0.5-1%. Several low geometry counting systems using two apertures for the determination of the geometric factors are employed Measurements with different apertures in front of the foil allow the estimation of the inhomogeneity From differences greater than the statistical uncertainty a further contribution to the overall error, mostly in the order of 0.5% is estimated by comparing neutron cone topography and inhomogeneity. It turned out that the errors of the target parameters were one of the most serious limitations for the further improvement of the accuracy of the fission cross section measurements of the RIL-TUD collaboration. Independent measurements of the areal density and the inhomogenuity on specially selected reference foils are suggested to be performed in different laboratories Thus, a intercomparison of geometric factors could be achieved, leading to more accurate foil parameters. At the TU Dresden a low geometry counter with several different apertures and a scanning setup were constructed to get a second independent set of foil data Preliminary results agree with the RI Leningrad values within the limits of uncertainty

2 3 Accidental Coincidences

The coincidence resolution time determined by a fast coincidence unit was 10-20 ns in the measurements carried out at the TUD The random coincidence rate amounted to some percent of the true events The time distribution between the fission and associated particle signals was taken in order to determine the background of random coincidences. A signal was derived from the AP-detector containing both the fast timing and the slow pulse height window information in order to obtain one random coincidence correction only For this purpose special electronic equipment was developed for fast pulse height processing [10] The uncertainty of the random coincidence correction is well below the statistical uncertainty of the true events

3 Neutron Flux Uncertainty for the TCAPM

The counting rate of the associated particle detection system differs slightly from the neutron flux reaching the fission foil Therefore several small corrections must be applied to account for AP-detector background, scattering of incoming and associated charged particles, and neutron scattering

3 1 Background of the AP-Detector

Three different methods are used to detect the associated particles in the 2 6, 8 5 and 14 7 MeV set-ups [1] During the development of the detection systems the main effort was concentrated on the background minimization and the determination of the appropriate corrections and their uncertainties At 14 7 MeV the use of a plastic scintillation detector in connection with a differential discriminator provides the separation of the alpha peak from the proton and triton ones arising due to the self-target build-up The background caused by neutron and gamma-rays was 0 3% (Fig 5) with an uncertainty of less than 0 1%

In the 2 6 MeV experiment the ^{3}He-particles had to be separated from the tritons and protons caused by the D (d,p) T reaction The background underlying the low energetic ^{3}He peak was determined applying an Al-foil in front of the silicon surface barrier detector sufficient to stop the ^{3}He's, but not the tritons and protons (Fig 6) The background correction due to the low energy tails of the triton and proton peaks was 2 4% with an estimated uncertainty of 0 5% In the 8 5 MeV measurements the associated *Helions were detected by a* $\Delta E - E_r$-telescope to distinguish them from the alpha background in the same alpha peak in the particle identifier output spectrum was determined by replacement of the deteriorated polyethylene target by a non-deteriorated one (Fig 7) The appropriate correction was in the order of 1-3%, depending mainly on the quality of the used ΔE detector with an uncertainty of less than 0 5% Effective pile-up rejection is employed in all cases in order to reduce spectrum distortions due to undetected pile-up to a value less than 0 1%

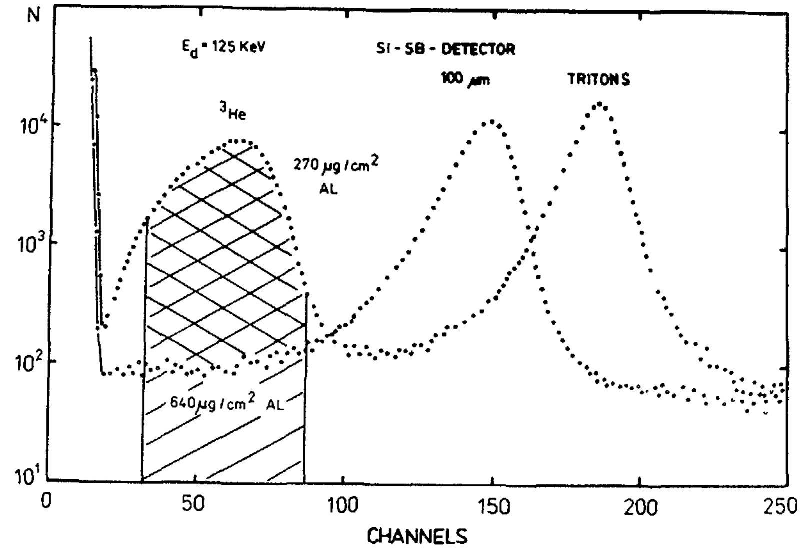

Fig 6 Background determination in the 2 6 MeV experiment by stopping the ^{3}He particles The higher energetic proton peak is not shown

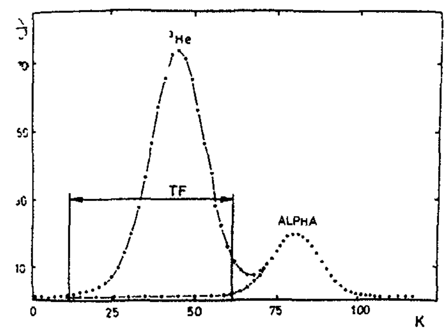

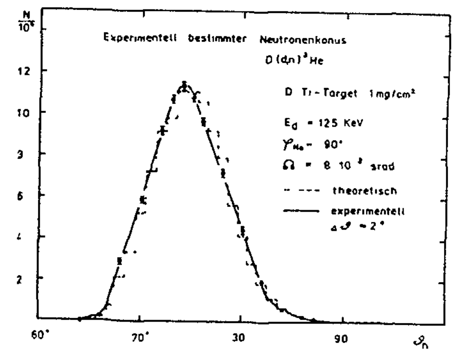

Fig 7 Particle identifier output spectra for CD_2 and CH_2 foils in the 8 5 MeV experiment TF particle window

Fig 8 Calculated and measured cone profiles in the 2 6 MeV experiment

3 2 Scattering and Straggeling of the Incoming and the Associated Particles

The neutron cone profile and the neutron energy distribution are mainly determined by the geometrical conditions and the slowing-down of the incoming deuterons and associated particles along their path in the neutron producing target Both distributions were calculated and the neutron cone was scanned experimentally A comparison of the calculated and measured neutron cone profiles (Fig 8) shows that the influence of the small angle multiple scattering and the energy straggeling is small compared with the factors mentioned above As for the determination of the fission chamber position in all experiments the measured neutron cone profiles were employed usually and no corrections for the broadening of the neutron cone had to be performed In the 2 6 MeV case however the probability of large angle Rutherford scattering cannot be neglected due to the low helion energy A helion emitted originally in another direction, can reach the AP detector after a scattering act This leads to diffusely distributed associated neutrons far away from the cone, which cannot be distinguished from the background experientally within reasonable measurement time A Monte Carlo simulation showed the necessity of a 0,5-1% correction with 0.5% uncertainty as a preliminary result

3 3 Neutron Scattering

The calculation of the neutron scattering correction was performed at the RI Leningrad [7] The uncertainties are in the order of 0,2-0,4%

4 The Total Uncertainty

In the 14 MeV region several groups reached the 1% level with excellent an agreement of their results (see for example [4] and the references therein) This fact, however, should be estimated not too optimistically, because the same method - TCAPM was used by all groups Similar methods for the theoretical calculation of the fission chamber inefficiency, which can be connected with systematical errors up to 1% had been employed in every case Since the TCAPM seems to be the only method giving a 1% uncertainty this approach has to be investigated very carefully in order to exclude unidentified sources of systematical uncertainties. At the TU Dresden, 8 5 MeV [8] and 2 6 MeV [9] measurements standard deviations of 2 4% and 1.6% respectively, were reached. These values are determined mainly by the counting statistics and the uncertainties of the foil parameters

5. References

[1] R. Arlt, et al; Proc. Int. Conf Nuclear Cross Sections for Technology, Knoxville, USA, October 22-26, 1979

[2] R. Arlt, et al; Preprint 05-5-79 of Technical University of Dresden, Dresden, GDR, 1979; and references therein

[3] P H White; Nucl Instr. a Meth., 79 (1970) 1

[4] O.A Wasson, A D Carlson and K D. Duvall; Nucl. Science and Engineering, 80 (1982) 282

[5] H W. Schmitt and R.B. Leachman; Phys. Rev. 102 (1956) 183

[6] L C. Northcliff and R.F Shilling; Nuclear Data Tables; A 7 (1970) 233

[7] V N. Dushin, In Proc. of VIII Internat Symp. on the Interact of Fast Neutr. with Nucl ; Gaussig, GDR, 1978, ZfK-382, p.153

[8] W Wagner; Dissertation, Technical University of Dresden; GDR, 1982

[9] R Arlt, et al, Preprint 05-22-81, Tech. University of Dresden; Dresden, GDR, 1981

[10] H.G. Ortlepp, Proc XII International Symposium on Nuclear Physics; Gaussig, 1982; Zfk-491, 1982, p 141

EXPERIMENTAL AND THEORETICAL INVESTIGATION OF THE ENERGY DISTRIBUTION OF CALIFORNIUM-252 SPONTANEOUS FISSION NEUTRONS

O. I. Batenkov, M. V. Blinov, G. S. Boykov,
V. A. Vitenko, V. A. Rubchenya

V. G. Khlopin Radium Institute,
197022, Leningrad, USSR

ABSTRACT

The results of recent measurements of the spectrum of californium-252 fission neutrons in a broad energy range are presented in the report. Some results of measurements and of theoretical calculations of angular and differential energy distributions of californium-252 fission neutrons are presented too.

INTRODUCTION

In the recent years investigations of the spectrum of californium-252 (international standard) spontaneous fission neutrons are carried out intensively in a broad energy range from hundreds eV to tens MeV. The shape of the spectrum at energies lower than 0.5 MeV has been specified considerably due to increase of measurements precision. A marked difference in the shape of the spectrum in the range 3-10 MeV from the data of other works was observed in /1/. A relatively high intensity in the region 20-25 MeV was found in /2/. There is still high uncertainty of the spectrum shape in the energy interval 10-15 MeV. Thus, the obtaining of precise data on the spectrum is still an urgent task.

In our work /3/ there were considered the results of ^{252}Cf neutron spectrum measurements in the energy range 0.01-7 MeV that had been obtained by the time-of-flight method using a fast ionization chamber with uranium-235 layers as a neutron detector.

New experimental data on the spectrum of californium-252 fission neutrons (energy interval 0.01-10 MeV) are presented in this paper. The data present the results of two sets of measurements - the first, reported in /3/ and the second, fulfilled recently. In the first set the main attention was paid to the low energy range and in the second one - to higher energies. A set-up described earlier /3/ was used, but in the second set the experimental conditions and some characteristics of the spectrometer were improved. In the report there is information on the designs and characteristics of the fragments and neutron detectors, on the characteristics of the fissionable layer, on the values of some corrections and the procedure of data processing. Besides, in the report there are given some results obtained both experimentally and by calculations on angular and differential energy distributions of californium-252 fission neutrons. It is supposed that these investigations will help to provide a theoretical base for understanding of formation of the integral spectrum - international standard - from many energy distributions of neutrons, depending on the mass, the charge of the fragment, its excitation energy and the angle of the neutron emission.

FISSIONABLE LAYER. DETECTORS.

Californium-252 layers were prepared by the method of thermovacuum sputtering of a californium nitrate on polished platinum backings 0.1 mm thick. A preheating of the californium sample at the temperature of 1000 °C was carried out for elimination of impurities. Evaporation of the californium was done at the temperature 1600-1700 °C. Californium was sublimated on the backing as an oxide. Spontaneously fissile isotopes of californium (except californium-252) and curium gave a contribution less than 0.2 % into the total number of the registered fragments. Two californium layers (diameter 4 mm) were prepared: 0.75 μg and 0.3 μg. The quality of the layer 0.75 μg and its absolute intensity was determined by measuring the amplitude spectra of the fission fragments at various angles in respect to the plane of the californium layer (fig. 1). The measurements were done by means of a silicon semiconductor detector, being at a distance of 100 cm from the center of the layer (angular uncertainty $\pm$ 0.5). The ratio of the number of the fragments registered at the angle of 90 ° to the layer plane to the number of the ones registered at the angle 4° was 1.02. The intensity of the layer was equal to $(5.12 \pm 0.05)10^5$ fiss/s.

For registration of californium-252 fission fragments during the measurements of the neutrons spectrum, a miniature current ionization chamber was constructed similar in the design to the one described in /4/. The construction of the chamber is shown in fig. 2. The chamber consisted of a hemisphere 16 mm in diameter made of stainless steel (0.1 mm thick) to the butt-end of which a platinum backing (0.1 mm thick) was soldered with a layer of californium-252. The collecting electrode was made of platinum also 0.1 mm thick. Methane was blown through capillary inlets at atmospheric pressure. The signal from the anode was fed by a cable with air insulator into the preamplifier located at 10 cm from the californium layer. The total weight of the chamber with the cable was 1.5 g, the weight of the preamplifier was 5.1 g. In fig. 3 the amplitude spectrum of the fragments is presented; the threshold at which all the measurements were carried out is shown there too. The fission fragments registration efficiency was more than 99 % at the working threshold.

A multilayer ionization chamber with uranium-235 layers was used as a neutron detector. Electrodes (100 mm in diameter) were made of aluminium foil 0.05 mm thick on both sides of which there were layers of uranium, containing 99.9 % of uranium-235. At manufacturing the layers by the method of multiple deposition of uranyl nitrate organic compound with the subsequent tempering at the temperature 550 °C special attention was paid to their homogeneity by the thickness; the former depending in particular on the keeping to the stoichiometric composition of the salt. The degree of homogeneity was determined by measurement of the α-activity of different parts of the layer by a semiconductor detector and in our case was $\pm$ 5 % at an average thickness of the layer 1 mg/cm^2. For improved current collection each layer was covered with gold (thickness 0.05 mg/cm^2) by the method of thermosputtering in vacuum. The relatively small thickness of the uranium layer enabled to obtain a sufficient efficiency of the chambers, on the one hand, and good discrimination of α-particles from fragments, on the other hand. The distance between the plates was chosen to be 3 mm. The amplitude distribution of the fission fragments and of alpha-particles, obtained using the chamber in the fission neutrons flux, is shown in fig. 4. Due to good discrimination of uranium-235 fission fragments from alpha-particles, the efficiency of fragments registration was more than 85 %. The chamber's casing was made of thin cadmium foil (0.2 mm thick), with the background of thermal neutrons being considerably lowered. The weight of the completely assembled chamber with the preamplifier was 65 g.

The full time resolution of the spectrometer using two chambers was 1.5 ns. The time resolution contributed by the californium chamber equalled 0.49 ns and was determined by the generally accepted method.

There were certain difficulties when measuring the resolution time of the uranium chamber. Therefore, a supplementary chamber differed from the working one by one of the uranium layers was substituted for a uranium layer with homogeneously imbedded californium-252 isotope (intensity 1 x 10^3 fiss/s). The measurement of the time resolution was carried out by the standard method (registration of fragments gamma-quanta coincidences) and the resolution time appeared to be equal 1.2 ns.

In order to find out the value of the relative angular dependence of the number of fragment-neutron coincidences, a control test was carried out. It showed that the efficiency of neutrons registration did not change (accuracy 1 %) with the change of neutrons emission angle from 90° to 4° in respect to the plane of the backing.

RESULTS OF THE MEASUREMENTS. CORRECTIONS

Neutron spectra were measured on three flight distances: 25, 50 and 100 cm. In order to exclude scattering from the walls of the room, the measurements were carried out outdoors at a distance of 8 m from the earth. The random coincidences background decreased by several times and constituted 20 % of the value for the neutron energy 30 keV on the base 25 cm and 2 % for the neutron energy 10 MeV on the base 50 cm.

Because of high intensity of spontaneous fissions in the used californium layers the background stimulated by the true-random coincidences (recycle neutrons) was rather high. Thus, at the energy 150 keV it constituted 30 % of the value of the effect. To suppress this background, a block (pile up controller) was used /5/ that analysed the time intervals between pulses from fission fragments and excluded those events for which this interval was less than 200 ns. As a result the background of the true-random coincidences was reduced to 1.9 % at the energy 150 keV without distortion of the spectrum. The residual background was due to the dead time of the californium chamber / τ_M = 25 ns/. The value of this background was calculated by the formula:

$$N_{tr}(j+1) = \left(N_o \tau_c + N_o^2 \tau_c^2 j\right) \sum_{i}^{j} N_K$$

$$i = \begin{cases} j - \dfrac{\tau_M}{\tau_c} & \text{at } j > \dfrac{\tau_M}{\tau_c} \\ 0 & \text{at } j \leq \dfrac{\tau_M}{\tau_c} \end{cases} \qquad j = 0, 1 \ldots n$$

where τ_c - channel value, N_o - number of fissions, τ_M - dead time of the californium chamber, N_K - number of counts in the channel, $N_{tr}(j+1)$ - value of the true-random background in $j+1$-channel. The time counting is from the "zero" time.

In the second set of measurements the precision of the "zero" time determination was improved to ± 0.08 ns. Increasing of the precision enabled to introduce small corrections in the data of the first set. The summary results of the two sets are presented in fig. 5. The neutron spectrum in the region 0.01-6 MeV in general is close to the Maxwellian distribution with T = 1.42 MeV. Some local deviations (∾ 5 %) may be connected with uncertainty of the applied values of the reaction $^{235}U(n, f)$ cross-section. Above 6 MeV gradual deviation from the Maxwellian distribution with T = 1.42 MeV was observed.

MEASUREMENTS OF DIFFERENTIAL NEUTRON DISTRIBUTIONS

The results of immediate measurements of ^{252}Cf neutron fission spectrum should be confirmed by the data based on theoretical calculations. Unfortunately, the fission theory and the theory of particle emission from excited nuclei are still unable to predict the spectrum as an international standard with adequate accuracy. Partly it is due to insufficient information on dynamics of fission process and on the character of neutron emission in this process. In order to elucidate these problems, we carry out experimental and theoretical investigations on the emission mechanism of fission neutrons.

These investigations are supposed to provide a theoretical basis for better understanding of the shape of standard spectrum. We conduct experimental work on precision measurements of angular and energy distributions of fission neutrons.

The measurements of kinetic energies of fission fragments were carried out by means of semiconductor detectors; neutron energies were measured by time-of-flight method using stilbene crystal with photomultiplier. Californium-252 was deposited as a spot 3 mm in diameter on aluminium oxide film 10 $\mu g/cm^2$ thick. Neutron characteristics were registered in computer by recording neutron flight time, amplitudes and parameters of pulse shape. The time resolution of set-up was about 1 ns, angular resolution changed in different experiments within 2-10°.

Angular distribution averaged over all the fission types is shown in fig 6. As it is seen from the figure, the increased yield at small angles was not observed. The difference of this result from the conclusions /7, 8/ is connected with the fact that the c. m. spectrum determined by us is somewhat softer than in the work /7/. Angular distribution for M = 108 ± 5 MU in dependence on the total kinetic fragments energy E_k is shown in fig. 7. As follows from the figure 6, the effect of increased neutron yield along fission axis does not appear within the limits of experimental error even in the case of great deformation of fragments. So, the effects of "shock wave" and "polar" emission type were not observed in the present work. The c. m. spectrum for fragment mass M = 108 MU obtained from the data at the angle 0° in l. s. is shown in fig. 8. The measurements and processing of c. m. spectra for different masses and kinetic energies of fragments are being continued.

DIFFERENTIAL SPECTRA CALCULATIONS

The present theoretical calculations of the prompt neutron spectra are done in statistical approaches. But even in this case, the problem of the integral spectra calculations is difficult, since one needs to take into account the different fragment parameters: charge, mass, kinetic and excitation energy distributions, statistical properties of fragments that are not observed experimentally. Taking all these factors into account makes the problem not only multidimensional, but also arbitrary. A large number of parameters used might lead to a good agreement with experiment for the initial approximations which can hardly be approved of. This makes the problem of clarification of the physical mechanism of fission neutron emission a rather difficult one. The reliability of integral calculations can be checked by comparison of the intermediate theoretical results with experimental data on differential measurements. The most important among them are the c. m. spectra for given masses and kinetic energies.

Madland and Nix /9/ obtained good agreement with experimental integral spectra of fission prompt neutrons, but had to suppose the equality of the c. m. spectra for light and heavy fragments. This suggestion does not seem to be a realistic one. They used in their calculations the evaporation spectrum with asymptotics, that does not correspond to the limited fragments excitation energies. They also used the one-stage approximation and triangular temperature distribution which differs from the known distributions of fragment excitation energies.

One can consistently take into consideration the fission fragment characteristics by applying the statistical Hauser-Feshbach theory /10/ to the calculations of fission prompt neutron spectra /11, 12/. The c. m. spectrum of neutrons emitted by a fragment with mass number A and charge Z in a compound state with excitation energy E^* and spin distribution $\omega(I, E^*)$ is given by

$$\varphi(\varepsilon, E^*) = \sum_I \omega(I, E^*) \frac{\sum_{I'} \rho(E^* - B_n(A,Z) - \varepsilon, A-1, Z, I') \sum_{\ell j} T_{\ell j}(\varepsilon)}{\Gamma(A, Z, E^*, I)} \qquad (1)$$

where Γ is proportional to the total decay width, including γ-emission:

$$\Gamma(A,Z,E^*,I) = \int_{\delta(A-1,Z)}^{E^*-B_n(A,Z)} dU \sum_{I'} \rho(U, A-1, Z, I') \Big[\sum_{\ell i} T_{lj}(E^* - U - B_n(A,Z) \Big] + \int_{\delta(A,Z)}^{E^*} dU \sum_{I'} T_{\gamma}(E^* - U, I') \, \rho(U, A, Z, I') \qquad (2)$$

Here we used the following notations:

ε – c. m. neutron kinetic energy;

I, I' – fragment spins before and after the particle emission;

$B_n(A,Z)$ - neutron binding energy in a nucleus with mass number A and charge Z;

$\rho(E^*,A,Z,I)$ - nuclear level density;

$T_{\ell j}$, T_j - transmission coefficients for neutrons and γ-quanta;

$\delta(A,Z)$ - even-odd correction in the mass formula.

If the nuclear excitation energy distribution is $P(E^*)$, one should make the averaging

$$n(\varepsilon) = \int_{B_n(A,Z)+\delta(A-1,Z)+\varepsilon}^{E^*_{max}} dE^* P(E^*)\varphi(\varepsilon,E^*) \qquad (3)$$

Since fission fragments have excitation energy several times in excess of neutron binding energy, one should take into account the cascade character of neutron emission which leads to a significant softening of spectra with respect to a single-stage approximation. One should use the expressions (1)-(3) at each stage of the cascade calculations and take into account the redistributions of spin and excitation energies. Neutron multiplicities are calculated together with neutron spectra. This gives additional information and serves as a good checking for the correctness of the calculations. The partial spectra at different stages are summed with the appropriate weights to give the total c. m. spectrum. Neutron binding energies were calculated according to Myers-Swiatecky /13/. The energy dependence /14/ of the level-density parameter was used in level-density calculations. The optical model was used to calculate the neutron transmission coefficients $T_{\ell j}$, while T_γ were calculated in the dipole approximations We have taken spin distributions from the expressions for spin-dependent level densities. The initial fragment energy distribution was taken to be Gaussian, while the maximum energy in (3) was equal to a sum of the average value plus three values of the excitation energy dispersions σ_{E^*}. Fig. 8 shows the example of c. m. fission prompt neutron spectrum for spontaneous fission of ^{252}Cf and fragments with A = 108, Z = 42, σ_{E^*} = 4,7 MeV and the fragment average excitation energy $\bar{E}^*$ = 22 MeV which corresponds to the experimental observed value of average neutron multiplicity from this fragment. One can see that the theoretical spectrum agrees well with the experimental one. This allows to use the above method for the calculation of fission prompt neutron integral spectra.

CONCLUSION

It should be noted that the works in the last years in some laboratories had shown the higher accuracy of measurements, the improved experimental conditions and the use of different neutron detectors. However essential discrepancies between the experimental data are still observed, particularly in the high energy region (above 6÷7 MeV). Further measurements within the whole energy range of spectrum of ^{252}Cf spontaneous fission prompt neutrons are needed for determination of the important standard to a high degree of accuracy.

The elucidation of mechanism of spontaneous fission neutron emission, experimental investigations and theoretical calculations are desirable for the better understanding of integral spectrum formation and for the higher reliability of immediate measurements.

It seems to be advisable to conduct consultative meetings supported by the IAEA and to exchange the detailed experimental information in order to elaborate the international standard - the spectrum of ^{252}Cf spontaneous fission neutrons - as soon as possible.

REFERENCES

1. R. Böttger, H. Klein et al., Nuclear Data for Science and Technology (Proc. of Intern. Conf. Antwerp, 1982), Geel 1983 (in press).
2. H. Maerten, O. Seeliger et al., INDC(GDR)-17/L, 1982
3. M. V. Blinov, G. S. Boykov, V. A. Vitenko, Nuclear Data for Science and Technology (Proc. of Intern. Conf. Antwerp, 1982), Geel 1983 (in press)
4. A. Chalupka, NIM 164 (1979) 105
5. M. V. Blinov, V. A. Vitenko, Y. I. Yurevich, Neutron Physics (Proc. Fifth All-Union Conference on Neutron Physics, Kiev, 1980) Moscow, 1980, part 4, p. 96 (in Russian)
6. J. Grundl, C. Eisenhauer, NBS Special publ. NBS-493 (1977)
7. H. R. Bowman et al, Rhys. Rev. 126 (1962), 2120
8. V. M. Piksaikin, P. P. D'yachenko et al., Nuclear Physics 2 (8) (1978) 324 (in Russian)
9. D. G. Madland, I. R. Nix, Nucl. Sci. Eng., 81 (1982), 213
10. W. Hauser, W. Feshbach, Phys. Rev. 87, (1952), 366
11. I. C. Browne, F. S. Dietrich, Phys. Rev. C 10, (1974) 2445
12. B. F. Gerasimenko, V. A. Rubchenya, A. V. Pozdajkov, Neutron Physics (Proc. Fifth All-Union Conference on Neutron Physics, Kiev, 1980) Moscow, 1980, 3, p. 137 (in Russian)
13. W. D. Myers, W. J. Swiatecki, Nucl. Phys. 81, (1966), 1
14. A. V. Ignatjuk, Nuclear Physics, 1, (1975) 485 (in Russian)

List of Figures

Fig. 1. Amplitude spectra of fission fragments measured at the angles 90 °(•), 10 °(▲) and 4 °(+) with respect to the plane of californium layer.

Fig. 2. Design of ionization chamber: 1 - platinum backing with californium layer, 2 - collecting electrode, 3 - insulator, 4 - capillary input, 5 - preamplifier.

Fig. 3. Amplitude spectrum of ^{252}Cf fission fragments pulses.

Fig. 4. Amplitude distribution of fission fragments and α-particles of ^{235}U. Fragment registration threshold at operating measurements is indicated by arrows.

Fig. 5. The ratio of the experimental results obtained in the present work to Maxwellian distribution (T = 1,42 MeV). The indicated errors are full ones, but uncertainties of fission cross-section are not included. Dotted line - data of the evaluation /6/.

Fig. 6. Angular distribution of neutrons averaged for all the fission types. The present work - •, /7/ - o, /8/ - Δ.

Fig. 7. Angular distribution of fission neutrons in l. s. for M = 108 MU as a function of the total kinetic energy of fragments.

Fig. 8. Energy distribution of ^{252}Cf fission neutrons in c. m. for M = 108 MU and E_k = 175 MeV. Points - experimental data, solid line - calculated data.

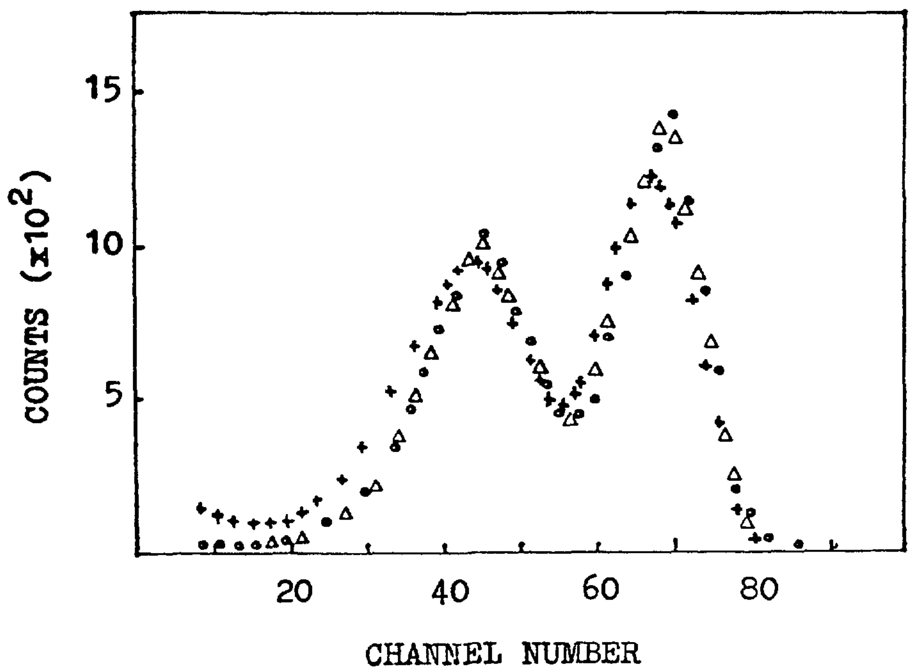

Fig. 1

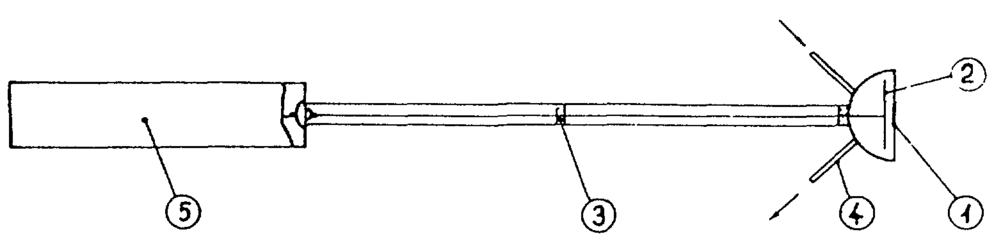

Fig. 2

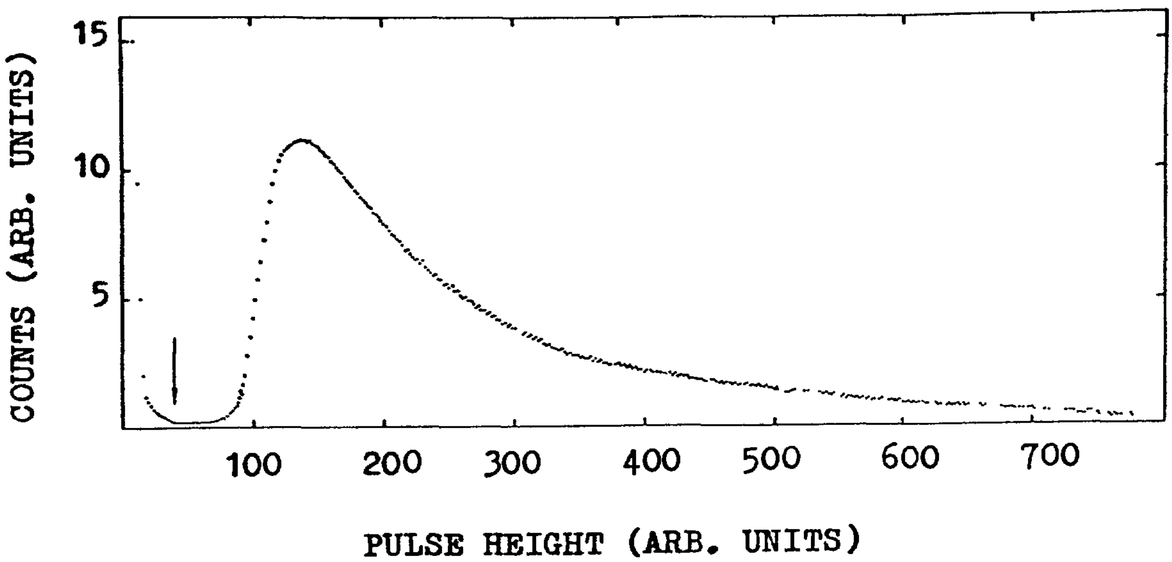
15
10
5
COUNTS (ARB. UNITS)
100
200
300
400
500
600
700
PULSE HEIGHT (ARB. UNITS)

Fig. 3

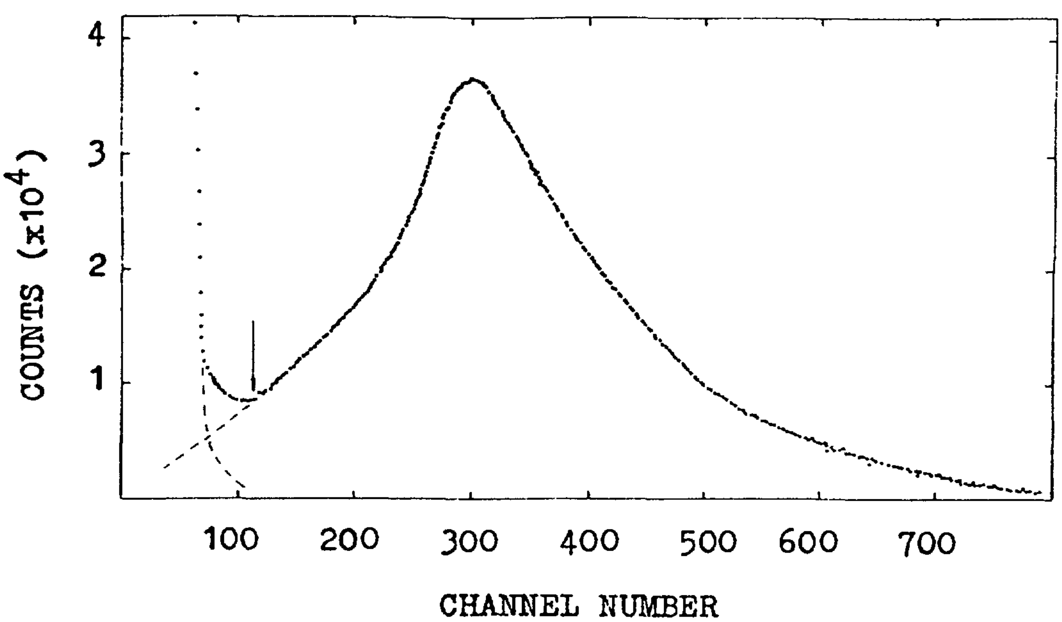
4
3
2
1
COUNTS (x10⁴)
100
200
300
400
500
600
700
CHANNEL NUMBER

Fig. 4

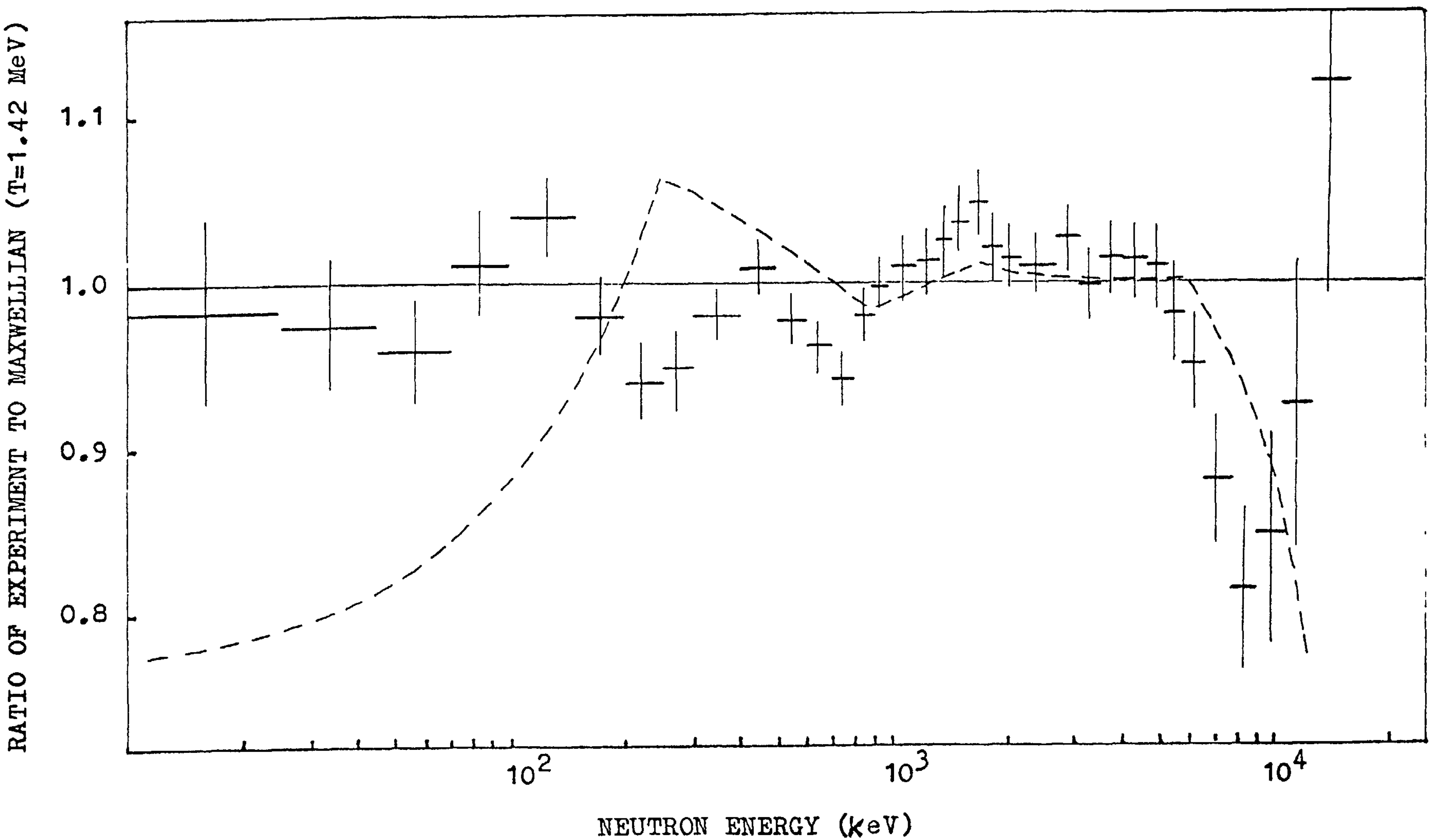
RATIO OF EXPERIMENT TO MAXWELLIAN (T=1.42 MeV)
1.1
1.0
0.9
0.8
10^2
10^3
10^4
NEUTRON ENERGY (keV)

Fig. 5

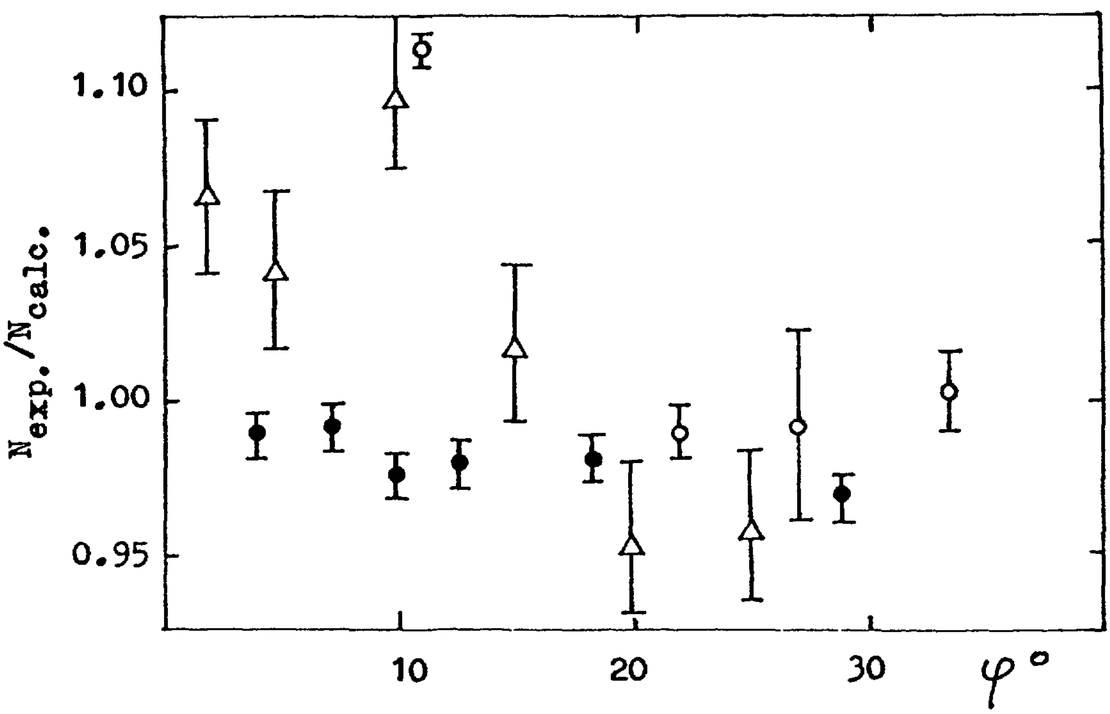

Fig. 6

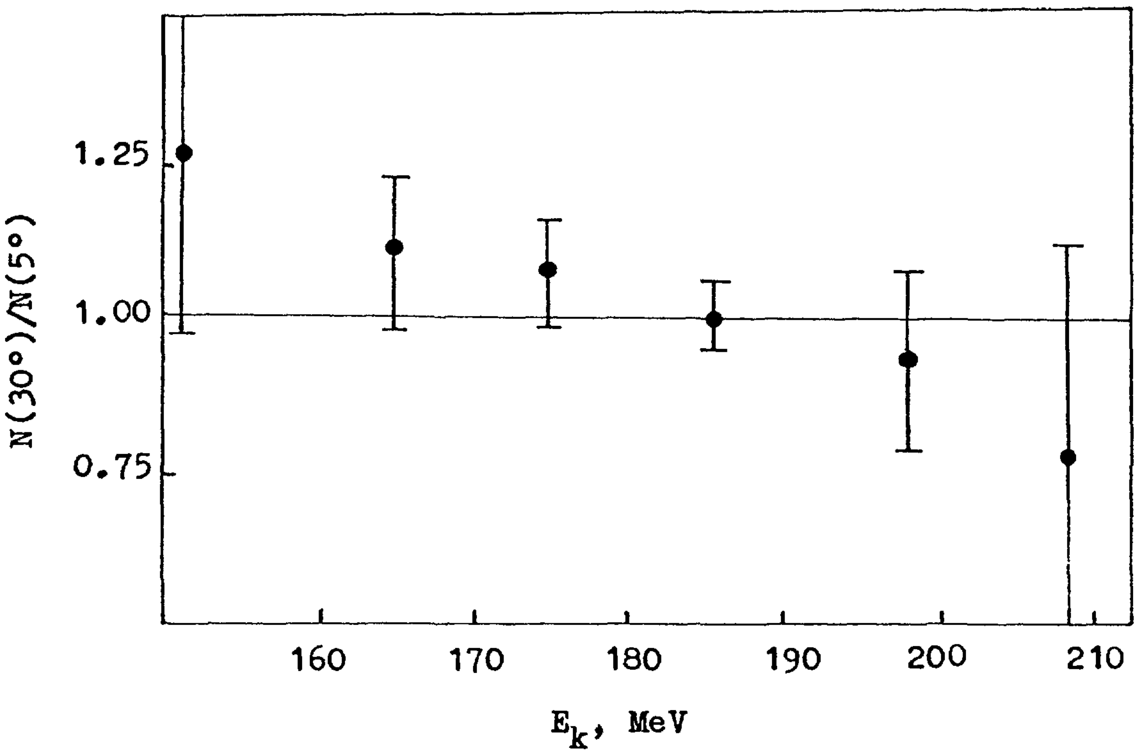

Fig. 7

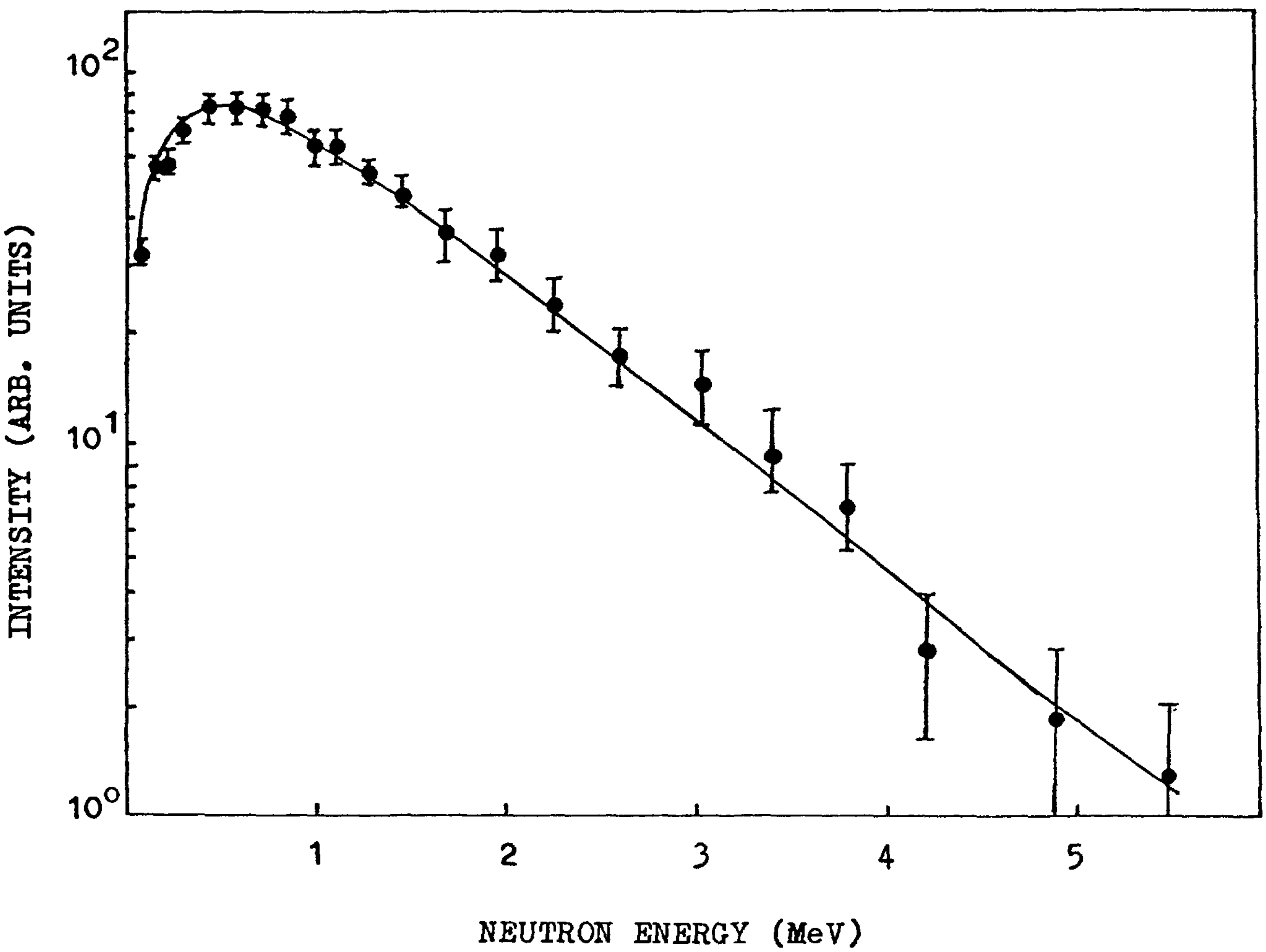

Fig. 8

Cf-252 Prompt Fission Neutron Spectrum Measurements*

by

W. P. Poenitz and T. Tamura**
Argonne National Laboratory
Argonne, Ill. 60439, U. S. A.

The prompt-fission-neutron spectrum of Cf-252 has been measured in the energy range 250 keV to 9.3 MeV. A gas-scintillation counter was used for the detection of the fission events. Two black neutron detectors with pulse-shape discrimination were used as detectors for a collimated neutron beam. Measurements were carried out at flight paths of 2.6 and 3.5 m. The energy was determined by time-of-flight, taking into account the detector response and varifying it with well-known carbon resonances. Corrections were applied for accidental coincidence gains and losses; transmission through various materials in the flight path; scattering from the sample backing, fission-detector windows, air, neutron-detector structural materials; fission-fragment absorption, and various other effects. A more detailed description and preliminary results were given in Ref. 1. Calculation of the detector efficiency above 7 MeV neutron energy requires knowledge of the (n,α) cross section of carbon. Data of Ref. 2 were previously used and substitution of this (n,α) cross section with more recent data (3) caused a reduction of the measured Cf-252 data by 1-4% for the four highest-energy points. The $C(n,\alpha)$ cross section was still assumed to be isotropic in these recalculations and inclusion of the anisotropy is expected to further reduce these four data values. A minor revision ($\lesssim$1%) was made for an adjustment of the total fission-fragment absorption. The data are still preliminary pending Monte-Carlo simulations of some of the measurement effects.

The present status of the data is shown in Figure 1 relative to a Maxwellian spectrum of the same average energy. The present data show a similar deviation from a Maxwellian spectrum shape as the recent theoretical calculation by Madland and Nix (4) which is also shown in the figure. The deviations from a Maxwellian spectrum shape, specifically at higher neutron energies, suggest that the use of a Maxwellian spectrum for the calculation of average cross sections for threshold-type dosimetry reactions would result in nonsensical values.

* This work has been supported by the US Department of Energy

** Present address: Tohoku University, Sendai, Japan

References

(1) W. P. Poenitz and T. Tamura, Proc. Conf. Nucl. Data for Sci. and Techn., 465, Antwerp (1982).
(2) E. A. Davis et al., Bull. Am. Phys. Soc. 8,115 (1963).
(3) G. Dietze et al., in: loc. cit. (1), p. 930.
(4) D. G. Madland and J. R. Nix, in: loc. cit. (1), p. 473.

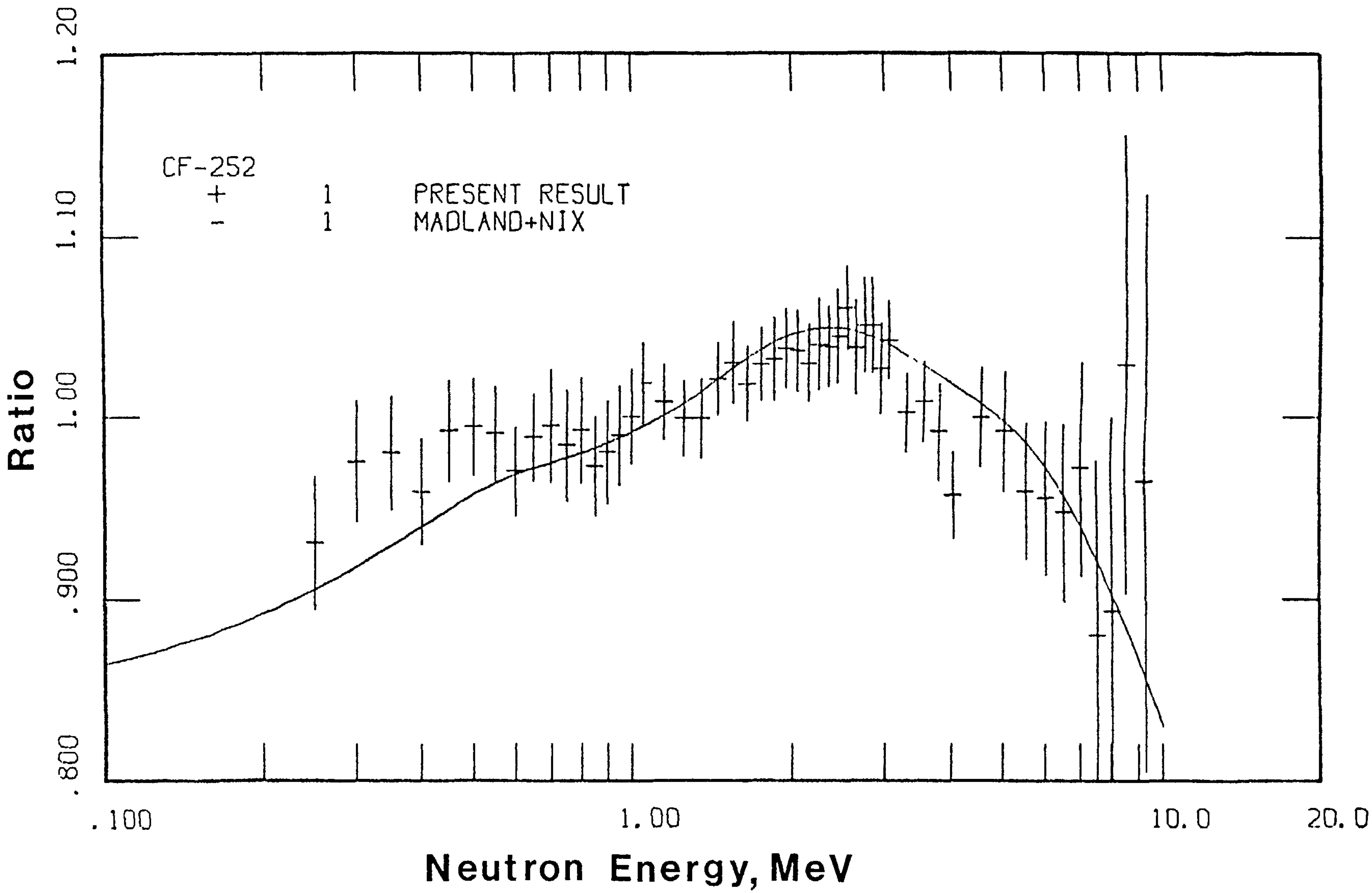
CF-252
+ 1 PRESENT RESULT
- 1 MADLAND+NIX
Ratio
1.20
1.10
1.00
.900
.800
.100
1.00
10.0
20.0
Neutron Energy, MeV

An absolute measurement of ^{252}Cf prompt fission neutron spectrum at low energy range

A. Lajtai
Central Research Institute for Physics
Budapest, Hungary

P.P. Dyachenko, L.S. Kutzaeva, V.N. Kononov, P.A. Androsenko, A.A. Androsenko
Institute of Physics and Power Engineering
Obninsk, USSR

Abstract

Prompt neutron energy spectrum at low energies /25 keV $< E_n <$ 1,2 MeV/ for ^{252}Cf spontaneous fission has been measured with a time-of-flight technique on a 30 cm flight -path. Ionization chamber and lithium-glass were used as fission fragment and neutron detectors, respectively. Lithium glasses of NE-912 /containing ^{6}Li/ and of NE-913 /containing ^{7}Li/ 45 mm in diameter and 9.5 mm in thickness have been employed alternatively, for the registration of fission neutrons and gammas. For the correct determination of the multiscattering effects - the main difficulty of the low energy neutron spectrum measurements - a special geometry for the neutron detector was used. A special attention was paid also to the determination of the absolute efficiency of the neutron detector. The real response function of the spectrometer was determined by a Monte-Carlo calculation. The scattering material content of the ionization chamber containing a ^{252}Cf source was minimized.

As a result of this measurement a prompt fission neutron spectrum of Maxwell type with a T = 1.42 MeV parameter was obtained at this low energy range. We did not find any neutron excess or irregularities over the Maxwellian.

1. Introduction

^{252}Cf fission prompt neutron energy spectrum is proposed as a reference standard. Californium sources are widely used for neutron detector calibration, in different neutron scattering and capture experiments, in fission, heavy-ion, reactor physics, defence physics, medical investigations and so a high accuracy of the spectrum in a wide energy range is required. A number of spectrum measurements have been done and being carried on recently [1-5]. One can conclude that ^{252}Cf fission prompt neutron spectrum at the 1 MeV $< E_n <$ 6 MeV energy range can be described by a Maxwellian distribution with T = 1.42 MeV and with a not more then 3-5 % deviation. Outside of this energy range the complex experimental difficulties are arising. At low energies up to 1 MeV there are two different groups of results. In the first one [6-9] essential deviations /up to 30 %/ were found to the Maxwell spectrum, extrapolated from data measured at high energies. On the countrary, in the second group of experimental results, the energy spectra from 10 keV to 6 MeV can be fitted well by a Maxwellian distrubution of T = 1.42 MeV [1-3].

In an attempt to solve this discrepancy we have repeated the low energy californium spectrum measurements paying special attention to get absolute spectrum data and to minimize the uncertainities due to backgrounds of different type and the neutron detector efficiency.

2. Experimental method

The experimental arrangement is shown in Fig. 1. The fragment detector was a fast ionization chamber 38 mm in diameter and 120 mm in length made of 0.1 mm stainless steel filled with 3 atm. of gas mixture /Ar-90 %, CO_2-10 %/. Electrodes were of 0.1 mm stainless steel too. Diameters of electrodes and the distance between them were 25 mm and 1.5 mm respectively. The ^{252}Cf source of 10^4 fissions per second 6 mm in diameter was volatilized onto one of electrodes.

NE-912 lithium glass /45 mm in diameter and 9.5 mm in thickness/ and FEU-30 photomultiplier were used as neutron detector. For measuring the background of delayed gamma rays the NE-912 glass was replaced by NE-913 lithium glass of same dimensions because it is insensitive to neutrons in the studied energy range [10]. The glass was fixed in the centre of a thin-wall aluminium cell mounted at the photocatode of the photomultiplier. Details of the construction and characteristics of the detector can be find in Ref. [11,12]. This arrangement of neutrons and fission detectors essentially reduces the amount of scattering materials in the solid angles of neutron detection.

It is very important because the background due to neutron scattering on these materials cannot be measured directly in the experiment. Distortion of the spectrum due to these neutrons was taken into account by using the response function of the spectrometer.

The background component due to the neutron scattering on materials out of neutron detection solid angle Ω was determined in shadow cone experiments.

The effect of systematic random coincidencies was eliminated by a pile up rejector, which discriminates the double stop signals [13].

General characteristics of the spectrometer are follows: the neutron flight path was 30 cm, while the channel width of the analyser was 0.704 nsec. Amplitude spectra of neutron and fragment detectors, thresholds in the fast and slow channels are shown in Fig.2. The apparatus response functions of the fast channels were measured using an additional scintillation /stylbene/ detector for the fission gamma rays and for measuring γ-γ coincidences from ^{60}Co in the fission fragment and neutron channels, respectively, as shown in Fig. 3. Differential and integral nonlinearities of the spectrometer did not exceed 0.7 and 0.5 %, respectively.

Measurements have been performed in a cycle regime, each of them consists of four series of measurements of 24 hours: with NE-912 and NE-913 scintillators both with and without shadow cone, respectively. The total number of fission events recorded was $N_f = 1.523 \cdot 10^{10}$ for each of the four arrangements.

3. Data treatment

In general case the measured neutron spectrum can be described by a Fredholme's integral equation of the second kind:

$$P(t) = \int F(E,t)\varphi(E)dE$$

where $P(t)$ is the measured spectrum, $\varphi(E)$ is the prompt fission energy spectrum and $F(E,t)$ is the spectrometer response function.

Unfortunately, the function $F(E,t)$ for thick lithium glass cannot be determinated with sifficient accuracy, and some difficulties can take place at solving this equation.

In the present work the data were processed as follows: at the first step the background of random coincidencies was subtracted from the measured spectra. Then using of expression

$$P(t) = P_1(t) - P_2(t) - P_3(t) + P_4(t)$$

where $P(t)$ is the flight time spectrum of fission neutrons, as shown in Fig. 4. $P_1(t)$, $P_2(t)$, $P_3(t)$, and $P_4(t)$ are the flight time spectra from measurements with NE-912, NE-913 scintillators, without and with shadow cone, respectively. At the same time the $P_3(t)$ spectrum has been corrected for some possible shadow cone transmission.

The $P(t)$ distribution has been corrected for the deviation of the real response function of spectrometer from the δ-function:

$$P'(t) = \alpha(t)P(t)$$

The correction factor $\alpha(t)$ was calculated by the following expression

$$\alpha(t)=\left\{\int\delta[t-t(E)]\mathcal{E}'(E)\varphi(E)dE\right\}/\left\{2\int F(E,t)\varphi(E)dE\right\} \;,$$

where $\varphi(E)$ is a Maxwellian distribution with $T = 1.42$ MeV and $\mathcal{E}'(E)$ is the theoretical efficiency of neutron detection. $\mathcal{E}'(E)$ was calculated by the following expression:

$$\mathcal{E}'(E)=\int F'(E,t)dt \;,$$

where $F'(E,t)$ is the probability of detection of a neutron, at the time t, emitted from the source with energy E, at t=0 into solid angle Ω, when the source and the detector are in vacuum /see Table 1/. $F(E,t)$ is the real response function of the spectrometer determined as

$$F(E,t)=\int F''(E,t)F'(t,t')dt'$$

where $F''(E,t)$ the same as $F'(E,t)$ but when the source and detectors are in the real experimental conditions /see Table 1/. $F'(t,t')$ is the response function of the apparatus. The distribution $F'(t,t')$ was obtained by the following expression:

$$F'(t,t')=\int F_f(t,t'')F_n(t',t'')dt'' \;,$$

where $F_f(t,t'')$ and $F_n(t',t'')$ are apparatus response functions of fast channels for fragments and neutrons, respectively /Fig. 3/.

Functions $F'(E,t)$ and $F''(E,t')$ were calculated by Monte-Carlo method, basic input data of which are presented in Table 1. The concentration of ^{6}Li in the lithium glass NE-912 was determined by the data of Nuclear Enterprises Ltd. Catalogue [10]. The ^{7}Li, O, Si concentrations were determined by using data from Ref. [14]. The neutron cross-section data for ^{6}Li, for ^{7}Li, Si, O, N and for Fe were taken from the file ENDF/B-V from file ENDF/B-IV and from Ref. [15] respectively.

It was assumed in the calculations that the neutrons are detected only by $^6Li(n,\alpha)^3T$ reaction. The Monte-Carlo programme BRAND [16] for 200 energies of monoenergetic source of neutrons in the energy range $0 < E_n < 2$ MeV was used. Results of calculations for $F''(E,t')$ functions at neutron energies 0.025, 0.245, 0.445 and 1.005 MeV are shown in Fig. 3, while Fig. 5 shows the correction factor $\alpha(t)$. It can be seen that the difference of the real spectrometer response function from the δ-function is essential. When this correction is ignored, a softening of the measured spectrum and essential spectrum oscillations near the strong resonances of lithium and oxygen of energies 0.242 and 0.442 MeV, respectively, can be observed. For example, the response function broadening on the high time side due to the before-detection-scattering of neutrons at the 0.442 MeV oxygen resonance can lead to a dip of 25 % in the spectrum at this energy /Fig. 5/.

For speeding of the Monte-Carlo calculation of $F''(E,t)$ function /see Table 1/ some simplifications have been used. In particular instead of the gas mixture of the fission chamber air, instead of stainless steel iron were assumed, respectively. The window thickness /80 micron thick aluminium foil/ of the neutron detector has been ignored. Estimated errors caused by these simplifications are within the statistical accuracy of the Monte-Carlo calculation.

4. Neutron detection efficiency

The efficiency of the thick lithium glass detector was measured [11] by time-of-flight method with IPPE pulsed Van de Graaff neutron generator, using the efficiency of 0.835 mm thin NE-908 ^{6}Li glass detector as a reference. For efficiency determination cross section data for $^6Li(n,\alpha)^3T$ were taken from the ENDF/B-V file. To get more precise neutron detection efficiency data a Monte-Carlo calculation were performed for the thin NE-908 glass scintillator, too [16]. The calculation model was the same as for calculation of $F'(E,t)$ with an exception in the zone 10 /see Table 1/, where the zone thickness and the ^{6}Li, ^{7}Li, O and Si concentrations were 0.0835 cm, 172.4, 8.0, 480.7 and 182.1 nuclei/cm^3 x 10^{20} [17], respectively. Table 2 shows the real detection efficiency data for the NE-912 glass obtained from the evaluation of the measured data for thick NE-912 scintillator [11] with the help of the calculated detector efficiency values of the thin NE-908.

Errors include the statistical errors of measurements [11], the statistical accuracy of the calculation of the thin glass efficiency and the accuracy of the $^{6}Li(n,\alpha)^{3}T$ cross sections. The last one was taken to be equal $\pm$ 2 % for the energy range E_n < 100 keV and $\pm$ 5 % for higher energies.

5. Results and discussion

^{252}Cf fission prompt neutron spectrum N(E) /shown in Fig. 6. and Table 2/ was obtained using the following expression

$$N(E) = \frac{P(E)}{N_f\, \Omega \cdot \mathcal{E}(E)}$$

P(E) is the converted to energy scale P'(t) distrubution N_f is number of fission events, Ω and $\mathcal{E}(E)$ are the solid angle and efficiency of the neutron detection. The spectrum data errors include the statistical errors of the measurements of $P_1(t)$, $P_2(t)$, $P_3(t)$, $P_4(t)$ distributions, the errors of the $\alpha(t)$ correction, the error of the neutron detection efficiency, the errors of N_f and Ω. The error of $\alpha(t)$ which less then 2 % was obtained from the deviation of two $\alpha(t)$ calculated for different Maxwellians with parameters T of 1.2 and 1.6 MeV, respectively, taking into account the statistical accuracy of calculations. The error in N_f was determined using the fission fragments spectrum /see Fig. 2/ and was equal $\pm$ 3 %. Error in Ω, defined by the accuracy of the flight path determination and the diameter of the lithium glass, was equal to $\pm$ 2 %.

Fig. 6 shows a Maxwellian distribution with parameter $\bar{\nu}_p$ = 3.757 /ENDF/B-V/ and T = 1.42 MeV, which describes the experimental data quite well. With some exceptions the deviation of experimental data from the values of a Maxwellian distribution do not exceed $\pm$ 5 %. The ratio of the three-point averaged experimental data to the same Maxwellian is shown in Fig. 7. This result confirms the conclusion made by M.V. Blinov and his coworkers [1-3] and contradicts to experimental data of Ref. [6-9], where essential deviations were found from a Maxwellian distribution extrapolated from higher energies.

It is difficult to find the exact reasons for these disagreements, including our earlier measurements, too [7,8]. We can point out only some factors which were not taken into account in our earlier measurements [7,8]. For example the real response function of the spectrometer was not taken into account though it plays a very important role specially at the geometry used in Ref. [7]. Inclusion of delayed neutrons might cause a softening of the measured spectrum [8].

6. Acknowledgements

The valuable assistance in electronics of E.D. Poletaev and N.N. Semenova are gratefully acknowledged. The authors are indebted to V.N. Dushin for helpful discussions in process of the data treatment.

Table 1: Models for Monte-Carlo calculations of functions F'(E,t) and F''(E,t)

No of zone	r [cm]	h [cm]	Concentration [nucl. x cm^{-3} x 10^{20}]											
			^{6}Li		^{7}Li		N		O		Fe		Si	
			F'(E,t)	F''(E,t)	F'(E,t)	F''(E,t)	F'(E,t)	F''(E,t)	F'(E,t)	F''(E,t)	F'(E,t)	F''(E,t)	F'(E,t)	F''(E,t)
1	2.25	100	-	-	-	-	-	0.42	-	0.12	-	-	-	-
2	2.25	0.01	-	-	-	-	-	-	-	-	-	8.5	-	-
3	2.25	1.73	-	-	-	-	-	0.42	-	0.12	-	-	-	-
4	2.25	0.01	-	-	-	-	-	-	-	-	-	8.5	-	-
5*	2.25	0.15	-	-	-	-	-	0.42	-	0.12	-	-	-	-
6	2.25	0.01	-	-	-	-	-	-	-	-	-	8.5	-	-
7	2.25	1.88	-	-	-	-	-	0.42	-	0.12	-	-	-	-
8	2.25	0.01	-	-	-	-	-	-	-	-	-	8.5	-	-
9	2.25	27.62	-	-	-	-	-	0.42	-	0.12	-	-	-	-
10	2.25	0.95	175.4	175.4	8.6	8.6	-	-	477.8	477.8	-	-	191.2	191.2
11	2.25	100	-	-	-	-	-	0.42	-	0.12	-	-	-	-

*Source is located on the boundary between 5 and 6 zone.

Table 2: Efficiency of neutron detection $\mathcal{E}(E)$ [%] and prompt neutron spectrum N(E) for spontaneous fission of ^{252}Cf [neutr. x $fission^{-1}$ x MeV^{-1} x $sterad.^{-1}$ x 10^{-2}]

E_n, keV	$\mathcal{E}(E)$	N(E)	E_n, keV	$\mathcal{E}(E)$	N(E)
25	1.89±0.04	3.27±0.46	35	1.70±0.04	2.72±0.45
45	1.53±0.03	4.34±0.48	55	1.39±0.03	4.37±0.49
65	1.35±0.03	4.55±0.48	75	1.29±0.03	5.05±0.49
85	1.29±0.03	4.89±0.46	95	1.32±0.03	5.67±0.45
105	1.34±0.03	5.67±0.50	115	1.38±0.04	6.44±0.53
125	1.40±0.05	7.35±0.56	135	1.48±0.07	7.12±0.52
145	1.58±0.08	6.86±0.50	155	1.74±0.09	7.83±0.54
165	1.94±0.10	7.72±0.53	175	2.65±0.14	7.05±0.48
185	2.62±0.14	8.39±0.56	195	3.78±0.20	7.38±0.49
205	4.58±0.24	7.12±0.47	215	5.38±0.28	8.39±0.55
225	5.40±0.28	8.02±0.53	235	6.52±0.34	7.76±0.51
245	6.54±0.34	7.83±0.51	255	5.72±0.30	8.02±0.52
265	5.00±0.26	8.95±0.58	275	5.16±0.27	8.47±0.56
285	4.54±0.23	8.35±0.55	295	3.35±0.17	9.55±0.63
305	2.97±0.15	9.21±0.61	315	2.70±0.14	9.19±0.61
325	2.69±0.14	8.64±0.57	335	2.19±0.11	9.38±0.63
345	2.04±0.11	8.88±0.60	355	1.88±0.10	9.32±0.61
365	1.89±0.10	9.14±0.62	375	1.79±0.09	9.17±0.68
385	1.62±0.08	9.40±0.64	395	1.59±0.08	9.06±0.62
410	1.48±0.08	9.70±0.65	430	1.36±0.07	9.99±0.67
450	1.28±0.07	9.43±0.63	470	1.11±0.06	9.73±0.66
490	1.00±0.05	9.39±0.63	510	0.89±0.05	9.85±0.67
530	0.82±0.04	10.14±0.68	550	0.76±0.04	10.03±0.68
570	0.74±0.04	9.66±0.66	590	0.71±0.04	9.85±0.67
610	0.68±0.04	10.10±0.69	630	0.65±0.03	10.03±0.69
650	0.63±0.03	10.07±0.69	670	0.62±0.03	10.03±0.69
690	0.60±0.03	9.99±0.69	710	0.56±0.03	10.37±0.71
735	0.54±0.03	10.41±0.70	765	0.52±0.03	10.55±0.71
795	0.53±0.03	10.22±0.69	825	0.54±0.03	9.99±0.68
855	0.54±0.03	9.66±0.65	885	0.53±0.03	10.07±0.68
915	0.53±0.03	9.73±0.66	945	0.53±0.03	9.70±0.66
975	0.54±0.03	9.47±0.64	1005	0.54±0.03	9.51±0.64
1020	0.53±0.03	9.40±0.63	1060	0.52±0.03	10.03±0.67
1100	0.50±0.03	10.0 ±0.67	1140	0.51±0.03	10.07±0.67
1180	0.50±0.03	9.66±0.63	1220	0.50±0.03	10.0±0.67

References

[1] M.V. Blinov, V.A. Vitenko, V.T. Touse, NBS Spec. Publ. 493 /1977/ 194

[2] M.V. Blinov, INDC /NDS/ 114 GT /1980/ 79/Review/

[3] M.V. Blinov, G.S. Boykov, V.A. Vitenko, Antwerp Conference 2 /1983/ 479 /International Conference on Nuclear Data for Science and Technology, Antwerp 6-10 Sept 1982. Proceedings edited by K.H. Bockhoff, Reidel Publishing Company 1983/

[4] W.P. Poenitz, T. Tamura, Antwerp Conference 2 /1983/ 465

[5] R. Bottger, H. Klein, A. Chalupka, B. Strohmaier, Antwerp Conference 2 /1983/ 484

[6] J.W. Meadows, Phys. Rev. 157 /1967/ 1076

[7] L. Jéki, et al., Prompt Fission Neutron Spectra IAEA, Vienna /1972/ 81

[8] P.P. Dyachenko, et al., At. Energ. 42 /1977/ 25

[9] B.I. Starostov, A.F. Semenov, V.N. Nefedov, INDC /CCP/ 164L /1981/

[10] Nuclear Enterprises Ltd Catalogue /1977/

[11] V.N. Kononov et al., Preprint KFKI 1979-72

[12] V.N. Kononov et al., Prib. i Techn. Experimenta 3 /1979/ 77

[13] P.P. Dyachenko, V.S. Nesterenko, V.M. Piksajkin, Prib. i Techn. Experimenta 3 /1981/ 95

[14] F. Wider, Eir-Bericht 217 /1975/

[15] V.M. Bichkov et al., Nuclear Contant Series Atomizdat 1 /36/ - M /1980/ 65

[16] P.A. Androsenko, A.A. Androsenko, Preprint FEI-1300 /1982/

[17] J.M. Neill, D. Huffman, C.A. Preskitt, J.C. Young, Nucl. Instr. Meth. 82 /1970/ 162

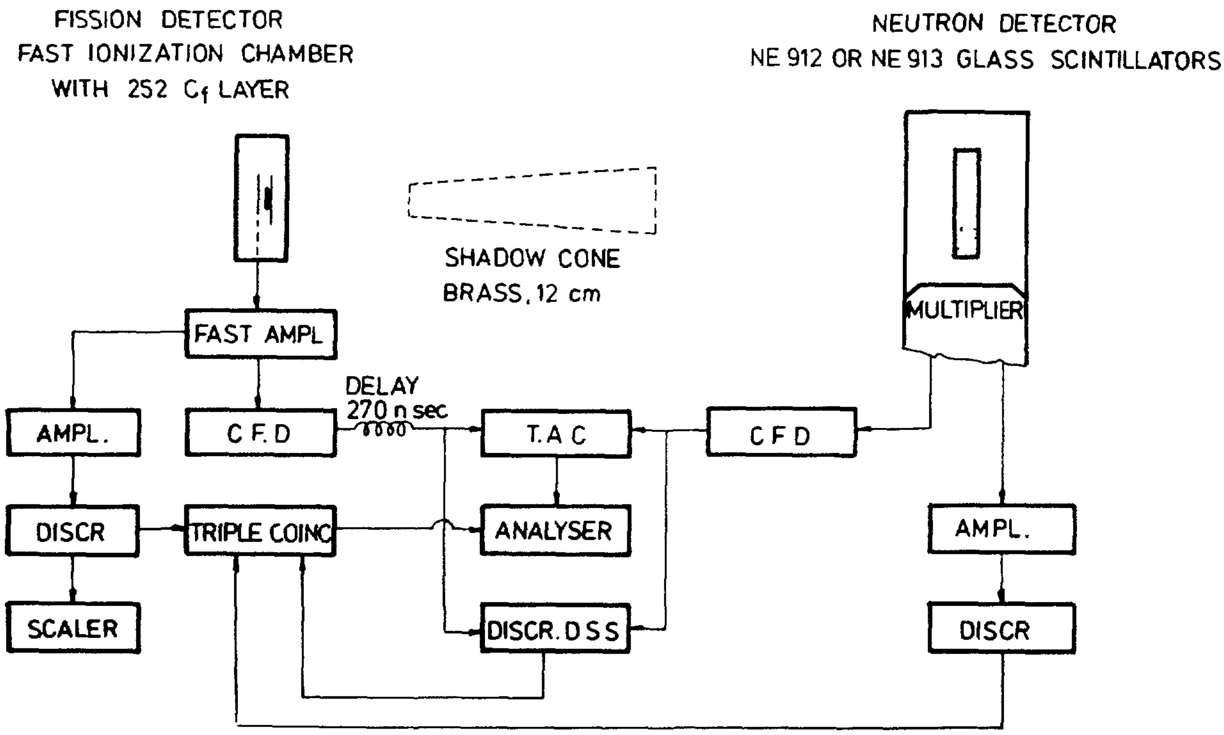

Fig. 1. Schematic drawing of experimental arrangement.

Fig. 2. Fission fragment amplitude spectrum of ionization chamber /top/ and thermal-neutron spectrum of NE-921 scintillator /bottom/.

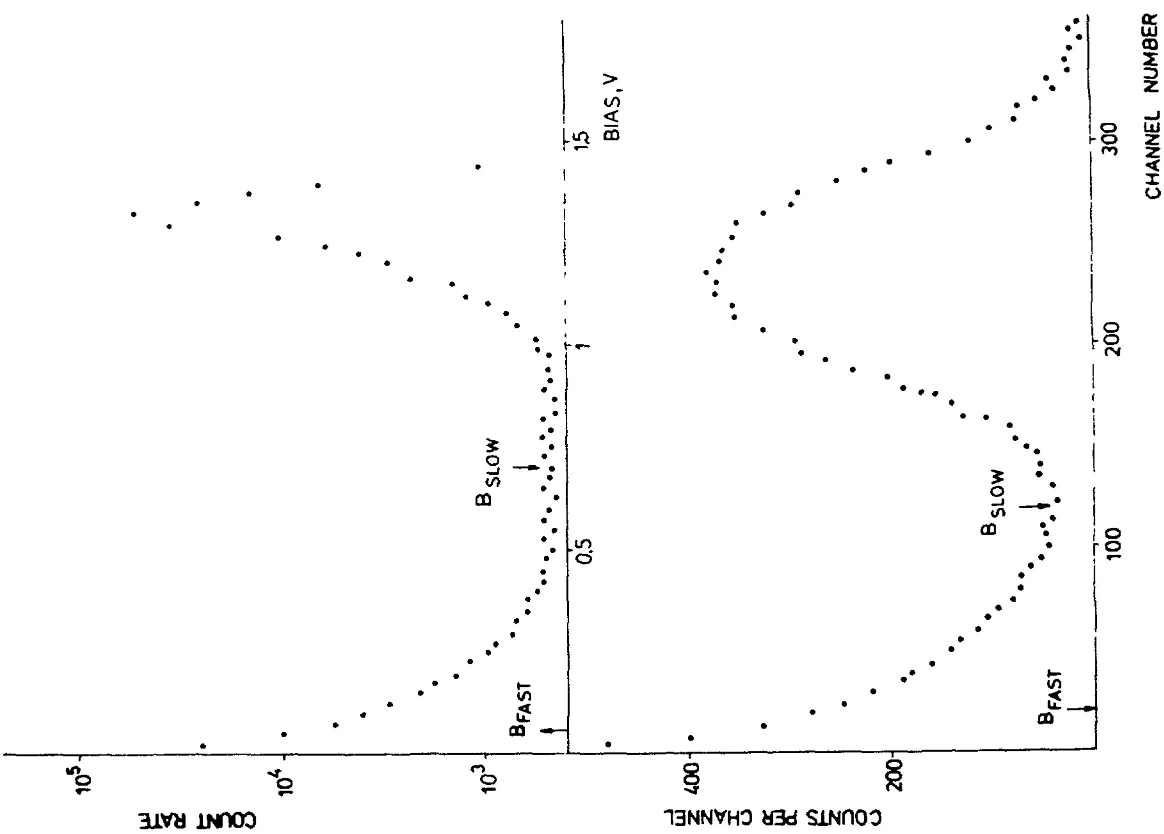

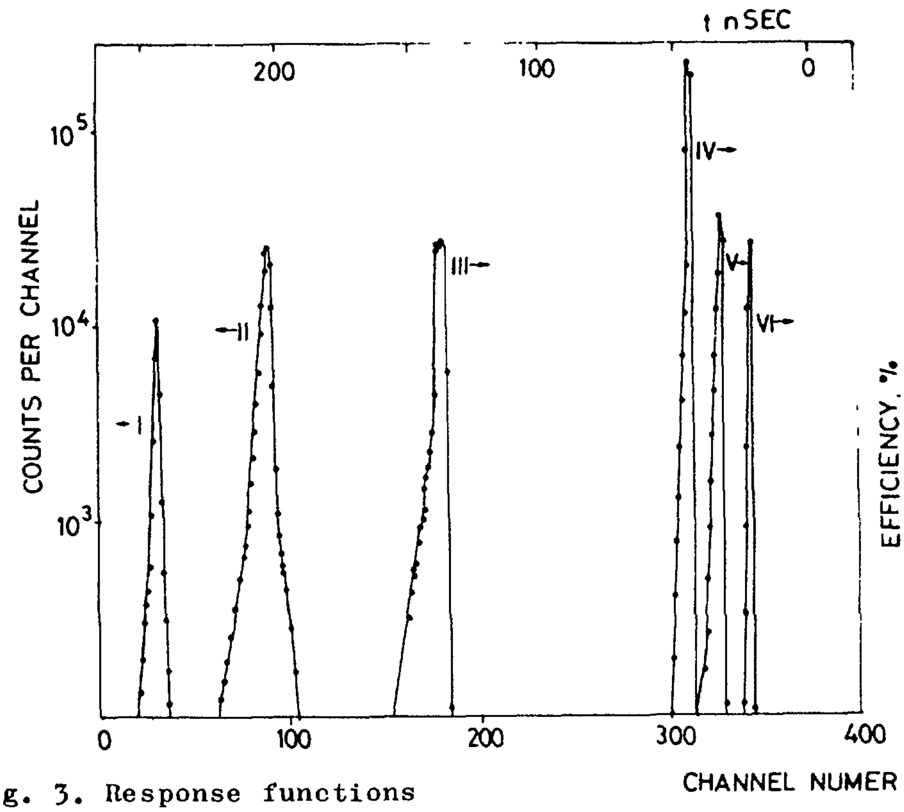

Fig. 3. Response functions

I-II the measured $F_f(t,t')$ and $F_n(t,t')$ response function

III-IV the calculated $F''(E,t)$ response function at neutron energies 0.0025, 0.245, 0.445 and 1.005 MeV.

Fig. 4. Fission neutron flight time spectrum P(t).

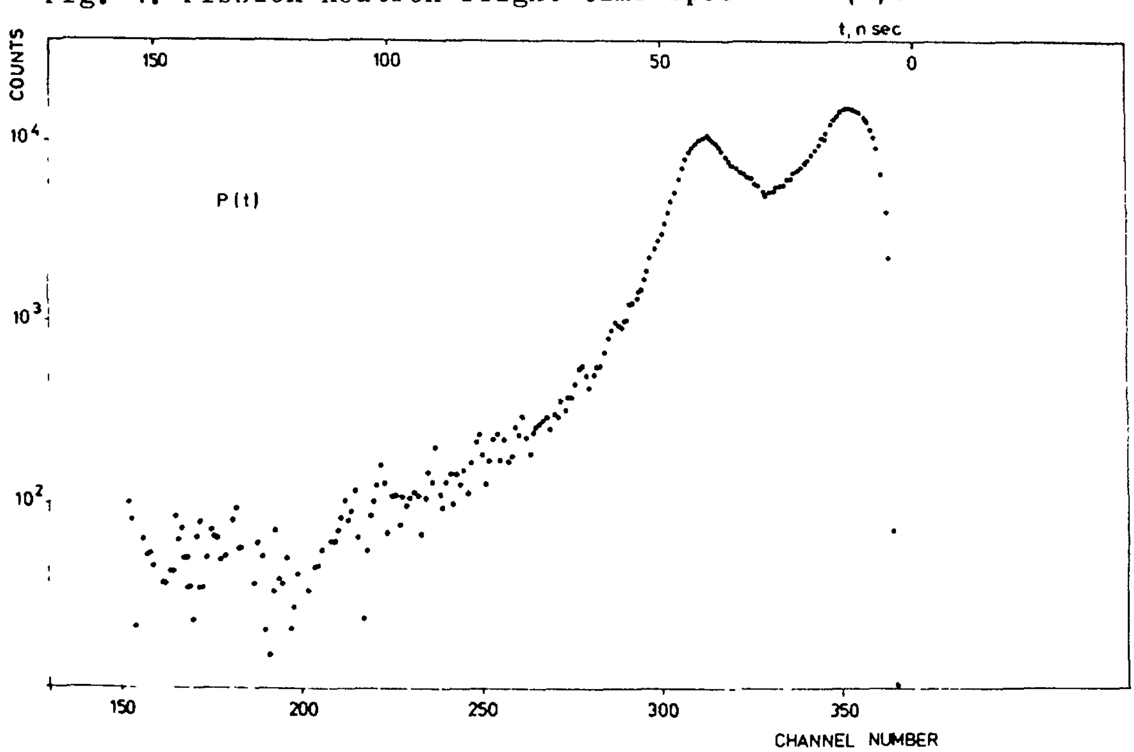

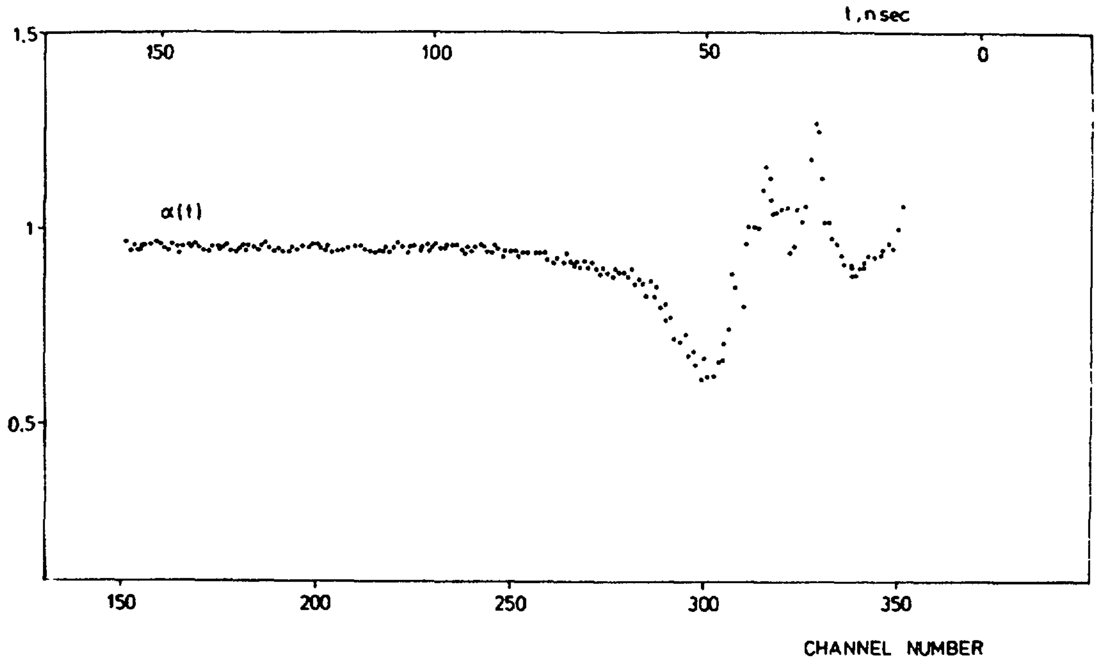

Fig. 5. $\alpha(t)$ response function correction

Fig. 6. Prompt fission neutron spectrum N(E) of ^{252}Cf

recent experimental data

- calculated Maxwell spectrum

$$N(E) = \bar{\nu}_p (2\pi)^{-3/2}\ T^{-3/2} \sqrt{E}\ \exp(-E/T)$$

with $\bar{\nu}_p = 3.757$ and T = 1.42 MeV

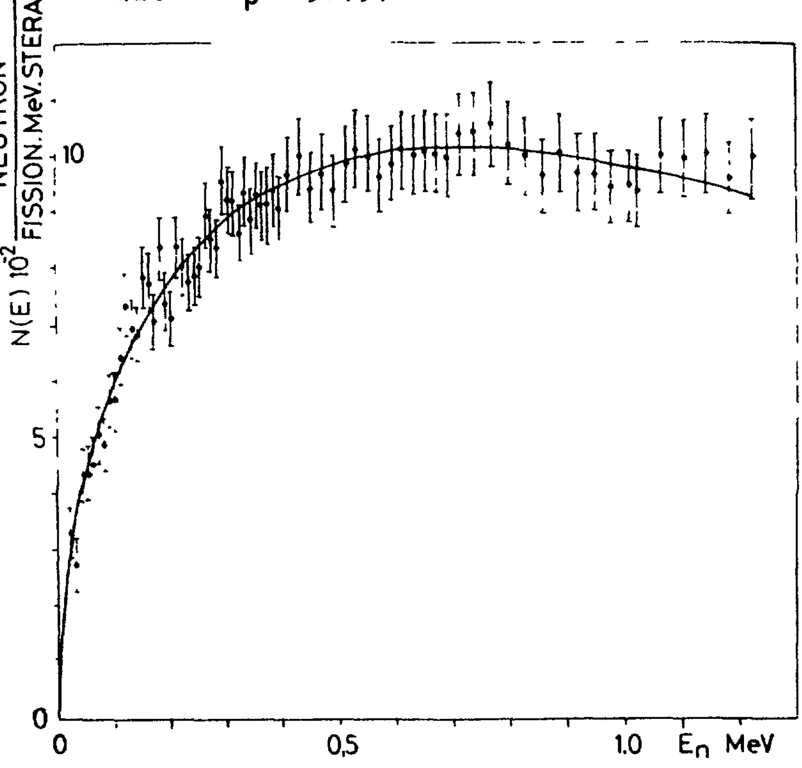

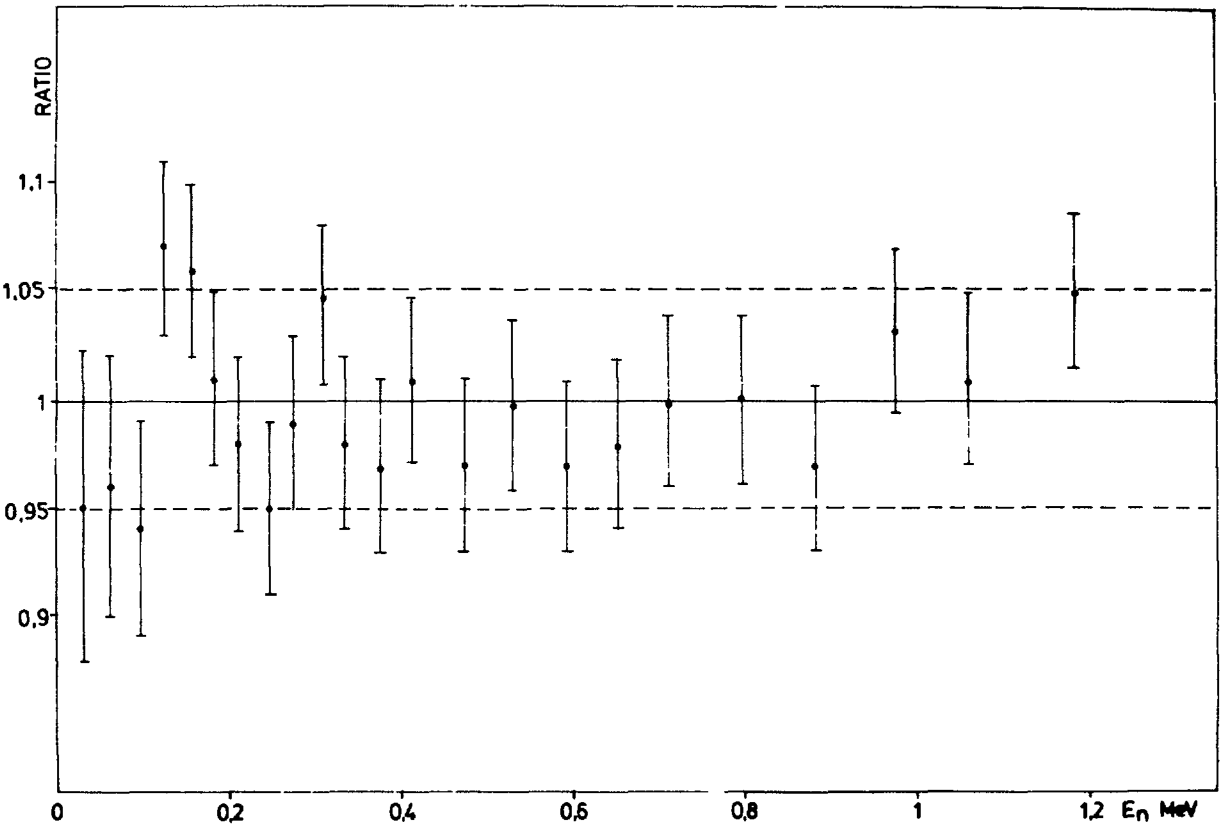

Fig. 7. Ratio of the present results to Maxwellian with a temperature of 1.42 MeV.

PROPERTIES OF FISSION FRAGMENT DETECTORS FOR TOF MEASUREMENTS

A. Chalupka, B. Strohmaier IRK, Vienna, Austria
H. Klein, R. Böttger PTB, Braunschweig, FRG

Summary of the paper presented at the IAEA Consultants' Meeting on the ^{252}Cf Fission Neutron Spectrum, Smolenice, ČSSR, 28 March-1 April, 1983.
Detailed publication forthcoming.

1. General requirements to be met by a fission fragment detector for TOF measurements of the ^{252}Cf fission neutron spectrum

a. The ^{252}Cf neutron spectrum should be disturbed as little as possible.
Obviously, the measured neutron spectrum contains contributions due to neutron scattering and neutron producing reactions in the detector material. Since these contributions are not accessible to direct measurement, they have to be accounted for either by means of theoretical calculations or experimentally by extrapolating a series of appropriate measurements to zero detector mass. In any case, geometry and material of the detector should be chosen such that this correction and hence the relative error due to it are as small as possible.

b. A source strength of some 10^5 fissions/s should be possible. In order to achieve high energy resolution in TOF experiments long flight paths are required. This results in small solid angles suspended by the neutron detector.
Within reasonable measuring times, statistical significance is obtained by using fission rates of some 10^5 s^{-1}.

c. Discrimination against the associated α-activity should be possible to keep the number of random coincidences in TOF experiments small.

d. A time resolution of $<$ 1 ns should be obtained to match the resolution of present TOF systems.

e. The fragment detection efficiency ε_f should be close to unity and its dependence on the neutron energy should be known. The higher the detector efficiency the smaller the relative contribution of non-correlated events. If the fission fragment detection efficiency ε_f is less than unity, the question of whether there is any dependence of ε_f on the neutron energy has to be answered.

2. Possible detection systems

Detector type/Ref.	Disturbance	Source strength	α-Discrimination	Time resolution	ε_f
Plastic sandwich Knitter 1973/1/	Window of PM, scintillator	5 10^3 fissions/s	not possible	1.5 ns	
Surface barrier det. Kotel'nikova 1976 /2/	Counter, backing	∿ 10^4 fissions/s limited by radiation damage	good, but worsening	∿ 2 ns	.9
Avalanche detector Eyal 1978 /3/	Backing, plates	> 10^5 fissions/s	very good	< 400 ps	> .95
Gas scintillator Green 1973 /4/ Guenther 1976/5/ Pönitz 1982 /6/	Backing, PM	> 10^5 fissions/s	very good	∿ 1 ns	.7-1.0
Ionization chamber Chalupka 1979 /7/ Böttger 1982 /8/	Backing, chamber can	10^5 fissions/s	very good	1 ns	.955

From this table it can be seen that the detector preferred by the authors is an ionization chamber. Therefore, the following refers only to this type of detector.

3. The IRK/PTB type fission chamber

For a ^{252}Cf neutron spectrum measurement, a description of the properties of a fission chamber similar to the one presented in ref. 7 was attempted by means of calculational studies. It was found that the contributions from neutron scattering and neutron producing reactions below 1 MeV are also essential for such a low-mass detector. As mentioned in the contribution to the 1982 Antwerp conference, calculations were made in order to reproduce the energy loss spectrum of fission fragments as well as the dependence of the fragment detection efficiency on the angle ϑ between the chamber axis and the neutron emission direction. A comparison of calculated and experimental results supports the assumptions on which the calculations were performed. From these assumptions, the dependence of the fragment detection efficiency on the neutron energy can be extracted, and an example is given in fig. 1. It is found that for $\vartheta \sim 60^\circ$, the efficiency shows the least variation with neutron energy.

References

/1/ H.H. Knitter et al., Atomkernenergie 22 (1973) 84

/2/ G.V. Kotel'nikova et al., Rept. INDC(CCP)-81/U (1976)

/3/ Y. Eyal, H. Stelzer, Nucl. Instr. Meth. 155 (1978) 157

/4/ L. Green et al., Nucl. Sci. Eng. 50 (1973) 257

/5/ P. Guenther et al., Rept. ANL/NDM-19 (1976)

/6/ W.P. Pönitz, Proc. Int. Conf. Nucl. Data for Science and Technology, 6-10 Sept. 1982, Antwerp, p. 465

/7/ A. Chalupka, Nucl. Instr. Meth. 164 (1979) 105

/8/ R. Böttger et al., Proc. Int. Conf. Nucl. Data for Science and Technology, 6-10 Sept. 1982, Antwerp, p. 484

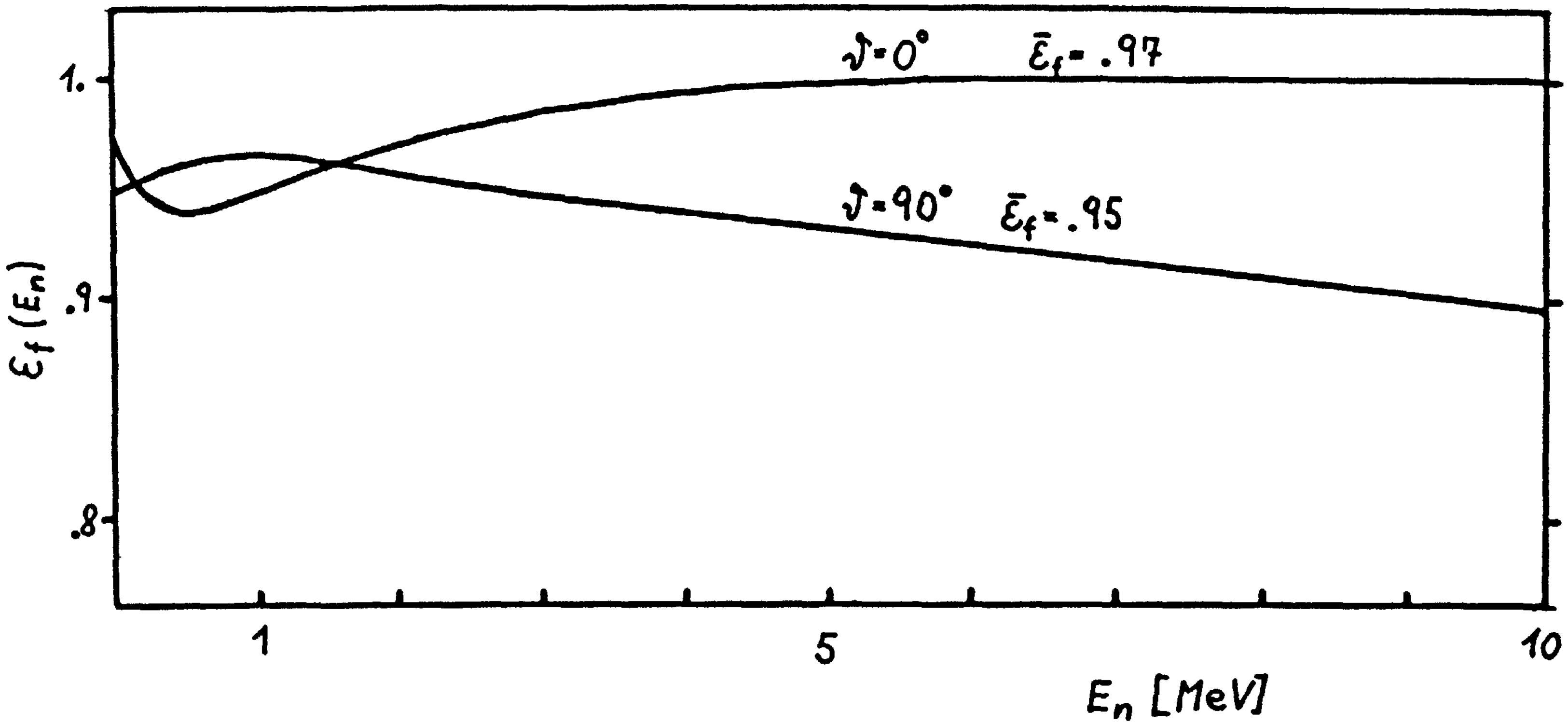

Fig. 1. Fission fragment detection efficiency as function of neutron energy for $\vartheta = 0^{\circ}$ and $\vartheta = 90^{\circ}$. $\bar{\varepsilon}_f$ is the respective spectrum averaged efficiency.

Investigation of the neutron energy spectrum from the spontaneous fission of Cf-252 by means of time-of-flight spectroscopy

H. Klein, R. Böttger, PTB, Braunschweig, FRG and
A. Chalupka, B. Strohmaier, IRK, Wien, Austria

1. Introduction

The continuous neutron energy spectrum from the spontaneous fission of Cf-252 is recommended for use as a reference standard, i.e. for absolute scaling or calibration purposes[1)]. In particular, neutron time-of-flight spectrometers may be checked for the low energy threshold and calibrated for the neutron detection efficiency by means of Cf sources deposited within gas scintillation detectors or low mass ionization chambers. Up to 10^6 fissions/s can be processed, including complete α-particle suppression, high detection efficiency and excellent timing properties. For these reasons, most of the recent experiments[2-5)] aimed at determining the neutron energy spectrum more precisely have been performed with a calibrated tof spectrometer using flight paths from 20 cm for the keV region[2)] up to 12 m for the high energy part[4)].

In this paper we describe the iteration method generally applied in analyzing the measured tof-spectra.

2. Time-of-flight spectroscopy

Detectors with sub ns-timing properties are used to define the start time of the neutrons by means of the associated fission fragments and the arrival time in the neutron detector by means of neutron induced reactions (fig. 1). While up to 10^6 f/s are processed in the FF detector, only a few events are expected in the neutron detectors due to the finite solid angle and the limited neutron detection efficiency. In order to avoid deadtime losses in the time-to-amplitude converter (TAC), the time scale is inversed by starting with the low neutron event rate and stopping with the fission events which for that reason have to be delayed by at least the largest flight time to be measured. In this method, which is generally applied for investigating regularly pulsed neutron sources, there are inherent problems if continuous time-statistical sources are involved in the stop channel and if non-extended deadtimes comparable with the inversed fission rate $1/A$ have to be considered.

Various density distributions superimpose to the tof distribution $p_m(t)\cdot\Delta t$ finally observed:

(a) the time interval distribution $p_r(t)$ due to random events without any correlated fission signal (background, inefficiency of the Cf detector etc, see fraction a in fig. 2)

(b) a modified random time distribution due to uncorrelated stop signals from fission events statistically preceding the associated fission (fraction (b-a) in fig. 2) and

(c) the remaining fraction of the tof distribution $p_u(t)$ to be investigated.

Defining the normalized net distribution $p'(t)$ by

(1a) $p'(t)\cdot\Delta t = \{p_m(t) - \alpha\cdot p_r(t)\}\cdot\Delta t$

the general solution, which will be derived in a more extensive paper[6], is given by:

(1b) $$p'(t)\cdot\Delta t = (1+A\cdot\tau)^{-1}\cdot\{p_u(t)\ \Delta t + A\cdot\Delta t\cdot\int_0^t p_u(t_1)\cdot\frac{A\cdot(\tau-t_1)}{1+A(\tau-t_1)}\,dt_1 + A\cdot\Delta t\cdot\int_t^\infty p_u(t_1)dt_1\}$$

for $0 \le t \le \tau$

(1c) $$p'(t)\cdot\Delta t = (1+A\cdot\tau)^{-1}\cdot\exp(-A(t-\tau))\cdot\{p_u(t)\cdot\Delta t + A\cdot\Delta t\cdot\int_0^\tau p_u(t_1)\cdot\frac{A\cdot(\tau-t_1)}{1+A(\tau-t_1)}\,dt_1 + A\cdot\Delta t\int_t^\infty p_u(t_1)dt_1\}$$

for $\tau < t \le \infty$ (T_R)

From these formulas it can generally be concluded that the distribution $p_u(t)$ can only be extracted from the measured distribution $p_m(t)$ by means of an iterative analysis. It should be noted that besides the calibration constant Δt(ns/channel) and the range T_R of the TAC (including PHA) and the Cf event rate A corrected for the losses due to the non-extended deadtime τ, the PHA channel corresponding to a vanishing time difference has to be known. This time difference $t = 0$ between START and STOP signal is defined by the fact that the TAC first accepts a stop event after being started (commonly indicated by a TRUE STOP signal).

The random background $\alpha\cdot p_r(t)$ may be measured in a separate run with a completely shielded FF detector or may be fitted mainly in the region above the prompt photon peak considering the time-interval distribution for statistical pulse sequences with nonextended deadtime[6]:

(2a) $p_r(t) = A/(1+A\cdot\tau)$ $\quad 0 \le t < \tau$

(2b) $p_r(t) = A\cdot(1+A\cdot\tau)^{-1}\exp\ (-A\cdot(t-\tau))$ $\quad \tau \le t$

In order to simplify the iterative analysis for further investigations or applications, it is advisable to minimize the deadtime $\tau < T_R$ without influencing the timing properties and to adjust the delay in such a way that the distribution $p_u(t)$ contributes only in the time range $\tau \le t \le T_R$. The general solutions of eq. 1 then reduce to:

(3a) $$p'(t)\cdot\Delta t = REN(t)\cdot\{p_u(t)\Delta t + A\cdot\Delta t\cdot\int_t^{T_R} p_u(t_1)dt_1\}$$

with the renormalization factor REN(t) given by:

(3b) $$REN(t) = \begin{cases} (1+A\tau)^{-1} & 0 \le t < \tau \\ (1+A\cdot\tau)^{-1}\exp(-A(t-\tau)) & \tau \le t \end{cases}$$

This approximation may be solved in practice by fitting the random fraction $I_r(ch) = \beta\cdot p_r(t)\cdot\Delta t$ of the measured TAC-pulse height spectrum $I_m(ch)$ in the upper region above the prompt photon peak

(4a) $I_1(ch) = I_m(ch) - I_r(ch)$

and iterating according to

(4b) $$I_n(ch) = REN(ch)^{-1} \cdot \left\{ I_1(ch) - REN(ch)\cdot A\cdot\Delta t\cdot \sum_{ch' \geq ch}^{max} I_{n-1}(ch') \right\}$$

In general, the third iteration already gives the final result. It should be emphasized that even in this approximation for certain experimental situations a channel-dependent renormalization factor must be considered which may significantly modify the shape of the net spectrum given in the brackets of eq. 4b.

If delay generators are used instead of delay lines ($\tau > T_R$), the approximation eq. 4b cannot be applied, due to the different shape of the uncorrelated background (compare with eq. 1b).

3. Conclusion

It has been shown that tof spectra measured with continuous neutron sources must be iteratively analyzed with care. Adequate procedures have been reported only in recent papers[3,4]. It is to be expected that some ealier experiments will have to be reanalyzed, particularly, if a high fission rate and a delay generator were involved[7].

Finally it should be mentioned that the uncorrelated background can be excluded by introducing a pile-up inspector[8] in the FF detector channel which rejects all FF signals with time differences of less than T_R (extended deadtime!). The statistical uncertainties can be considerably reduced in the low energy region, but problems will arise in the case of absolute calibration measurements.

References

(1) Nuclear Standards File
INDC (NDS) 114/GT (1980) 79 - 106

(2) M. V. Blinov, G. S. Boykov, V. A. Vitenko
Proceeding of the International Conference on "Nuclear Data for Science and Technology", ed. by K. H. Böckhoff,
D. Reichel Publ. Comp. Eindhoven (1983) 479 - 483

(3) W. P. Pönitz, T. Tamura
ibd. p. 465 - 472

(4) R. Böttger, H. Klein, A. Chalupka, B. Strohmaier
ibd. p. 484 - 487

(5) H. Märten, S. Seeliger, B. Stobinski
ibd. p. 488 - 491

(6) R. Böttger, H. Klein, A. Chalupka, B. Strohmaier
to be published

(7) L. Green, J. A. Mitchel, N. M. Steen
NSE 50 (1973) 257 - 272

(8) O. I. Batenko, M. V. Blinov, G. S. Boykov, V. A. Vitenko,
V. A. Rubchenya
contribution to these proceedings

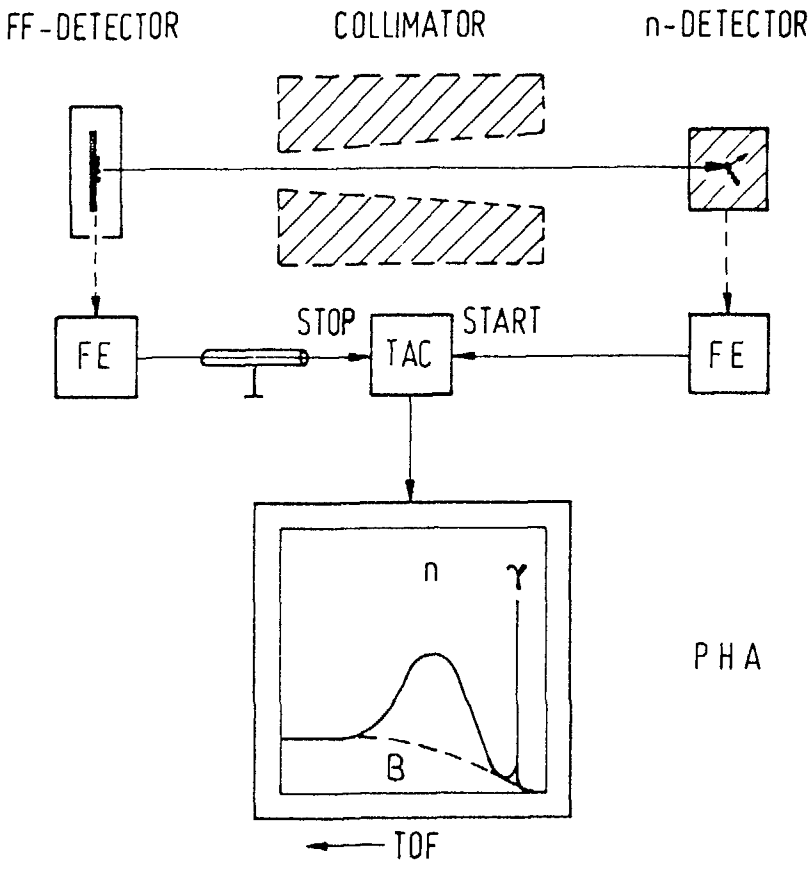

Fig. 1: Typical set-up for neutron tof spectroscopy with a Cf-252 fission source including a fission fragment detector, a neutron detector, a collimator between these detectors, fast timing electronic modules (FE), a time-to-amplitude converter (TAC), a delay line in the STOP channel and a pulse height analyzer (PHA)

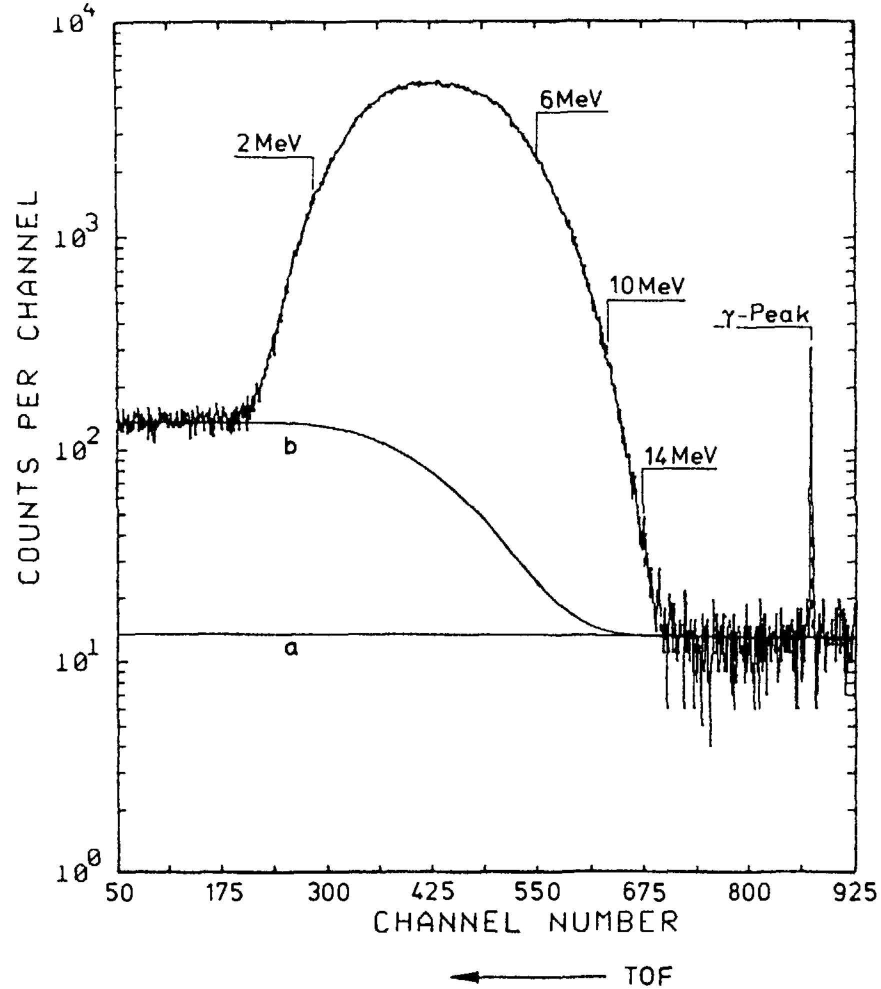

Fig. 2: Typical neutron tof spectrum (histogram) with random background (fraction a) and iteratively calculated "uncorrelated" background (fraction (b-a)). (see fig. 3 of ref. 4)

THE HIGH-ENERGETIC PART OF THE NEUTRON SPECTRUM FROM SPONTANEOUS FISSION OF ^{252}Cf

H. Märten, D. Seeliger, and B. Stobinski

Technische Universität Dresden
Sektion Physik
Mommsenstr. 13, DDR-8027 Dresden
German Democratic Republic

The high-energy end of the neutron spectrum from spontaneous fission of ^{252}Cf has been measured by the use of a very sensitive neutron spectrometer. The experimental data which were corrected for different apparatus effects indicate a hard emission component predominant at energies higher than 20 MeV. In this energy range, the measured spectrum cannot be described in the framework of a complex cascade evaporation model, whereas the calculated data agree with experimental ones up to 20 MeV satisfactorily. Non-equilibrium emission of fission neutrons is considered in interpretation.

[^{252}Cf(sf), prompt fission neutron spectrum, E_n = 10-30 MeV]

Introduction

Properly fission neutron spectra extend to relatively high emission energies. Considering the energy balance in fission, on principle, energies up to about 40 MeV are conceivable. Because of the very low emission cross sections in the high-energy range, fission neutron spectra are measurable up to about 15 MeV commonly. The physical interest in this matter stimulated our effort to determine the high-energy end of fission neutron spectra experimentally as high as possible [29, 30]. The importance of such measurements is confirmed in the case of the neutron emission spectrum from spontaneous fission of ^{252}Cf, because it was recommended as a standard [1]. Hitherto, its validity at high emission energies is not founded due to the high experimental errors above 10 MeV. Data of different authors diverge substantially [2]. The result of the NBS evaluation [3] was stated by a correction function $\mu(E)$ with reference to the Maxwellian distribution with kT = 1,420 MeV:

$$N(E) = \mu(E)\cdot 0{,}6672\cdot E^{1/2}\cdot \exp(-E/1{,}420). \qquad (1)$$

Some recent measurements [4] and evaluations [5] are consistent with that of Grundl and Eisenhauer (NBS) [3].

The main mechanism of neutron emission in low-energy fission reactions is the evaporation from fully accelerated fragments. Experimental results on the prompt neutron anisotropy have led to the conclusion that a small fraction (about 10 %) of the total number of fission neutrons is emitted isotropically in the compound nucleus frame [6]. Further experimental data on scission neutron emission are poor and partially contradictory [8, 9, 10, 11]. Corresponding theoretical investigations have been based on typical rapid changes of nuclear potential in fission (move of the fissioning nucleus from saddle to scission point [12], transition of strongly deformed fragments into the equilibrium state [13]). Hitherto, the partial spectra of the different eventual kinds of scission neutrons are not founded theoretically. One way to obtain more informations about neutron emission in fission is the measurement of the high-energy spectrum parts, because scission neutrons which should be emitted due to strong one-particle excitations in fission may influence the neutron spectrum at high energies especially.

Experimental method

The employed high-sensitive neutron spectrometer, its coupling to a minicomputer as well as the analysis of experimental data were already described in detail [14, 15]. Therefore, only a brief summary is given here. A high-efficient neutron detector with a voluminous NE 213 scintillator is located in a heavy shielding. The electronic system for particle discrimination by the charge comparison method is used to suppress the background counts of the detector caused by γ-rays and penetrating components of the cosmic rays. Especially cosmic myons with energies around 1 GeV give rise to a background part with about 3,5 s^{-1} event rate and an average pulse of about 25 MeV with reference to proton recoil energy (PRE). The n/μ-discrimination method enables the suppression of the cosmic background to less than 0,2 % in the region of the myon hump of the pulse height background spectrum (see Fig. 1).

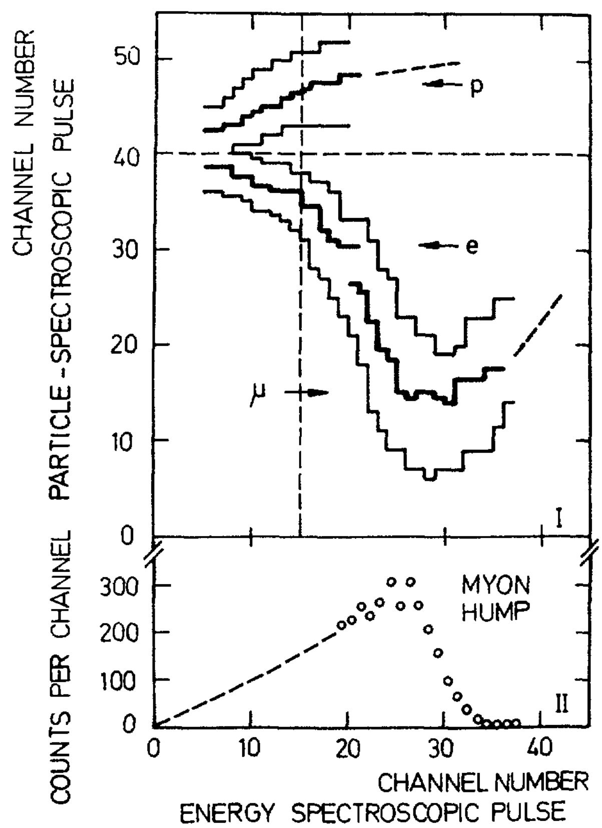

Fig. 1/I. Two-dimensional representation of the performance of the particle discrimination system (p, e, μ - particle branches of recoil protons, Compton electrons and cosmic myons respectively).

Fig. 1/II. Pulse height spectrum of cosmic myons.

Besides the use of the electronic n/γ-discrimination method, i. e. effective background suppression, the high sensitivity of the spectrometer is based on the two-dimensional measurement of neutron time-of-flight (TOF) and PRE. In this way, one is able to select the optimum (regarding background conditions) PRE-range for a given TOF-channel or channel range in analysis which is carried out cyclicly in connection with PRE-interval variation. Fig. 2 shows typical neutron-TOF-distributions which were obtained from a two-dimensional (TOF,PRE)-measurement for selected threshold energies.

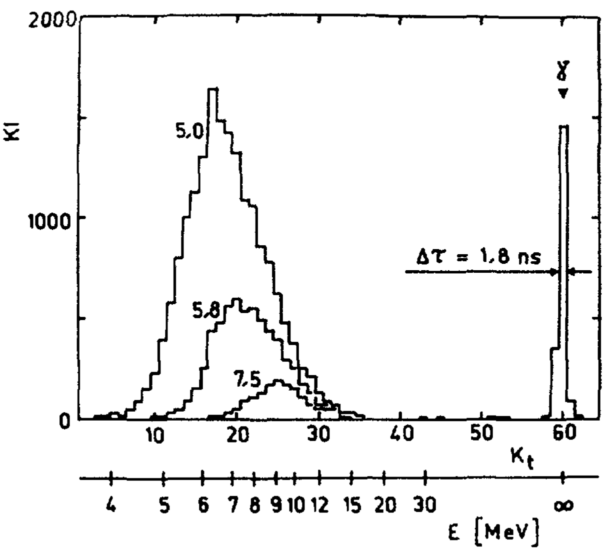

Fig. 2. Typical neutron-TOF-spectra from spontaneous fission of ^{252}Cf deduced from the two-dimensional (TOF,PRE)-measurement for selected PRE-threshold energies (4 m flight path, 62,0 h measuring time; KI - counts per channel; K_t - TOF-channel number; E - neutron energy).

The background level per TOF-unit, PRE-unit and measuring time respectively was found to be smaller than $1{,}5\cdot10^{-4}$ ns^{-1} MeV^{-1} h^{-1} in the PRE-ranges which were used in the analysis of the long-time measurement [25]. The stated value illustrates the sensitivity of the experiment.

The zero-time signal is obtained employing a fast ionization chamber [16] for direct fission fragment detection. It is characterized by a very light construction. The fission event rate amounted to $3{,}40\cdot10^4$ s^{-1} at the beginning of the measurement. The whole time resolution of the experimental arrangement is 1,8 ns regarding FWHM of the γ-peak. It is somewhat higher for neutrons due to the dimension of the scintillator and, hence, neutron energy dependent. To guarantee a sufficiently good energy resolution for high neutron energies a relatively high flight path is required (more than 4 m).

The spectrometer is coupled to a minicomputer which arranges the control of the two-dimensionally working multi-channel analyser for data acquisition, for the check (regarding TOF-peak and PRE-edge positions) and correction of the spectra as well as their analysis. The corresponding programme system was elaborated by the use of the high-level language FORTRAN 4000/42// including CAMAC and display application subroutines [15].

The calibration of the time coordinate is carried out by additional measurements using a defined delay device and considering the γ-peak as a fixed TOF-point. The PRE-edge position (point of inflexion) for a given TOF-channel or neutron energy EN corresponds to EN but a systematic deviation because of the distortion of the PRE-response function by multiple detection processes. This effect was studied by the use of the Monte Carlo code NEUCEF [17] after determining an effective parameter which characterizes the finite pulse height resolution of the detector by a fit of calculated PRE-response functions to experimental ones. Considering the corresponding correction factor the calibration of the PRE-coordinate is possible by the use of the measured continuous spectrum itselves due to the energy selection by the TOF-measurement.

Generally the background is a function of TOF. This effect doesn't appear at sufficiently high PRE, i. e. above about 5 MeV in the present case. Therefore, it is possible to reduce the common conception of the alternating measurements with and without sample on the sole measurement with sample. In this case, the background is determined from a defined region of the (TOF,PRE)-plane, where no effect events appear for physical reasons.

The detector efficiency was calculated by the use of the code NEUCEF [17] accepting the light output data of Verbinski et al. [18] and realistic values of the mentioned pulse height resolution parameter and geometric factors. A first measurement of the $^{252}Cf(sf)$ neutron spectrum, which is known with an uncertainty of less than 2,5 % between 0,4 and 7 MeV [5], was aimed at the comparison of the calculated efficiency data with the measured ones for relatively high bias energies and EN up to 10 MeV. We assumed the NBS evaluated spectrum for efficiency determination. The deduced efficiency functions depending on the bias energy confirm the NEUCEF data absolutely within an error which is EN and PRE-threshold dependent. It amounts to about 5 % in the ranges of best statistics (bias around 4 MeV, EN around 7 MeV) [25]. It is emphasized that the description of the experimental efficiency data is rather good in the PRE-threshold region due to the realistic consideration of resolution effects.

The long-time experiment (1218,5 h measuring time, 4,5 m path of flight) was subdivided in single runs. It is described in Ref. [25] in detail. The deduced energy distribution, i. e. the sum of the spectra from the single runs, which were obtained for PRE-thresholds around 8 MeV, was corrected for TOF-channel width and time resolution. The latter influences the measured spectrum in the high-energy region especially. Dead-time corrections were neglegible because of the low event rate. The results of the experiment are summarized below. Here it should be mentioned that the measured spectrum extends to about 30 MeV. Therefore, the interpretation of the experiment has to be based on an enlarged spectrum calculation which has been carried out in the framework of a complex cascade evaporation model presuming suitable approximations to guarantee a sufficient accuracy at high emission energies. This implies that the first theoretical analysis is founded on the main mechanism of fission neutron emission, i. e. the evaporation from fully accelerated fragments.

Cascade evaporation model

Because of the availability of necessary experimental data, the calculation was performed for different fragment mass numbers A by averaging the initial parameters over corresponding pairs of proton and neutron numbers. To consider the excitation energy distribution $P_o(E^x)$ and the cascade evaporation of fission neutrons by steps i as well as the energy balance, i. e. introduction of the spectrum dependence on the total kinetic energy TKE, one has to generalize the equation of the standard evaporation theory for the description of the emission spectrum f(e) in the center-of-mass frame and obtains

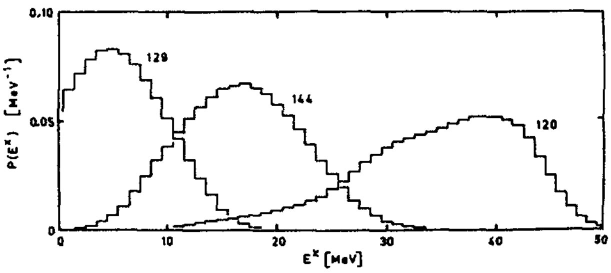

Fig. 3. Initial distributions of excitation energy for typical fragment mass numbers

$$f(e:A,TKE) = \sum_{i=0}^{i_{max}} \int_{B_{ni}}^{\infty} dE^x \cdot f(e,E^x:A-i) \cdot P_i(E^x:A,TKE) \cdot P(A,TKE), \quad (2)$$

where B_n is the neutron separation energy. P(A,TKE) is the occurance probability of fission events with the stated characteristics. The analysis was based on the nuclear-level density description by Ignatyuk et al.[20] including the excitation energy dependence of shell effects. The transformation of eq. (2) into the laboratory system, which was carried out considering a small emission anisotropy in the center-of-mass frame [22], results in the spectrum F(E:A,TKE). The integral energy spectrum is given by

$$N(E) = \sum_A \int_{TKE} dTKE \cdot F(E:A,TKE) \cdot P(A,TKE). \quad (3)$$

In the final calculation, we neglected the TKE dependence in the expressions (2) and (3), because this approximation influences the integral spectrum weakly [19]. Consequently, the laboratory system spectrum as a function of A has to be calculated by the use of the average kinetic energy of the fragments with given A. The initial distributions $P_o(E^x:A)$ have been deduced on the base of experimental data on neutron and γ-emission as a function of both A and TKE of the fragments [21] by

$$P_o(E^x:A) = \int_{TKE} dTKE \cdot P(E^x:A,TKE) \cdot P(TKE:A). \quad (4)$$

The $P_o(E^x:A,TKE)$ distributions were assumed to be Gaussian. Fig. 3 shows obtained $P_o(E^x:A)$ for typical A. The dependence of the average emission energy in the center-of-mass frame on A is illustrated in Fig. 4 in comparison with experimental data. The discrepancy between evaporation theory and experiment regarding the $\bar{e}(A)$ curve around A = 132 may be explained qualitatively considering the data on the scission neutron yield as a function of both A and TKE obtained by Samyatnin et al.[10] and the fact that the average emission energy of such neutrons is somewhat higher than the corresponding value for evaporated fission neutrons. Further details of the used model, the method of determining the excitation energy distributions and obtained results are described in Ref.[19]

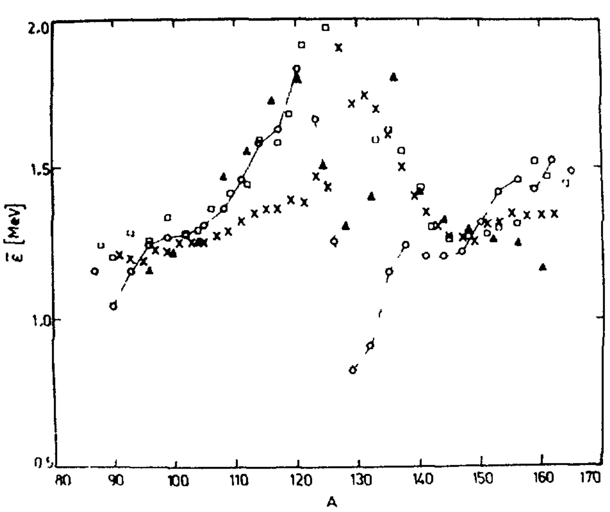

Fig. 4. The calculated average emission energies in the center-of-mass frame (o) in comparison with results deduced from experimental data (□ - Ref.[7], x - Ref.[23], ▲ - Ref.[9]).

Results and discussion

Our experimental results on the high-energy end of the neutron spectrum from the spontaneous fission of ^{252}Cf are represented in Fig. 5 and may be summarized as follows:

i) Within the experimental errors, the NBS evaluated spectrum was confirmed up to 20 MeV (in a qualified sense for the range from 16 to 20 MeV).

ii) For the energy interval from 20 to 28 MeV, the correction function

$$\mu(E) = \exp(+0{,}65 \cdot (E-20{,}65)) \quad (5)$$

with reference to the Maxwellian distribution with kT = 1,42 MeV (eq. (1)) was determined. The integral over N(E) from 21,5 to 26,7 MeV amounts to $(6{,}0 \pm 3{,}4) \cdot 10^{-6}$. This neutron yield is much more higher as expected [25].

Furtheron, we present a comparison of our experimental data with those of other groups (Fig. 6). It illustrates the discrepancies of experimental data determined by different authors in the energy range above 8 MeV.

The integral fission neutron spectrum obtained by weighted concentration of the l. s. spectra of the fragments with A between 87 and 165 by steps 3 is

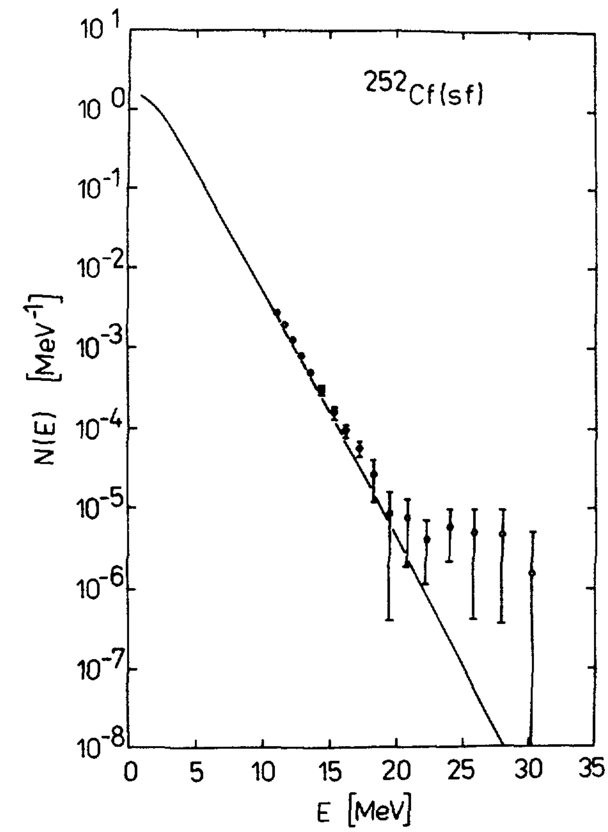

Fig. 5. The experimental data on the high-energy end of the neutron spectrum from spontaneous fission of ^{252}Cf compared with the result of the complex cascade evaporation calculation.

shown in Fig. 5 in comparison with the results of the described experiment. We were able to obtain good agreement with the experimental data on the neutron spectrum from ^{252}Cf up to the energy of about 20 MeV using the cascade evaporation model and realistic initial distributions of excitation energy. No arbitrary normalizations or free parameters were introduced. The experimental data indicate the existence of a hard emission component of fission neutrons. A similar result was already found in a measurement of the neutron spectrum from 14,5 MeV-neutron induced fission of Uranium by the use of the same experimental method [29, 30]. The high-energy component of fission neutron emission is predominant at extremely high emission energies (above 20 MeV) and cannot be explained assuming neutron evaporation from fully accelerated fragments. Hence, one should take into account non-equilibrium neutron emission which may be attributed to the typical rapid changes of nuclear potential in fission [24]. Further conclusions and outlooks are described in Ref.[19]

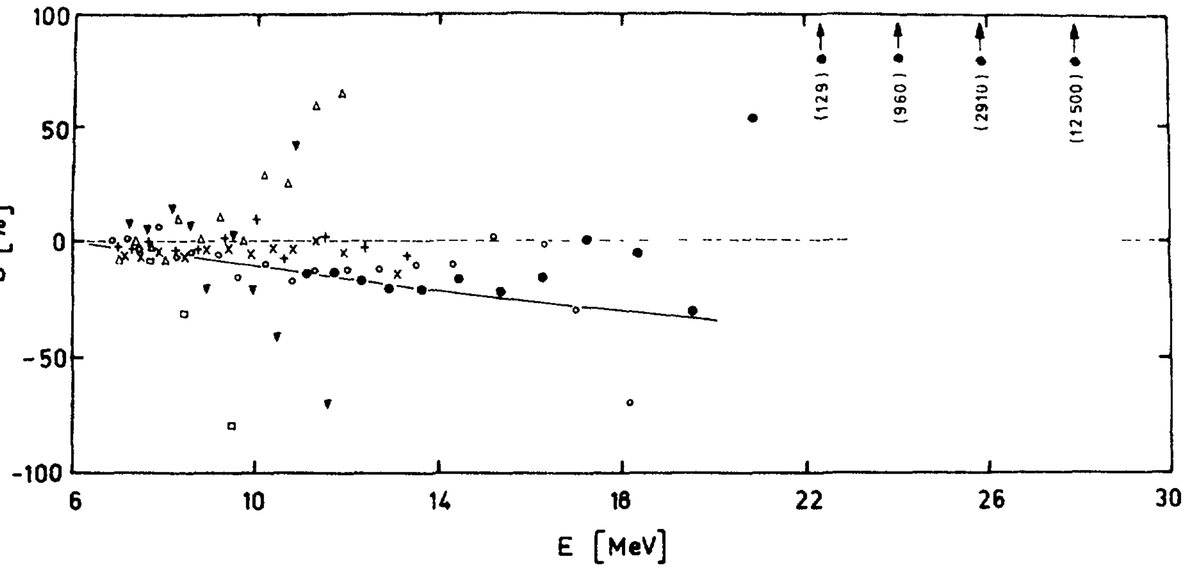

Fig. 6. Percentage departure of our data (o - 1st experiment with 62,0 h measuring time; • - 2nd experiment with 1218,5 h measuring time) from the Maxwellian distribution with kT = 1,42 MeV in comparison with the results of other groups (+ - Ref.[4]; x - Ref.[26]; ▼△ - Ref.[27]; □ - Ref.[28]) as well as with the NBS evaluated spectrum (continuous line). The representation is a supplemented one of Ref.[2]

References

1. Report INDC-36/LN, INDC/NEANDC, Nuclear Standards File, 1980 version, p. B-38.
2. M. V. Blinov, Proc. IAEA Consultants Meeting on Neutron Source Properties, Debrecen, 1980, INDC(NDS)-114/GT (1980).
3. J. Grundl, C. Eisenhauer, Natl. Bur. Stds. Publ., NBS-493 (1977).
4. J. Boldeman et al., Trans. Am. Nucl. Soc. 32, 733 (1979).
5. B. I. Starostov, A. F. Semenov, V. N. Nefedov, Yad. Konst. 2(37), 3 (1980).
6. H. R. Bowman, S. G. Thompson, J. C. D. Milton, W. J. Swiatecki, Phys. Rev. 126, 2120 (1962).
7. H. R. Bowman, J. C. D. Milton, S. G. Thompson, W. J. Swiatecki, Phys. Rev. 129, 2133 (1963).
8. M. V. Blinov, N. M. Kazarinov, I. T. Krisyuk, Yad. Fiz. 16, 1155 (1972).
9. V. M. Piksaikin, P. P. Dyatchenko, L. S. Kazaeva, Yad. Fiz. 25, 723 (1977).
10. Ju. S. Samyatnin, D. K. Ryasanov, B. G. Basova, V. A. Rabinovitch, V. A. Kostilev, Yad. Fiz. 29, 595 (1979).
11. P. Riehs, AIAU 81201 (1981).
12. Y. Boneh, Z. Fraenkel, Phys. Rev. C 10, 893 (1974).
13. V. A. Rubtchenya, Report RI-28 (Leningrad, 1974).
14. W. Grimm, H. Märten, D. Seeliger, Nejtronnaya Fizika (Proc. Vth All Union Conf., Kiev, 1980) 3, 3 (Moscow, 1980).
15. W. Grimm, H. Märten, D. Seeliger, B. Stobinski, Proc. XIth Int. Conf. on the Interaction of Fast Neutrons with Nuclei, Rathen, 1981, to be published.
16. M. Adel-Fawzy, H. Förtsch, S. Mittag, W. Pilz, D. Schmidt, D. Seeliger, T. Streil, Kernenergie 24, 107 (1981).
17. N. R. Stanton, COO-1545-92 (1971); D. Hermsdorf, ZfK-315, 192 (1977).
18. V. V. Verbinski et al., Nucl. Instr. Meth. 65, 8 (1968).
19. H. Märten, D. Seeliger, submitted to J. of Phys. G.
20. A. V. Ignatyuk, K. K. Istekov, G. N. Smirenkin, Nejtronnaya Fizika (Proc. IVth All Union Conf., Kiev, 1977) 1, 60 (1977).
21. H. Nifenecker et al., Proc. 3rd IAEA Symp. on the Physics and Chemistry of Fission, Rochester, 1973, vol. II, 117 (Vienna, IAEA).
22. A. Gavron, Phys. Rev. C 13, 2561 (1976).
23. A. Gavron, Z. Fraenkel, Phys. Rev. C 9, 632 (1974).
24. H. Märten, thesis, TU Dresden (1981).
25. H. Marten et al., INDC(GDR)-17/L (1982).
26. Z. A. Alexandrova et al., Atomnaya Energiya 36, 282 (1974).
27. H. N. Knitter et al., Atomkernenergie 22, 84 (1974).
28. H. Werle, H. Bluhm, Prompt Fission Neutron Spectra (Proc. IAEA Consultants Meeting, Vienna, 1971) p. 65 (1972).
29. H. Märten, D. Seeliger, ZfK-459, 98 (1981).
30. H. Märten, D. Seeliger, B. Stobinski, Proc. Europhysics Topical Conf. on Neutron Induced Reactions, Smolenice, 1982, to be published.

THEORETICAL ANALYSIS OF THE CF-252 FISSION NEUTRON SPECTRUM

H. Märten, D. Neumann and D. Seeliger
Technische Universität Dresden, GDR

Abstract

A complex cascade evaporation model is used to analyse energy and angular distributions of Cf-252 fission neutrons for specified scission configurations. The sensitivity of the calculation with regard to the most important input data as well as certain approximations has been studied for typical fragment mass numbers.

The paper includes a brief summary on the characteristics of the scission neutron component and its influence on energy spectra and angular distributions of fission neutrons. The model was also applied to calculate the distortion of the measurable Cf-252 fission neutron spectrum by the anisotropic fragment detection in time-of-flight spectrometer arrangements.

1. Introduction

In general, one has to distinguish between different mechanisms of fission neutron emission. The bare main one, i. e. the evaporation from fully accelerated fission fragments, is a rather complex process. In this case, detailed calculations of emission spectra in the framework of statistical models have to account for many characteristics of fission and fission neutron emission:

i) nucleon (N, Z, A=N+Z), excitation energy (E^x), kinetic energy (E_k) and spin (I) distribution of the fission fragments (which depends on the features of the fissioning nucleus);

ii) cascade neutron emission from highly excited, neutron-enriched fragments (in competition to γ-emission).

The fragment distribution of item i) is not derivable from fission theory completely or/and with sufficient accuracy. Therefore, one has to consider experimental data and/or special assumptions. Table 1 summarizes selected theoretical works [1-10] which take into consideration the items i) and ii) to a certain degree. The first complex analysis of fission neutron spectra in the framework of the Weisskopf formalism [12] was given by Terrell [1]. Nardi et al. [5] introduced a microscopic calculation of nuclear level densities. Browne and Dietrich [6] presented the first calculation in the framework of the Hauser/Feshbach formalism [13]. The references [9-11] take into account a more detailed consideration of different scission configurations defined by asymmetry and elongation, i. e. by the fragment mass number ratio A_L/A_H and the total kinetic energy TKE of the fission fragments respectively. Moreover, Table 1 illustrates the hitherto existing restricted theoretical treatments of fission neutron spectra. This concerns induced fission reactions especially. The model proposed by Madland and Nix [8] was based on rough approximations concerning the description of level density and excitation energy distribution, but it is easily applicable to any fission reactions. Therefore, it should be a possible reference to experimental data on fission neutron spectra.

In this work, the cascade evaporation model (CEM, see paragraph 2) is used to calculate energy spectra and angular distributions of Cf-252 fission neutrons (paragraph 4). We discuss the sensitivity of the CEM calculation with regard to the most important input parameters and approximations (paragraph 3).

A brief review on experimental and theoretical works about the emission of scission neutrons as well as their influence on energy and angular distributions of fission neutrons is given in paragraph 5.

The Cf-252 fission neutron spectrum is widely used as a standard (reference) in fast-neutron physics. However, the result of its measurement using time-of-flight arrangements is influenced by fission fragment absorption in the Cf sample and, in general, angle-dependent [24,40,41]. This appearance was studied on the base of the CEM calculation considering the scission neutron component. General conclusions are discussed in paragraph 6.

<u>Table 1</u>

Comparison between different fission neutron spectrum calculations which include a more complex consideration of emission characteristics than simple evaporation assumptions concerning the whole fission reaction:

Ref.	Basic formalism	Level density decription	σ_{inv} / T_{lj}	Sc. config. specification	$P(E^x)$	Remarks
1	Weisskopf cascade emission	Constant T approximation/ Fermi-gas m.	Constant σ_{inv}	By some typical A	Gaussian	Deduced: Rest-temperature distribution and $\bar{E}(\bar{\nu})$
2	Weisskopf cascade emission	Constant T approximation	Constant σ_{inv}	By A	-	Analytic solution of the cascade emission spectrum
3	Weisskopf cascade emission	Fermi-gas model (modified)	Constant σ_{inv}	By A	Gaussian	Deduced: a(A) for fission fragments
4	Weisskopf cascade emission	Constant T approximation/ Fermi-gas model	Semi-empirical σ_{inv}	By A	-	In addition: Study of possible scission neutron influences

Table 1 (continued)

Ref.	Basic formalism	Level density description	σ_{inv} / T_{lj}	Sc. config. specification	$P(E^x)$	Remarks
5	Weisskopf cascade emission	Nilsson model (shell model plus pairing Hamiltonian)	σ_{inv}: Optical m., square-wall potential	By A	Gaussian	Monte Carlo calculation. Deduced: $\bar{\varepsilon}(A)$ and $\bar{E}_\gamma(A)$
6	Hauser/ Feshbach cascade emission	Semi-empirically (Gilbert/ Cameron)	T_{lj}: Wilmore/ Hodgson potential	By A	Gaussian	Deduced: N(E) up to 14 MeV
7	Hauser/ Feshbach cascade emission	Semi-empirically (Ignatyuk) a(U)	T_{lj}: Square-wall potential Lagrange potential	By A	Gaussian	Deduced: $\bar{\varepsilon}(A)$ for different $P(E^x)$

Table 1 (continued)

Ref.	Basic formalism	Level density decription	σ_{inv} / T_{lj}	Sc. config. specification	$P(E^x)$	Remarks
8	Weisskopf	Constant T approximation	σ_{inv}: Optical m., Becchetti/ Greenless potential	By the light and heavy fragment group	Rect-angular (to simu-late the cascade emission)	Deduced: N(E) up to 14 MeV and $\bar{\nu}$. The model is applicable to induced fission reactions
9 10 11	Weisskopf cascade emission	Semi-empirically (Ignatyuk) a(A)	σ_{inv}: Optical m. or semi-empiri-cally	By A as well as by TKE / by A	Gaussian for fixed A and TKE	Deduced: $P(E^x:A)$, $\bar{\varepsilon}(A)$, N(E) up to 30 MeV, $N(E,\Theta)$, $N(E,\Theta:A,TKE)$

(T_{lj}: transmission coefficients)

2. Complex cascade evaporation model for fission neutron spectrum calculations (summary [10])

The energy spectrum $\varphi(\epsilon)$ in the center-of-mass system (CMS) for fixed A and E^x is given by [12]

$$\varphi(\epsilon : E^x, A) = C \cdot \sigma_{inv}(\epsilon : A-1) \cdot \epsilon \cdot \rho(E^x - B_n - \epsilon, I=0 : A-1) \tag{1}$$

(σ_{inv} - inverse cross-section, B_n - neutron separation energy, ρ - level density). C normalizes the spectrum to unit. To consider the items i) and ii) of paragraph 1 one has to introduce an initial excitation energy distribution of single fragments $P_{i=0}(E^x)$, the cascade emission by steps i as well as the energy balance in fission, i. e. the TKE dependence of the emission spectrum. This generalization results in

$$\varphi(\epsilon : A, TKE) = \sum_i \int_{B_{ni}}^{\infty} dE^x \cdot \varphi_i(\epsilon ; E^x, A-i) \cdot P_i(E^x : A, TKE) \tag{2}$$

with

$$P_i(E^x) = \int d\widetilde{E^x} \cdot \varphi_{(i-1)}(\widetilde{E^x} - B_{n(i-1)} - E^x) \cdot P_{(i-1)}(\widetilde{E^x}) \tag{3}$$

A small CMS emission anisotropy caused by the fragment spin [19] may be considered by

$$\varphi(\epsilon, \vartheta) = \varphi(\epsilon) \cdot (1 + B \cdot \cos^2\vartheta)/(1 + B/3). \tag{4}$$

The corresponding laboratory system (LS) distribution $N(E,\Theta)$ is obtained by

$$E = E_f + \epsilon + 2 \cdot (\epsilon \cdot E_f)^{1/2} \cdot \cos\vartheta \tag{5}$$

$$E_f = E_k/A = (1/A - 1/A_{CN}) \cdot TKE \tag{6}$$

$$N(E, \Theta : A, TKE) = (E/\epsilon)^{1/2} \cdot \varphi(\epsilon, \vartheta : A, TKE) \tag{7}$$

(A_{CN} - mass number of the fissioning nucleus) [1].

The distributions $N(E,\Theta:A)$ or $N(E,\Theta)$ may be deduced taking into account the occurance probability $P(A,TKE)$ (in the case of the Cf-252 fission, see for instance Ref. [21,22]).

<u>σ_{inv} description:</u> The computer code for the CEM calculations includes the following variants:

i) σ_{inv} = constant,
ii) σ_{inv} description according to Ref. [16],
iii) σ_{inv} calculated on the base of the optical model (OM),
iv) $\sigma_{inv}(\epsilon) \sim \epsilon^{-m}$ as an approximation of the results of OM calculations accepting the Becchetti/Greenless potential [17]. This approximation is feasible for neutron-enriched nuclei like fission fragments especially. m amounts to about 0.144 for the mass number range of fission fragments.

<u>Level density description:</u> In the CEM calculation, we apply the Ignatyuk treatment of the level density description [14,15] which takes into account the excitation energy (U) dependence of shell effects. The Fermi-gas formulae of nuclear level density is modified by

$$a(U) = \tilde{a}\cdot(1+f(U)\cdot\delta W/U) \tag{8}$$

with

$$f(U) = 1-\exp(-\gamma\cdot U) \tag{9}$$

(a - level density parameter, $\tilde{a}$ - asymptotic value of a, δW - shell correction energy, γ - parameter which amounts to about (0.05 - 0.06) MeV^{-1}

<u>Excitation energy distribution:</u> The distribution $P_0(E^x:A,TKE)$ is assumed to be Gaussian. In the case of the Cf-252 spontaneous fission, the distribution parameters are derivable from measured data on neutron multiplicity and γ-emission [20]. One may deduce

$$P_0(E^x:A) = \int dTKE\cdot P_0(E^x:A,TKE)\cdot P(TKE:A). \tag{10}$$

<u>A possible approximation:</u> Eq. 2 may be simplified by

$$\varphi(\epsilon:A) = \sum_i \int_{\bar{B}_n}^{\infty} dE^x\cdot\varphi(\epsilon:E^x,A)\cdot P_i(E^x:A) \tag{11}$$

introducing Eq. 10. The transformation into the LS is based on $\bar{E}_k(A)$.

<u>3. The sensitivity of the CEM calculation with regard to input data and approximations</u>

The study of sensitivity effects is a necessary precondition for the evaluation of the calculation accuracy as well as for the interpretation of systematic deviations between measured and calculated spectra. The influence of input parameter variations on the LS spectrum shape was investigated for some typical fragments from Cf-252 spontaneous fission on the base of the approximation according to Eq. 11. To modify $P_0(E^x:A)$ in a defined manner we have approximated it by a Gaussian distribution (compare paragraph 4) and varied the average value $\bar{E}^x$ and the variance parameter σ_{Ex}. The results are represented in the Figures 1 - 8 and Table 2.

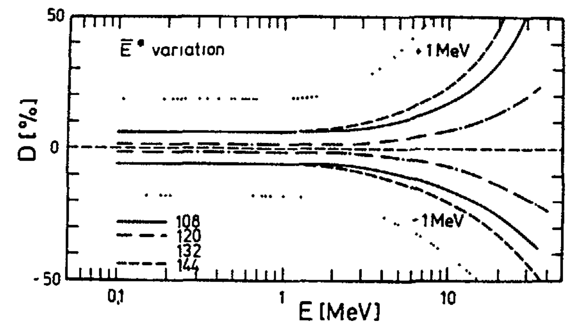

Fig. 1
Percentage departures of LS spectra, which have been calculated for plus/minus 1 MeV variations of the average excitation energy, from the corresponding reference spectra for typical fragment mass numbers

The most significant deviations from the reference spectrum appear at high emission energies in each case. The calculated average number of emitted neutrons $\bar{\nu}$ is strongly changed by $\bar{B}_n$ and $\bar{E}^x$ variations as expected (Figures 1 and 3, Table 2). The shape of the calculated spectrum (expressed by $\bar{E}$ in Table 2) is very sensitive to $\bar{E}^x$, σ_{Ex} and $\tilde{a}$ variations. The other parameters give rise to spectrum modifications in the order of some percents.

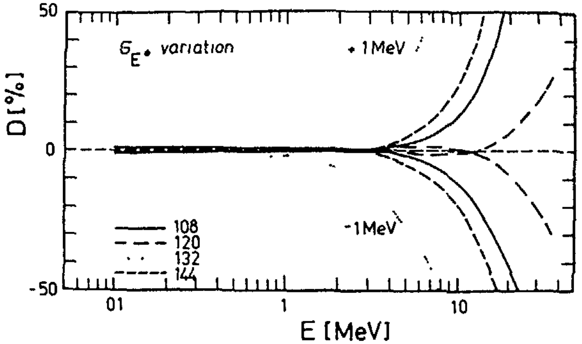

Fig. 2

The same as Fig. 1 for plus/minus 1 MeV variations of the variance parameter of the assumed Gaussian shape distribution of *excitation energy* in each case of the selected fragment mass number.

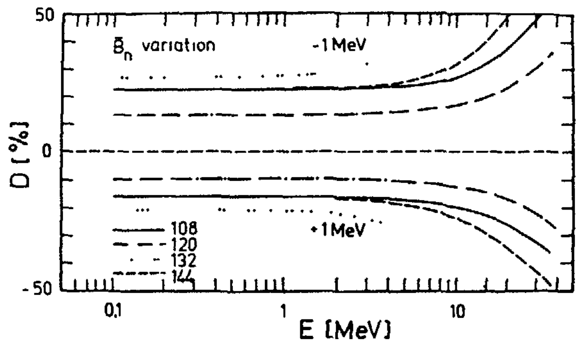

Fig. 3

The same as Fig. 1 for variations of the average neutron separation energy (compare Eq. 11).

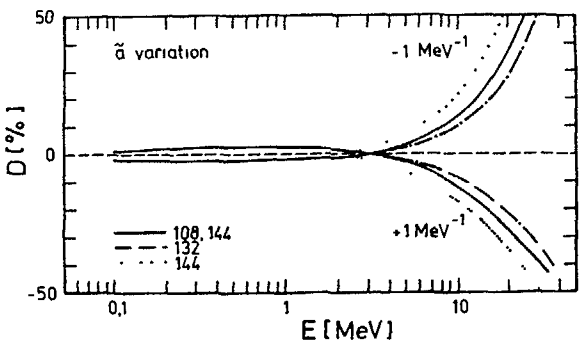

Fig. 4

The same as Fig. 1 for plus/minus 1 MeV^{-1} variations of the asymptotic level density parameter (compare Eq. 8). a itselves depends on the excitation energy of the residuel nucleus.

The calculated spectrum of the low-excited fragment with A = 132 shows considerable uncertainties at energies higher than about 3 MeV.

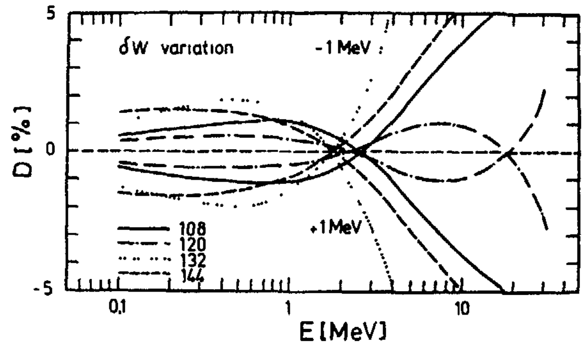

Fig. 5

The same as Fig. 1 for plus/minus 1 MeV variations of the shell correction energy (compare Eq. 8).

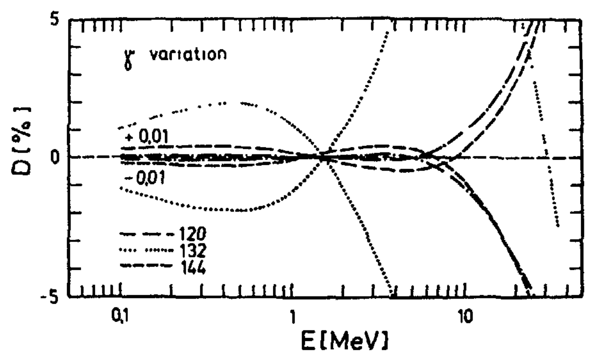

Fig. 6

The same as Fig. 1 for plus/minus 0.01 variations of the γ-parameter which appoints the excitation-energy-dependent shell influence on the level density description. γ amounts to about (0.05 - 0.06) MeV^{-1} (compare Eq. 9).

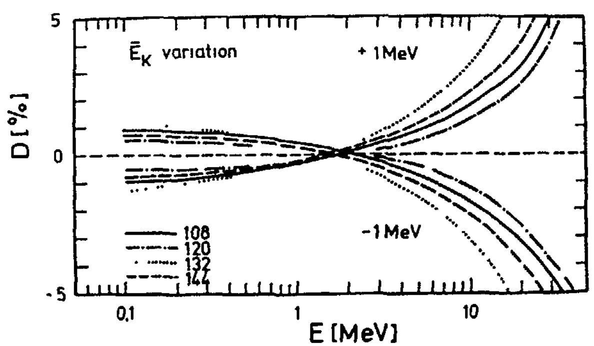

Fig. 7

The same as Fig. 1 for plus/minus 1 MeV variations of the average kinetic energy of the fission fragments for fixed A.

The description of σ_{inv} in the framework of the OM reduces the average emission energy by about (5 - 6)% (Fig. 9).

Table 2

The sensitivity of the CEM calculation with regard to selected input parameters expressed by the derivations of $\bar{\nu}$ and $\bar{E}$ for typical mass numbers of fragments from the spontaneous fission of Cf-252

Derivation	Fragment mass number			
	108	120	132	144
$\frac{d\bar{\nu}}{d\bar{E}^x}$ / MeV^{-1}	0.139	0.079	0.110	0.147
$\frac{d\bar{\nu}}{d\sigma_{Ex}}$ / MeV^{-1}	0.003	0.000	0.037	0.001
$\frac{d\bar{\nu}}{d\bar{B}_n}$ / MeV^{-1}	-0.388	-0.494	-0.137	-0.407
$\frac{d\bar{E}}{d\bar{E}^x}$	0.029	0.023	0.036	0.027
$\frac{d\bar{E}}{d\sigma_{Ex}}$	0.028	0.002	0.072	0.026
$\frac{d\bar{E}}{d\bar{E}_k}$	0.012	0.008	0.007	0.006
$\frac{d\bar{E}}{d\bar{B}_n}$	-0.007	-0.017	-0.028	-0.012
$\frac{d\bar{E}}{d\delta W}$	-0.018	-0.010	-0.022	-0.016
$\frac{d\bar{E}}{d\tilde{a}}$ / MeV^2	-0.041	-0.046	-0.022	-0.027

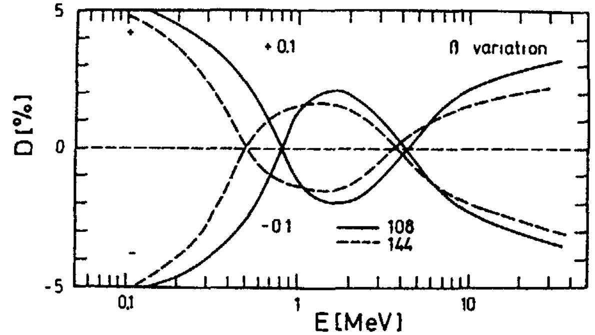

Fig. 8

The same as Fig. 1 for plus/minus 0.1 variations of the CMS anisotropy parameter β (compare Eq. 4).

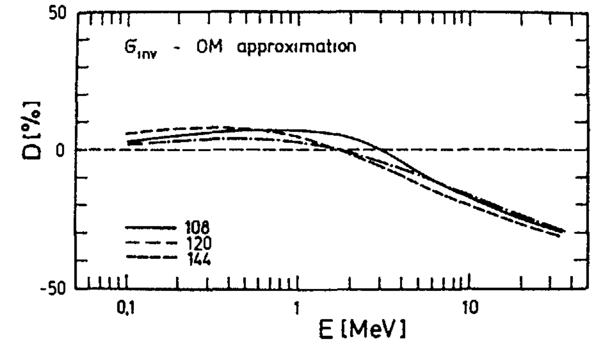

Fig. 9

Percentage departures of the LS spectra calculated on the base of the σ_{inv} approximation according to the OM with reference to the corresponding constant-σ_{inv} calculation in the case of some typical fragment mass numbers.

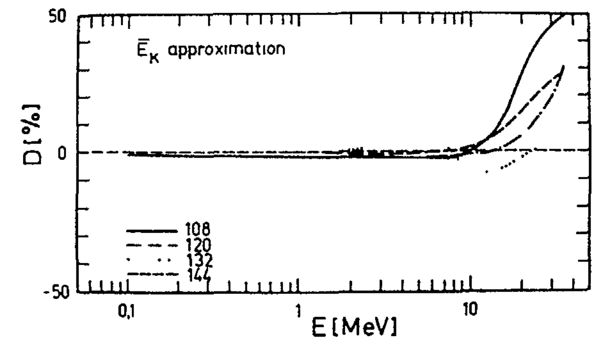

Fig. 10

The influence of the $\bar{E}_k$ approximation on the calculated LS spectrum with reference to the "exact" calculation (D - percentage departure).

The $\bar{E}_k$ approximation according to Eq. 11 modifies the calculated spectrum at high emission energies strongly (Fig. 10).

It is applicable to common spectrum descriptions, i. e. up to about 10 MeV.

Eq. 11 includes further simplifications:

i) the approximation of B_{ni} in Eq. 2 by $\bar{B}_n$,

ii) the approximation of the emission-step-dependent CMS spectrum $\varphi_i(\epsilon:E^x,A-i)$ (Eq. 2) by $\varphi(\epsilon:E^x,A)$.

Both approximations give rise to spectrum modifications lower than about 1.5 %.

4. Application of the CEM to the Cf-252 spontaneous fission

Assuming Gaussian $P_0(E^x:A,TKE)$ distributions with parameters deduced from Ref. [28] the initial E^x distributions for fixed A were obtained by the use of Eq. 10 [10]. They are represented in Fig. 11 for some selected fragment mass numbers.

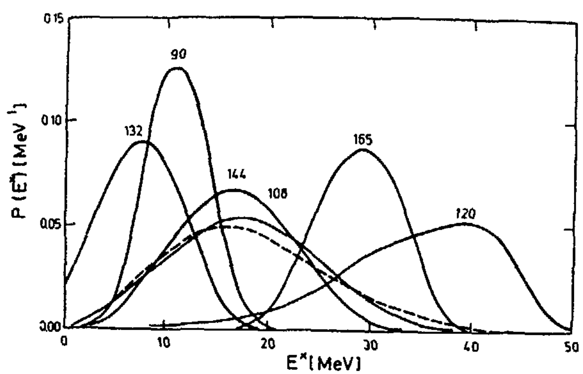

Fig. 11
Initial excitation energy distributions for selected fragment mass numbers (parameter). The dashed line represents the weighted average $\bar{P}^A(E^x) = \sum_A P(E^x:A)\cdot P(A)$.

These curves show the influence of shell effects on the partition of the total excitation energy which originally appears as deformation energy at scission point mainly. As discussed in Ref. [10] in more detail, the ratio of the average excitation energies of complementary fragments depends on TKE. Moreover, it is emphasized that $P_0(E^x:A)$ does not correspond with a Gaussian distribution, if one of the fragments is nearly (double-)magic.

Fig. 12
LS spectra for selected fragment mass numbers weighted by the fission fragment yield in each case.

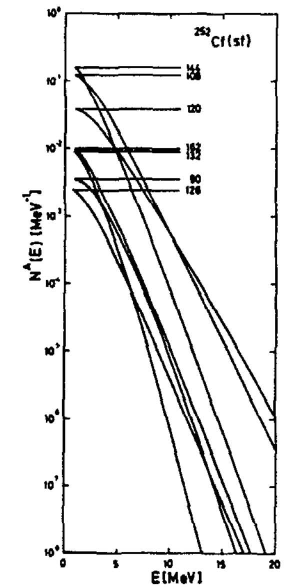

Fig. 12 represents calculated LS neutron spectra of selected primary fission fragments weighted by the fragment yield. It is shown that the integral Cf-252 fission neutron spectrum in the energy ranges from 0 to 2 MeV, from 2 to 12 MeV and above 12 MeV are predominantly formed by the heavy fragment group, by the light fragment group and by highly excited fragments with A around 120 respectively.

The calculated integral neutron spectrum (integral with regard to A and TKE) is represented in Fig. 13 in comparison with recent experimental results [9,23,24,39] as well as with the NBS evaluated spectrum [42] and a Madland/Nix model (MNM) calculation. The MNM (constant-σ_{inv} version) spectrum was obtained assuming such a maximum-temterature parameter T_m which guarantees the best spectrum description between 1 and 6 MeV (NBS evaluated spectrum as a reference). The comparison between both the CEM and the MNM calculation has shown that the Madland/Nix model is applicable up to relatively high emission energies (about 20 MeV), if one uses a reasonable T_m value (determined by TKE and the level density parameter). The experimental data on the high-energy end of the spectrum [9] cannot be decribed in the framework of the CEM.

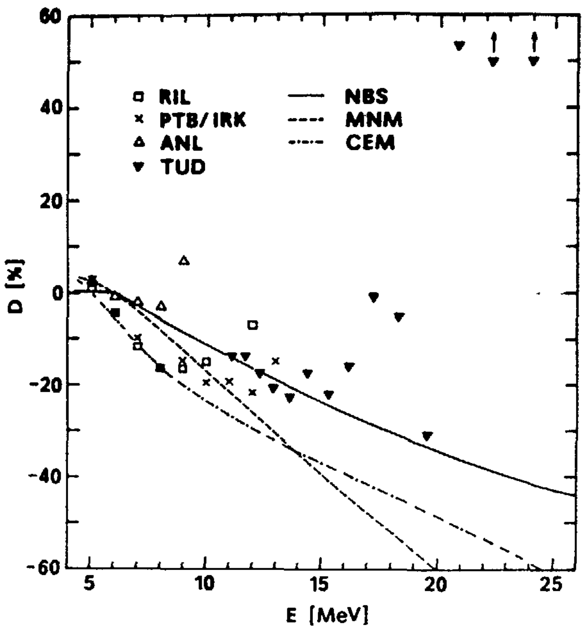

Fig. 13
Recent experimental results (RIL [39], PTB/IRK [23], ANL [24], TUD [9]), the NBS evaluated spectrum [42] and energy distributions calculated in the framework of the CEM and the MNM (see text) represented by percentage departures D from a Maxwellian with a temperature parameter of 1.42 MeV.

As discussed in the Refs. [9,10], the appearance of a hard emission component at energies above 20 MeV should be caused by non-equilibrium fission neutron emission due to strong single-particle excitations during rapid changes of nuclear potential (descent from saddle to scission point, transition of strongly deformed fragments into the equilibrium shape).

Furtheron, we analysed the double-differential emission probability N(E,Θ). Typical examples of the results are shown in the Figures 14 - 16. The shape of angular distributions of complementary fragments depends on the E^x partition as

Fig. 14
The angular distributions of Cf-252 fission neutrons for selected LS energies (parameter in MeV). The calculation was performed in the framework of the complex CEM.

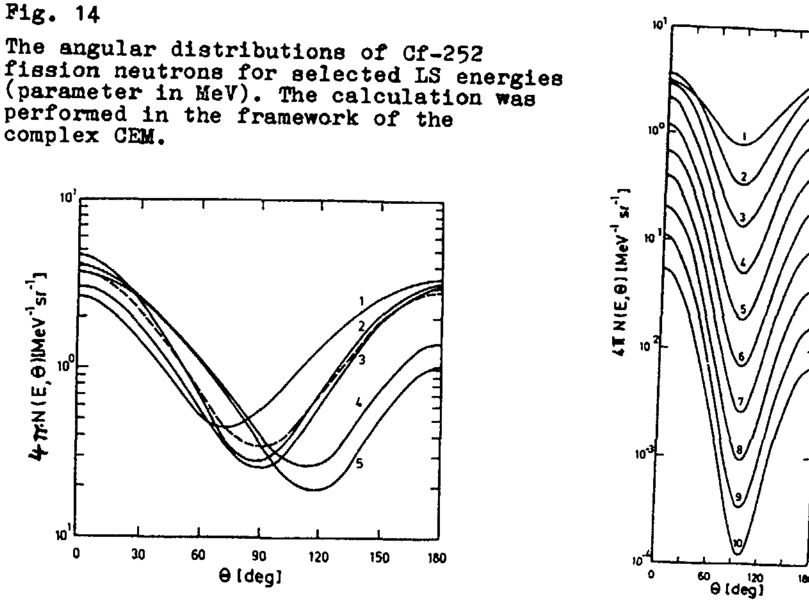

Fig. 15
The angular distributions of Cf-252 fission neutrons at the LS energy of 2 MeV for selected fragment mass number ratios (1 - 90/162, 2 - 108/144, 3 - 126/126, 4 - 120/132, 5 - 123/129. dashed curve - integral distribution).

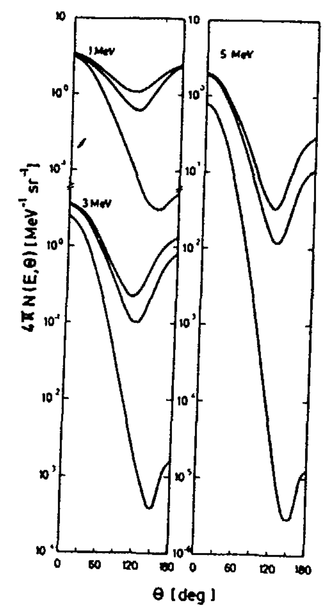

Fig. 16
Angular distributions of Cf-252 fission neutrons at three LS emission energies (parameter in MeV) calculated for the 120/132 configuration and different TKE values. The upper (middle, lower) curve corresponds to the minimum (average, maximum) TKE in each case.

discussed above as well as on the difference between their kinetic energies. Fig. 16 represents the TKE dependence of the angular distribution for the fragment mass number ratio 120/132. In this case, one should expect a considerable amount of the scission neutron yield [30] (compare paragraph 5).
On the base of the CEM calculation, one may draw the conclusion that a corresponding measurement should be sensitive to the angular distribution of scission neutrons at angles higher than about 40 deg.

5. The influence of the scission neutron component on energy spectra and angular distributions

The used complex CEM refers to the main mechanism of fission neutron emission. It was found by Bowman et al. [25] at first that a 10 %-component is emitted isotropically in the LS.
In spite of many further investigations summarized in Table 3 (Cf-252 spontaneous fission) our knowledge about the so-called scission neutron emission is poor and partially contradictory. This concerns the scission neutron yield as a function of A_L/A_H and/or TKE especially. The energy spectrum of this central component is usually approximated by

$$N_{sc}(E) \sim E \cdot \exp(-E/T_{sc}). \tag{12}$$

Considering the published yields and average emission energies of scission neutrons from the spontaneous fission of Cf-252 (see Table 3) one may assume:

$$\bar{T}_{sc,1} \approx (1.0 - 1.2)\ \mathrm{MeV}, \quad \bar{\nu}_{sc,1}/\bar{\nu}_{total} \approx 0.1.$$

The figures 17 and 18 illustrate the comparison between the CEM calculation results (no additional normalizations!) and experimental data of Ref. [25]. Obviously, the central component becomes more predominant at higher emission energies. By a comparison of experimental 90 deg-spectra of the Refs. [25,27,31] with the CEM calculation, we deduced (in addition to previous treatments) a second, much harder central component characterized by

$$\bar{T}_{sc,2} \approx (2.0 - 2.5)\ \mathrm{MeV}, \quad \bar{\nu}_{sc,2}/\bar{\nu}_{total} \approx (0.001 - 0.01).$$

The higher value of the relative scission neutron yield of the second component corresponds to the results of the Refs. [25,27], the lower one to the data of Ref. [31].
The given result does not contradict to the measured high-energy end of the Cf-252 fission neutron spectrum [9] (E higher than 20 MeV).

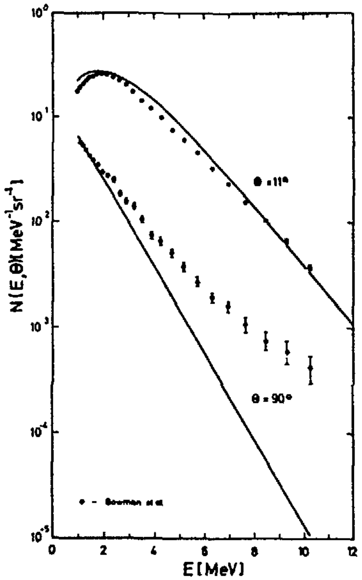

Fig. 17
The calculated A-integrated energy spectra in 11 deg- and 90 deg-direction with reference to the light-fragment direction in comparison with experimental data [25].

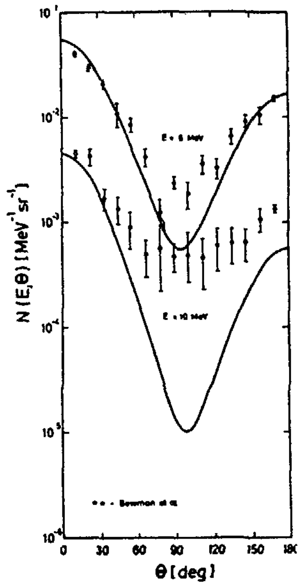

Fig. 18
The calculated A-integrated angular distributions of Cf-252 fission neutrons at two selected emission energies in comparison with experimental data (Ref. [25]).

The energy spectra as well as the angular distributions of the different eventual kinds of scission neutrons are not founded theoretically. The hitherto published papers [32-36] consider possible yields but not the energy spectra on the

Table 3

Summary of experimentally determined features of scission neutron emission in the Cf-252 spontaneous fission

Reference	$\bar{\nu}_{sc}/\bar{\nu}_{tot}$/%	$\bar{E}_{sc}$/MeV	Further results
25	10	2.6	-
26	20 - 25	2.4	$\bar{\nu}_{sc}$(TKE) is nearly constant
27	$5.6^{+1.5}_{-1.3}$	-	-
28	10.5 ± 2.6	-	-
29	20	1.65	$\bar{\nu}_{sc}$(TKE) is decreasing; $\bar{\nu}_{sc}$(A) is nearly constant
30	20 ± 12	-	$\bar{\nu}_{sc}$(TKE) is increasing; $\bar{\nu}_{sc}(A_H/A_L)$ is predominant, if A_H or A_L is nearly (double-)magic
31	13.2 ± 3.1	2.0 ± 0.2	-

base of different models, because the model parameters concerning the time-dependent parameterization of nuclear potential at different stages of the fission process are known roughly. The most probable characteristic time τ of the descent from saddle to scission point deduced by Negele et al. [37] amounts to $3.4\ 10^{-21}$ s. The average experimental value of $\bar{\nu}_{sc}$ and the scission neutron yield which corresponds to the stated value of τ according to the results of Ref. [35] are nearly identical. However, it would be early to draw conclusions regarding the predominance of this kind of scission neutron emission.

6. Correction of measured Cf-252 neutron spectra for the influence of the anisotropic fragment detection

The Cf-252 fission neutron spectrum measured by the use of time-of-flight spectrometers is influenced by the anisotropic fragment detection (timing signal) caused by absorption in the sample plane (deposit thickness, roughness) [24,40,41]. As an alternative of the Monte Carlo study presented by Chalupka at this meeting [41], we calculated the measurable Cf-252 neutron spectrum assuming an angular distribution of detected fragments given by

$$W(\beta) = (1/4\cdot\pi)\cdot(1-\exp(-\cos^2\beta/(2\cdot\sigma^2))) \tag{13}$$

(β - fragment direction angle with reference to the direction perpendicular to the sample plane). This function should be a sufficiently good approximation in the case of parallel-plate ionization chambers. Its inefficiency depends on the distribution parameter σ according to

$$1-\varepsilon = (\pi/2)^{1/2}\cdot\sigma \tag{14}$$

Using the Legendre-polynominal representation of N(E,Θ), i. e.

$$N(E,\Theta) = \sum_i C_i(E)\cdot P_i(\cos\Theta), \tag{15}$$

we obtain the measurable neutron energy distribution by numerical solution of

$$G(E,\beta) = \sum_i C_i(E)\cdot P_i(\cos\beta)\cdot\int_{-1}^{1} W(\Theta)\cdot P_i(\cos\Theta)\cdot d(\cos\Theta). \tag{16}$$

Fig. 19 shows the ratio G(E,β)/N(E) which was calculated for a 5 % inefficiency on the base of the CEM N(E,Θ) (see paragraph 4) introducing a 10 % scission neutron component according to Eq. 12 (T = 1.0 MeV). At an angle of about 60 deg, this ratio is a nearly constant function of E and amounts to about ε. It is emphasized that the result of this analysis is not very sensitive to the shape of W(β). Using a rectangular

W(θ) distribution we obtained quite similar results.

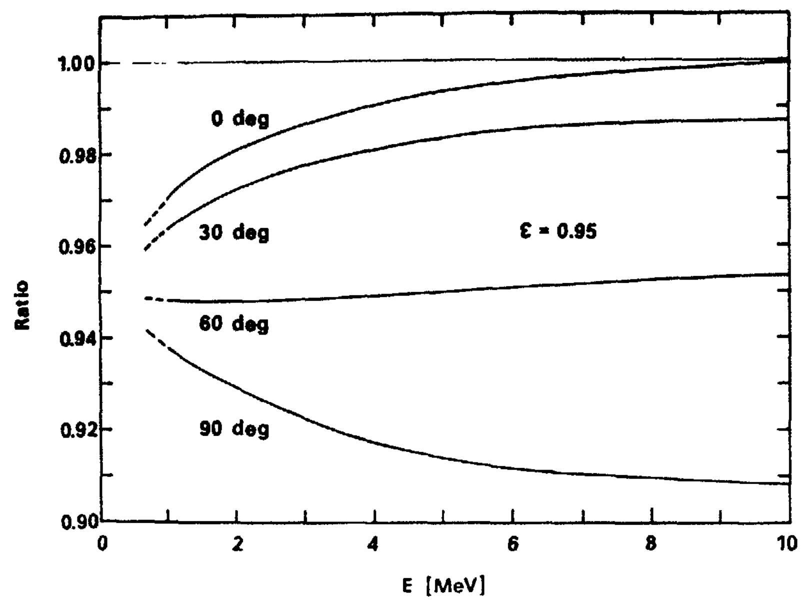

Fig. 19
The calculated ratio of the measurable and the actual fission neutron spectrum (in the case of a 5 % fragment detector inefficiency) represented as a function of the LS neutron energy for selected angles (with reference to the sample plane normal).

7. Conclusions

Using the CEM in a complex form we were able to obtain a rather good description of the neutron energy spectrum from Cf-252 spontaneous fission up to about 20 MeV. The angular distributions cannot be deduced satisfactorily because of the existence of scission neutrons. It is indicated that this component should be subdivided in a weak 10 % and a hard (0.1 - 1) % part with $\bar{T}_{sc}$ parameters (Eq. 12) of about 1.1 and 2.3 MeV respectively.

More detailed experimental as well as theoretical investigations are necessary to clarify our knowledge about the nature of scission neutron emission. This concerns the measurement of N(E,θ:A,TKE) especially (for first results see for instance the Refs. [38,39]), but one should analyse the results carefully regarding necessary corrections of experimental effects and reference calculations on the base of evaporation models.

The presented study of the influences of input data and approximations on the calculated energy spectra are useful to evaluate the accuracy of evaporation calculations in general. It may give some clues for the further developement of fission neutron evaporation models.

In paragraph 6, we deduced necessary corrections of measured fission neutron spectra due to the anisotropic fragment detection. In general, this appearance cannot be neglected in precise spectrum measurements.

References

1 J. Terrell, Phys. Rev. 113(1959)527

2 D. W. Lang, Nucl. Phys. 53(1964)113

3 V. P. Sommer, A. E. Saval'ev, S. V. Shuchareva, Atomnaya Energiya 23(1967)327

4 G. Kluge, Phys. Lett. 37B(1971)217 and Proc. IAEA Consultants' Meeting on Prompt Fission Neutron Spectra (Vienna, 1971), IAEA, Vienna(1972)149

5 E. Nardi, L. G. Moretto, S. G. Thompson, Phys. Lett. 43B(1973)259

6 J. C. Browne, F. S. Dietrich, Phys. Rev. C10(1974)2545

7 B. F. Gerassimenko, V. A. Rubtchenya, A. V. Posgnyakov, Proc. 5th All Union Conf. on Neutron Physics (Kiev, 1980), Vol. III, 114

8 D. G. Madland, J. R. Nix, Proc. Int. Conf. on Nuclear Data for Science and Technology (Antwerp, 1982), in print

9 H. Märten, D. Seeliger, B. Stobinski, ibid.

10 H. Marten, D. Seeliger, submitted to J. of Phys. G

11 H. Marten, D. Neumann, D. Seeliger, Int. Conf. on the Interaction of Fast Neutrons with Nuclei (Gaußig, 1982), in print

12 V. F. Weisskopf, Phys. Rev. 52(1937)295 and J. M. Blatt, V. F. Weisskopf, Theoretical Nuclear Physics (New York, 1952)365

13 E. Vogt, in Advances in Nuclear Physics, edited by M. Baranger and E. Vogt (Plenum, New York, 1968), Vol. I,270

14 A. V. Ignatyuk, G. N. Smirenkin, A. S. Tishin, Yad. Fiz. 21(1975)485

15 A. V. Ignatyuk, K. K. Istekov, G. N. Smirenkin, Proc. 4th All Union Conf. on Neutron Physics (Kiev, 1977), Vol. I, 60

16 J. Dostrovsky et al., Phys. Rev. 116(1959)683

17 F. D. Becchetti, G. W. Greenless, Phys. Rev. 182(1969)1190

18 D. G. Madland, J. R. Nix, Nucl. Sci. Eng. 81(1982)213

19 A. Gavron, Phys. Rev. C13(1976)2561

20 H. Nifenecker, C. Signarbieux, R. Babinet, J. Poiton, Proc. 3rd IAEA Symp. on the Physics and Chemistry of Fission (Rochester, 1973), Vol. II, 117

21 A. Gavron, Z. Fraenkel, Phys. Rev. C9(1974)632

22 H. W. Schmitt, J. H. Neiler, F. J. Walter, Phys. Rev. 141(1966)1146

23 R. Böttger, H. Klein, A. Chalupka, B. Strohmaier, Proc. Int. Conf. on Nuclear Data for Science and Technology (Antwerp, 1982), in print

24 W. P. Poenitz, T. Tamura, ibid.

25 H. R. Bowman, S. G. Thompson, J. C. D. Milton, W. J. Swiatecki, Phys. Rev. 126(1962)2120

26 M. V. Blinov, N. M. Kazarinov, I. G. Krisyuk, Yad. Fiz. 16(1972)1155

27 C. J. Bishop, I. Halpern, R. W. Shaw, R. Vandenbosch, Nucl. Phys. A198(1972)161

28 Z. Fraenkel, I. Mayk, J. P. Unik, A. J. Gorski, W. D. Loveland, Phys. Rev. C12(1975)1809

29 V. M. Piksaikin, P. P. Dyatchenko, L. S. Kazaeva, Yad. Fiz. 25(1977)723

30 Ju. S. Samyatnin, D. K. Ryazanov, B. G. Basova, A. D. Rabinowitsch, V. A. Korostilev, Yad. Fiz. 29(1979)595

31 P. Riehs, Acta Physica Austriaca 53(1981)271

32 V. S. Stavinski, J. E. T. P. 36(1959)629

33 R. W. Fuller, Phys. Rev. 126(1962)684

34 G. A. Pik-Pitschak, Yad. Fiz. 10(1969)321

35 Y. Boneh, Z. Fraenkel, Phys. Rev. C10(1974)893

36 V. A. Rubtchenya, Preprint RI-28 (Leningrad, 1974)

37 J. W. Negele, S. E. Koonin, P. Möller, J. R. Nix, A. J. Sierk, Phys. Rev. C17(1978)1098

38 Yu. A. Vasil'ev et al., INDC(CCP)-177/L(1982)49

39 O. I. Batenkov, M. V. Blinov, G. S. Boykov, V. A. Vitenko, V. A. Rubtchenya, Contribution to this Meeting

40 H. Klein, Int. Conf. on the Interaction of Fast Neutrons with Nuclei (Gaußig, 1982), in print

41 A. Chalupka, Talk Presented at this Meeting

42 J. Grundl, C. Eisenhauer, Natl. Bur. Stds. Pub., NBS-493 (1977)

Information on the Cf-252 fission-neutron spectrum deduced from integral experiments

W. Mannhart
Physikalisch-Technische Bundesanstalt,
3300 Braunschweig, FR Germany

Abstract

Integral data (spectrum-averaged neutron cross sections) measured in the Cf-252 neutron field are compared with calculations mainly based on ENDF/B-V cross-section data and various spectrum representations. The experiments cover the energy range of the neutron spectrum between 1 MeV and 18 MeV. After a few ENDF/B-V data sets have been replaced by more recent evaluations, a fair consistency between experiments and calculations has been established. Two spectrum representations were identified which fit the experimental data over the whole energy range very well: the NBS segment fit evaluation and the evaporation theory of Madland and Nix in the version presented at the Antwerp conference.

1. Introduction

The measurement of spectrum-averaged neutron cross sections in a Cf-252 neutron field can be performed with high accuracy. Due to relatively small corrections, necessary to arrive at cross sections in an undisturbed neutron spectrum, the relative uncertainties which can be achieved are of the order of 2 - 3 % /1,3/. In the past, the comparison between experimentally determined spectrum-averaged cross sections, $\langle\sigma\rangle_{EXP}$, and calculated ones

$$\langle\sigma\rangle_{CALC} = \int_0^\infty \sigma(E)\ \chi(E)\ dE \quad \text{with} \int_0^\infty \chi(E)\ dE = 1 \qquad (1)$$

$\chi(E)$ being the normalized spectral distribution, has been chiefly used for cross-section validation purposes. With a sufficiently well-established neutron cross-section data base, Eq. (1) can also be applied for checking the shape of the neutron spectrum. In both cases, the calculated/experimental (C/E) ratio is an indicator of the quality of the data. For neutron spectrum validation purposes, the C/E value of an individual neutron reaction is of little use, due to the danger of a hidden error in the cross-section data base for this specific reaction. However, the bulk of C/E data covering a large energy range gives sufficient information on the shape of a smooth spectrum, i.e., integral data allow global effects to be recognized but should not be interpreted to deduce structural effects in the spectrum; a single C/E data point different from unity should be handled with particular care regarding its interpretation. An additional advantage of integral data is that the results of high-threshold reactions give access to the neutron energy range above 12 MeV where direct spectrum measurements are sparse due to inherent problems with adequate counting statistics.

2. Spectrum representations used

Only a selected set of the available spectrum representations has been used in the present comparison. The selection was governed by two facts: the spectrum representation should be valid over the whole energy range between 0 and 20 MeV and the normalization condition of Eq. (1) must be fulfilled. From the large set of direct spectrum measurements, only a single experiment has been chosen as representative. Due to the limited energy range covered by such experiments, special attention should be given to the fact that only integral detectors with energy responses within the energy range covered by the spectrum measurement can be compared.

2.1. NBS evaluation /4/

The NBS evaluation is based on experimental data up to 1974 and is a segment-adjusted fit. Relative to a Maxwellian of an average neutron energy of $\bar{E} = 2.13$ MeV (corresponding to a temperature parameter of T = 1.42 MeV), five energy-dependent correction segments have been applied. Between 0 and 6 MeV, the correction function is given by four linear segments and above 6 MeV, an exponential correction term is stated. Between 0.8 MeV and 6 MeV, the evaluation is, in essence, identical with the pure Maxwellian. Above 6 MeV, a deficit of neutrons compared to the Maxwellian is shown. In Fig. 1 all other spectrum representations are plotted relative to the NBS evaluation.

2.2. Evaporation theory of Madland and Nix /5-7/

Besides the neutron energy spectrum, the evaporation theory of Madland and Nix also allows the prompt neutron multiplicity $\bar{\nu}_p$ to be determined. This quantity can be used as an independent test parameter of the validity of the theory. The neutron spectrum is available in numerical form. The theory accounts for the following effects:

(a) the motion of the fission fragments

(b) the distribution of fission-fragment residual nuclear temperature

(c) the energy dependence of the cross section for the inverse process of compund-nucleus formation (based on optical potential parameters taken from Becchetti-Greenless; detailed references in /5/).

The result of the theory mainly depends on two parameters: the average energy release, $\langle E_r \rangle$, and the level density parameter, a. The average energy release is connected with $\langle E^* \rangle$, the initial total average fission-fragment excitation energy, by:

$$\langle E^* \rangle = \langle E_r \rangle - \langle E_f^{tot} \rangle \qquad (2)$$

with $\langle E_f^{tot} \rangle$ being the total average fission-fragment kinetic energy (185.9 MeV for Cf-252). The energy release for division into a pair of fission fragments is the difference between the mass of the fissioning compound nucleus and the masses of the two fission fragments. Its average is determined by integration over all fission-fragment mass and charge distributions. The maximum residual nuclear temperature is given by:

$$T_m = \sqrt{\langle E^* \rangle / a} \qquad (3)$$

The different versions of the theory are listed in Table I. The parameters used in the calculation of the average energy release and the value adopted for the level density parameter are given. In addition, the resulting average neutron energy and the $\bar{\nu}_p$ value are shown. The differences between the various versions of the theory are briefly reviewed. In the first version, M-N-1, the mass values were taken from 1977 Wapstra-Bos mass evaluation and in the missing case from the mass formula of Myers. The numbers in brackets indicate the number of masses taken from each source. The integration over the mass and charge distribution has been done in a 7-point approximation. The level density parameter has been assumed as A/11 (A being the mass number). The second version, M-N-2, differs from the first one in that the mass sources are replaced. The 1981 Wapstra-Bos mass evaluation and the Möller-Nix mass formula were used. All other parameters remained the same as before. The last version, M-N-3, replaced the 7-point approximation by an exact integration formula, and the somewhat arbitrary value of the level density parameter has been adjusted by fitting the theory with the experimental data of Boldeman /8/. Considering that problems also exist with Boldeman's data at higher neutron energies (see below), the last version of the evaporation theory gives values of the average neutron energy as well as of the neutron multiplicity which seem to be relatively realistic. The agreement of $\bar{\nu}_p$ with the experimental value of Spencer /9/ is satisfactory.

2.3. PTB/IRK experiment /10/

This TOF experiment has been analysed in the neutron energy range between 3 MeV and 13 MeV. The experimental points are shown in Fig. 1. The data were fitted with a Maxwellian with a temperature parameter of 1.355 MeV and a scaling factor of 1.08.

For comparison the data points of a recent ANL experiment /11/ are also shown in Fig. 1. This experiment covered the energy range between 0.25 MeV and 10 MeV. On the assumption of a Maxwellian distribution, a temperature parameter of 1.439 MeV, valid in this energy range, was determined.

3. Sources of $\sigma(E)$ data

Most neutron cross-section data were taken from ENDF/B-V. In addition, recent evaluations /12-16/ mainly performed at the IRK, Vienna, were also taken into account. A detailed list of the data sets used is given in Table II. In a few cases, the ENDF/B-V data should be replaced by other evaluations:

$^{27}Al(n,\alpha)$

The relatively old ENDF/B-V evaluation should be replaced by the new evaluation of Vonach /14/.

$^{47}Ti(n,p)$

For this reaction, a 30 % discrepancy between integral and energy-dependent cross-section data has been well-known for a long time. This discrepancy seems to have been eliminated by recent ANL/PTB cooperation. In a parallel work, the energy-dependent cross section and the Cf-252 spectrum-averaged cross section have been remeasured. The experiments were interconnected by using the same activity counting detector for both groups of data. Work is in progress on the final analysis /17/.

^{58}Ni(n,2n)

The recent evaluation and measurements performed by Winkler /15/ are more consistent with integral data experiments.

^{63}Cu(n,α)

The ENDF/B-V data set of this reaction presents some problems. It should be replaced by a recent evaluation by Winkler /16/.

In the case of the reaction ^{59}Co(n,p), two different data sources were used. From threshold up to 10 MeV, the data are based on Ref. /18/. Above 10 MeV, data were taken from Ref. /19/.

4. Results

In Fig. 2 the data are given in the form of ratios of calculated Cf-252 spectrum-averaged cross sections relative to the experimental values. The C/E values were determined with different spectrum representations. The NBS evaluation /4/ as well as a pure Maxwellian with a temperature parameter of 1.42 MeV were applied. In the figure the results obtained with the versions M-N-1 and M-N-2 of the Madland-Nix theory are also shown. The reactions are selected in such a way that their energy responses overlap with the range from 3 to 13 MeV covered by the PTB/IRK spectrum experiment /10/. The reactions are ordered according to their energy response ranges (for details, see Figs. 4 and 5) with ranges at lower energies on the left-hand side and at higher energies on the right-hand side of the figure.

It should be mentioned that such a comparison cannot be based alone on the uncertainties of the integral data. The energy-dependent neutron cross-section data, with relative uncertainties mostly larger than 5 %, represent an essential uncertainty source which must be taken into account. These uncertainties, taken from the covariances files, have therefore been processed to the $\langle\sigma\rangle$ values. The given error bars (shown alone for the NBS evaluation) include the combined uncertainty of the integral experiments and of the σ(E) data.

The sensitivity of the integral data as regards the shape of the neutron spectrum can easily be understood from the plots of Fig. 2. Taking the reaction ^{63}Cu(n,α) with an energy response range between 4.9 MeV and 11.5 MeV as an example, one recognizes from Fig. 1 that the theory M-N-1 overestimates the neutron spectrum in this range by between 12 % and 47 % in comparison with the NBS evaluation. This situation is clearly reflected in the data point based on this version of the theory which, due to the averaging process, is about 26 % higher than that obtained with the NBS evaluation.

Fig. 2 shows that versions M-N-1 and M-N-2 of the Madland-Nix theory disagree with the experimental data points. The values based on the PTB/IRK spectrum experiment are compatible with the integral data within the error bars. Above 6 MeV, these data are approximately 5 % lower than those obtained with the NBS evaluation and in most cases lie at the lowest boundaries of the error bars. One also recognizes that at lower neutron energies, the results obtained with the NBS evaluation and with a pure Maxwellian (T = 1.42 MeV) are relatively similar. Above 6 MeV both groups of data show a clear tendency to diverge.

This effect is even more pronounced in Fig. 3, which covers the neutron energy range between 9 MeV and 18 MeV. The fact that the integral data are in better agreement with the NBS evaluation than with the Maxwellian at high neutron energies is additionally confirmed by a recent spectrum experiment /20/ covering the neutron energy range above 10 MeV. This is all contrary to Boldeman's spectrum results /8/ indicating a Maxwellian of T = 1.424 MeV between 0.6 MeV and 15 MeV. Fig. 3 also shows that at high neutron energies, the data points obtained with the theory M-N-2 become lower than those obtained with the pure Maxwellian. This fact is understandable if we look at Fig. 1. Nevertheless, neither of the spectrum representations is compatible with the integral data at high neutron energies.

Figs. 4 and 5 summarize all the integral data experiments performed at the PTB. For each reaction the 90 % energy response range (i.e., the energy corresponding to a response of 5 % and 95 %) in the Cf-252 neutron spectrum is shown. The experimental data points are compared with calculations based on the NBS spectrum representation /4/ and on the recent version (M-N-3) of the Madland-Nix evaporation theory /7/. The various sources of $\sigma(E)$ data are indicated in Table 2. In the case of the reaction ^{47}Ti(n,p), the improvement due to the preliminary ANL/PTB data /17/ compared with the ENDF/B-V is obvious. The same is valid for ^{63}Cu(n,α) if the ENDF/B-V data set is replaced by Winkler's evaluation /16/. Also in the case of the reaction ^{27}Al(n,α), consistency is increased by replacing the ENDF/B-V cross-section data with Vonach's evaluation /14/. There is also real improvement of the integral data point at the highest neutron energy range ^{58}Ni(n,2n) when the ENDF/B-V set is replaced by a recent evaluation /15/.

The data in Figs. 4 and 5 show that the NBS evaluation of the neutron spectrum as well as the recent Madland-Nix theory (M-N-3) are almost compatible with the whole set of integral data experiments within the given error bars. The only exception is the data point of the reaction ^{60}Ni(n,p). Due to the results of reactions with similar energy response ranges, namely ^{63}Cu(n,α) and ^{56}Fe(n,p), it is obvious that the discrepancy cannot be attributed to the neutron spectrum. At present it is not clear whether the integral data point or the $\sigma(E)$ data are wrong. Investigations to solve this problem are being carried out.

The data in Fig. 5 do not clearly confirm the trend of the evaporation theory (M-N-3) above 13 MeV, which indicates an additional deficit of neutrons in comparison with the NBS evaluation as shown in Fig. 1. It must also be mentioned that the fair consistency of the integral data with the NBS evaluation does not extend to the energy range below 1 MeV. In this energy range the NBS evaluation indicates some structure. It is beyond the scope of the present data to confirm this structure. Recent spectrum experiments /21/ have produced results contrary to such a structure.

5. Conclusions

The results of integral experiments were compared with calculations with the aim of testing the validity of various representations of the fission-neutron spectrum of Cf-252. After the ENDF/B-V cross section data sets of ^{27}Al(n,α), ^{47}Ti(n,p), ^{58}Ni(n,2n) and ^{63}Cu(n,α), had been replaced by other evaluations, a fair consistency between experiments and calculations was found. Only neutron threshold reactions which covered the neutron energy range between 1 MeV and 18 MeV were investigated. Within this range two spectrum representations were identified as in general adequate: the NBS evaluation and the last version of the Madland-Nix evaporation theory. The trend of this theory at high neutron energies (above 13 MeV) remains somewhat questionable. The integral data also showed a fair consistency with recent spectrum experiments (ANL, PTB/IRK and Blinov's work) within the energy ranges covered by these experiments.

References:

/1/ W. Mannhart, Nucl. Sci. Eng. 77, 40 (1981)

/2/ "Nuclear Data for Science and Technology" (ed. K.H. Bockhoff), Proc. Int. Conf., Antwerp, 6-10 September 1982, D. Reidel Publishing Company (1983)

/3/ W. Mannhart, Antwerp Conference /2/, p. 429 (1983)

/4/ J. Grundl, C. Eisenhauer, IAEA-TECDOC 208, Vol.I, p. 53 (1978)

/5/ D.G. Madland, J.R. Nix, Nucl. Sci. Eng. 81, 213 (1982)

/6/ D.G. Madland, priv. comm. (1982)

/7/ D.G. Madland, J.R. Nix, Antwerp Conference /2/, p. 473 (1983)

/8/ J.W. Boldeman, D. Culley, R.J. Cawley, Trans. Am. Nucl. Soc. 32, 733 (1979)

/9/ R.R. Spencer, R. Gwin, R. Ingle, Nucl. Sci. Eng. 80, 603 (1982)

/10/ R. Böttger, H. Klein, A. Chalupka, B. Strohmaier, Antwerp Conference /2/, p. 484 (1983)

/11/ W.P. Poenitz, T. Tamura, Antwerp Conference /2/, p. 465 (1983)

/12/ B. Strohmaier, S. Tagesen, H. Vonach, Physics Data 13-2 (1980)

/13/ S. Tagesen, H. Vonach, B. Strohmaier, Physics Data 13-1 (1979)

/14/ S. Tagesen, H. Vonach, Physics Data 13-3 (1981)

/15/ G. Winkler, A. Pavlik, H. Vonach, A. Paulsen, H. Liskien, Antwerp Conference /2/, p. 400 (1983)

/16/ G. Winkler, D.L. Smith, J.W. Meadows, Nucl. Sci. Eng. 76, 30 (1980)

/17/ D.L. Smith, J.W. Meadows, W. Mannhart, preliminary data (1983)

/18/ D.L. Smith, J.W. Meadows, Nucl. Sci. Eng. 60, 187 (1976)

/19/ G. Vasiliu, S. Mateescu, INDC(NDS)-103/M, p. 26 (1979)

/20/ H. Maerten, D. Seeliger, B. Stobinski, INDC(GDR)-17/L (May 1982)

/21/ M.V. Blinov, G.S. Boykov, V.A. Vitenko, Antwerp Conference /2/, p. 479 (1983)

Table I

Evaporation theory of Madland-Nix

Version	Average Energy Release			Level Density Parameter MeV^{-1}	Average Neutron Energy MeV	Prompt Neutron Multiplicity $\bar{\nu}_p$	Ref.
	$\langle E_r \rangle$ MeV	Mass Source	Integration				
M-N-1	219.408	WAPSTRA 77 (7) MYERS (7)	7-point approx.	a = A/11	2.2791	3.803	/5/
M-N-2	216.581	WAPSTRA 81 (10) MÖLLER-NIX (5)	7-point approx.	a = A/11	2.2167	3.554	/6/
M-N-3	218.886	WAPSTRA 81 (10) MÖLLER-NIX (5)	exact	a = A/9.6	2.168	3.791	/7/
				EXPERIMENT		3.773 (7)	/9/

Table II

Sources of $\sigma(E)$ data

Reaction	$\sigma(E)$-data from			
	ENDF/B-V	to be replaced by	Other	Ref.
$^{19}F(n,2n)$			Vonach	/12/
$^{24}Mg(n,p)$			Vonach	/13/
$^{27}Al(n,p)$	x			
$^{27}Al(n,\alpha)$	x	→	Vonach	/14/
$^{46}Ti(n,p)$	x			
$^{47}Ti(n,p)$	x	→	ANL/PTB	/17/
$^{48}Ti(n,p)$	x			
$^{55}Mn(n,2n)$	x			
$^{54}Fe(n,p)$	x			
$^{56}Fe(n,p)$	x			
$^{59}Co(n,p)$			Smith/Vasiliu	/18,19/
$^{59}Co(n,\alpha)$	x			
$^{59}Co(n,2n)$	x			
$^{58}Ni(n,p)$	x			
$^{58}Ni(n,2n)$	x	→	Winkler	/15/
$^{60}Ni(n,p)$	x			
$^{63}Cu(n,\alpha)$	x	→	Winkler	/16/
$^{63}Cu(n,2n)$			Vonach	/13/
$^{64}Zn(n,p)$			Vonach	/13/
$^{90}Zr(n,2n)$			Vonach	/13/
$^{115}In(n,n')$	x			
$^{197}Au(n,2n)$	x			

Figure Captions

Fig. 1: Various neutron spectrum representations compared with the NBS evaluation /4/. On the right-hand side of the figure the corresponding average neutron energies, $\bar{E}$, are given. The Maxwellian with $\bar{E}$ = 2.13 MeV corresponds to a temperature parameter of T = 1.42 MeV. The curves indicated by M-N-x are based on different versions of the Madland-Nix evaporation theory (see Table I). The experimental data are from Refs. /10/ and /11/.

Fig. 2: Comparison between calculated and experimental responses of neutron activation detectors. The figure covers the neutron energy range of the PTB/IRK spectrum experiment /10/. The data marked with (+) correspond to the theory M-N-1 and those with (Δ) to the theory M-N-2.

Fig. 3: As in Fig. 2, but for high-threshold reactions.

Fig. 4 and Fig. 5: Same representation as in Fig. 2. For each reaction the neutron energy corresponding to a response of 5 % and 95 % is shown. A distinction is made between $\sigma(E)$ data taken from ENDF/B-V and those from other sources (see table II). The spectrum representations used are the NBS evaluation /4/ and the modified Madland-Nix evaporation theory (M-N-3) /7/.

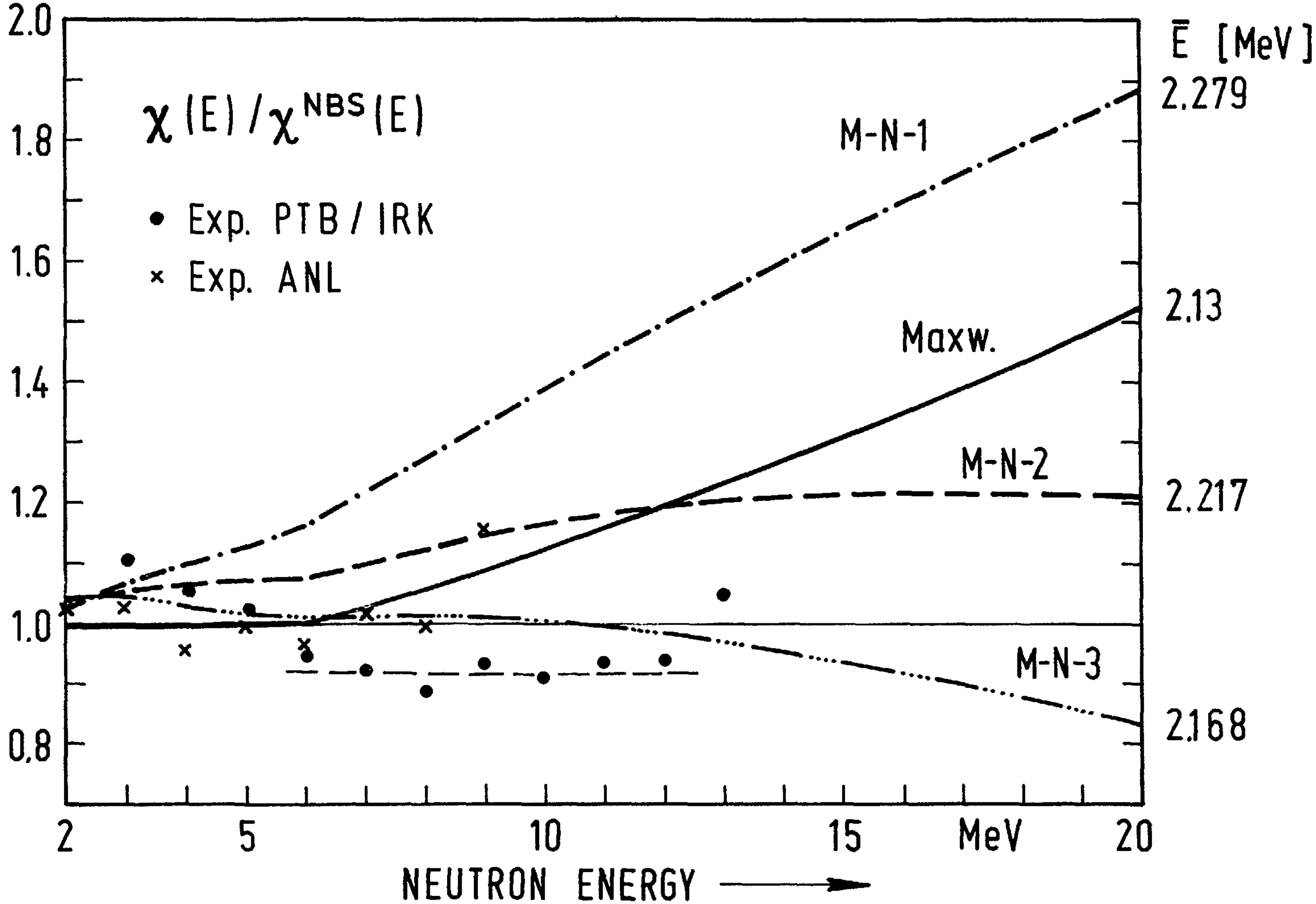
χ(E)/χ^NBS(E)
• Exp. PTB/IRK
× Exp. ANL
M-N-1
Maxw.
M-N-2
M-N-3
Ē [MeV]
2.279
2.13
2.217
2.168
2.0
1.8
1.6
1.4
1.2
1.0
0.8
2
5
10
15
MeV
20
NEUTRON ENERGY

Fig. 1

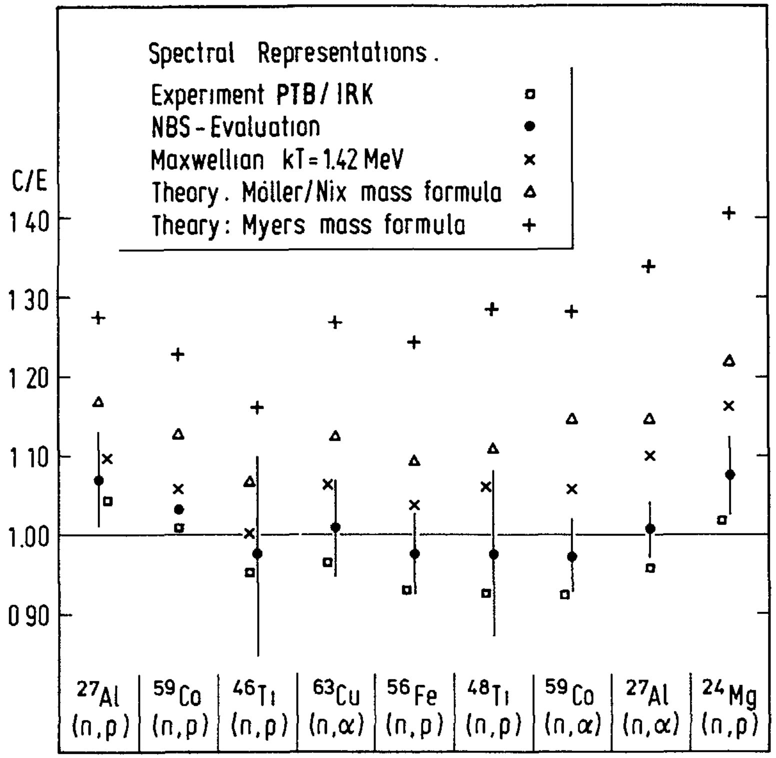

Spectral Representations.
Experiment PTB/IRK
NBS-Evaluation
Maxwellian kT = 1.42 MeV
Theory. Möller/Nix mass formula
Theory: Myers mass formula
C/E
1.40
1.30
1.20
1.10
1.00
0.90
27Al (n,p)
59Co (n,p)
46Ti (n,p)
63Cu (n,α)
56Fe (n,p)
48Ti (n,p)
59Co (n,α)
27Al (n,α)
24Mg (n,p)

Fig. 2

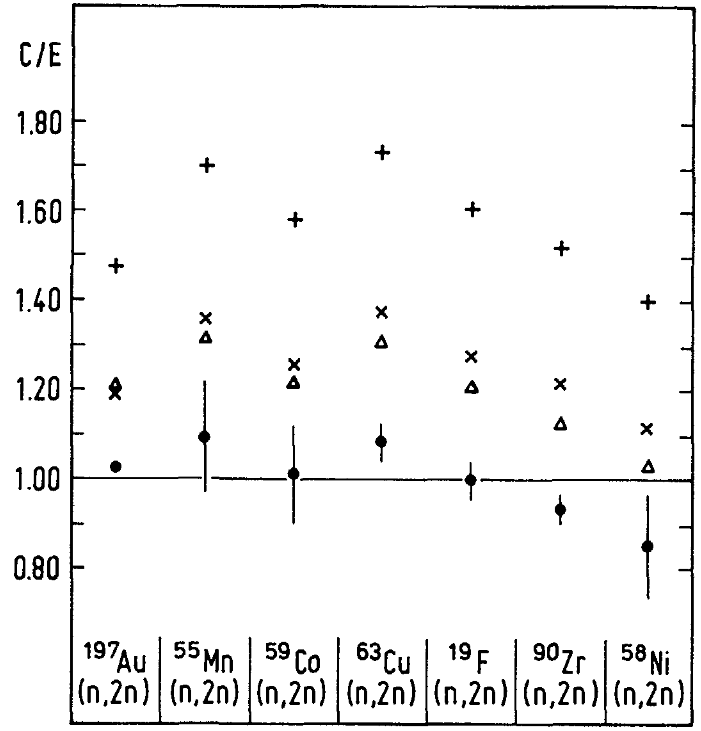

C/E
1.80
1.60
1.40
1.20
1.00
0.80
197Au (n,2n)
55Mn (n,2n)
59Co (n,2n)
63Cu (n,2n)
19F (n,2n)
90Zr (n,2n)
58Ni (n,2n)

Fig. 3

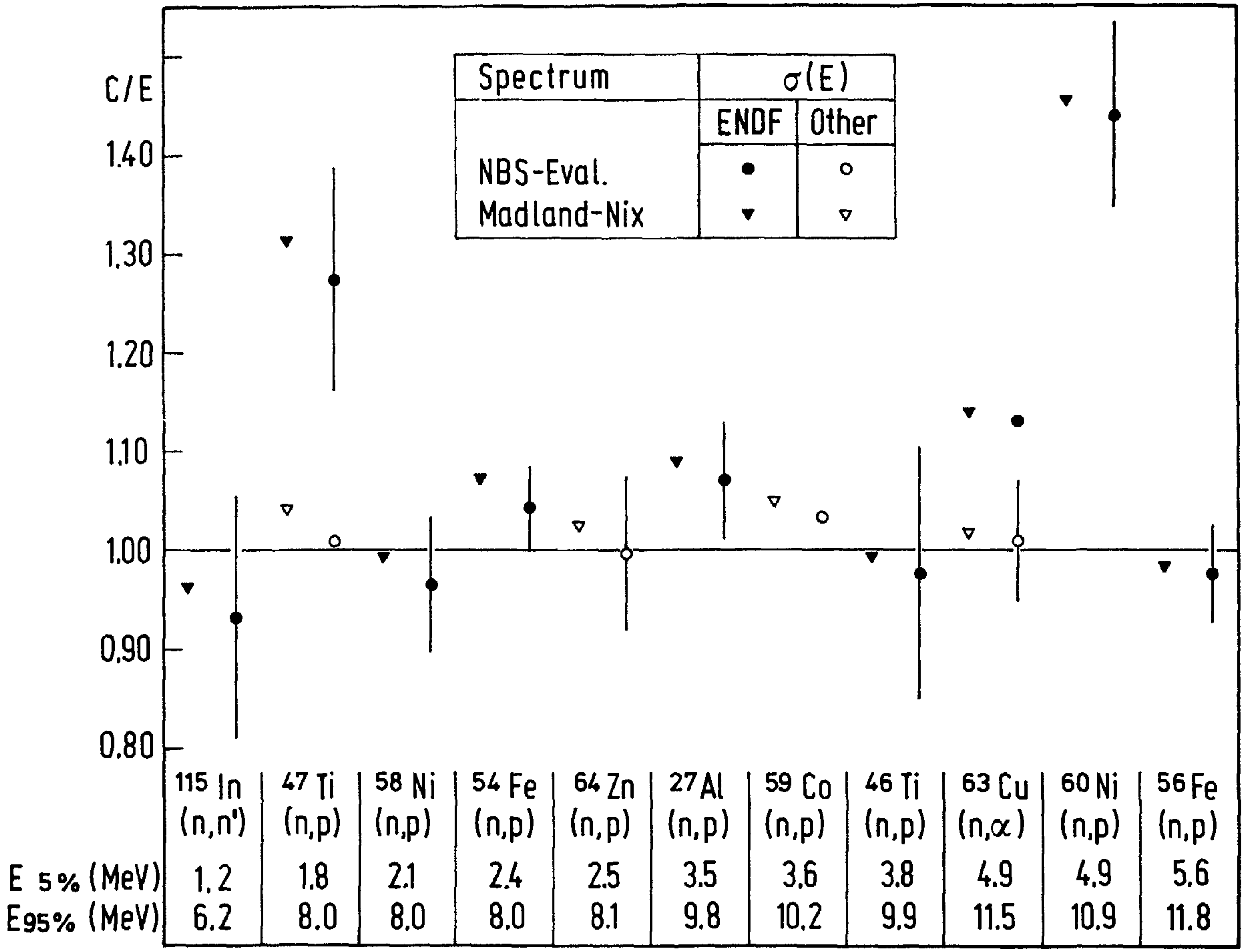
C/E
1.40
1.30
1.20
1.10
1.00
0.90
0.80
Spectrum
σ(E)
ENDF
Other
NBS-Eval.
Madland-Nix
115 In (n,n')
47 Ti (n,p)
58 Ni (n,p)
54 Fe (n,p)
64 Zn (n,p)
27 Al (n,p)
59 Co (n,p)
46 Ti (n,p)
63 Cu (n,α)
60 Ni (n,p)
56 Fe (n,p)
E 5% (MeV) 1.2 1.8 2.1 2.4 2.5 3.5 3.6 3.8 4.9 4.9 5.6
E95% (MeV) 6.2 8.0 8.0 8.0 8.1 9.8 10.2 9.9 11.5 10.9 11.8

Fig. 4

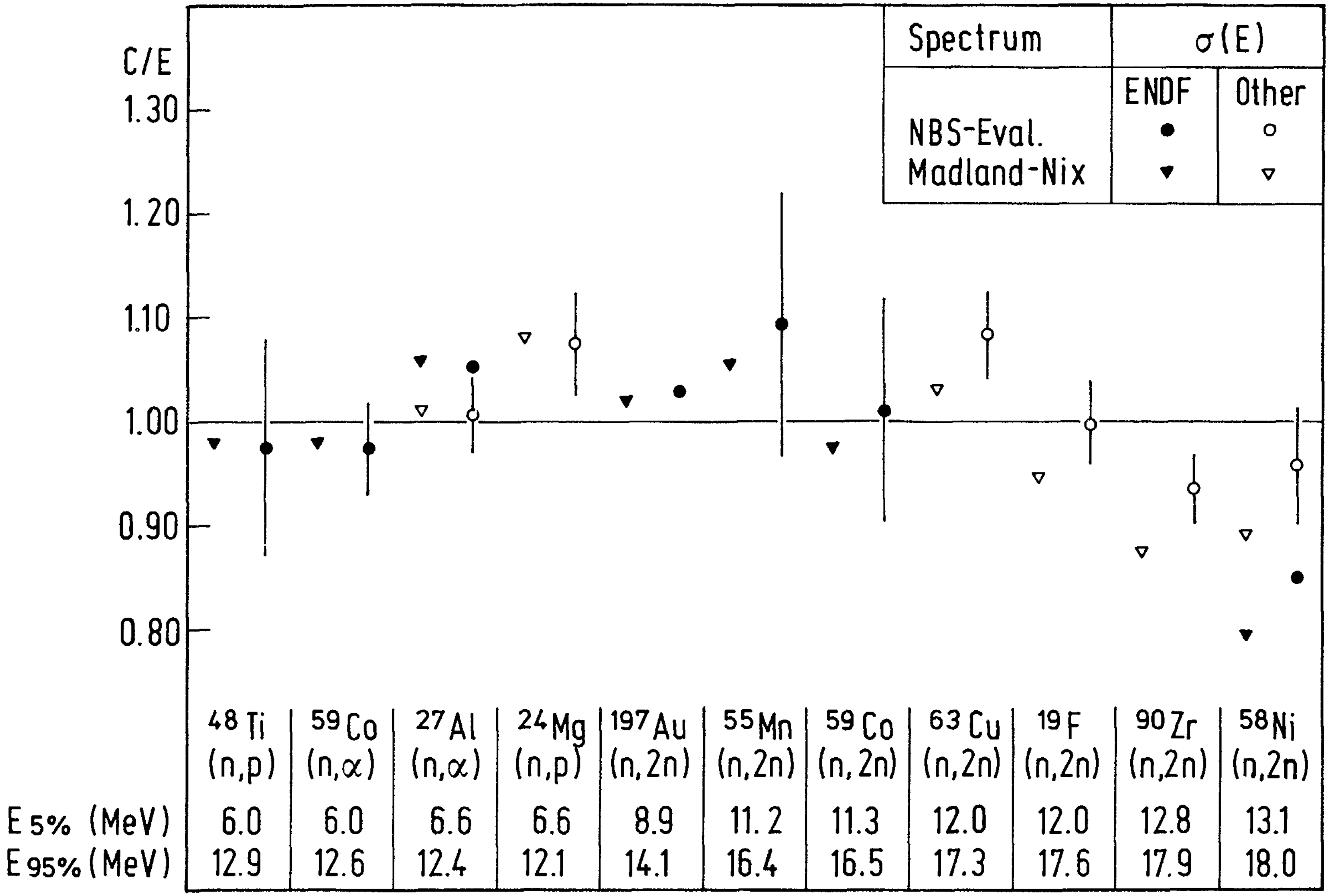
C/E
1.30
1.20
1.10
1.00
0.90
0.80
Spectrum
σ(E)
ENDF
Other
NBS-Eval.
Madland-Nix
48 Ti (n,p)
59 Co (n,α)
27 Al (n,α)
24 Mg (n,p)
197 Au (n,2n)
55 Mn (n,2n)
59 Co (n,2n)
63 Cu (n,2n)
19 F (n,2n)
90 Zr (n,2n)
58 Ni (n,2n)
E 5% (MeV) 6.0 6.0 6.6 6.6 8.9 11.2 11.3 12.0 12.0 12.8 13.1
E 95% (MeV) 12.9 12.6 12.4 12.1 14.1 16.4 16.5 17.3 17.6 17.9 18.0

Fig. 5

Measurements of Cf-252 Spectrum Averaged Cross Sections

Z. Dezső and J. Csikai

Institute of Experimental Physics, Kossuth University
H-4001 Debrecen, P.O.Box 105
Hungary

Abstract

Reaction rate measurements have been performed for eight reactions-having well characterized nuclear parameters in a pure Cf-252 fission neutron field relative to the $^{115}In/n,n'/\ ^{115m}In$ reaction. Results obtained under modified experimental conditions compared to our recently published data show better reproducibility and are in general agreement with other $\bar{\sigma}$ data in the literature.
In order to establish integral cross sections for Cf-252 fission neutrons with high accuracy experimental investigations have also been started to study the effect of source encapsulation on neutron flux perturbation.
This short communication reports our preliminary results.

Introduction

Californium-252 spectrum averaged cross sections are of great importance especially for reactor neutron dosimetry applications. Using reactions with well known energy dependent cross sections it is also possible to test the fission neutron spectrum representations obtained in the different experiments or using theoretical calculations. This kind of application of integral data has now become especially important if one considers, that most of the recently reported experimental data for Cf-252 spontaneous fission neutron spectrum are based on very similar experimental methods.
In this respect even simple integral data might be useful as can give indication on some systematical errors of the

differential spectrum measurements.

The work reported here is a continuation of our work begun previously [1-3] on integral cross section data in the Cf-252 spontaneous fission neutron field. The recently published new data [4] have been derived from reaction rate measurements made under improved experimental conditions using a small Cf-252 source. The overall reproducibility of these new measurements was found not to be better than ± 2 percent and thus can not be considered adequte to result $\bar{\sigma}$ data with high precision. Therefore additional measurements have been done for some of the reactions investigated using modified irradiation geometry. The so called compensated beam geometry [5] used in this set of measurements made it also possible to perform some experiments for the investigation of the effect of source encapsulation for the $\bar{\sigma}$ data. In addition to the new cross section values this paper reports also the preliminary results of these measurements.

Experimental

The californium source used in this experiment contains about 35 μg of ^{252}Cf and is double encapsulated in a stainless steel cylinder. The diameter and height of the source are 7 mm and 14 mm respectively.
For the irradiations the source is put in a Aluminium container having 0.25 mm wall thickness and 16 mm height. The exact location of the Ø 3x3.5 mm^3 ^{252}Cf core have been determined experimentally [4]. All irradiations have been performed in the open air as described in ref. [4].
The irradiation facility consists of a 0.2 mm thick Aluminium frame which holds on its opposite sides the two identical foils of 10 mm in diameter and 0.2 mm thick to be activated.

The samples are positioned using Aluminium rings with 0.5 by 0.5 mm^2 cross section which are constantly fixed on the frame. The frame has a Ø 7.6 mm hole on the top and the source is introduced through this for the irradiations. In this arrangement the separation between the foils is about 14 mm.
To the investigation of effect of source encapsulation for the reaction rates 14 mm long stainless steel cylinders with different outer but the same I.D. have been put between the source and the foils. Using this "extra encapsulation" in four steps the wall thickness of the source could be doubled. Under such experimental conditions both gold and indium foils have been irradiated.
The time of irradiations were set according to the half-life of the investigated radionuclide but lasted at least for 5 hours to decrease uncertainties in irradiation time. The longest activation lasted 10 days in this set of experiments.
The γ-activity of the foils have been measured by an efficiency- calibrated Ge/Li/ detector, in most cases using two counting geometry with different distance from the detector.
Since these integral cross section measurements are not considered to be complete at the moment details of corrections applied and method of data evaluation are not given here.

Results

Since there was not any direct measurement to determine the source strength of the ^{252}Cf-source, all $\bar{\sigma}$ values are given relative to the ^{115}In/n,n'/^{115m}In reaction accepting $\bar{\sigma}$=196.4 mb for the latter as reported in ref[6]. Spectrum averaged cross section data obtained in the present experiment are presented in Table 1. For comparison the evaluated $\bar{\sigma}$ values of Mannhart [6] are also given with their

quoted overall uncertainties.
Although detailed analysis of uncertanintıes is not yet available a rough estimate shows that the total uncertainty of the presently reported $\bar{\sigma}$ data will not exeed ±3 %.

Table 1. Measured averaged cross sections in mb.

Reaction	$\bar{\sigma}_{measured}$	$\bar{\sigma}_{evaluated}$
$^{27}Al/n,p/^{27}Mg$	4.80	4.825/±3.2 %/
$^{54}Fe/n,p/^{54}Mn$	85.1	85.58 /±2.0 %/
$^{56}Fe/n,p/^{56}Mn$	1.41	1.446/±2.1 %/
$^{58}Ni/n,p/^{58}Co$	117.2	115.0 /±1.7 %/
$^{113}In/n,n'/^{113m}In$	161.9	160.8 /±2.0 %/
$^{115}In/n,\gamma/^{116}In$	123.2	124.6 /±2.6 %/
$^{197}Au/n,\gamma/^{198}Au$	76.0	76.17/±2.0 %/
$^{197}Au/n,2n/^{196}Au$	5.55	5.461/±2.2 %/

Several measurements on the same reaction resulted better reproducibility of $\bar{\sigma}$ values in this case than prevously reported [4]. Since counting geometry basically were the same in both cases this is certainly due to the more precise irradiation arrangement.
The presently achived ± 1.4 % reproducibility can probably be further improved if two indium foils are simultanously activated with the foil to be irradiated, one being in front of and the other behind the sample. Measurements in this sandwich geometry are now in progress for all the reactions having been involved in this experiment.
Up to now the results of two complete set of measurements for neutron flux perturbation of source encapsulation are available.
The reaction rates obtained with the different additional cylinders clearly show the effect of encapsulation in case of $^{197}Au/n,\gamma/$ reaction as they tend to increase as the thickness of stainless steel increases. In the case of $^{197}Au/n,2n/$ the opposite trend can be observed, however it is not so significant as in the previous case. Using the $^{115}In/n,n'/$ reaction for such investigations no effect of encapsulation could be observed. It should be noted that the effects mentioned above are relatively small and do not exeed 3 percent. To get more reasonable figures on flux perturbation, measurements with higher precision are needed than the presently available 1.4%. Using the sandwich technique it is hoped to achive the required accuracy both for gold and indium foils.
The final results of averaged cross section measurements together with their covariance matrix and also the results of flux perturbation measurements are planned to be completed by July of this year.

References

1. Z. Dezső, J. Csikai, Proc. IV. All Union Conf. on Neutron Physics, Kiev, Vol. III., pp 32 /1977/ Atomizdat.
2. Z. Dezső, J. Csikai, Proc. VII. Symp. on Interactions of Fast Neutrons with Nuclei. Gaussig, pp.44 /1977/
3. Z. Dezső, J. Csikai, INDC/NDS/-1o3/M, pp. 176 /1979/
4. Z. Dezső, J. Csikai, Proc. Int. Conf. on Nuclear Data for Science and Technology /Antwerp, 1982/, in print
5. H. T. Heaton II, et al., Proc. Conf. on Nucl. Cross Sections and Techn. , NBS Special Publication 425, Vol. 1, pp. 266. /1975/
6. W. Mannhart, Proc. Int. Conf. on Nuclear Data for Science and Techn. /Antwerp, 1982/, in print

Approaches for the generation of a covariance matrix for the Cf-252 fission-neutron spectrum

W. Mannhart
Physikalisch-Technische Bundesanstalt
3300 Braunschweig, FR Germany

Abstract

After a brief retrospective glance is cast at the situation, the evaluation of the Cf-252 neutron spectrum with a complete covariance matrix based on the results of integral experiments is proposed. The different steps already taken in such an evaluation and work in progress are reviewed. It is shown that special attention should be given to the normalization of the neutron spectrum which must be reflected in the covariance matrix. The result of the least-squares adjustment procedure applied can easily be combined with the results of direct spectrum measurements and should be regarded as the first step in a new evaluation of the Cf-252 fission-neutron spectrum.

1. Introduction

The generation of a covariance matrix for the Cf-252 neutron spectrum has been an outstanding problem for some time. Up to now, the only approach made towards finding a solution has been an attempt to generate the matrix by attributing a 2 % uncertainty to a temperature parameter of T = 1.42 MeV of a Maxwellian /1/. This approach is far from satisfactory, as it is not based on any experimental data. The reason for this surprising lack of information is due to an inherent problem in earlier neutron spectrum measurements. None of these experiments provides enough information to allow a reliable covariance matrix to be deduced. It is also probably unrealistic to expect that such experiments can be re-analysed in detail to obtain the necessary covariance information.

Since the Antwerp conference /2/, a real improvement of this situation can be anticipated. A few recent spectrum measurements /3-6/ were presented, most of which were at a preliminary stage, i.e., the final analysis of these data has still to be made. In this context, there is a great demand to take advantage of the opportunity to use the final analysis for a parallel generation of a covariance matrix of the experimental data.

Within the scope of generating a covariance matrix valid over the whole energy range (between 0 MeV and 20 MeV) of the Cf-252 neutron spectrum, the spectrum measurements can only attribute partial components, due to the limited energy ranges of the individual experiments. A way out of this situation would be the combination of these data with those obtained from integral experiments /7/. In the following, the principles of a least-squares adjustment procedure based on integral data with the aim of generating a covariance matrix are shown. The result of this procedure can be regarded as the first step towards a new evaluation of the Cf-252 neutron spectrum in the future. The later combination of this result with the partial covariances of the spectrum experiments seems to be a sound basis for a realistic evaluation of the Cf-252 neutron spectrum and its covariance matrix.

2. Least-squares adjustment based on integral data

2.1. Principles

The methodology is first shown in a general form. Necessary modifications for application to the Cf-252 problem are explained in the following sections.

In the given notation, capital letters indicate vectors or, if underlined, matrices. Small letters with subscripts are used to indicate their components. The superscript (T) stands for a transpose and (-1) indicates an inversion.

A set (dimension m) of experimental activation detector responses described by a vector and an appropriate covariance matrix /8/ are assumed:

$$A^o = (a_i^o) \text{ with an (absolute) covariance matrix } \underline{N}_{A^o}. \qquad (1)$$

The index i stands for a specific neutron reaction. The components of this vector are compared with calculated results (prior information)

$$a_i = \int_0^\infty \sigma^i(E) \quad \phi(E) \; dE, \qquad (2)$$

with $\sigma^i(E)$ being the energy-dependent cross section of the neutron reaction i and $\phi(E)$ being the neutron flux density describing the neutron spectrum. In a group representation, Eq. (2) is replaced by

$$a_i = \sum_{j=1}^{n} \sigma_j^i \; \phi_j \qquad (i=1,m) \quad . \qquad (3)$$

The calculated data are summarized by the vector

$$A = (a_i) = (\Sigma_i^T \; \Phi) \qquad (4)$$

with the group cross section and group flux density vectors

$$\Sigma_i = \begin{pmatrix} \sigma_1^i \\ \sigma_2^i \\ \vdots \\ \sigma_n^i \end{pmatrix} \quad \text{and} \quad \Phi = \begin{pmatrix} \phi_1 \\ \phi_2 \\ \vdots \\ \phi_n \end{pmatrix} \qquad (5)$$

The least-squares adjustment minimizes the expression /9/

$$\chi^2 = (A^o - A)^T \left[\underline{N}_A + \underline{N}_{A^o}\right]^{-1} (A^o - A) \qquad (6)$$

with

$$\underline{N}_A = \underline{G} \; \underline{N}_P \; \underline{G}^T \; . \qquad (7)$$

The parameter vector and its covariance matrix are given by

$$P = \begin{pmatrix} \Phi \\ \Sigma \end{pmatrix} \quad \text{and} \quad \underline{N}_P = \begin{pmatrix} \underline{N}_\Phi & 0 \\ 0 & \underline{N}_\Sigma \end{pmatrix} \qquad (8)$$

The vector Σ contains the vectors of the individual cross-section sets Σ_i

$$\Sigma = \begin{pmatrix} \Sigma_1 \\ \Sigma_2 \\ \vdots \\ \Sigma_m \end{pmatrix} \qquad (9)$$

$\underline{G}$ is a sensitivity matrix which transforms the parameters to the measured quantities:

$$\underline{G} = \frac{dA}{dP} = \begin{pmatrix} \Sigma_1^T & \Phi^T & 0 \; \ldots\ldots \; 0 \\ \Sigma_2^T & 0 & \Phi^T \ldots\ldots \; 0 \\ \vdots & \vdots & \vdots \\ \Sigma_m^T & 0 & 0 \; \ldots\ldots \; \Phi^T \end{pmatrix} \qquad (10)$$

The solution of Eq. (6) results in a new, adjusted parameter vector P' and a corresponding covariance Matrix $\underline{N}_P'$:

$$P' = P + \underline{N}_P \; \underline{G}^T \left[\underline{N}_A + \underline{N}_{A^o}\right]^{-1} (A^o - A) \qquad (11)$$

and

$$\underline{N}_P' = \underline{N}_P - \underline{N}_P \; \underline{G}^T \left[\underline{N}_A + \underline{N}_{A^o}\right]^{-1} \underline{G} \; \underline{N}_P^T \qquad (12)$$

Two facts should be noted: the covariance matrix of the parameter vector (prior information) $\underline{N}_P$ shows no correlations between cross sections and neutron spectrum (see Eq. (8)). This does not remain valid after the adjusting process, i.e., $\underline{N}_P'$ of Eq. (12) establishes such correlations. Secondly, the matrix which is to be inverted (see Eqs. (6), (11) and (12)) is of the dimension m of the set of activation detectors and does not depend on the fineness of the group structure chosen.

The solution of Eqs. (11) and (12) can be found using the computer codes STAY'SL /9/ and FERRET /10/. The difference between these codes is that STAY'SL solves Eqs. (11) and (12) only for ϕ, whereas the FERRET code offers the full solution.

2.2 Special case: normalized spectrum

Up to now, we have not considered that the Cf-252 fission-neutron spectrum is normalized in the sense that its total energy integral is unity. Special attention should be paid to this fact, otherwise the result of the procedure described in Section 2.1. applied to Cf-252 would be wrong. The neutron activation detector responses measured in the Cf-252 neutron field in form of spectrum-averaged cross sections /7/ are normalized quantities:

$$\langle\sigma\rangle_i = \sum_{j=1}^{n} \sigma_j^i \, \phi_j / Q \quad \text{with} \quad Q = \sum_{j=1}^{n} \phi_j \tag{13}$$

or written in a modified notation

$$\langle\sigma\rangle_i = \sum_{j=1}^{n} \sigma_j^i \, \chi_j \quad \text{with} \quad \chi_j = \frac{\phi_j}{Q} \tag{14}$$

with the normalization condition of

$$\sum_{j=1}^{n} \chi_j = 1, \tag{15}$$

i.e., in the case of the Cf-252 neutron spectrum, we must replace the following quantities of Section 2.1. by:

$$\begin{aligned} a_i^o &\longrightarrow \langle\sigma\rangle_i \\ \phi &\longrightarrow \chi \\ \underline{N}_\phi &\longrightarrow \underline{N}_\chi \end{aligned} \tag{16}$$

Due to the side condition of Eq. (15), the covariance matrix of the normalized neutron spectrum, $\underline{N}_\chi$, has a special structure in that the sum over each row and over each column of the <u>absolute</u> covariance matrix must be zero. This can easily be understood. The adjustment of the Cf-252 neutron spectrum in a certain energy range requires a compensation in other energy ranges to conserve the normalization of Eq. (15). The special structure of the absolute covariance matrix automatically takes this into account. It can be shown that the least-squares formalism conserves such a normalization, i.e., with normalized prior information in Eq. (8) in the form of χ and $\underline{N}_\chi$, the adjusted result of Eqs. (11) and (12), χ' and $\underline{N}_\chi'$, remains normalized.

The covariance matrix of a neutron spectrum which does not take the normalization into account can easily be transformed to the normalized case. The transformation rule is given by

$$\underline{N}_\chi = \underline{S} \; \underline{N}_\phi \; \underline{S}^T \tag{17}$$

The elements of the transformation matrix $\underline{S}$ are:

$$S_{ij} = \frac{d\chi_i}{d\phi_j} = \begin{cases} \dfrac{Q-\phi_i}{Q^2} & \text{for } i = j \\[2ex] -\dfrac{\phi_i}{Q^2} & \text{for } i \neq j \end{cases} \tag{18}$$

For the example of the NBS evaluation /11/ of the Cf-252 neutron spectrum, the transformation of Eq. (17) is demonstrated. The uncertainties originally quoted comprise only diagonal elements of the covariance matrix and therefore neglected the normalization. The result before and after the application of Eq. (17) is shown in Table I. The data are shown in the form of a relative covariance matrix. The group structure is the one originally quoted. The group-averaged spectral distribution $\bar{\chi}(E)$ is also given. The relative uncertainty of 15 % between 12 MeV and 20 MeV is based on an estimation. The uncertainty information in both cases shown in Table I is exactly the same. The small modifications of the relative standard deviations in the normalized case are due to off-diagonal elements of the matrix. Only the normalized case can be applied in the least-squares adjustment procedure.

2.3. Transformation of $\sigma(E)$ data to a specific group structure

The group structure of the NBS spectrum evaluation shown in Table I is not appropriate for the procedure described in Section 2.1., i.e.,the neutron spectrum as well as the neutron cross-section data must be transformed to a specific group structure. In the case of neutron cross sections taken from ENDF/B-V or from other evaluations (see. Ref. /7/), care must be taken to process the covariance information correctly.

The transformation of ENDF/B-V neutron cross sections can be performed with modules of the NJOY system /12/, for example. Due to the application of the transformation to other cross-section sets (see Ref. /7/, for example) not given in the ENDF format, it appears expedient to give a brief review of the principles of such transformations. The samples given are based on ENDF data but can also be applied to other forms of data. The method shown requires direct access to the original ENDF file. In the case of data already processed, the methodology can also be applied with minor modifications (see Ref. /13/, for example).

The correct transformation of cross sections and covariances from one group structure to another requires the conservation of energy integrals independent of the specific group structure to be taken into account.

Fig.1 Transformation of the group structure

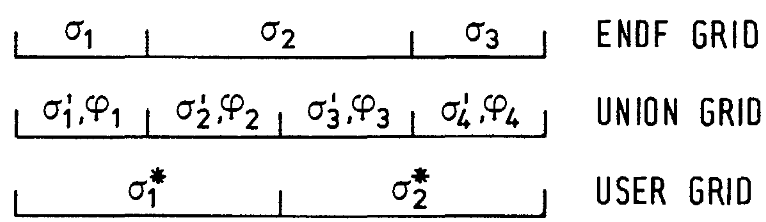

As shown in Fig. 1 this effect can be obtained by introducing a "union" group structure with group boundaries fitting the original ENDF structure as well as the final "user" structure. After a straightforward transformation from the ENDF structure to the "union" structure, the final group cross-section data can be obtained by

$$\sigma_i^* = \sum_{k\in i} \sigma_k' \phi_k \Big/ \sum_{k\in i} \phi_k \qquad (19)$$

with ϕ_k being the group fluxes of the union structure. The absolute covariance matrix of the final structure is then given by

$$\mathrm{cov}(\sigma_i^*, \sigma_j^*) = \sum_{k\in i} \sum_{l\in j} a_{ik} \, a_{jl} \, \mathrm{cov}(\sigma_k', \sigma_l') \qquad (20)$$

with

$$a_{ik} = \phi_k \Big/ \sum_{k\in i} \phi_k \qquad (21)$$

In the case of a relative covariance matrix, the transformation is similar:

$$\mathrm{rcov}(\sigma_i^*,\sigma_j^*) = \sum_{k\epsilon i} \sum_{j\epsilon l} f_{ik} f_{jl} \; \mathrm{rcov}(\sigma_k', \sigma_l') \qquad (22)$$

with

$$f_{ik} = \sigma_k' \quad \phi_k \quad / \sum_{k\epsilon i} \sigma_k' \quad \phi_k \qquad (23)$$

3. State of information available for the adjustment procedure and action still to be taken

a) The first step is the definition of an appropriate group structure. Due to the fact that covariance matrices of a large dimension contain a lot of redundant information and are difficult to handle, a compromise has to be found in the form of a dimension of the matrix which contains sufficient detail but avoids unnecessary redundancy. A dimension of 20 x 20 elements of the matrix is probably sufficient.

b) Integral experimental data for A^o (Eq. (1)) are available (see Ref. /7/). The covariance matrix has been constructed for a subset of this data /14/. The generation of the matrix for the remainder is in progress.

c) As prior information on the neutron spectrum, the NBS evaluation /11/ can be applied. The normalization of its covariance matrix is shown in Table I and does not present any problems.

d) The transformation of neutron cross section data and their covariances to the above-mentioned group structure, according to Section 2.3, is a task which still has to be done. As shown in Ref. /7/, data taken from ENDF/B-V as well as from other evaluations will be used. In most cases covariance files are available.

e) The solution of the least-squares of Section 2.1 aimed at obtaining an evaluated Cf-252 neutron spectrum with a covariance matrix based on integral data depends on the time needed to process the input data of the procedure. Final results can be expected at the end of 1983.

4. Summary

The evaluation of the spectrum and its covariance matrix based on integral experiments is proposed within the framework of a new evaluation of the Cf-252 neutron spectrum. The present state of information and future action are reviewed. Such an evaluation can be regarded as the first step in the whole evaluation process. The disadvantage of the least-squares adjustment procedure in interlinking neutron spectrum and neutron cross-section data can be sufficiently diminished in further steps of the evaluation combining the result based on integral data with that of direct spectrum measurements.

References:

/1/ J.J. Wagschal, B.L. Broadhead, R.E. Maerker, NBS Spec. Publ. 594, 956 (1980)

/2/ "Nuclear Data for Science and Technology" (ed. K.H. Böckhoff), Proc. Int. Conf., Antwerp, 6 - 10 September 1982, D. Reidel Publishing Company (1983)

/3/ W.P. Poenitz, T. Tamura, Antwerp Conference /2/, p. 465 (1983)

/4/ M.V. Blinov, G.S. Boykov, V.A. Vitenko, Antwerp Conference /2/, p. 479 (1983)

/5/ R. Bottger, H. Klein, A. Chalupka, B. Strohmaier, Antwerp Conference /2/, p. 484 (1983)

/6/ H. Märten, D. Seeliger, B. Stobinski, Antwerp Conference /2/, p. 488 (1983)

/7/ W. Mannhart, this meeting

/8/ R.W. Peelle in "Advances in Nuclear Science and Technology, 14, 11 (1982)

D.L. Smith, Report ANL/NDM-62 (1981)

W. Mannhart, Report PTB-FMRB-84 (1981)

German Standard: DIN 1319 part 4, (ed. K. Weise), draft, (1983)

/9/ F.G. Perey, Report ORNL/TM-6062 (1977)

/10/ F. Schmittroth, Report HEDL/TME 79-40 (1979)

/11/ J. Grundl, C. Eisenhauer, IAEA-TECDOC-208, Vol. I, p. 53 (1978)

/12/ R.E. MacFarlane, D.W. Muir, R.M. Boicourt, Report LA-9303-M (May 1982)

/13/ W. Mannhart, IAEA-TECDOC-263, 47 (1982)

/14/ W. Mannhart, F.G. Perey; EUR 6813, Vol. II, p. 1016 (1980)

Table I

Relative Covariance Matrix of the NBS evaluation without and with regard of the normalization

CF-252 NBS-EVALUATION UNNORMALIZED

ENERGY RANGE MeV		$\bar{\chi}(E)$	REL. STD.DEV. %								
0.00	0.25	4.70E-2	13.0	100							
0.25	0.80	1.84E-1	1.1	0	100						
0.80	1.50	2.20E-1	1.8	0	0	100					
1.50	2.30	1.94E-1	1.0	0	0	0	100				
2.30	3.70	2.00E-1	2.0	0	0	0	0	100			
3.70	8.00	1.46E-1	2.1	0	0	0	0	0	100		
8.00	12.00	8.70E-3	8.5	0	0	0	0	0	0	100	
12.00	20.00	5.80E-4	15.0	0	0	0	0	0	0	0	100

CF-252 NBS-EVALUATION NORMALIZED

ENERGY RANGE MeV		$\bar{\chi}(E)$	REL. STD.DEV. %								
0.00	0.25	4.70E-2	12.4	100							
0.25	0.80	1.84E-1	1.3	-46	100						
0.80	1.50	2.20E-1	1.6	-38	-3	100					
1.50	2.30	1.94E-1	1.2	-48	29	-2	100				
2.30	3.70	2.00E-1	1.8	-35	-7	-22	-6	100			
3.70	8.00	1.46E-1	2.0	-31	0	-15	1	-16	100		
8.00	12.00	8.70E-3	8.5	-7	0	-3	0	-4	-2	100	
12.00	20.00	5.80E-4	15.0	-4	3	0	3	-0	0	0	100

March 2, 1983

Work Planned on the Prompt Fission Neutron Spectrum for the Spontaneous Fission of ^{252}Cf

David G. Madland and J. Rayford Nix

Our intention is to compare the following representations of the ^{252}Cf(sf) prompt fission neutron spectrum with existing high quality experimental data:

(a) Maxwellian spectrum, with parameter T_M;

(b) Watt spectrum, with parameters E_f and T_W;

(c) Watt spectrum composed of two contributions, one from each mass peak, with parameters E_f^L, E_f^H, and T_W;

(d) Madland and Nix spectrum, for a constant compound-nucleus cross section, with parameters E_f^L, E_f^H, and T_m; and

(e) Madland and Nix spectrum, for an energy-dependent compound-nucleus cross section, with parameters E_f^L, E_f^H, and T_m.

We intend to present pure calculated results and results obtained in the least-squares adjustment of various spectrum parameters to the experimental data. Since the values of E_f, E_f^L, and E_f^H are very well known, from experiment, we will vary only T_M, T_W, and T_m. In the case of T_m, a calculated temperature in the Madland and Nix theory, the nuclear level-density parameter, a, will actually be adjusted since it is the least well known quantity in the theory. Note that T_m is proportional to $1/\sqrt{a}$.

We expect to publish the results of our comparisons within the year.

UNITED STATES DEPARTMENT OF COMMERCE
National Bureau of Standards
Washington, D.C. 20234

May 17, 1982

MEMORANDUM FOR Allan Carlson
Chairman, CSEWG Sub-Committee on Standards

From: James Grundl, David Gilliam, Dale McGarry, Charles Eisenhauer (NBS), and Pat Soran (LANL)

Subject: Revised Value for the ^{252}Cf Fission Spectrum-Averaged Cross Section for ^{235}U Fission, $\bar{\sigma}_f(\mathrm{U235}, \chi_{Cf})$

Pursuant to our recent discussion this memorandum provides an updated value for the subject cross section last reported in Ref. 1 and used by W. Poenitz in Ref. 2 to evaluate the U235 fission cross section.

Three features of the measurement have been reworked in recent times: (1) the ^{252}Cf neutron source strength; (2) the mass scale of the NBS U235 fissionable isotope mass standard; and (3) neutron scattering in the fission chamber and fissionable deposit backing. The resulting change in the measured cross section is modest; the error reduction however, is more substantial. The new cross section value is

$$\bar{\sigma}_f(\mathrm{U235}, \chi_{Cf}) = 1216 \pm 1.6\%(1\sigma)$$

On an rms scale the error has been reduced by about a factor of 2, while the value itself is 0.9% higher than previously reported.

It should be noted that the value of this integral cross section measurement as a test of ENDF/B data is not significantly affected by uncertainties in the ^{252}Cf neutron spectrum. Since the ^{235}U fission cross section is relatively flat over the major response range and since the ^{252}Cf neutron spectrum uncertainties are small (Ref 3.), the result is that a spectrum averaged cross section based on ENDF/B data has a propagated uncertainty of only $\pm$ 0.30%(2σ) due to the ^{252}Cf neutron spectrum uncertainties.

A brief description of the reworked features are included for the benefit of the evaluators. Further inquiries can be directed as a start to David Gilliam, Charlie Eisenhauer, or Jim Grundl of NBS.

<u>(1) Neutron source strength</u>. The absolute neutron source strength of NBS-I, the National Standard Photoneutron Source has been checked against modern values of $\bar{\nu}_{Cf}$ in a series of experiments involving low-geometry fission fragment counting and manganous-sulfate bath source intercomparisons. The resulting agreement of the historic NBS-I neutron source strength with $\bar{\nu}_{Cf}$ is within(0.7 $\pm$ 0.6)%. On this basis, the error in the NBS-I source strength has been reduced from its long-standing and conservatively derived value of $\pm$ 1.1%(1σ) to $\pm$ 0.8(1σ). The high-intensity Cf sources are calibrated relative to NBS-I with an accuracy of $\pm$ 0.4% (Ref. 5). Hence the Cf source strength error has been reduced from 1.2% to 0.9%.

(2) Fissionable deposit mass. A sustained program to improve the mass scale of NBS fissionable isotope mass standards employs standardized low-geometry alpha counting and fission fragment counting comparisons along with various inter-laboratory comparisons of well-studied fissionable deposits. This accumulated effort has led to an error assignment of $\pm$ 0.5%(1σ) to the isotopic mass of the NBS U235 fissionable deposit mass standard. The mass of the U235 deposits used in the subject measurements are traceable to these archive standards with an accuracy of better than $\pm$ 0.5%. Thus, the largest error in the original report of the measurement of $\bar{\bar{\sigma}}_f$(U235, χ_{Cf}) has been reduced to $\pm$ 0.7%(1σ).

(3) Neutron scattering corrections. Scattering corrections for the fission chambers (and the source capsule as well) have been estimated for once scattered neutrons by means of an elementary geometry code without a detailed articulation of energy and angle transport. Within this limitation scattering corrections of up to 1.2% were entered with errors of between 1/3 to 4/3 of the correction itself. The error assessment of the source capsule correction has been revised slightly due to differences found in subsequent Monte-Carlo calculations. Very recently a high-precision Monte-Carlo calculation has been undertaken at Los Alamos which accounts for the effect upon the U235 fission rate of neutrons scattered at the fission chamber, and most importantly for scattering within the fissionable deposit backing. The new corrections are 0.9873 $\pm$ 0.2% and 0.990 $\pm$ 0.2% for the fission chamber and deposit backings, respectively. These corrections are very nearly the same as had been previously estimated, but the residual uncertainties in the corrections are now reduced from the level of major contributors to the level of insignificance.

A revision of the summary table of error components which appeared in Ref. 1 is attached. The new error estimates and corrections are given along with the values applied in the original work.

References

1. Fission Cross Sections of ^{235}U, ^{238}U, and ^{239}Pu Averaged Over the ^{252}Cf Neutron Spectrum, H. T. Heaton II, D. M. Gilliam, V. Spiegel, C. Eisenhauer, and J. A. Grundl, Proceedings of the NEANDC/NEACRP Specialist Meeting on Fast Neutron Fission Cross Sections of U-233, U-235, U-238 and Pu-239, Argonne National Laboratory (June 1976).

2. ^{235}U Fission Mass and Counting Comparison and Standardization, W. P. Poenitz, J. W. Meadows and R. J. Armani, ANL/NDM-48, Argoone National Laboratory (1979).

3. Fission Spectrum Neutrons for Cross Section Validation and Neutron Flux Transfer, J. A. Grundl and C. M. Eisenhauer, Nuclear Cross Sections and Technology Conference, Washington, D.C., NBS Special Publ. 425, U.S. Dept. of Commerce (March 1975).

4. ^{235}U Cavity Fission Neutron Field Calibration via the ^{252}Cf Spontaneous Fission Neutron Field, V. Spiegel, C. M. Eisenhauer, D. M. Gilliam, J. A. Grundl, E. D. McGarry, I. G. Schroder, W. E. Slater, and R. S. Schwartz/ IAEA Consultant's Mtg. on Neutron Source Properties, Debrecen, Hungary (March 1980).

5. Absolute ^{235}U Fission Cross Section for ^{252}Cf Spontaneous Fission Neutrons, H. T. Heaton II, J. A. Grundl, V. Spiegel, Jr., D. M. Gilliam, and C. Eisenhauer, Nuclear Cross Sections and Technology Conference, Washington, D.C., NBS Special Publ. 425, U. S. Dept. of Commerce, (March 1975).

Error Components for NBS Measurement of $\bar{\sigma}_f(U235, \chi_{Cf})$
(Revision of Table II, Ref. 1; May 1982)

	Correction		Percent Error in Cross Section	
	Old	New	Old	New
Fissionable Deposit Mass	--	--	±1.3%(1σ)	±0.7%
Cf Neutron Source Strength	--	--	±1.2%	±0.9%
Fission in Other Isotopes	0.9987	same	±0.1%	same
Geometrical Measurements				
Fissionable Deposit Separation	--	--	±0.6%	same
Deposit Diameter	1.0075	same	±0.1%	same
Source Position	1.001	same	±0.2%	same
Undetected Fission Fragments				
Extrapolation to Zero Pulse Height	1.009	same	±0.5%	same
Absorption in Fissionable Deposit	1.0132	same	±0.3%	same
Neutron Scattering				
Room Return	0.9955	same	±0.2%	same
Source Capsule	0.9922	same	±0.3%	±0.4%
Fission Chamber	0.9888	0.9873	±0.4%	±0.2%
Support Structures	0.9945	same	±0.5%	same
Deposit Backing (Pt.)	0.987	0.990	±0.8%	±0.2%
TOTAL ERROR			±2.25%(1σ)	1.61%(1σ)

NEW VALUE 1216 mb (± 1.61%)

FISSION CROSS SECTION MEASUREMENTS IN REACTOR PHYSICS AND DOSIMETRY BENCHMARKS

J.A. Grundl, and D.M. Gilliam (NBS)

Fission cross sections for eight fissionable isotopes of importance for nuclear technology have been measured in three fission neutron spectra and one fission-neutron-driven standard neutron field. New measurements for ^{240}Pu, ^{241}Pu, ^{233}U, and ^{232}Th accompany revised values from earlier determinations for ^{239}Pu, ^{235}U, ^{238}U, and ^{237}Np.

For all of these measurements, the starting point is an absolute cross section for ^{252}Cf fission spectrum neutrons based upon determination of a neutron source strength, a source-to-detector distance and an absolute fission rate.[1] For the fission-neutron-driven Intermediate-Energy Standard Neutron Field (ISNF), a neutron flux transfer procedure from the ^{252}Cf fission source is employed (Refs. 2-5 for ISNF facility description); for ^{235}U fission spectrum neutrons, cross section ratios are determined with a cavity fission source and subsequently normalized to the Cf fission spectrum measurement of σ_f (^{235}U)[6,7]; results for ^{239}Pu fission neutrons have been derived from earlier ratio measurements designed to compare ^{235}U and ^{239}Pu fission neutron spectra.[8,9]

Major components of these cross section measurements are the same for all of the benchmarks but one and can be summarized individually. Errors are similar also and they will be assessed together for each measurement component.[10] Specialized activation techniques for the ^{239}Pu fission spectrum measurements have been described previously.[8,9]

Fission rate detection. Double fission ionization chambers with detection efficiencies between 0.97 and 0.998 depending upon the thickness of fissionable deposits, were employed in these measurements.[11] Errors for fission fragment loss corrections were ± (0.6-0.8)%; counting statistics were <± 0.2% except for ^{252}Cf where counting errors for some isotopes were as high as ± 0.6%.

Isotopic mass. Fissionable deposits in a thickness range 8 to 600 $\mu g/cm^2$ were used in the fission chambers.[11,12] Deposit masses were ascertained by a multiplicity of techniques including advantageous comparisons among the isotopes and selective intercomparisons with archive deposits from other laboratories: (1) low-geometry alpha counting; (2) isotope dilution mass spectrometry (^{235}U and ^{238}U only); and (3) Maxwellian and thermal-neutron fission counting. A new set of isotopic mass uncertainties for the NBS fissionable isotope mass standards are now available and they supercedes all previously reported values are set out below at one standard deviation:

previously reported[10]	new isotopes
^{235}U: ± 0.5%	^{232}Th: ± 2.0%
^{238}U: ± 0.7%	^{233}U: ± 1.5%
^{237}Np: ± 1.0%	^{240}Pu: ± 0.8%
^{239}Pu: ± 0.4%	^{241}Pu: ± 4.0%

Corrections for fission in other than the principle isotope were between 0% and 1% for all but ^{240}Pu and ^{241}Pu where the corrections were 3.0% and 21% respectively.

Neutron flux. The free-field neutron flux at 5 cm from the ^{252}Cf fission source can be established to ± 1.1% on the basis of a measured detector separation distance and a neutron source strength determination performed at the NBS $MnSO_4$ Bath Facility. Neutron fluence transfer from the ^{252}Cf Irradiation Facility to the ISNF and to the ^{235}U fission spectrum irradiation facilities is carried out by means of the ^{239}Pu and ^{235}U fission reactions as as indicated in Table 1.

Scattering corrections. Monte-carlo calculations have been performed for the Cf irradiation facility in order to determine fission rates attributable to source neutrons once-collided in the source capsule, the fission chambers, and the support structures. Total corrections is 3.5% for fissile isotopes and % for the other isotopes; errors have been set at ± %.

Fission rates in fissile isotopes due to environmental return at the Cf Facility is aroung 0.5% based on both measurment and calculation. At ISNF the fission chamber is the only significant scattering element in a neutron flux that is nearly isotropic. Corrections are ( )%. Cavity fission source arrangements for ^{235}U fission spectrum measurements (and ^{239}Pu) are less ideal for scattering calculations and larger corrections and uncertainties are involved.

Fission cross section results are presented in Table 1, along with selected cross section ratios for which errors are significantly less than for the individual cross sections. Corresponding section values predicted by ENDF/B-V are within experimental errors for many of the isotope reported. Some exceptions are ^{232}Th and ^{238}U for which calculated-to-experimental ratios are 0.885 and 0.955 respectively, for both the ISNF and Cf benchmarks.

TABLE 1. Fission Cross Sections For Reactor Physics and Dosimetry Benchmarks

Isotope	ISNF (mb)	[a] Fission ^{252}Cf (mb)	Spectra ^{235}U (mb)
^{232}Th	38.4 ± 1.2	89.4 ± 2.7	-
^{233}U	2424 ± 65	1893 ± 48	-
*^{235}U	1606 ± 35	1216 ± 19	(b)
*^{238}U	149.0 ± 3.6	326 ± 6.5	309 ± 8
*^{237}Np	829 ± 22	1366 ± 27	1344 ± 54
*^{239}Pu	(b)	1824 ± 35	1832 ± 55
^{240}Pu	824 ± 23	1337 ± 32	-
^{241}Pu	2152 ± 108	1616 ± 80	-
$^{235}U/^{238}U$	10.78 ± 1.1%	3.73 ± 1.2%	3.94 ± 2.0%
$^{235}U/^{239}Pu$	0.866 ± 1.0%	0.666 ± 0.9%	0.664 ± 2.5%
$^{237}Np/^{238}Pu$	5.56 ± 1.7%	4.19 ± 1.5%	4.35 ± 3.0%

[a] Two Cross sections for the ^{239}Pu fission spectrum may be derived from ^{235}U and ^{239}Pu fission spectra comparison experiments: $\sigma_f(^{238}U) = 319 \pm 0.09$; $\sigma_f(Np) = 1346 \pm 44$ mb.

[b] Neutron fluence transfer reactions are $\sigma_f(^{235}U,X_{25})/\sigma_f(^{235}U,X_{Cf}) = 1.000 \pm 0.004$ (2 std. dev.), and $\sigma_f(^{239}Pu, ISNF)/\sigma_f(^{239}Pu, X_{Cf}) = 1.018 \pm 0.006$ (2 std. dev.).

*Previous work reported in Refs. 7, and 12-14.

REFERENCES

1. J.A. Grundl, V. Spiegel, C.M. Eisenhauer, H.T. Heaton II, and D.M. Gilliam (NBS), and J. Bigelow (ORNL), "A Californium-252 Fission Spectrum Irradiation Facility for Neutron Reaction Rate Measurements," Nucl. Tech. 32, 315 (1977).

2. C.M. Eisenhauer and J.A. Grundl, "Neutron Transport Calculations for the Intermediate-Energy Standard Neutron Field (ISNF) at the National Bureau of Standards," Proc. International Symposium on IAEA Consultants Meetings on Prompt Fission Neutron Spectra, Vienna, Austria (1971).

3. P.D. Soran, R.J. LaBauve, and D.C. George (LASL) C.M. Eisenhauer, (NBS), "Neutronic Analysis of the NBS Intermediate-Energy Standard Neutron Field (ISNF)," Trans. Am. Nucl. Soc. 32 (1979).

4. B.L. Broadhead and J.J. Wagschal, "The ISNF: A New CSEWG Dosimetry Benchmark (Computational Problems and Their Solutions)," Trans. Am. Nucl. Soc. 35, p. 466 (1980).

5. R.J. LaBauve, D.C. George, D.W. Muir, P.D. Soran, and C.M. Eisenhauer, "Nuclear Data Development Work in Support of the National Bureau of Standards ISNF Project," Los Alamos Scientific Lab. Report LA-8638-SR (1980).

6. A. Fabry, G. Minsart, F. Cops, and S. DeLeeuw, "The Mol Cavity Fission Spectrum Standard Neutron Field and Its Applications," Proc. Fourth ASTM-EURATOM Symposium on Reactor Dosimetry, Washington, D.C. (1982)

7. J.J. Wagschal, B.L. Broadhead, "Evaluation of the New ISNF One-Dimensional Model," Trans. Am. Nucl. Soc. 39, p. 887 (1981).

8. J.A. Grundl, "A Study of Fission-Neutron Spectra with High-Energy Activation Detectors, Part II, Fission Spectra," Nucl. Sci. Eng., 31, 191 (1968).

9. J.A. Grundl, "Brief Review of Integral Measurements with Fission Spectrum Neutrons," Proc. International Symposium on IAEA Consultants Meetings on Prompt Fission Neutron Spectra, Vienna, Austria (1971).

10. J.J. Wagschal, R.E. Maerker (ORNL), D.M. Gilliam (NBS), "Detailed Error Analysis of Average Fission Cross-Section Measurements in NBS Standard Neutron Fields," Trans. Am. Nucl. Soc. 33, 823 (November 1979).

11. J.A. Grundl, D.M. Gilliam (NBS), and N.D. Dudey and R.J. Popek (ANL), "Measurement of Absolute Fission Rates," Nucl. Tech. 25, 237 (1975).

12. D.M. Gilliam, C. Eisenhauer, H.T. Heaton II, and J.A. Grundl, "Fission Cross Section Ratios in the ^{252}Cf Neutron Spectrum (^{235}U, ^{238}U, ^{239}Pu, ^{237}Np)," Proceedings of a Conference on Nuclear Cross Sections and Technology, NBS Special Publication 425, Dept. of Commerce, Washington, D.C. Vol. I, p. 270 (March 1975).

13. H.T. Heaton II, J.A. Grundl, V. Spiegel Jr., D.M. Gilliam, and C. Eisenhauer, "Absolute ^{235}U Fission Cross Section for ^{252}Cf Spontaneous Fission Neutrons," Proceedings of a Conference on Nuclear Cross Sections and Technology, NBS Special Publication 425, U.S. Dept. of Commerce, Washington, D.C., (1975).

14. A. Fabry (CEN/SCK, Belgium), J.A. Grundl, and C. Eisenhauer (NBS), "Fundamental Integral Cross Section Measurements in the Thermal-Neutron-Induced Uranium-235 Fission Neutron Spectrum," Proceedings of a Conference on Nuclear Cross Sections and Technology, NBS Special Publication 425, U.S. Dept. of Commerce, Washington, D.C., p. 254 (1975).

February 25, 1983

Description of Cf neutron spectrum work of R. R. Spencer and D. K. Olsen (ORNL).

Most of the measurement problems and their solutions have been discussed by reviewers, particularly by Adams at the Harwell Conference, Browne at the BNL Workshop, and Blinov. In fact, all or almost all the problems and their solutions have been discussed in the various experimental papers. The challenge is to incorporate all these ideas successfully into a single series of definitive TOF measurements. Phase 1 will complete a measurement from 30 keV to 15 MeV of the standards neutron spectrum from spontaneous fission of ^{252}Cf. This measurement will be done in the 15- x 15- x 6-m shield test station of ORELA using a spherical, low-mass, $\sim 10^5$ f/s chamber and employing rejection electronics to eliminate complicated deadtime corrections. Three detector systems for different energy regions will be required. A segment from 0.1 to 2.0 MeV will be measured at 2 m with a 7-x 10-cm, NE110 detector which has been extensively studied and documented. A 0.5-to-15.0-MeV segment will be measured at 4 m with a 7-x 10-cm, NE 213 detector employing n-γ discrimination. Data for very-low-energy neutrons will be obtained with either a Li-glass detector or a NE110 detector using single photoelectron coincidence from multiple phototubes. Low-energy background events due to delayed γ's will be determined with the aid of variable flight-path lengths. Room-return backgrounds will be determined with shadow bars. Energy scales will be determined with a precision EG&G TDC 100 time digitizer and verified, with the resolution function, by observing resonance dips in an auxiliary carbon transmission measurement.

An important feature will be the simultaneous recording, event by event, of the neutron TOF, the detector pulse height, the fission chamber pulse height, and the n-γ discrimination pulse height for the NE213 detector. The recording system will allow variable bias levels to be set in this four dimensional space after data accumulation, and in particular allow the construction of pulse-height spectra for particular neutron energy intervals. These pulse-height spectra will allow comparison with measured and calculated neutron response functions and confirm that the time-dependent and time-independent backgrounds have been accounted for correctly.

For both low and high neutron energies the hydrogen-recoil detector efficiencies will be calculated and verified with the pulse-height spectra. At low neutron energies where the detectors are nearly black to incident neutrons this procedure is probably sufficient. At high neutron energies the NE213 efficiency calculation will need to be verified by auxillary measurements. The efficiency effect of n-γ discrimination will be determined in the ORELA beam. Since all measurements will be absolute, overlap regions will provide a check of detector efficiency determination. Over 99% of the fission neutrons are detected in a 30-keV to 15-MeV measurement so the ^{252}Cf $\bar{\nu}$ will provide an overall verification of the efficiency determinations. Other techniques for detector efficiency calibrations will be utilized as required.

Using the same fast neutron detector systems, phase 2 will include simultaneous measurements of the spectra of ^{233}U, ^{235}U, and ^{239}Pu with respect to this ^{252}Cf standard with the ^{233}U, ^{235}U, and ^{239}Pu fissions induced by thermal and eV

neutrons from ORELA. The ORELA facility and the ORELA staff's experience are unique for this task. A ^{233}U, ^{235}U, and ^{239}Pu multiple plate fission chamber with ^{252}Cf would supply a timing signal and a target and would allow relative spectral measurements with common detector efficiency and background conditions. ORELA would be operated at 1000 pps with the counting system off for 200 µs after γ-flash so 80% of all incident neutrons below 55 eV at 20 m, for example, would be useable. A feasibility study with the above ORELA conditions and an existing ^{235}U chamber has shown that these measurements are possible. Nearly all recent spectral results have been obtained with Van de Graaff neutron sources and massive samples. A fission chamber measurement employing low-energy neutrons from ORELA would allow: (1) simultaneous relative results to ^{252}Cf eliminating many systematic sources of uncertainty, (2)alow-background environment, (3) results for low spectral energies, and (4) the use of small samples eliminating much of the uncertainty from multiple scattering corrections. Angular distribution effects would be eliminated by summing results taken at several angles. Though some of the basic experimental parameters have been worked out, many experimental difficulties must yet be overcome.

Phase 3 will attempt to measure the changes in the ^{233}U, ^{235}U, and ^{239}Pu spectra with increasing incident neutron energy and also the spectra from ^{232}Th and ^{238}U. This task is substantially more difficult than phase 2 because of the relatively low high-energy neutron flux from ORELA. Almost no experimental information presently exists on these spectra above an MeV.

ANGULAR DISTRIBUTIONS OF FISSION FRAGMENTS FROM ^{235}U, ^{238}U AND ^{237}Np NEAR THE /n,2nf/ TRESHOLD*

S. Ouichaoui +, S. Juhász and J. Csikai, M. Várnagy

Institute of Experimental Physics, Kossuth University
4001. Debrecen, Pf. 105, Hungary

The angular distributions of fission fragments from fast neutron induced fission on ^{235}U, ^{238}U and ^{237}Np were determined near the /n,2nf/ threshold using the track-etched technique. A function of the form $W/\vartheta/= a_0+a_2\cos^2\vartheta$ has been fitted to the data. The anisotropy parameters obtained around 14 MeV show a strong energy dependence.

*This work was supported in part by the IAEA, Vienna and the Hungarian Academy of Sciences

+Permanent address: Institut de Physique Nucleaire, Commissariat aux Energies Navelles, B.P. 1017, Alger-gare, Algerie

1. Experimental procedure

Fissionable samples of 19 mm diam. deposited onto aluminium backing plate of 0.2 mm thickness and 40 mm diam. were placed in a vacuum chamber together with the Makrofol KG detector foils. The samples, placed at 5 cm from the target spot, were oriented at on angle of 45° to the neutron beam. Neutrons were produced in the D+T reaction using analysed D^+ beam of 200 μA. Schematic drawing of the experimental arrangement is shown in Fig.1.

The isotopic composition and the areal density of the samples are given in Table I. These detector foils having about 1000-1500 tracks/cm^2 were evaluated by a Jumping Spark Counter.

2. Results and discussion

The angular distributions for all fragments have been determined at 14.1, 14.45 and 14.8 MeV neutron energies. Results for the anisotropy parameter in comparision with the calculated values are given in Table II-IV. The differential cross sections as a function of angle are indicated in Figs. 2-4.

Table 1. Isotopic composition and areal density of the utilised fissile samples

Sample	Isotopic composition			Areal density / $\mu g/cm^2$/
^{235}U	^{234}U 0.0010	^{235}U 99.9955	^{236}U 0.0035	170
^{238}U	is depleted by a factor of 230			190
^{237}Np	^{237}Np 99.9933	^{239}Pu 0.0062	^{241}Am 0.0005	148

Table 2, The parameters of the fitted angular distribution functions

Target	En/MeV/	a_o	a_2	R	$/Z^2/A/C.N.$
^{235}U	14,12	143,99±2,339	63,48±8,062	1,441±0,056	35.86
	14,45				
	14,80	150,52±0,930	50,13±3,118	1,333±0,022	
^{238}U	14,12	76,63±1,192	40,48±4,254	1,528±0,055	35.41
	14,45	79,58±0,900	39.77±3.183	1,499±0,040	
	14,80	83,63±0,905	35,20±3,120	1,421±0,037	
^{237}Np	14,12	166,71±1,250	62,50±4,244	1,375±0,025	36,34
	14,45	175,20±1,396	48,40±4,589	1,276±0,026	
	14,80	181,00±1,126	41,91±3,647	1,232±0,020	

Table 3. Experimental anisotropy values compared to literature data

Target	E_n/MeV/	R	Reference	E_n/MeV/	Present work
^{235}U	14.0	1.27±0.17	12 /25/		
	14.0	1.27±0.08	13,14/13,26/		
	14.0	1.23±0.08	15 /4/		
	14.1±0.1	1.27±0.10	4 /10/	14.12±0.08	1.441±0.06
	15.8±0.5	1.27±0.08	9. /21/		
	14.8±0.1	1.28±0.07	19 /29/	14.80±0.17	1.333±0.02
^{238}U	14.0	1.31±0.05	13,14/13,26/		
	14.0	1.37±0.13	15 /4/		
	14.1	1.30±0.03	7 /19/		
				14.12±0.08	1.528±0.055
	14.1±0.1	1.31±0.02	4 /10/		
	14.5±0.5	1.40±0.14	16 /7/	14.45±0.12	1.499±0.040
	14.7	1.43±0.05	7 /19/		
				14.80±0.17	1.421±0.037
	14.9	1.25±0.02	17 /27/		
	15.8±0.5	1.66±0.10	9		
^{237}Np	14.0	1.15±0.04	13,14/13,26/		
	14.0	1.14±0.04	15 /4/		
	14.1±0.1	1.12±0.05	4 /10/	14.12	1.375±0.025
				14.45	1.276±0.026
	14.7	1.16±0.02	18 /28/		
				14.80	1.232±0.020
	15.8±0.5	1.23±0.06	9 /21/		

Table 4. Comparison of experimental anisotropy values with calculated ones

Nuclide	E_n/MeV/	Experimental anisotropy	Calculated anisotropy /a/	Calculated anisotropy /b/	σ_0 /Barn/	σ_1 /Barn/	σ_2 /Barn/	A_0 /c/	A_1 /c/
^{235}U	14.12±0.08	1.441±0.56	1.296±0.01	1.669±1.06	1.15	0.67	0.55	0.16	0.4
	14.80±0.17	1.333±0.021	1.271±0.02	1.493±0.42					
^{238}U	14.12±0.08	1.528±0.055	1.299±0.015	1.628±1.12	0.56	0.44	0.20	0.20	0.3
	14.45±0.12	1.499±0.040	1.294±0.010	1.550±0.74					
	14.80±0.17	1.421±0.037	1.281±0.007	1.496±0.52					
^{237}Np	14.12±0.08	1.375±0.025	1.271±0.004	1.554±0.85	1.43	0.94	0.26	0.16	0.41
	14.45±0.12	1.276±0.026	1.261±0.002	1.434±1.6					
	14.80±0.17	1.232±0.020	1.256±0.001	1.379±4.1					

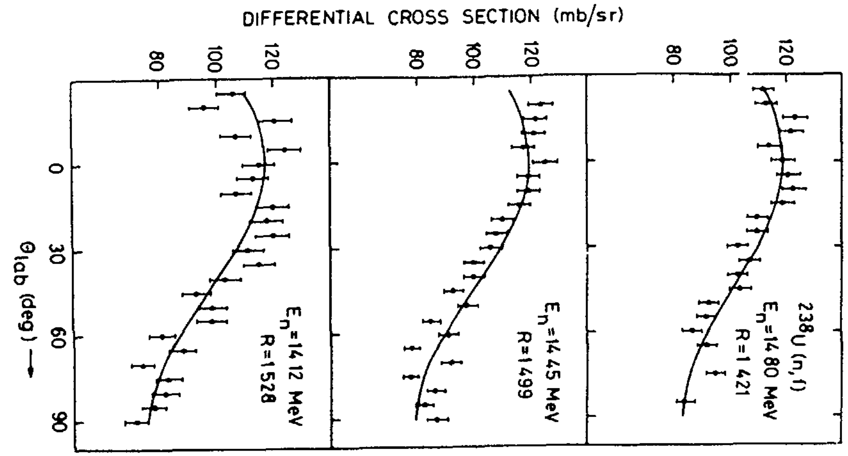

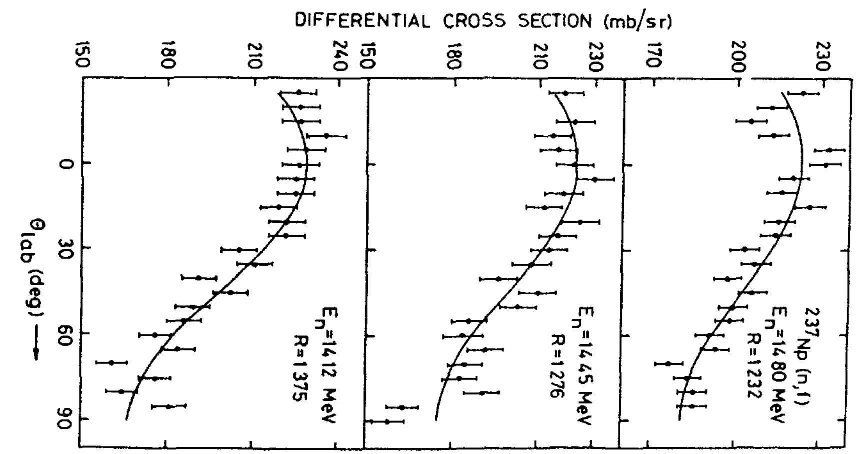

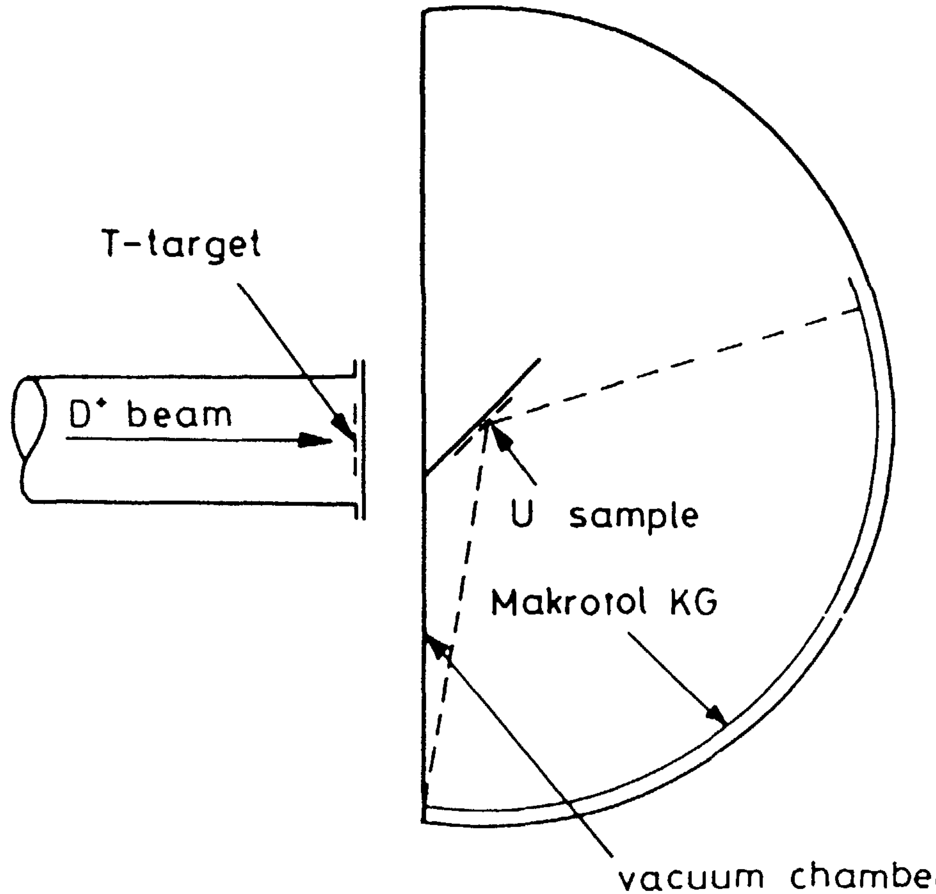

Fig 1. Schematic diagram of the experimental arrangement